Specific Sulphation Modifications of Heparan Sulphate Regulate Distinct Aspects of Axon Guidance in the Developing Mouse Central Nervous System.

Christopher Conway

Thesis submitted for the Degree of Doctor of Philosophy at the University of Edinburgh.

October 2008

This Thesis is Dedicated to my Loving Grandparents

Grandma Fletcher	
Grandpa Fletcher	1927-2005
Grandad	1924-1997
Nan	1925-1995
Auntie Molly	1921-2008

Disclaimer

I (Christopher Conway) composed this thesis and performed all of the experiments presented herein unless otherwise clearly indicated in the text. No part of this work has been, or is being submitted for any other degree or professional qualification.

Signed……..

Date……..

Acknowledgements

I would like to thank the “three wise men”, John Mason, Tom Pratt and David Price for providing excellent advice and encouragement throughout my PhD. Not only were they great supervisors, but they also contributed to one of the best working environments I have ever experienced.

Thanks go out to past and present members of the Mason/Price/Kind/Spears/Theil labs who helped to create such a positive working atmosphere. Thanks to Linda Wilson and Trudi Gillespie for their amazing skills in confocal imaging and Martin Simmen for guidance in statistical analysis. I must also thank the men of the animal house who had the thankless job of checking whether my mice had “got their groove on”. And finally, a big thank you to Katy Gillies for excellent technical support and for ensuring that my lab coat was always on.

A special thanks to the people that have made my stay in Edinburgh a wonderful one. Mike and Mark for football games and pub crawls. Catherine, Tammy, Dennis, Natasha and Dario for entertainment inside and outside of the lab. All the friends from Mylne’s Court, too many to name. And last, but not least Petrina for being a caring and helpful girlfriend.

There are not enough pages in this thesis to describe the contributions I have received from my parents over the years. Learning from their example, they have instilled in me the insatiable drive and determination to accomplish my goals. Thank you for your unconditional support (emotional and financial). I am honored to have you as my parents. Thanks to my brother whose over-achieving nature has always forced me to aim high.

To the “DOC”, I could not have a better group of friends.

Finally I would like to thank Rudy of Rudy’s Sandwich Shop for supplying me with excellent food at a reasonable price.

“Of all the things I miss, I miss my mind the most…”

Ozzy Osborne

Table of Contents

List of Figures

Chapter 1

Chapter 3

Chapter 4

Chapter 5

Chapter 6

Chapter 7

Chapter 8

List of Tables

Chapter 1

Chapter 2

Chapter 4

Chapter 6

Abbreviations

A	anterior
bp	base pairs
CNS	central nervous system
CTA	corticothalamic axons
d	dorsal
ddH_2O	distilled deionized water
dLGN	dorsal lateral geniculate nucleus
DN	dorso-nasal
DNA	deoxyribonucleic acid
dNTP	deoxyribonucleotide triphosphates
DTB	diencephalic telencephalic boundary
E	embryonic age
ECM	extracellular matrix
epiT	epithalamus
GAG	glycosaminoglycan
GW	glial wedge
hPLAP	human placental alkaline phosphatase
HS	heparan sulphate
HSPG	heparan sulphate proteoglycan
Hst	heparan sulphate sulphotransferase
Hs2st	heparan sulphate-2-O-sulphotransferase
Hs6st1	heparan sulphate-6-O-sulphotransferase-1
HypoT	hypothalamus
IGG	indusium griseum
l	lateral
m	medial

MZG	midline zipper glia
n	number of samples
OC	optic chiasm
OFL	optic fiber layer
OT	optic tract
PSPB	pallial subpallial boundary
PBS	phosphate buffered saline
PCR	polymerase chain reaction
PFA	paraformaldehyde
POA	pre-optic area
Q-RTPCR	quantitative-reverse transcriptase PCR
RGC	retinal ganglion cell
RNA	ribonucleic acid
RPE	retinal pigmented epithelium
rpm	rotations per minute
SC	superior colliculus
SEM	standard error of the mean
stm	striatum
T	temporal
TCA	thalamocortical
V	ventral
VT	ventro-temporal

Abstract

Development of the visual system involves the precise orchestration of neural connections between the retina of the eye, the thalamus (dorsal lateral geniculate nucleus; dLGN) and the superior colliculus (SC). During early development, receptor molecules on the growth cones of retinal ganglion cell (RGC) axons sense molecular guidance cues in the extra cellular matrix (ECM) that define their route and branching behaviour within the visual system. Heparan sulphate proteoglycans (HSPGs) are ECM molecules composed of a core protein and a variable number of disaccharide residues that have been implicated in mediating axon guidance. HSPGs are modified by a number of enzymes that contribute to their structural diversity. Based on this structural diversity; the "heparan sulphate code" hypothesis of Bulow and Hobert (2004) postulated that different HSPG modifications confer different axon navigation responses as the growth cones traverse the local environment. To investigate the roles played by specific modifications of HSPG molecules in the guidance of axons, we examined two lines of mutant mice harbouring mutations in the genes encoding HSPG modifying enzymes, Heparan sulphate-6-O-sulphotransferase-1 (Hs6st1) and Heparan sulphate-2-O-sulphotransferase (Hs2st). These two mutant lines were generated through the use of gene trapping. Previous observations of RGC axon development in the two mutant lines revealed distinct axon guidance errors at the optic chiasm. Loss of Hs6st1 sulphation resulted in RGC axons navigating ectopically into the contralateral eye. Loss of Hs2st sulphation resulted in RGC axons navigating outside the normal boundary of the optic chiasm. Early observations suggested that both Hs2st sulphation and Hs6st1 sulphation have distinct, non-overlapping actions and thus, influence different axon guidance signalling pathways at the optic chiasm.

Based on our findings and previous work describing the expression patterns and functions of the chemo-repellent axon guidance molecules, Slit1 and Slit2 at the optic chiasm and their Robo2 in the retina, we formulated the hypothesis of an HSPG sulphation code where Hs2st sulphation is specifically required for Slit1-Robo2

signalling and Hs6st1 sulphation is specifically required for Slit2-Robo2 signalling at the optic chiasm.

To further our understanding of the roles Hs2st sulphation and Hs6st1 sulphation have on axon guidance, we looked at a number of key choice points that navigating axons encounter and are known to be influenced by Slit signalling. Further observations of RGC axons at the optic chiasm of *Hs2st*$^{-/-}$ mutants and *Hs6st1*$^{-/-}$ mutants showed distinct axon guidance phenotypes, both resulting in statistically significant increases in the width of the optic chiasm at the midline. While Hs6st1 sulphation had no effect on RGC axon navigation within the eye (possibly due to 6-O-sulphation compensation by Hs6st3); the loss of Hs6st1 sulphation at the dLGN resulted in a significant increase in the defasciculation of the optic tract.

Observations of other axonal tracts influenced by Slit signalling revealed the importance of Hs2st and Hs6st1 sulphation in aiding callosal axons to successfully traverse the midline in corpus callosum development. Observations of the thalamocortical (TCA)/corticothalamic (CTA) tracts revealed that neither Hs2st sulphation nor Hs6st1 sulphation was required for the development of the mouse TCA tract (the latter may be explained by 6-O-sulphation compensation by Hs6st2).

To test whether Hs2st and Hs6st1 enzymes have redundant functions in optic chiasm development, we attempted to create *Hs2st*$^{-/-}$*/Hs6st1*$^{-/-}$ double mutants. A PCR genotyping strategy was developed for the identification of *Hs6st1* animals and showed that *Hs6st1*$^{-/-}$ mutants had high postnatal lethality with only 3% of the offspring surviving to weaning while *Hs2st*$^{-/-}$*/Hs6st1*$^{-/-}$ double mutants all died very early during embryonic development. Observations of *Hs2st*$^{-/-}$*/Hs6st1*$^{+/-}$ mutants and *Hs2st*$^{+/-}$*/Hs6st1*$^{-/-}$ mutants that lacked three of the four Hst alleles showed no differences when compared to single Hst knockouts.

Finally, we showed that altered *Slit* expression at the optic chiasm and *Robo* expression in the retina could not explain the mutant phenotypes observed in *Hs2st*$^{-/-}$ mutants and *Hs6st1*$^{-/-}$ mutants, and therefore we hypothesized that Hs2st sulphation and Hs6st1 sulphation regulate distinct aspects of Slit-Robo signalling at the surface of the navigating axon growth cone.

Chapter 1: Introduction

In this introduction I will describe some of the mechanisms and factors involved in guiding navigating axons during development. Focusing primarily on the development of the mouse visual system and the corpus callosum, I will describe how receptors located on the surface of growth cones detect axon guidance cues in the ECM and on cell surfaces through receptor-ligand interactions to direct axon navigation from origin to target. Furthermore I will describe the structure and function of HSPGs with particular emphasis on their roles in axon guidance. Finally, I will introduce the "heparan sulphate code hypothesis" which suggests that different HSPG modifying enzymes confer different axon guidance attributes and how we might test this hypothesis through the method of gene trapping in mice.

1.1 Developing connections in the brain

Brain function depends on highly regulated developmental events that act collectively to establish precise connections between specific populations of neurons. These connections number in the billions and contribute to the incredible function and complexity of the vertebrate central nervous system (CNS). The mammalian brain can be subdivided into a number of functional neuronal domains characterized by the processes (i.e. motor, sensory, autonomic, etc.) they control. These functional domains send information in the form of electrical impulses carried through long processes known as axons and synapse with dendrites on the surfaces of their target cells. Axons link sensory organs and other neuronal domains through these synapses and together, create elaborate neuronal networks. Recent years have seen major advances in understanding the mechanisms involved in establishing neuronal connectivity and their importance in brain function.

1.2 Axon navigation

During development of the brain, neuronal cells project their axons into the extra cellular matrix (ECM) often traversing long intricate paths towards their eventual targets. Receptors located on the growth cones of navigating axons detect chemical guidance cues within the ECM and on cell surfaces which communicate navigational information. Guidance cues dictate where axons will project, how fast they will navigate, and what targets they will innervate. These chemical guidance cues are regulated spatiotemporally to generate precisely stereotyped axonal tracts that make up the complex CNS.

1.2.1 The motile growth cone

Growing axons sample their environment for guidance cues through a highly motile structure located at the tip of the axon known as the growth cone (Farrar and Spencer, 2008). The growth cone navigates through the ECM via the extension and retraction of finger-like projections called filopodia and veil-like projections called lamellopodia. The extension and retraction of these filopodia and lamellopodia are controlled by a highly dynamic, intracellular cytoskeleton constructed from actin filaments. These actin filaments are rapidly assembled and/or dissembled to create directed axonal navigation depending on the instructions received by the chemical guidance cues (Suter and Forscher, 1998).

The growth cone detects chemical guidance cues through receptors located on the surface of the growth cone. Binding of these guidance cues to their appropriate receptors triggers intracellular signalling cascades that alter the dynamic cytoskeleton of the growth cone (Song and Poo, 1999). The extension and retraction necessary for axonal navigation involves linking the dynamic cell cytoskeleton with the ECM mediated by adhesion molecules and a number of different classes of adaptor molecules. Detection of guidance cues that result in disassembly of the actin

cytoskeleton are known as chemo-repulsive cues and act to cause growth cone retreat. Detection of guidance cues that result in assembly of the actin cytoskeleton are known as chemo-attractive cues and act to cause growth cone advance. Asymmetric growth cone detection of a guidance cue results in turning of the growth cone through the assembly of the actin cytoskeleton on one side and the disassembly of the actin cytoskeleton on the other side (Chilton, 2006).

1.2.2 Chemical guidance cues direct navigating axons

There are an ever increasing number of guidance molecules being implicated in axon guidance (Dickson, 2002; Tanaka et al., 2008). Early identification and classification of guidance molecules reported them as being either repulsive or attractive in their ability to influence axon navigation. However, further characterization of these molecules has shown that the functions of many of the guidance cues are not absolute, but rather, reflective of the context in which they are encountered and also on the type of axon they encounter. This allows a relatively small number of guidance cues to orchestrate a multitude of axon guidance functions. Deciphering these interactions has been a monumental task that scientists have only begun to tackle.

Four evolutionarily conserved families of axon guidance ligand molecules are the Ephrins, Semaphorins, Netrins, and Slits and their receptors Ephs, Plexins/Neuropillins, DCC/unc5, and Robos, respectively (Dickson, 2002). These axon guidance molecules have been extensively studied in a wide range of model organisms including both invertebrates (*C. elegans* and *Drosophila*) and vertebrates (Zebrafish, *Xenopus*, and Mouse) (Goodman and Shatz, 1993; Goodman, 1996; Bulow and Hobert, 2004; Garbe and Bashaw, 2004; Chisholm and Jin, 2005). These guidance molecules are not the only ones known (more will be introduced later in this chapter), however they are by far the best ones characterized to date.

1.2.2.1 Eph-ephrin signalling

Ephrins are short range guidance cues that signal through their Eph receptors to initiate repulsion (Klein, 2004; Kruger et al., 2005). Eph-ephrin signalling requires cell-cell contact and has been shown to function bi-directionally, where the ligand can initiate intracellular signalling as well as the receptor (Davy and Soriano, 2005; Egea and Klein, 2007). Eph-ephrin signalling has been shown to be a prominent feature of neuronal topographical mapping (McLaughlin and O'Leary, 2005; Flanagan, 2006). Quoting McLaughlin and O'Leary, 2005, "A topographical map is a projection from one set of neurons to another wherein the receiving set of cells reflects the neighbour relationships of the projecting set". Through the graded expression of *ephrin-As* and *ephrin-Bs,* functional maps have been described in a number of axonal tracts in the mouse including the RGC axon projection and the thalamocortical (TCA) axon projection (Hansen et al., 2004; Cang et al., 2005). Best described in the mapping of the visual system, ephrin-As (anchored to the cell membrane via GPI-linkage) have been shown to have a key role in anterior-posterior retino-tectal topography, while ephrin-Bs (anchored to the cell membrane via transmembrane domain) have been shown to have a key role in dorsal-ventral retino-tectal topography (Hindges et al., 2002; Mann et al., 2002; McLaughlin et al., 2003b; McLaughlin et al., 2003c; Hansen et al., 2004).

1.2.2.2 Semaphorin-Plexin/Neuropillin signaling

Semaphorins constitute a large family of secreted and cell surface guidance molecules usually associated with chemo-repulsion (Winberg et al., 1998). Semaphorins signal through multimeric receptor complexes consisting of a number of proteins including plexins and neuropilins (Bagnard et al., 1998; Artigiani et al., 1999; Raper, 2000; Fujisawa, 2004; Negishi et al., 2005). Semaphorin 5a has been shown to be capable of bi-functional activity switching from chemo-repulsion to

chemo-attraction based on the composition of the ECM. The presence of HSPGs results in chemo-attraction while the presence of chondroitin sulphate proteoglycans (CSPGs) results in chemo-repulsion within the fasciculus retroflexus, a diencephalon fibre tract associated with the limbic system (Kantor et al., 2004).

1.2.2.3 Netrin-DCC/UNC5 signalling

Netrins were first identified in vertebrates as chemo-attractant molecules acting on commissural axons in the spinal cord (Kennedy et al., 1994; Serafini et al., 1996; Bradford et al., 2008). Further characterization revealed Netrin-1 to be a bi-functional, long-range guidance molecule repelling some types of axons and attracting others (Colamarino and Tessier-Lavigne, 1995; Barallobre et al., 2005; Moore et al., 2007). Netrin's bi-functional ability was shown to be due, at least in part, to two different receptors, namely DCC and UNC-5. DCC receptors were generally associated with netrin induced chemo-attraction; however there is also evidence for chemo-repulsion in some circumstances (Keino-Masu et al., 1996). UNC-5 has been associated with chemo-repulsion (Round and Stein, 2007). Netrin-1 has also been shown to alter their response from chemo-attraction to chemo-repulsion in the presence of the ECM molecule Laminin-1 in the *Xenopus* eye. This was shown to be important in attracting RGC axons to the optic disc and then to repel the same axons from the optic disc towards the optic nerve (Hopker et al., 1999).

1.2.2.4 Slit-Robo signalling

Slits were first characterized as evolutionarily conserved long range guidance cues that act through their Robo receptors to repel many types of axons (Seeger et al., 1993; Tear et al., 1993; Brose et al., 1999; Kidd et al., 1999; Nguyen Ba-Charvet et

al., 1999). To date, there are 3 known mammalian Slits (Slit1, Slit2, and Slit3) as well as 3 Robo receptors (Robo1, Robo2, and Robo3) (Nguyen-Ba-Charvet and Chedotal, 2002). Further research established Slit2 as having dual branch promoting-arborisation and elongation activities (Wang et al., 1999). This property was shown to be dependent on whether Slit2 was proteolytically processed or not. The 200 kDa Slit2 protein was shown to have chemo-repellent activities towards navigating axons (Hu, 1999; Niclou et al., 2000; Ringstedt et al., 2000). The 140 kDa Slit2 N-terminal domain was shown to be responsible for initiating branching, elongation and arborisation of sensory axons in the mammalian CNS (Van Vactor and Flanagan, 1999; Brose and Tessier-Lavigne, 2000; Nguyen Ba-Charvet et al., 2001; Ozdinler and Erzurumlu, 2002; Ma and Tessier-Lavigne, 2007). Slit-Robo signalling has been shown to be a major player in the organization of a number of axonal tracts that cross the midline (Lindwall et al., 2007).

1.2.3 Guidance cues cooperate to direct axons across the midline

The ability of axons to cross the midline of bilaterally symmetrical organisms has been studied extensively (Kaprielian et al., 2000; Kaprielian et al., 2001). Commissural tracts link the two hemispheres of the brain providing avenues of communication between them. These commissural tracts form by sending axons from their origin on one side of the brain across the midline and toward their targets on the other side of the brain. Netrins and Slits have been shown to function cooperatively to ensure that commissural axons of the vertebrate spinal cord approach the midline (attraction), cross the midline (switch attraction to repulsion), and continue towards their eventual targets without re-crossing the midline (repulsion). In brief, using the mammalian spinal cord as a model system, Netrin-1 signalling has been shown to attract commissural axons toward the midline, while these same axons are insensitive to Slit signalling (Serafini et al., 1996; Tessier-Lavigne and Goodman, 1996; Long et al., 2004)s. At the midline, Netrin-1 signalling is silenced and Slit repulsion is up-regulated through a DCC/Robo receptor

complex (Stein and Tessier-Lavigne, 2001). Switching from attraction to repulsion in the spinal cord results in the exit of commissural axons from the midline as well as ensuring these axons do not re-cross the midline. How this switch from attraction to repulsion occurs is only now being deciphered in more detail. Recently, Robo3 splice variants (Robo3.1 and Robo3.2) have been implicated in the switch from axon attraction to axon repulsion at the midline (Black and Zipursky, 2008; Chen et al., 2008). Differing in their C-terminal domains, Robo3.1 has been shown to be insensitive to Slit repulsion and is up regulated on pre-crossing and crossing axons resulting in axon navigation across the midline. Robo3.2 has been shown to be up regulated on post-crossing axons and is responsive to Slit repulsion resulting in axon navigation away from the midline.

1.2.4 Other Molecules Implicated in Axon Guidance

Over the years a number of transcription factors have been identified as regulating the transcription of many chemical guidance cues and their receptors. Moreover, transcription factors, themselves have been shown to act as extracellular guidance factors (Brunet et al., 2005; Butler and Tear, 2007). Transcription factors that have been shown to regulate axon guidance include Zic2 (Herrera et al., 2003), Isl2 (Pak et al., 2004), Foxg1 (Pratt et al., 2004), Foxd1 (Herrera et al., 2004), Pax2 (Torres et al., 1996) and Pax6 (Manuel et al., 2008) just to name a few.

Traditionally, morphogens have been described as concentration dependant, diffusible molecules responsible for patterning naive cells into a more differentiated state based on their relative positions in the developing embryo. However many morphogens have also been implicated in directing axon guidance (Schnorrer and Dickson, 2004; Zou and Lyuksyutova, 2007). Morphogens that have been implicated in axon guidance include Shh (Charron et al., 2003; Bourikas et al., 2005), Wnt (Dickson, 2005), FGF (McFarlane et al., 1995), and BMP (Yamauchi et al., 2008).

While axons have been shown to respond to many axon guidance cues on their way to their eventual targets, less is known about the axon-axon interactions that direct axon navigation. Pioneer axons, the first axons to navigate their stereotyped path, can influence the guidance of later arriving axons through axon-axon interactions mediated by neural adhesion molecules (Walsh and Doherty, 1997; Pittman et al., 2008). Neural adhesion molecules implicated in axon guidance include L1 (Itoh et al., 2004), TAG-1 (Law et al., 2008), and NrCAM (Williams et al., 2006). A number of ECM molecules have been shown to influence axon guidance either directly (as a co-receptor) or indirectly (influencing the local environment) including CSPGs (Walsh and Doherty, 1997; Chung et al., 2000a; Chung et al., 2000b) and HSPGs (Lee and Chien, 2004). This thesis is devoted to HSPGs and will be discussed in detail later in this chapter.

1.3 The visual system

While the colloquialism goes "the eyes are the windows to the soul" to a developmental neuroscientist, the eyes are a window to the elaborate mechanisms required to generate, order, and maintain the billions of cells involved in central nervous system (CNS) development. The visual system is a precisely stereotyped neuronal network of the CNS that functions to collect light information from the outside world. This information is conducted in the form of electrochemical signals to the visual centres of the CNS for processing and interpretation. The visual system accounts for a substantial proportion of the sensory information received from the outside world. The central importance of this sensory system as well as its accessibility to scientific manipulation has propelled its research for decades.

1.3.1 Retinal ganglion cell axons connect the eyes to the visual centres of the brain

An intensively studied system, the retinal ganglion cell (RGC) axon projection of the visual system has been a particularly excellent model for elucidating the mechanisms axons use to navigate stereotyped, 3-dimensional spaces involving midline crossing, branching, and the generation of topographic neuronal maps (Mann et al., 2004; Inatani, 2005; Erskine and Herrera, 2007; Haupt and Huber, 2008).

In mice, RGCs are born in the ganglion cell layer of the retina in a central to peripheral order and project their axons to form the optic nerves at around E12.5 (Hinds and Hinds, 1974). The fasciculated optic nerves from each eye meet at the ventral surface of the hypothalamus at approximately E13.5 (Silver and Sidman, 1980). Here we define fasciculation as the tendency of developing neurites to grow along existing neurites and hence form bundles or fascicles, regardless of whether cells are interspersed among the fascicles. At this point a decision is made whether to cross the midline to form part of the contralateral optic tract or remain on the same side and form part of the ipsilateral optic tract. In mice, ~3% of RGC axons have an uncrossed projection and all originate in the ventro-temporal region of the retina (Drager and Olsen, 1980; Colello and Guillery, 1990; Sretavan, 1990). By ~E15.5 the characteristic "X" structure of the optic chiasm is established and by ~E16.5 the adult pattern of decussation has been established (Drager and Olsen, 1980; Drager, 1985). The optic tracts leave the optic chiasm and navigate over the surface of the thalamus, reaching the dorsal thalamus at ~E14.5 and then projecting caudally towards their targets in the superior colliculus (SC) at ~E16.5. While all RGC axons innervate the SC in rat (Linden and Perry, 1983), approximately 33% of them also send branches to their targets in the dorsal lateral geniculate nucleus (dLGN), but not until the primary axon growth cone reaches the SC at ~E16.5 (Godement et al., 1984; Martin, 1986; Bhide and Frost, 1991) (Figure 1). See table 1 for a more detailed account of the developmental timing of RGCs and their axonal projections.

Table 1. **Stages of RGC development and their axonal projections.** (Drager and Olsen, 1980; Godement et al., 1984; Drager, 1985; Colello and Guillery, 1990; Marcus et al., 1995; Marcus and Mason, 1995).

Stage	**Description of RGCs and their axon projections**
Birth of RGCs in the retina	At ~E11.5 the earliest RGCs are born starting in the dorso-central retina with later born RGCs radiating concentrically to the periphery. The earliest born RGCs show segregation of ipsilaterally projecting RGCs in the ventral retina and contralaterally projecting RGCs in the dorsal retina. This segregation is lost by ~E13.5 when contralaterally projecting RGCs also start arising from the ventral retina. While contralaterally projecting RGCs are born between E11.5 to E19.5, ipsilaterally projecting RGCs are born between E11.5 and E16.5.
Early stages of RGC axon projections	Between E12.5 and E13.5, the earliest born RGCs project their axons and reach the anatomical midline. Some of these pioneering RGC axons will cross the midline and enter the contralateral optic tract, whilst others will remain ipsilateral, entering the ipsilateral optic tract directly without approaching the midline. These early ipsilateral projections are only transient and are eliminated later on during postnatal development. These early projections establish the early optic chiasm.
Peak stage of RGC axon projections	E14.5 to E16.5 is the peak phase of RGC genesis and retinal axon growth through the optic chiasm. During this period the permanent ipsilateral RGC axon projection develops. Contralateral RGC axons arise from the entire retina, whereas ipsilateral RGC axons arise from a small region of the peripheral VT retina called the ventro-temporal crescent. The adult pattern of decussation is established by E15.5-E16.5 with a 97:3 ratio of contralaterally projecting RGC axons to ipsilaterally projecting

	RGC axons.
Late stages of RGC axon projections	From E16.5 to E19.5, all RGC axons project contralaterally, including those from the VTC. Starting around E16.5 RGC axons have started arriving at the SC. This also marks the time point at which collateral branches start projecting into the dLGN. While contralateral crossing RGC axons are observed to send branches to all areas of the dLGN at ~E16.5, ipsilateral RGC axon innervation of the dLGN is delayed until ~E18-P0 in mice. It is not until ~P2 that ipsilateral RGC axons are observed to invade the medio-dorsal region of the dLGN (the future binocular area). The segregation of crossed and uncrossed RGC axons starts at ~P4 and continues to ~P8; this is also the period where the refinement of region specific targeting occurs within the dLGN (mouse, Godement, et al., 1984; rat, Bhide and Frost, 1991).

Figure 1. **Development of the mouse visual system.** Retinal ganglion cells (RGCs) originate in the retina of the eye and project their axons to form the optic nerves (ON) at ~E12.5. The ONs from each eye meet at the surface of the ventral diencephalon at ~E13.5 and by E15.5 the characteristic "X" structure of the optic chiasm (OC) has formed. The OC is the site of decussation of RGC axons; where most RGC axons are observed to cross the midline and innervate contralateral targets, ~3% of RGC axons are repelled from the midline and innervate ipsilateral targets thus giving mice a small degree of binocular vision. The RGC axons exit the OC to form the optic tracts (OT) and the OTs navigate dorso-laterally over the surface of the diencephalon and then project caudally to the superior colliculus (SC), a major target for RGC axons at ~E16.5. While all RGC axons terminate at the SC, approximately 33% of all RGC axons also send branches to their targets in the dorsal lateral geniculate nucleus (dLGN) of the dorsal thalamus.

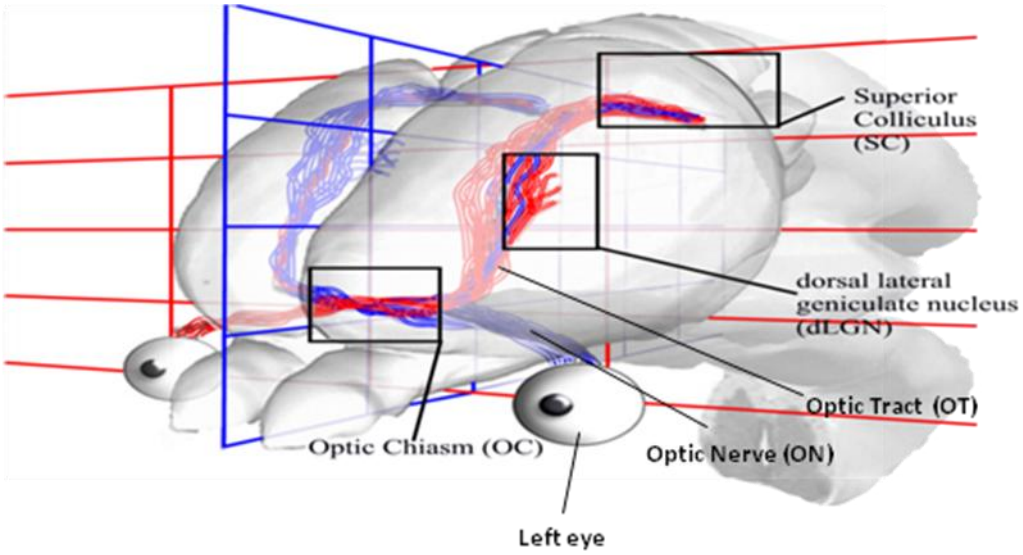
Superior
Colliculus
(SC)
dorsal lateral
geniculate nucleus
(dLGN)
Optic Tract (OT)
Optic Chiasm (OC)
Optic Nerve (ON)
Left eye

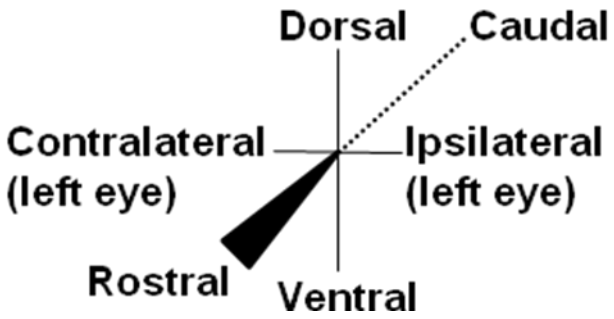
Dorsal
Caudal
Contralateral
(left eye)
Ipsilateral
(left eye)
Rostral
Ventral

1.3.1.1 The retina and retinal ganglion cell classes

The retina is a thin layer of neuronal cell types that collectively function to detect light (rod and cone photoreceptors) and transmit (retinal ganglion cells) the information to specified areas in the brain that function to process and interpret visual information. RGC axons have two main central nervous system (CNS) targets, namely the dLGN and the SC. Additionally, some RGC axons are observed to target the suprachiasmatic nucleus and the pretectal nucleus (Hattar et al., 2006).

The distribution of RGC bodies within the retina, show the highest density to be temporal to the optic disc and lowest density to be in the most dorsal retina (Drager and Olsen, 1981). An account of the various afferent projections observed in the developing visual system can be attributed, at least in part, to four morphologically and/or electro-physiologically distinct classes of RGCs (RG_A, RG_B, RG_C, and RG_D) in rat (Sefton and Swinburn, 1964; Perry, 1979; Huxlin and Goodchild, 1997; Sun et al., 2002a). In addition, there have been a number of subclasses described within each class constituting a total of at least 12 distinct groups to date (Huxlin and Goodchild, 1997; Sun et al., 2002a). Less is known about mouse RGC electro-physiology, however four distinct classes have been characterized based on soma size and dendritic field (RG_A, RG_B, RG_C, and RG_D) and 14 subclasses (Doi et al., 1995; Sun et al., 2002b). While the distribution of these classes within the retina has not yet been clearly ascertained in either mouse or rat RGCs have been regionalized based on their expression patterns of a number of transcription factors (Herrera et al., 2004; Pratt et al., 2004; Butler and Tear, 2007) and axon guidance receptors (Williams et al., 2003). These patterns of expression have been implicated in topographic mapping and in the decussation of RGC axons at the optic chiasm (Birgbauer et al., 2000; McLaughlin and O'Leary, 2005) (Figure 2).

Figure 2. **Position of ipsilaterally and contralaterally projecting RGCs in the retina of the eye.** RGCs are born in a roughly concentric central to peripheral order with older RGCs being closer to the optic disc and younger RGCs towards the periphery of the retina. RGCs in the RGC layer of the retina project their axons away from the neuroblastic layer (NL) and into the optic fibre layer (OFL) where they navigate towards the optic disc and exit the eye to form the fasciculated optic nerve. RGCs originating in the ventro-temporal crescent are responsible for the ipsilateral projection (red) of the visual system where their axons will be repelled from the midline and remain on the same side of the brain entering the ipsilateral optic tract. All other RGCs project their axons (blue) across the midline to form the contralateral optic tract.

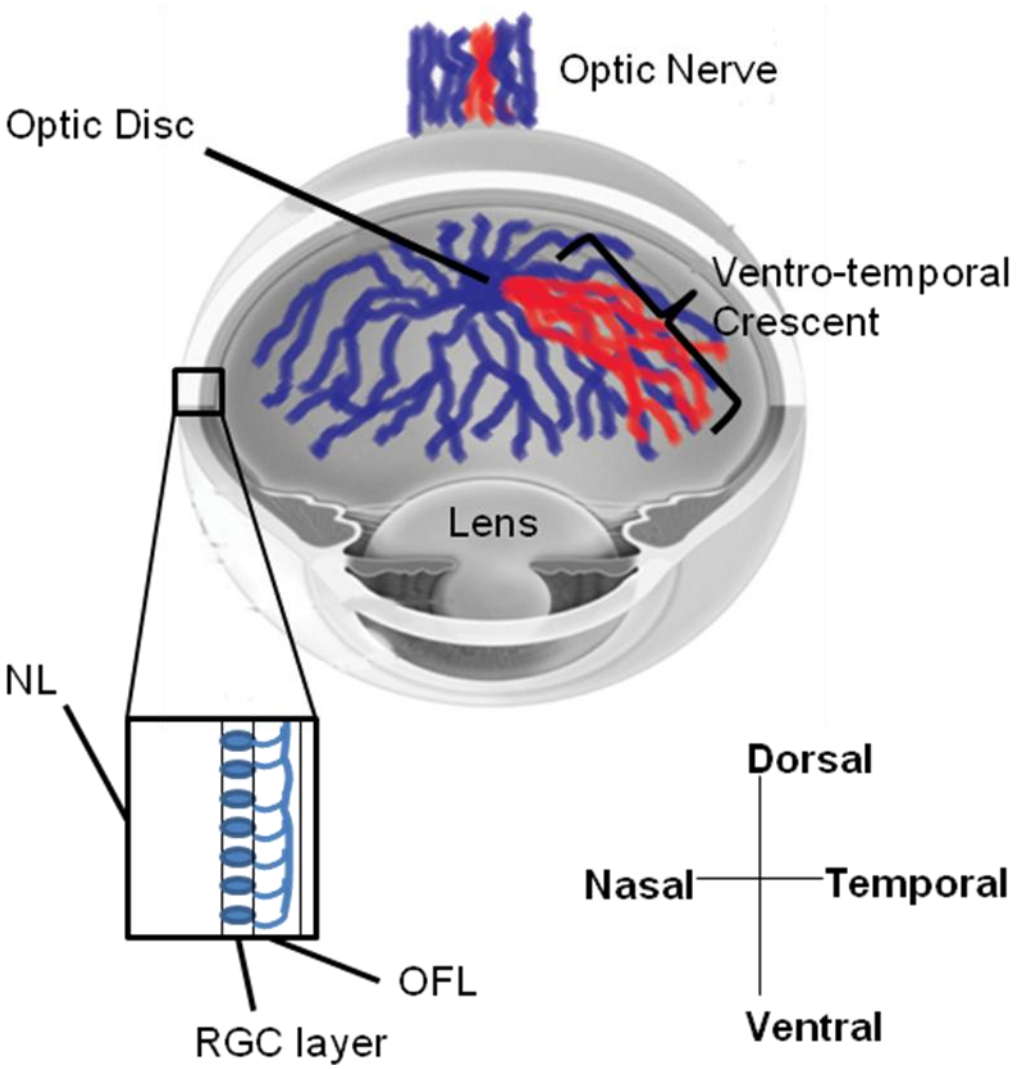
Optic Nerve
Optic Disc
Ventro-temporal
Crescent
Lens
NL
OFL
RGC layer
Dorsal
Nasal
Temporal
Ventral

1.3.1.2 Guidance cues involved in RGC axon navigation in the retina

All projecting RGC axons are restricted to the optic fibre layer (OFL) of the inner retina and project towards the optic disc through a balance of attractive and repulsive chemical guidance cues (Stier and Schlosshauer, 1995; Oster et al., 2004; Erskine and Herrera, 2007) (Figure 2). Slit1 and Slit2 have been shown to regulate distinct aspects of RGC axon guidance within the mouse dorsal and ventral retina. In *Slit1*$^{-/-}$ */Slit2*$^{-/-}$ double mutants, newly differentiated RGC axons in the dorsal retina, distal to the optic disc were shown to navigate aberrantly indicating a possible role in RGC axon guidance polarity. Furthermore, RGC axons were observed to exit the OFL ectopically in the ventral retina indicating the requirement for Slit signalling in OFL formation, at least in the ventral retina (Thompson et al., 2006b). Eph-ephrin signalling has been implicated in RGC axon guidance in the retina with a loss of EphB2/EphB3 receptors resulting in navigation errors towards the optic disc (Birgbauer et al., 2000). Netrin-1 has been shown to direct RGC axons through the optic disc to form the optic nerve. Loss of Netrin-1 resulted in RGC axons arriving to the optic disc, but unable to pass through which resulted in optic nerve hypoplasia. Furthermore, Netrin-1 in the presence of laminin was shown to be required for RGC axon exit into the optic nerve and away from the optic disc (Deiner et al., 1997; Hopker et al., 1999). Sema5a has been shown to corral RGC axons into the optic nerve (Oster et al., 2003).

1.3.2 Development of the optic chiasm

The optic chiasm is a key decision point for the development of the visual system as this is the site where binocular vision is established. In mice and other species with limited binocular vision a small proportion of RGC axons (3% in mice) do not cross the midline, but project to ipsilateral visual centres. As the degree of visual field overlap increases in other species (decrease in the laterality of the eyes) there is a

direct increase in the number of RGC axons that project to ipsilateral targets (Drager and Olsen, 1980; Colello and Guillery, 1990). Formation of the optic chiasm starts at around E13.5 in mice where pioneer axons from the dorso-central retina navigate towards the midline, on the ventral surface of the hypothalamus. Most of the RGC axons cross the midline and enter the optic tract towards their eventual targets in the dLGN and SC. By E15.5, the distinct "X" structure of the optic chiasm has formed consisting of the optic nerves from each eye ventro-rostrally and the projecting optic tracts dorso-caudally (Marcus et al., 1995; Marcus and Mason, 1995; Jeffery, 2001) (Figure 3).

Figure 3. **The optic chiasm**. The optic chiasm (OC) forms at the ventral surface of the diencephalon, caudal to the pre-optic area (POA) and is a key choice point for navigating RGC axons (red and blue). At the optic chiasm, RGC axons from each eye decide whether to cross the midline (contralateral) and target regions on the opposite side of the brain or remain on the same side (ipsilateral) and target regions on the same side of the brain. The presence of an ipsilateral projection gives rise to binocular vision, enabling visual information from both eyes to be processed in the same region of the brain. RGC axons enter of the region of the optic chiasm via the optic nerves (ON) and exit the region of the optic chiasm via the optic tracts (OT). The positioning of the chiasm is, at least in part, determined by the glial palisade (green) and the chemical guidance cues that are expressed in this region. SSEA-1 and CD44 (yellow) are cell surface molecules expressed on a population of early-differentiating neurons known to influence RGC axons at the optic chiasm. These SSEA-1/CD44 neurons first appear around E12.5 in a "V" shape and are believed to provide an anatomical scaffold for early RGC axon navigation at the OC.

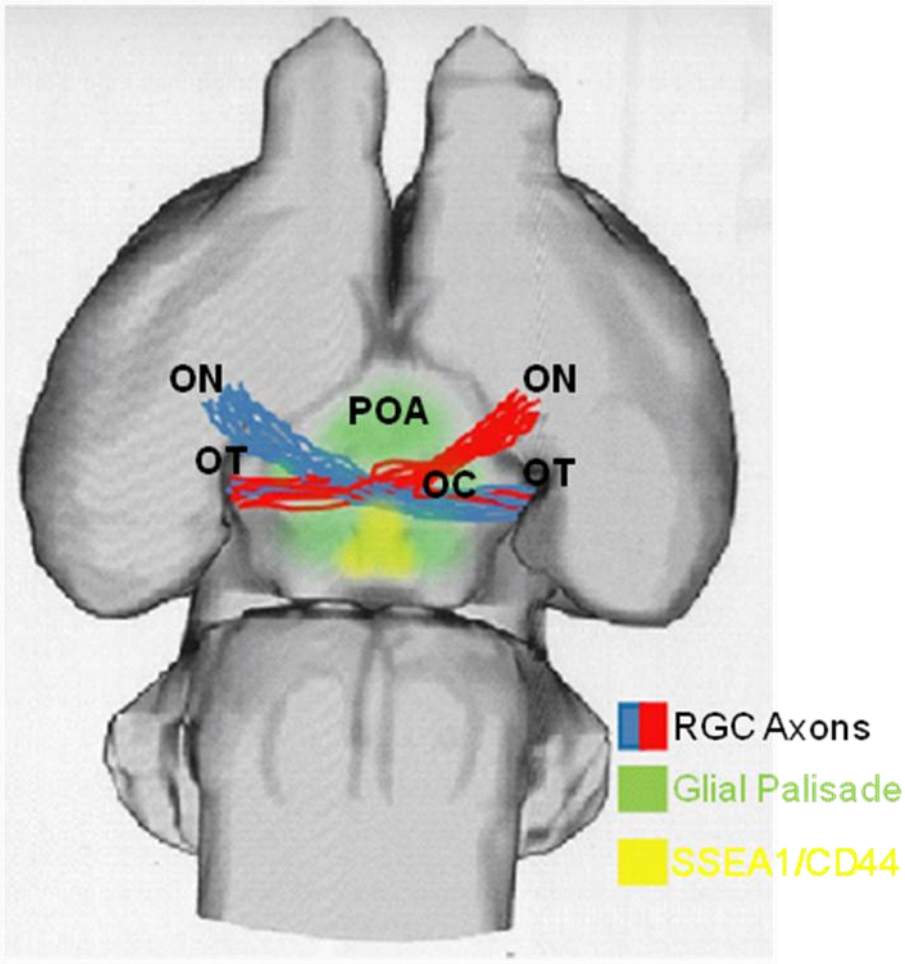
ON
ON
POA
OT
OC
OT
RGC Axons
Glial Palisade
SSEA1/CD44
Rostral
Caudal

1.3.2.1 Cellular and molecular interactions guide axons at the optic chiasm

The positioning of the optic chiasm is determined through a combination of cellular and molecular interactions. The cellular environment consists of radial glial cells (the glial palisade) and neuronal cell populations such as SSEA-1/CD44 positive neurons, both of which have been shown to be important in the development of the optic chiasm (Sretavan et al., 1994; Marcus et al., 1995; Marcus and Mason, 1995; Sretavan et al., 1995) (Figure 3). Consisting of a dense concentration of radial glial cells, the radial glial palisade is located on adjacent sides of the midline occupying the region where RGC axon divergence will occur. The radial glial palisade has been shown to contact both crossed and uncrossed RGC axons and it has been suggested that it functions in axon guidance (Marcus et al., 1995; Marcus and Mason, 1995).

The position and formation of the optic chiasm is established through interactions with many axon guidance cues (Erskine and Herrera, 2007). Slit-Robo signalling has been shown to channel incoming RGC axons into the mouse optic chiasm, but has not shown any effect on midline crossing of RGC axons. Loss of Slit-Robo signalling results in midline wandering as well as ectopic navigation to the opposite eye and ectopic chiasm formation in mice (Erskine et al., 2000; Plump et al., 2002; Plachez et al., 2008). Sema3D has been shown to direct navigating RGC axons across the midline and into the optic tract in Zebrafish (Sakai and Halloran, 2006).

Binocular vision is established at the optic chiasm through the decussation of RGC axons into contralaterally projecting axons and ipsilaterally projecting axons (Petros et al., 2008). EphrinBs were first implicated as having a role in binocular vision establishment in *Xenopus*. The axons of RGCs expressing EphB receptors in the ventral-region of the retina were observed to be repelled from the midline which starts to express *ephrinB* at the onset of metamorphosis to form part of the ipsilateral optic tract during metamorphosis from tadpole (no binocular vision because of laterally placed eyes) to frog (binocular vision due to visual field overlap) (Nakagawa et al., 2000). This observation of EphB-ephrinB signalling was later

shown to control decussation in the development of the mouse ipsilateral RGC axonal projection (Williams et al., 2003).

1.3.3 Development of the retino-thalamic projection

The dLGN is part of the thalamic sensory relay system and functions to link and refine visual stimuli through the visual cortex and the superior colliculus. A number of mammalian models have been used to characterize the developing retino-thalamic projection. While virtually all RGC axons send branches to the dLGN in cats and monkeys (Illing and Wassle, 1981; Perry et al., 1984), only a third of all RGCs have been shown to send branches to the dLGN in rodents (Martin, 1986; Bhide and Frost, 1991). dLGN innervation by RGC axons is established through the production of collaterals (branches) (Figure 4). These RGC axon collaterals are primarily generated through morphologically distinct interstitial budding of the axon trunk and not by bifurcation of the leading growth cone (Bhide and Frost, 1991; O'Leary, 1992). The origin of the RGC axons that send these permanent collaterals into the dLGN has been shown in co-culturing experiments to be primarily from the ventro-temporal region of the retina in mice, however it has not yet been ascertained whether specific types of RGCs are responsible for dLGN innervation (Chan et al., 2002).

While contralateral crossing RGC axons are observed to send branches at ~E16.5 to all areas of the dLGN, ipsilateral RGC axon innervation of the dLGN is delayed until ~E18-P0 in mice as revealed by HRP labelling at different ages (Godement et al., 1984). It is not until ~P2 that ipsilateral RGC axons are observed to invade the medio-dorsal region of the dLGN (the future binocular area). The segregation of crossed and uncrossed RGC axons starts at ~P4 and continues to ~P8; this is also the period where the refinement of region specific targeting occurs within the dLGN (Godement et al., 1984; Bhide and Frost, 1991). The retina maps over the dorso-lateral and posterior surfaces of the contralateral dLGN in rats, such that the

Figure 4. **The optic tract.** The RGC axons leave the region of the optic chiasm (OC) formed on the surface of the ventral diencephalon and form the optic tracts (red indicates ipsilaterally projecting RGC axons and blue represents contralaterally projecting RGC axons) as shown in the sagittal plane. The RGC axons of the optic tract navigate dorso-laterally over the surface of the diencephalon in a tightly grouped bundle over the hypothalamus. RGC axons lose this tightly bundled grouping as they reach the dLGN of the dorsal thalamus. This is believed to promote RGC axon branching at the dLGN where 1/3 of all RGC axons will send branches into the target dLGN and find their synaptic partners. All RGC axons within the optic tract steer away from the epithalamus (epiT) and the RGC axons of the optic tract navigate towards their final targets within the superior colliculus (SC).

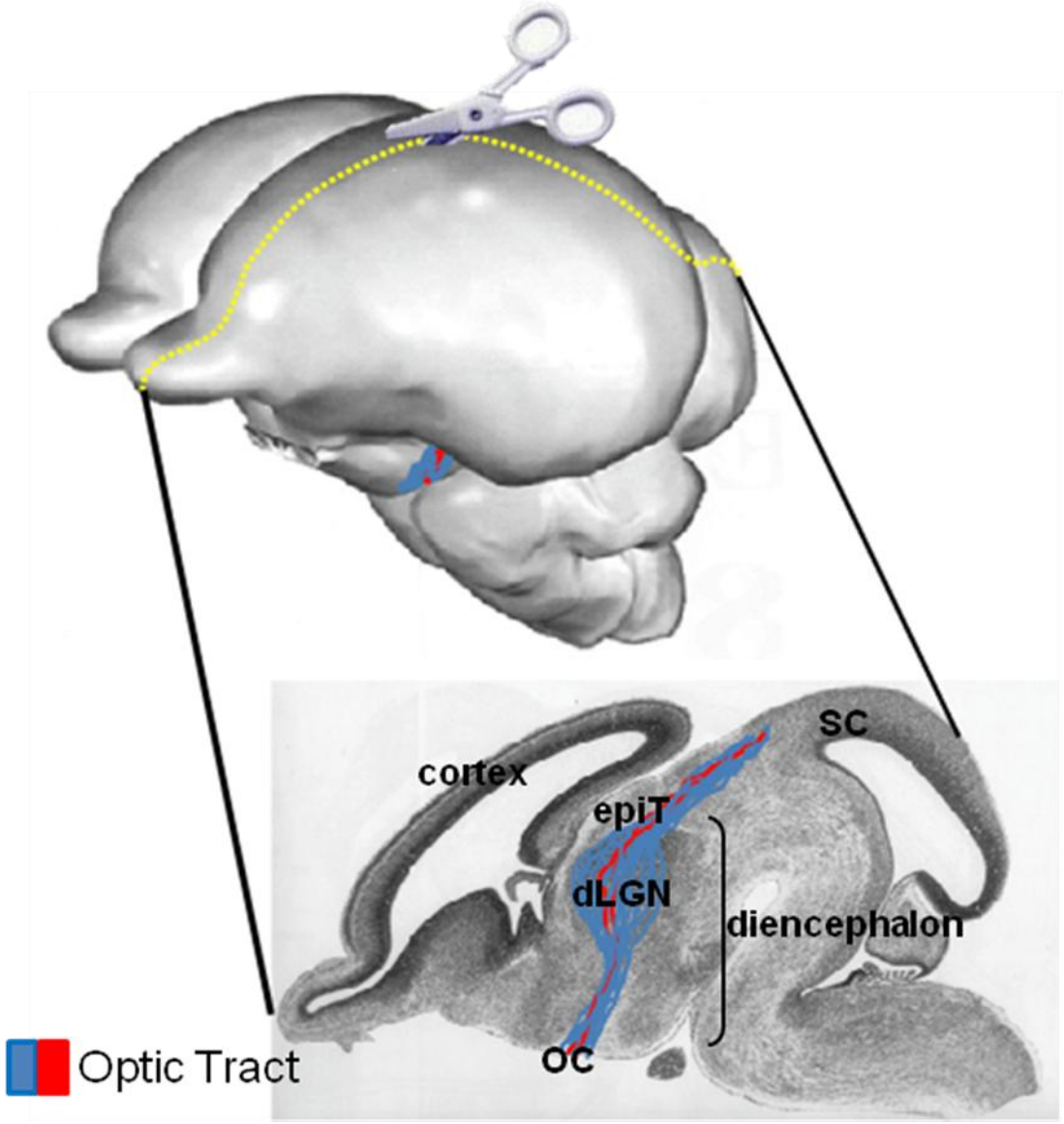
cortex
epiT
SC
dLGN
diencephalon
OC
Optic Tract

dorsal retina projects posteriorly and the ventral retina projects over the dorso-lateral surface. Nasal retina projects ventro-laterally and temporal retina dorso-medially (Lund et al., 1974).

1.3.3.1 Chemical guidance cues direct the development of the retino-thalamic projection

Axons exit the optic chiasm and form the optic tracts which are observed to navigate over the surface of the hypothalamus and the thalamus in a tightly fasciculated bundle until they reach the dLGN of the dorsal thalamus (figure 4). Little is known about the chemical guidance cues required in the formation of the optic tract. It has been shown that the exit of RGC axons from the optic chiasm into the optic tracts requires cell autonomous GAP-43 (a growth cone associated protein) to overcome inhibitory signals in this region in mice (Zhang et al., 2000). In Zebrafish it has been shown that RGC axon topographical ordering requires HSPGs as RGC axons enter the optic tract (Lee et al., 2004). Slit-Robo repulsive signalling has been shown to maintain the trajectory of RGC axons as they navigate over the surface of the diencephalon. Loss of Slit-Robo signalling has been shown to result in RGC axons mis-projecting into the telencephalon as well as RGC axons projecting ectopically into the epithalamus (Tuttle et al., 1998; Ringstedt et al., 2000; Thompson et al., 2006a). While very little is known about the guidance cues responsible for RGC innervation at the dLGN, recent evidence has implicated Slit-Robo signalling; as a loss of Robo2 resulted in increased defasciculation at the dLGN (Plachez et al., 2008). How Slit-Robo signalling may be involved in dLGN innervation is still not understood, but it may affect the formation of RGC collaterals as proteolytically cleaved Slit2-N has been shown to cause axon branching (Nguyen Ba-Charvet et al., 2001; Ozdinler and Erzurumlu, 2002). Topographic mapping of RGC axons in the dLGN has been shown to involve ephrinA-EphA signalling as well as neuronal activity (Huberman et al., 2005; Pfeiffenberger et al., 2005).

1.3.4 Development of the retino-collicular projection

The superior colliculus (SC) of the mouse or tectum in some vertabrates (eg. frogs, fish, and chick) is the major target for all RGC axons of the visual system. Located within the dorsal midbrain this structure is responsible for processing visual information and likely coordinating the orientation of the eyes, head, and body towards objects of interest in the visual field (Drager and Hubel, 1975). The mapping of RGC axons onto the SC has long been the predominant model for studying topographic maps. The retino-collicular map is established in a way that the Cartesian coordinates of the eye are precisely recapitulated in the SC where RGC axons originating from the ventral-dorsal axis of the retina map onto the medial-lateral axis of the SC and RGC axons from the temporal-nasal axis of the retina map onto the rostral-caudal axis of the SC. To explain the ability of RGC axons to topographically map to the tectum the "chemo-affinity" hypothesis was postulated (Sperry, 1963). Sperry postulated that RGC cells carry positional guidance labels, or chemo-affinity tags distributed in gradients that determine their position in the tectum. Evidence supporting this hypothesis has been well documented in the SC and is the dominant model for understanding how topographic maps develop in the CNS (Lemke and Reber, 2005; McLaughlin and O'Leary, 2005).

1.3.4.1 Chemical guidance cues direct the development of the retino-collicular projection.

The chemical guidance cues primarily responsible for establishing the retinotopic maps of the visual system belong to the Eph/ephrin family. Using a number of *in vitro* and *in vivo* techniques, Eph/ephrin signalling has been implicated in patterning along the rostral-caudal axis and the medial-lateral axis of the SC (McLaughlin and O'Leary, 2005). Retinotopic mapping along the rostral-caudal axis has been shown to be established through complementary gradients of ephrinA ligands and their

EphA receptors. EphrinAs are distributed in a high nasal to low temporal gradient in the eye and a high caudal to low rostral gradient in the SC (Frisen et al., 1998; Feldheim et al., 2000). EphAs are distributed in a high temporal to low nasal gradient in the eye and a high rostral to low caudal gradient in the SC (Brown et al., 2000; Feldheim et al., 2004). Retinotopic mapping along the medial-lateral axis has been shown to be established through complimentary gradients of ephrinB ligands and their EphB receptors. EphrinBs are distributed in a high dorsal to low ventral gradient in the eye and a high medial to low lateral gradient in the SC (McLaughlin et al., 2003b; McLaughlin et al., 2003c). EphBs are distributed in a high ventral to low dorsal gradient in the eye and a high lateral to low medial gradient in the SC (Hindges et al., 2002; McLaughlin et al., 2003b) (Figure 5). While there are other known mechanisms involved in retinotopic map refinement, the Eph/ephrin signalling is by far the best characterized to date (Lemke and Reber, 2005).

Figure 5. **The retino-collicular map.** RGCs project their axons from the retina to the superior colliculus (SC) in a topographic manner orchestrated through Eph-ephrin signalling gradients. RGCs originating in the nasal (N) region of the retina (low EphA) project their axons to the caudal (C) region of the SC (high ephrinA). RGCs originating in the temporal (T) region of the retina (high EphA) project their axons to the rostral (R) region of the SC (low ephrinA). RGCs originating in the dorsal (D) region of the retina (low EphB) project their axons to the medial (M) region of the SC (high ephrinB). RGCs originating in the ventral (V) region of the retina (high EphB) project their axons to the lateral (L) region of the SC (low ephrinB).

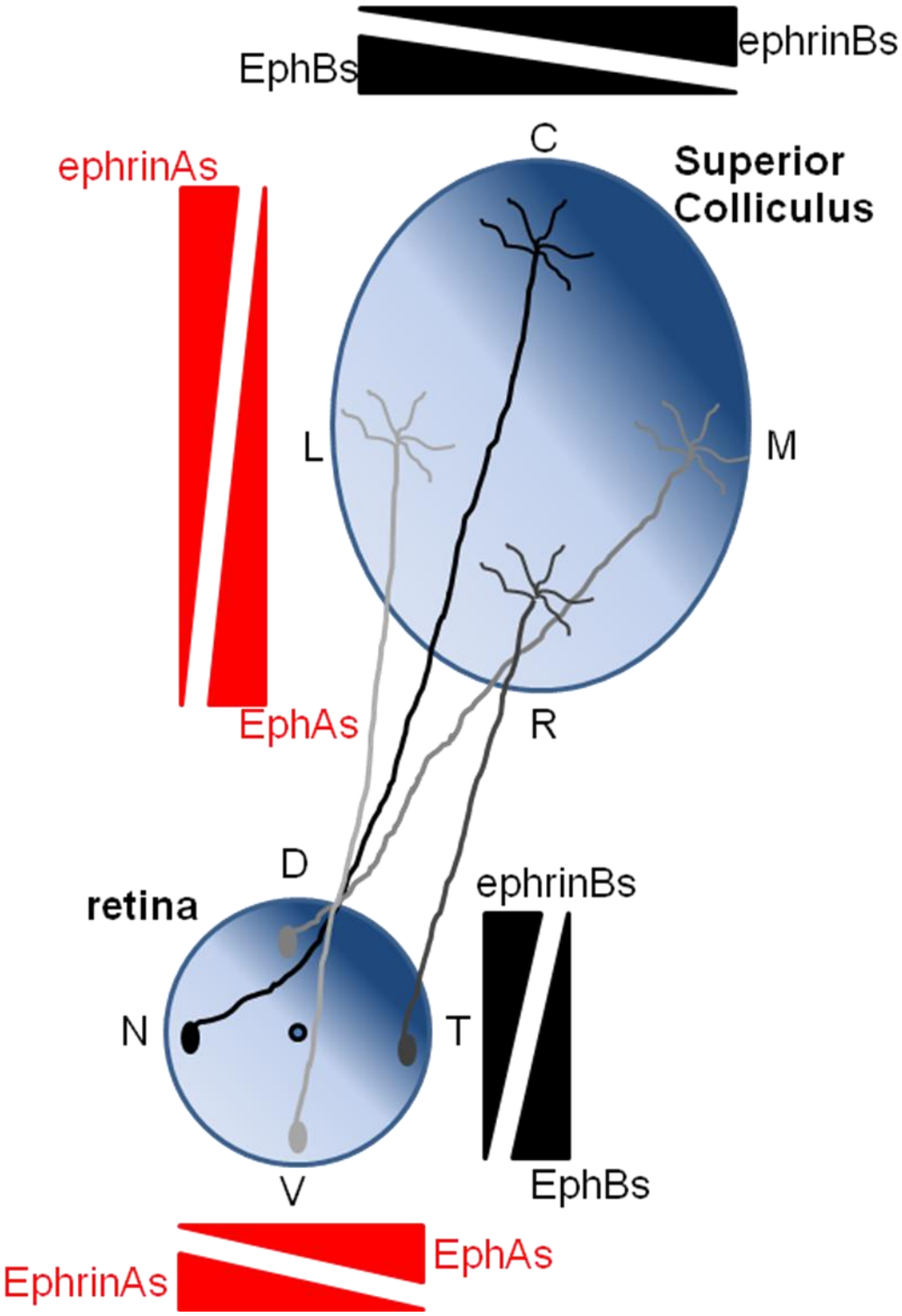
EphBs
ephrinBs
C
Superior
Colliculus
ephrinAs
L
M
EphAs
R
D
retina
ephrinBs
N
T
V
EphBs
EphrinAs
EphAs

1.4 Major forebrain tracts connect the cortex to the thalamus as well as the two hemispheres of the brain

There are many axonal tracts that make up the adult CNS. These tracts form between functional neuronal domains allowing for information to be passed and received from one region to another. The thalamocortical and corticothalamic (TCA and CTA) axonal tracts link the thalamus to the cortex relaying sensory information to higher order processing centres in the cortex. The corpus callosum is a major axonal tract that links and refines information received from one cerebral hemisphere to the other.

1.4.1 TCA and CTA tracts

As their names would suggest, the TCA tract and its reciprocal CTA tract link the cortex with the dorsal thalamus. The dorsal thalamus acts as a major relay system for sensory (except olfactory) and subcortical motor afferents which are organized into one or more specific thalamic nuclei. The information carried by these afferents is re-directed to particular regions of the cortex for higher order integration and processing. Between E13 and E18, these two tracts navigate intricate paths, which include crossing several emerging boundary zones including the diencephalic-telencephalic boundary (DTB) and the pallial-subpallial boundary (PSPB). TCA axons originating in the dorsal thalamus, extend ventrally through the ventral thalamus, turn dorso-laterally into the ventral telencephalon to form part of the internal capsule. TCA axons leave the internal capsule and turn dorsally to their targets in the cortex. CTA axons originating in the cortex follow a similar, but opposite path to their targets in the dorsal thalamus (Lopez-Bendito and Molnar, 2003) (Figure 6). See table 2 for a more detailed account of the developmental timing of TCA/CTA projections.

Table 2. **Stages of thalamocortical/corticothalamic projection neuron development and their axonal projections** (Rubenstein and Beachy, 1998; Lopez-Bendito and Molnar, 2003; Price et al., 2006)**.**

Stage	**Description of the TCA/CTA projections**
Early development of the TCA/CTA projection neurons	Starting around E11.5-E12.5 TCA neurons in the thalamus and CTA neurons in the cortex are born. This continues to ~E18.5. The CTA projection neurons are generated in the ventricular and sub-ventricular zones of the lateral ventricle. These neurons accumulate forming a new layer called the preplate. While TCA projection neurons develop synchronously with CTA projection neurons, the thalamic nuclei within the dorsal thalamus are not established until ~E16.5-E17.5.
Early stages of TCA/CTA projections	From E13.5 to E19.5 the reciprocal TCA and CTA tracts form. The TCA/CTA tracts must navigate through several emerging boundaries including the DTB and the PSPB and through the internal capsule. The TCAs navigate ventrally from the dorsal thalamus and arrive at the DTB at ~E12.5. By E13.5, TCAs have entered the internal capsule and by E14.5 they have reached the PSPB. The CTAs also arrive at the PSPB at ~E14.5 and by E15.5 both CTAs and TCAs have started crossing the PSPB on their way to their eventual targets in the dorsal thalamus and cortex, respectively.
Later stages of TCA/CTA projections	By E18.5, TCAs and CTAs have started arriving at their eventual targets in the cortex and dorsal thalamus, respectively. TCAs are observed to be primarily located in the intermediate zone and the subplate of the cortex with some side branches extending into the deep cortical plate. CTAs are observed to have arrived at the dorsal thalamus in a topographically ordered manner showing increased topographic ordering postnatally into distinct thalamic nuclei. It is not until P8 that segregation

	is complete.

Figure 6. **The thalamocortical/corticothalamic (TCA/CTA) tracts.** The TCA/CTA tracts are responsible for relaying sensory information between the dorsal thalamus and the cerebral cortex. The neurons of the TCA tract originate in the dorsal thalamus and send axons to their targets within the cerebral cortex while the neurons of the reciprocal CTA tract originate in the cerebral cortex and send axons to their targets in the dorsal thalamus. These tracts are observed to navigate through the internal capsule within the ventral telencephalon avoiding the hypothalamus on the way to their eventual destinations. Along their respective paths the TCAs/CTAs are observed to pass through a number of emerging boundaries such as the diencephalic/telencephalic boundary (DTB) and the pallial/sub-pallial boundary (PSPB).

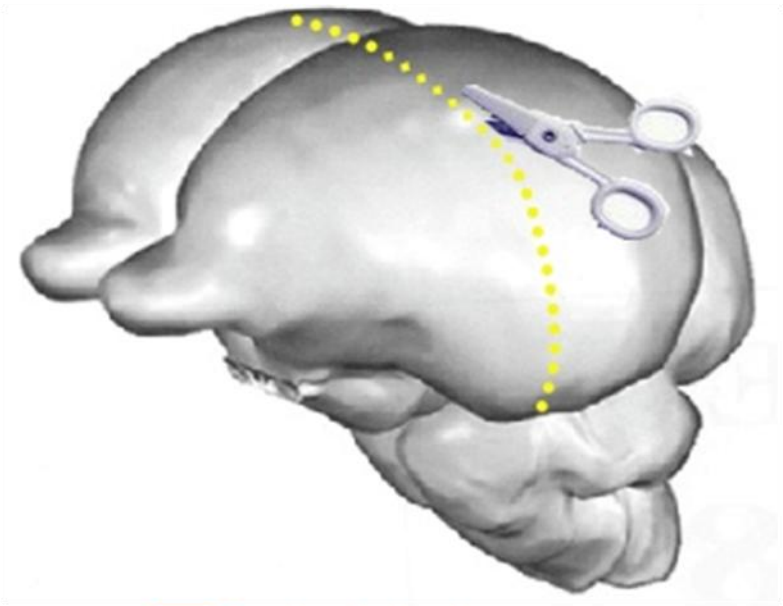

Corticothalamic

Thalamocortical

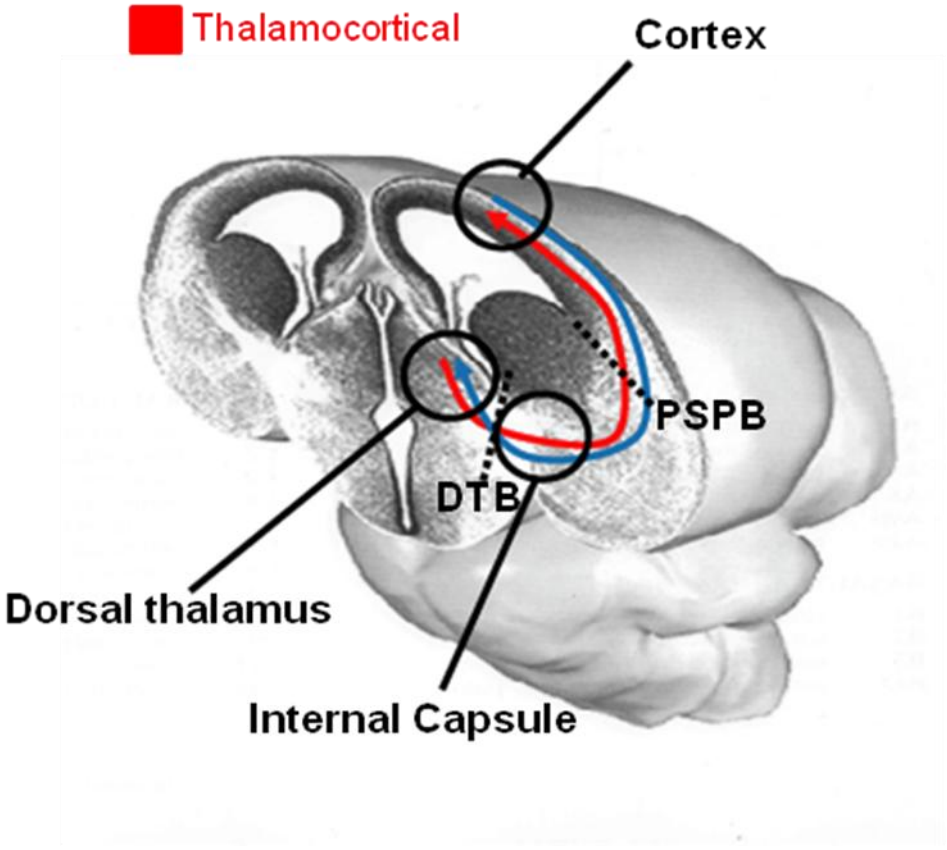

1.4.1.1 Cellular and molecular interactions guide the TCA tract

Many axon guidance molecules, transcription factors, and growth factors have been implicated in thalamocortical path finding (Price et al., 2006). Along the trajectory of the thalamocortical tract are a number of known guidance molecules that act to shape this pathway through chemo-repulsion and chemo-attraction. Netrin-1 is expressed in the ventral telencephalon when thalamocortical axons are traversing this region and it has been shown to act as a chemo-attractant to thalamocortical axons *in vitro* (Braisted et al., 2000). Further research has recently shown that a high rostral to low caudal gradient of Netrin-1 topographically sorts axons as they navigate the ventral telencephalon. In the presence of Netrin-1, rostro-medial thalamocortical axons were shown to be attracted via the expression of DCC receptor, while caudo-lateral thalamocortical axons were repelled via the expression of DCC as well as UNC5(A-C) receptors (Powell et al., 2008). A loss of Netrin-1 resulted in disorganization of the TCA tract at the ventral telencephalon with fewer axons making it to the cortex (Braisted et al., 2000). Ephrins have also been shown to have a role in topographic sorting of TCA axons at the ventral telencephalon (Bolz et al., 2004; Cang et al., 2005; Torii and Levitt, 2005; Uziel et al., 2006). Slit-Robo signalling has been shown to repel TCA/CTA axons from the hypothalamus in a manner that is consistent with directing CTA axons posteriorly towards the dLGN and directing TCA axons laterally into the telencephalon (Braisted et al., 1999; Bagri et al., 2002; Lopez-Bendito et al., 2007)

1.4.2 The corpus callosum

The corpus callosum is a major commissural tract which links the left and right cerebral hemispheres. This large commissural tract acts to coordinate and transfer information between the two hemispheres of the brain. Starting around E14.5, callosal neurons originating in layers 2/3 and 5 of the cortex project their axons

ventrally into the intermediate zone. These axons turn medially towards the midline and enter the cingulate cortex. Callosal axons then turn and navigate ventrally towards the corticoseptal boundary where they make a sharp turn medially to project across the midline at around E16.5. Once these axons have crossed the midline, they travel a similar route on the opposite side of the cortex towards their target cortical area for innervation. The corpus callosum continues to enlarge during development reaching maturity postnatally (Richards et al., 2004; Lindwall et al., 2007) (Figure 7). See table 3 for a more detailed account of the developmental timing of callosal axon projections.

Table 3. **Stages of callosal neuron development and their axonal projections** (Richards et al., 2004; Lindwall et al., 2007)**.**

Stage	**Description of callosal axon projections**
Early development of callosal neurons	Callosal neurons from layers 2/3 and 5 start projecting their axons ~E14.5 ventrally toward the intermediate zone. Around E15.5 callosal axons navigate towards the midline through the cingulate cortex. At the cingulate cortex, callosal axons project ventrally toward the corticoseptal boundary and then sharply towards the midline where they will cross.
Midline crossing of callosal axons	At ~E16.5 callosal axons start crossing the midline aided by pioneer neurons from the cingulate cortex, glial structures, and chemical guidance cues. Midline crossing of callosal axons continues to early postnatal development.
Later Stages of callosal axon navigation	By E17.5 the first callosal axons have crossed the midline and are observed to deflect dorsally through the contralateral cingulate cortex. By ~E18.5 callosal axons have arrived in the cortical plate where they innervate their correct cortical layer and innervate their target neurons.

1.4.2.1 Cellular and molecular interactions guide callosal axons

The development of the corpus callosum is determined through a combination of cellular and molecular interactions. Midline glia have been shown to be essential for the formation of commissures. In order for the corpus callosum to form, the two developing hemispheres of the brain must fuse at the point where callosal axons will cross the midline. Midline fusion is critical for the formation of corpus callosum because these axons cannot cross the midline if there is no substrate for them to grow and extend upon. Two populations of midline glia contribute to this fusion event

starting around E14.5 in mice; the midline zipper glia (MZG) and the indusium griseum (IGG). The observed medial deflection of callosal axons at the point just prior to crossing the midline have been shown to be due to the presence of a population of glial cells called the glial wedge (GW) (Shu and Richards, 2001). In addition, the glial sling (GS) has been shown to be important in midline crossing of callosal axons (Silver et al., 1982) (Figure 7).

A number of axon guidance cues have been implicated in corpus callosum development as well as a number of transcription factors, growth factors, and extracellular matrix molecules (Richards et al., 2004; Lindwall et al., 2007). The guidance molecule Sema3a has been shown to repel axons from the marginal zone and may act to repel layer 2/3 and 5 neuronal axons towards the intermediate zone (Polleux et al., 1998). Many guidance molecules (both receptors and ligands) have been implicated in midline crossing through loss of function experiments, where many or all of the callosal axons fail to cross the midline. These include Slits and Robos (Bagri et al., 2002; Andrews et al., 2006; Lopez-Bendito et al., 2007); netrin-1 and DCC (Serafini et al., 1996); and ephrins and Eph receptors (Mendes et al., 2006).

Figure 7. **The corpus callosum.** The corpus callosum is a major commissural tract that links and refines information from the two cortical hemispheres. Callosal neurons are born at ~E14.5 in layers 2, 3/5 of the cortex and project their axons to their eventual targets in the contralateral cortex. A key choice point for the navigating callosal axons is at the midline where they must decide to cross to the contralateral side of the brain. A number of glial structures have been implicated in mediating this decision. These glial structures (green) include the bi-symmetrical glial wedges (GW) located at the corticoseptal boundary as well as the midline zipper glia (MZG), indusium griseum (IGG), and the glial sling (GS).

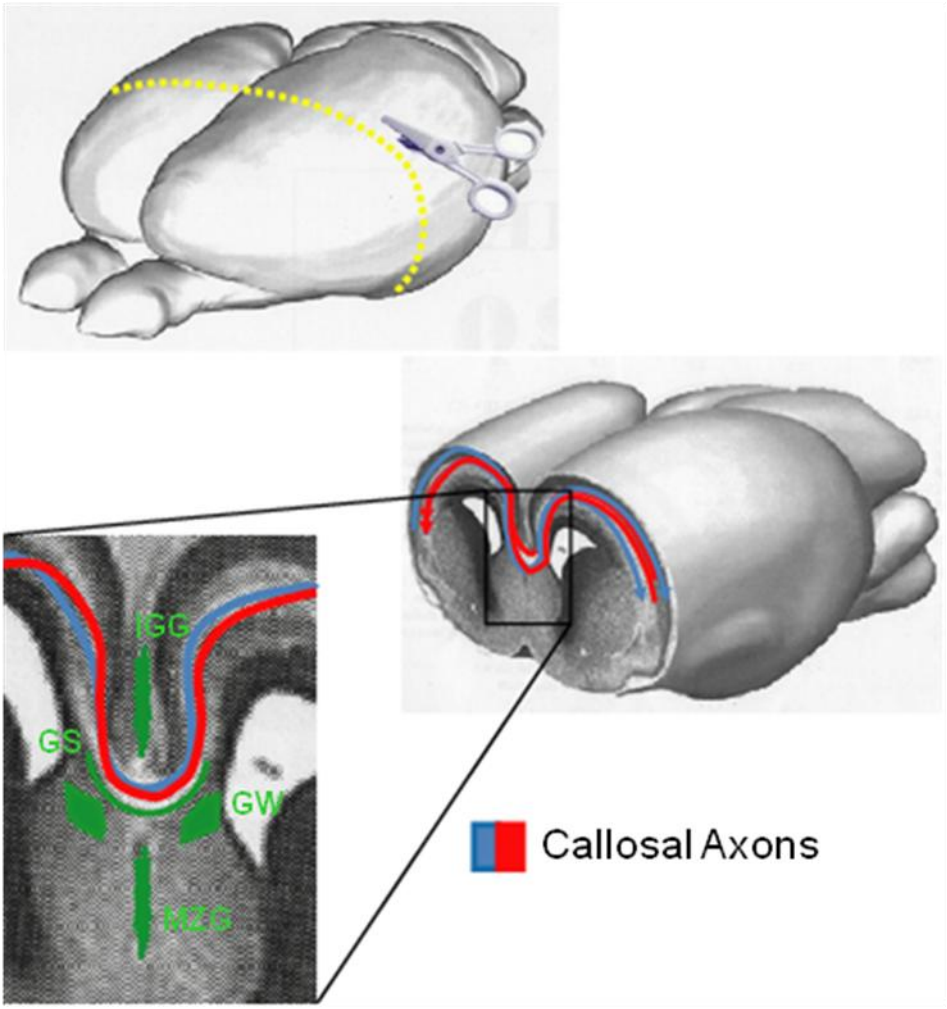
IGG
GS
GW
MZG
Callosal Axons

1.5 Proteoglycans and glycosaminoglycans

Proteoglycans (PGs) are cell surface and extracellular matrix macromolecules composed of a core protein and a variable number of covalently attached disaccharide residues known as glycosaminoglycans (GAGs). Widely distributed and structurally diverse, proteoglycans have been shown to influence a myriad of biological functions such as tissue morphogenesis, cell-to-cell signalling, and cell proliferation. The structural diversity of proteoglycans can be attributed to the protein core, the composition, number and branching of the GAGs, and the post-translational modifications that occur to the GAGs (Lin and Perrimon, 2002).

1.5.1 Heparan sulphate proteoglycans

The heparan sulphate proteoglycans (HSPGs) belong to a subgroup of proteoglycans (PGs) characterized by possessing at least one heparan sulphate (HS) chain. Heparan sulphate chains are unbranched, negatively charged (due to SO_4^{2-} moieties) GAGs composed of repeating disaccharide units of alternating hexuronic acid (either glucuronic acid or iduronic acid) and N-acetylglucosamine. The number of GAG chains attached (1 to >100) varies between different HSPGs, and the number of chains on a specific HSPG may vary, depending on the cell type that produces it (Bernfield et al., 1999; Esko and Selleck, 2002).

1.5.2 There are several groups of HSPG core proteins

All HS chains are covalently O-linked to serine residues in the core proteins via a GlcA-Gal-Gal-Xyl linkage region (Fransson et al., 2000). There are several types of HS core proteins that define the location and function of HSPGs. There are two cell

surface associated HSPGs; syndecans (4 different members known) are associated with the cell surface through a transmembrane domain and glypicans (6 known members) are associated with the cell membrane via a glycosylphosphatidylinositol (GPI) anchor. Syndecans and glypicans are widely expressed throughout development as well as in adulthood, but individual family members show specific spatiotemporal expression profiles. There are two extracellular matrix HSPGs called perlecan and agrin. Agrin is mainly found in the kidney and brain, while perlecan shows a wider tissue distribution. In addition to the above mentioned HSPGs, there are also surface HSPGs that can exist in both a glycosylated or non-glycosylated form; these are referred to as part-time HSPGs. A few examples of these include CD44, betaglycan and a unique isoform of fibroblast growth factor receptor 2 (FGFR2) (Bernfield et al., 1999; Esko and Selleck, 2002; Clark et al., 2004).

1.5.3 Structure and biosynthesis of HSPGs

The biosynthesis of HSPGs takes part in the Golgi apparatus in a complex multi-step process involving the concerted efforts of many enzymatic reactions (Gorsi and Stringer, 2007). Each step in the chain of assembly is catalyzed by a separate class of enzymes starting with the sugar transferases that create the GlcA-Gal-Gal-Xyl-O-serine linker. The exostosin (EXT)-family of sugar polymerases are responsible for the extension of the GAG chain while a number of enzymes act to modify the GAG chain through the actions of epimerization, sulphation, and de-acetylation. Epimerization of the hexuronic acid (Glucouronic acid to Idouronic acid) is carried out through the activities of C5 epimerase (Li et al., 2003). N-deacetylase/N-sulphotransferase (Ndst-1-4) acts to deacetylate N-acetylglucosamine and transfer a sulphate group to the 2 position of N-acetylglucosamine (Aikawa et al., 2001; Grobe et al., 2002). There are a number of enzymes that act to sulphate specific regions of the GAG chain and thus add the characteristic negative charge associated with HSPGs. Heparan sulphate-2-sulphotransferase (Hs2st) sulphates the 2 position of the hexuronic acid (Merry and Wilson, 2002; Wilson et al., 2002). There are three

isoforms of Heparan sulphate-6-sulphotransferase (Hs6st) 1-3 including one known splice variant of Hs6st2 in human (Habuchi et al., 2000; Habuchi et al., 2003; Sedita et al., 2004). These enzymes are responsible for the addition of sulphates to the 6-position of N-acetylglucosamine. Finally, Heparan sulphate-3-sulphotransferase (Hs3st-1-7) acts to sulphate the 3-position of N-acetylglucosamine (Guimond et al., 2001; Turnbull et al., 2003). In addition to the above enzymes that act to modify HSPGs in the Golgi apparatus, recent findings have shown that HSPG sulphation patterns can be additionally remodelled at the cell surface by extracellular heparan sulphate-6-endosulphatases (1-2) which acts to remove 6-O-sulphation (Morimoto-Tomita et al., 2002) (Figure 8).

Finally, taking into account that the modifications of HSPGs are generally accepted to be incomplete (i.e. enzymes do not always act on available substrates) and other enzymes may structurally alter HSPGs; the structural diversity of these macromolecules can theoretically accommodate a very large number of possible sequences. In practice, however, while the number of possible HSPG sequences is still astounding, the regulated expression and action of the biosynthetic enzymes and their restricted substrate specificities, limit the actual number of sequences expressed (Bernfield et al., 1999; Wei et al., 2000; Esko and Lindahl, 2001; Esko and Selleck, 2002; Nakato and Kimata, 2002).

Figure 8. **Synthesis and structure of HSPGs.** HSPGs are cell surface and ECM macromolecules composed of a core protein to which a number of disaccharide residues composed of hexuronic acid and N-acetylglucosamine are added through the activities of the exostosin (EXT-1) family of enzymes. To these disaccharide residues are a number of enzymes that act to modify the fine structure of HSPGs through such actions as epimerization (C5 epimerase) and sulphation (Hs2st) of hexuronic acid and deacetylation (Ndst) and sulphation (Hs3st, Hs6st1, and Ndst) of N-acetylglucosamine.

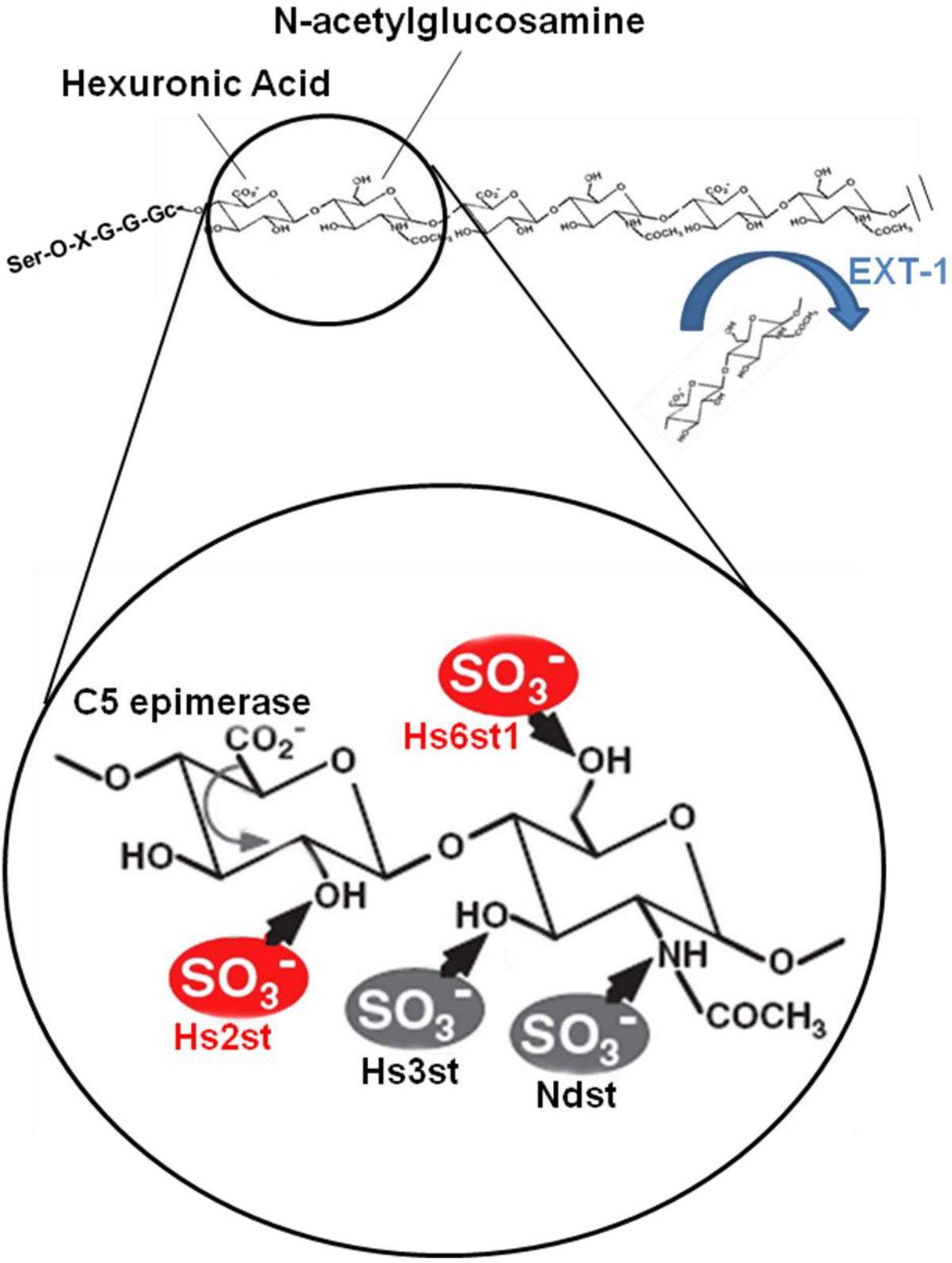
N-acetylglucosamine
Hexuronic Acid
Ser-O-X-G-G-Gc
EXT-1
C5 epimerase
Hs6st1
Hs2st
Hs3st
Ndst

1.5.4 HSPGs interact with many proteins

HSPGs physiological functions are closely related to their ability to selectively interact with various protein ligands and thereby affect many biological processes. The combinational possibilities in the biosynthesis of HSPGs offer considerable potential for multiple biological activities. The ligands include growth factors, morphogens, axon guidance cues, and ECM components. It is generally believed that the interactions between HS and various ligands depend on the relative positions of carboxyl and in particular sulphate groups within the HS chains. Positively charged patches of amino acids on the protein surfaces recognize these negatively charged groups within the HS chains (Bernfield et al., 1999; Esko and Selleck, 2002).

The structural diversity of HSPGs underlie their various functions (Bulow and Hobert, 2004). HSPGs have the ability to alter expression of a ligand through HS dependent signalling (Bernfield et al., 1999). HSPGs can alter the distance a ligand is transported away from the producing cell and also regulate the local concentration (i.e. protect from degradation) of the molecule available for receptor binding at the receiving cell (Esko and Selleck, 2002; Nybakken and Perrimon, 2002). Further, HSPGs can bind signalling inhibitory molecules and also itself work as an enhancer or inhibitor in a signalling system depending on sulphation patterns (Perrimon and Bernfield, 2000). HSPG interactions can modulate the actions of a protein in many ways. Because of the potential size of an HS chain, it has the ability to bind to several different molecules on the same chain and thereby increase the likelihood of interaction between the bound molecules, such as receptors and their ligands or enzymes and there inhibitors. In growth factor signalling, HSPGs can act to facilitate receptor dimerization and/or act as a co-receptor (McFarlane et al., 1995; Walz et al., 1997). HSPGs can function to retain growth factors and morphogens in the ECM, where they can be stored and/or protected from degradation. HSPGs can maintain concentration gradients of morphogens and growth factors at the cell surface (Strigini, 2005). The different modifications HSPGs contain directly influence their

ability to interact with proteins and have been shown to be individually critical to embryonic development (Table 4).

Table 4. **Lethality of mutations affecting HSPG modifications in mice.**

Gene name	Loss of function phenotype	Reference
Ext1	Defective gastrulation	(Lin et al., 2000)
Ext2	Defective gastrulation	(Stickens et al., 2005)
Ndst1	Perinatal lethality due to respiratory failure.	(Grobe et al., 2005)
C5-epimerase	Perinatal lethality due to respiratory failure.	(Li et al., 2003)
Hs2st	Perinatal death due to renal agenesis	(Bullock et al., 1998)
Hs3st1	Lethality depending on genetic background	(Shworak et al., 2002)
Hs6st1	Increased perinatal lethality due to placental defects	(Habuchi et al., 2007), Reported in this thesis
Hs2st/Hs6st1	Early embryonic death	Reported in this thesis
Hs6st1/Hs6st2	Early embryonic death	(Sugaya et al., 2008)

1.5.5 HSPGs have a role in the development of the CNS

The emergence of HSPGs as key regulators of developmental processes such as morphogen signalling and axon guidance has brought up the notion that these macromolecules evolved to modulate the interactions of receptor-ligand pairs. However, biochemical analysis, suggests that these ancient macromolecules predate most of the signalling molecules involved in the development of bilaterian organisms (nematodes, insects, and vertebrates, etc), and in fact have orthologs in Cnidaria. The neural net of Cnidaria is believed to be the oldest form of a CNS and it raises the interesting question as to the early role of HSPGs in CNS development (Medeiros et al., 2000; Van Vactor et al., 2006). It is interesting to think that many if not all chemical guidance cues evolved in a manner that utilized the presence of these ancient HSPGs.

Through such mechanisms, HSPGs have been shown to be important factors in regulating key developmental signalling pathways such as the Wnt (Yoshikawa et al., 2003), BMP (Augsburger et al., 1999), and Shh (Charron et al., 2003) signalling pathways; signalling by each of which is affected by alterations in HSPG structure (Lin, 2004; Hacker et al., 2005). The role HSPG function has on FGF signalling has been extensively studied. HSPGs act as co-receptors interacting with both the FGF ligand and the FGF receptor through a specific sequence of 3 disaccharide (glucosamine and iduronic acid) residues carrying specific sulphation modifications (Ornitz, 2000; Schlessinger et al., 2000; Pellegrini, 2001; Coumoul and Deng, 2003).

Recent years have implicated HSPGs in regulating axon guidance through its various interactions with chemical guidance cues and/or their receptors (Lee and Chien, 2004). HSPGs have been shown to be an integral component of Slit-Robo induced chemo-repulsion of axons both *in vitro* and *in vivo* (Hu, 1999; Liang et al., 1999; Johnson et al., 2004; Steigemann et al., 2004; Hussain et al., 2006). As previously described earlier in this chapter, HSPGs have been shown to influence Sema5a induced chemo-attraction (Kantor et al., 2004). Netrin-1/DCC signalling in commissural axon guidance in the spinal cord has revealed a cell autonomous

requirement for HSPGs *in vivo* (Matsumoto et al., 2007). Recently, HSPGs have been shown to regulate ephrinA3/EphA signalling (Irie et al., 2008).

1.5.6 Sulphotransferase enzymes responsible for HSPG modification contribute to CNS development

Previous work has shown mice completely lacking all heparan sulphation via a mutation in EXT-1 sugar polymerizing activity (cannot make functional HSPGs) die very early in development due to defective gastrulation (Lin et al., 2000). Conditional knockout of the HS sugar- polymerising enzyme EXT-1 in the embryonic mouse brain resulted in a number of developmental defects particularly in axonal tract formation. These *EXT-1* conditional mutants lacked the corpus callosum, hippocampal commissure, and the anterior commissure. Disruption of the anatomical structure of the developing mouse brain was evident with the absence of the olfactory bulbs, hypomorphic cortex, and deformed cerebellum. In addition, RGC axons were observed to project ectopically to the contralateral optic nerve (Inatani et al., 2003; Inatani and Yamaguchi, 2003).

1.5.6.1 Ndst1

As previously mentioned Ndst is responsible for removing the acetyl group at the C2 position on N-acetylglucosamine and replacing it with a sulphate group. Observations of mice harbouring a targeted disruption of HS Ndst1 showed severe defects in CNS development. These animals had severe cerebral hypoplasia and craniofacial defects, and lacked olfactory bulbs and eye lens. Axonal tract formation was also compromised with an absence of the hippocampal and anterior commissures as well as the olfactory tract. These defects have been attributed, at least in part, to Shh and FGF signalling defects (Grobe et al., 2005). Interestingly, Ndst-(2-4) were

unable to rescue the defects observed in the *Ndst1* mutant, suggesting the unique/non-redundant functions of this particular isoform.

1.5.6.2 Hs2st

Hs2st enzymes are Golgi located type II transmembrane proteins that are capable of transferring sulphate groups to the C2 positions of hexuronic acids. Hs2st was first purified from serum free medium of Chinese hamster ovary (CHO) cells (Kobayashi et al., 1997).

Mice deficient in Hs2st sulphation die perinatally due to renal agenesis (Bullock et al., 1998). *Hs2st*$^{-/-}$ mutant animals were also characterized as having defects in eye development (cataracts and colombomas of the iris) and also showed skeletal abnormalities. Also, *Hs2st* mutant embryos showed a significant reduction in the thickness of the cerebral cortex due to proliferation defects as well as defects in RGC axon guidance (Bullock et al., 1998; McLaughlin et al., 2003a; Pratt et al., 2006). In *Xenopus*, 2-O-sulphation was shown to be important, as exogenously added 2-0-sulphated heparins resulted in RGC axons failing to turn towards their targets in the tectum (Irie et al., 2002). Interestingly, loss of Hs2st sulphation has been shown to have a concomitant increase in both N-sulphation and 6-O-sulphation (Merry et al., 2001).

1.5.6.3 Hs6st

Hs6st enzymes are Golgi located type II transmembrane proteins that are capable of transferring sulphate groups to the C6 positions of N-acetylglucosamines. Hs6st was first purified from serum free medium of Chinese hamster ovary (CHO) cells and later cloned from human foetal brain cDNA (Habuchi et al., 1998). Three mammalian Hs6st isoforms (Hs6st1, Hs6st2, and Hs6st3) are known to date

including one splice variant of Hs6st2 in humans. These Hs6st isoforms show differential expression patterns, but similar substrate specificities suggesting that they are capable of functioning redundantly when co-expressed (Habuchi et al., 2000; Smeds et al., 2003; Sedita et al., 2004).

A loss of Hs6st1 sulphation results in increased neonatal lethality with only 3% of the offspring being homozygous mutant. The increase in lethality was reported to be a 50% reduction in foetal micro-vessels in the labyrinthine zone of the placenta (Habuchi et al., 2007). Similar to the RGC axon guidance defects observed in the *EXT-1* conditional knockout mice, *Hs6st1* mutants showed an increase in the number of RGC axons projecting to the opposite eye (Pratt et al., 2006). Systemic inactivation of Hs6st1 showed no major defects in organogenesis, however, lethality was observed in early adulthood in some cases (Izvolsky et al., 2008). In *Xenopus*, 6-O-sulphation was shown to be important, as exogenously added 6-O-sulphated heparins resulted in RGC axons failing to turn towards their targets in the tectum (Irie et al., 2002). Further to these results, observations to determine up-regulation of Hs6st2, Hs6st3, and/or Hs2st revealed no significant increase in the transcript levels of any of these enzymes in *Hs6st1* mutant animals (Habuchi et al., 2007). Characterization of animals lacking both Hs6st1 and Hs6st2 revealed a significant decrease in 6-O-sulphation. In the absence of both, Hs6st1 and Hs6st2, 2-O-sulphation was observed to be nearly twice as high and Hs2st enzyme activity was 1.5 fold higher than in wild type (Sugaya et al., 2008). These animals were observed to die slightly earlier than *Hs6st1* mutant animals.

1.5.7 The heparan sulphate code hypothesis

Based on the structural diversity that exists in HSPGs, the "heparan sulphate code" hypothesis was proposed by Bulow and Hobert, 2004. This hypothesis postulated that differential modifications of HSPGs contribute to different functions in development. This hypothesis was tested in the invertebrate model system, *C. elegans* using animals harboring mutations in three HSPG modifying enzymes;

Hs2st, *Hs6st*, and *C5-epimerase*. They showed that these mutants exhibited both overlapping and distinct axon guidance defects implicating the *sax-3/Robo* and *kal-1/Anosmin-1* axon guidance signaling pathways as being dependant on these specific HSPG modifications (Bulow and Hobert, 2004).

1.6 Gene trapping

A common method of determining protein function in a biological system is to remove or inactivate the protein and observe the phenotype that results. Gene trapping is a form of insertional mutagenesis specifically designed to disrupt gene function. The gene trap vector itself, carries one or more reporter genes. A productive integration event brings the reporter gene under the transcriptional regulation of the endogenous gene and thus, the expression pattern of the gene can be observed.

Gene trapping involves the random insertion of a vector into intronic DNA using a splice acceptor site located at the 5' end of the vector, entry of which creates a gene fusion, which essentially disrupts the endogenous gene. An important feature of the gene trap strategy is the presence of an N-terminal signal sequence (supplied by the endogenous gene) and a transmembrane domain (TM) (supplied by the gene trap vector), which allows the preferential targeting of membrane bound and secreted proteins. Containing the bicistronic β-geo (β-galactosidase fused to neomycin phosphotransferase) reporter gene, the gene trap vector allows the possibility to identify the expression patterns of the disrupted genes (Figure 9).

Figure 9. **The gene trap vector.** The gene trap vector is a tool used to disrupt gene function and identify cells that express this gene using gene trap reporter genes. Gene trapping involves the random insertion of a vector into intronic DNA using a splice acceptor (SA) site located at the 5' end of the vector. The transmembrane domain (TM) allows the preferential targeting of membrane bound and secreted proteins. Containing the bicistronic β-geo (β-galactosidase (LacZ, blue) fused to neomycin phosphotransferase (neo)) reporter gene, the gene trap vector allows the possibility to identify the expression patterns of the disrupted genes. While the β-geo transcript localizes to cell bodies (retained within an intracellular compartment), the secretory gene trap reporter uses the human placental alkaline phosphatase (hPLAP, purple), which is under the control of an internal ribosome entry site (IRES). This allows the hPLAP protein to localize away from the cell body; an important attribute when marking axonal projections of neurons.

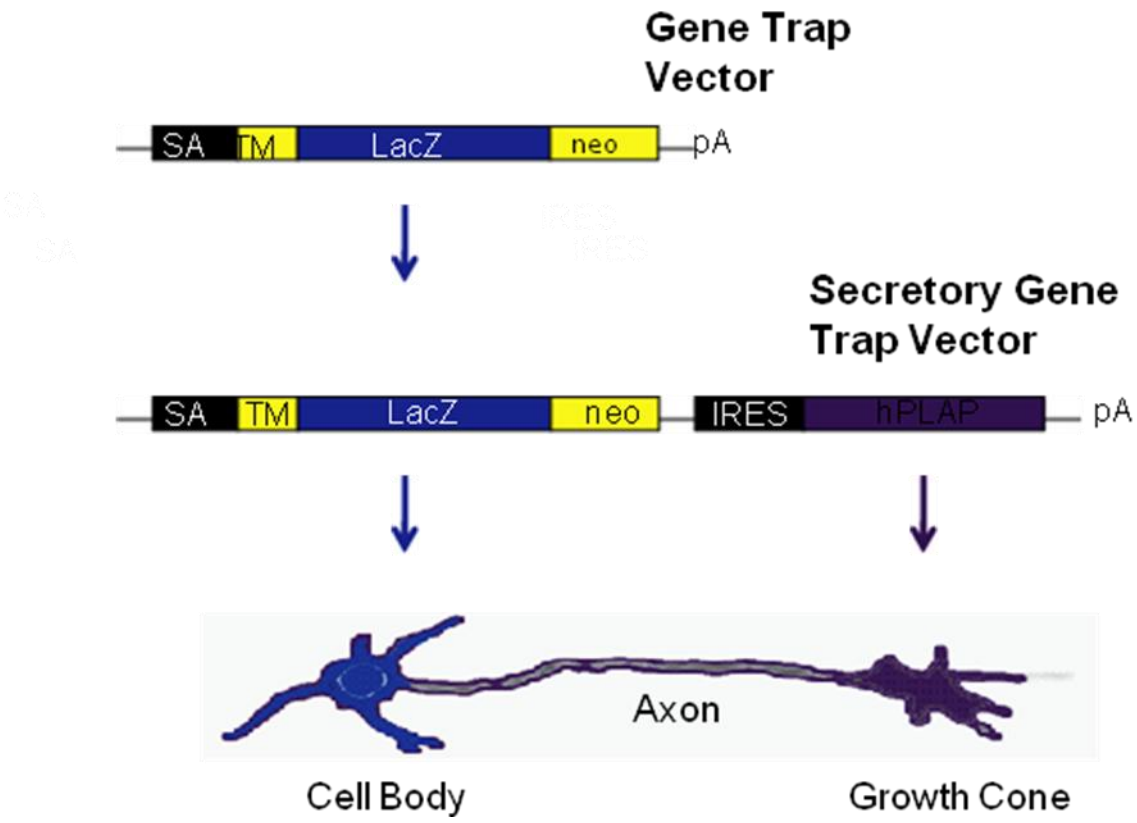
Gene Trap
Vector
SA
TM
LacZ
neo
pA
Secretory Gene
Trap Vector
SA
TM
LacZ
neo
IRES
hPLAP
pA
Axon
Cell Body
Growth Cone

While the β-geo transcript localizes to cell bodies (retained within an intracellular compartment), another (secretory gene trap) reporter used is human placental alkaline phosphatase (hPLAP), which is under the control of an internal ribosome entry site (IRES). This allows the hPLAP protein to localize away from the cell body; an important attribute when marking axonal projections of neurons (Skarnes et al., 1995; Stoykova et al., 1998; Leighton et al., 2001; Mitchell et al., 2001) (Figure 9).

There are some disadvantages of using gene trapping as a method of determining gene function. It is not possible to target a specific gene as the integration of the gene trap vector is a random event. Gene trapping involves the insertion of the vector into one of the introns of a gene, therefore, there is a bias towards genes that have larger or more numerous introns. There is the possibility that multiple copies of the gene trap vector insert into a single gene. It is also possible that while the gene trap vector inserts into a gene and is translated, it does not result in a complete loss of function for that gene (i.e. the functional domains remain intact).

1.7 Aims of the thesis

To investigate the roles played by specific modifications of HSPG molecules in the guidance of axons, we examined two lines of mutant mice harbouring mutations in the genes encoding HSPG modifying enzymes, Heparan sulphate-6-O-sulphotransferase-1 (Hs6st1) and Heparan sulphate-2-O-sulphotransferase (Hs2st). These two mutant lines were generated through the use of gene trapping. Previous observations of RGC axon development in the two mutant lines revealed distinct axon guidance errors at the optic chiasm. Loss of Hs6st1 sulphation resulted in RGC axons navigating ectopically into the contralateral eye. Loss of Hs2st sulphation resulted in RGC axons navigating along the ventral midline of the diencephalon and a general defasciculation of the optic chiasm. Early observations suggest that both Hs2st and Hs6st1 sulphation have distinct, non-overlapping actions and thus, influence different axon guidance signalling pathways at the optic chiasm.

Following these observations, I aimed to further characterize the defects at the optic chiasm in *Hs2st*$^{-/-}$ mutants and *Hs6st1*$^{-/-}$ mutants. *Hs2st*$^{-/-}$ mutant chiasms were previously described as disorganized however, no quantitative data was provided. Here I aimed to identify the source of this disorganization and quantify this defect through width measurements using a combination of DiI tract tracing and immunohistochemistry.

To test whether Hs2st and Hs6st1 enzymes act redundantly during optic chiasm development, I aimed to create *Hs2st*$^{-/-}$*/Hs6st1*$^{-/-}$ double mutants. Before this could be accomplished, I required a method of differentially identifying the *Hs6st1*$^{-/-}$ mutants. Using a combination of Southern blotting and PCR I aimed to characterize the *Hs6st1*-gene trap allele.

Finally, knowing that Hs2st sulphation and Hs6st1 sulphation had a role in RGC axon guidance at the optic chiasm, I hypothesized a possible role for Hs2st and/or Hs6st1 sulphation in guiding RGC axons in other key choice points within the visual system as well as other axonal tracts. Using a combination of LacZ reporter staining and *in situ* hybridization I aimed to characterize the expression patterns of *Hs2st* and *Hs6st1*. Based on these results, I looked at regions where Hs2st and Hs6st1 sulphation may be important in axon guidance; these regions included the dLGN (a major neuronal network in the visual system), the regions encountered by TCA/CTA tracts, and the regions encountered by callosal axons in the formation of the corpus callosum.

Chapter 2: Methods and Materials

2.1 Animals

Hs6st1$^{LacZ\text{-}IRES\text{-}hPLAP}$ (*Hs6st1*$^{+/-}$) mice were maintained on a pigmented CBA background by crossing wild type females with *Hs6st1*$^{+/-}$ males (Leighton et al., 2001; Mitchell et al., 2001). *Hs2st*^{LacZ} (*Hs2st*$^{+/-}$) mice were maintained on a pigmented CBA/C57Bl6 mixed background by crossing wild type females with *Hs2st*$^{+/-}$ males (Bullock et al, 1998 and Leighton et al, 2001). *Hs2st*$^{+/-}$ animals were subsequently bred onto and maintained on a pigmented CBA background. Compound *Hs2st*$^{+/-}$/*Hs6st1*$^{+/-}$ mutant animals were created by inter-crossing *Hs2st*$^{+/-}$ animals with *Hs6st1*$^{+/-}$ animals. All mice were housed and cared for under the rules and regulations of the Home Office. Embryos were taken from euthanized female mice where the day of insemination was designated as embryonic day (E) 0 and the plug day E0.5.

2.2 Genotyping

2.2.1 LacZ genotyping

Hs6st1$^{+/-}$ animals from *Hs6st1*$^{+/-}$ x wild type crosses were initially identified using the "knock-in" LacZ reporter of the gene trap vector. Ear clips were briefly LacZ fixed in 4% paraformaldehyde (PFA)/phosphate buffered saline (PBS) containing (0.02% NP40, 0.01% sodium deoxycholate, 5 mM EGTA, and 2 mM $MgCl_2$) on ice. The ear clips were washed several times in PBS and then incubated O/N at 37°C in LacZ staining solution (2mM $MgCl_2$, 0.02% NP40, 0.01% sodium deoxycholate, 5mM potassium ferricyanide, 5mM potassium ferrocyanide, and 1 mg/ml 5-bromo-4-chloro-3-indolyl-β-D-galactopyranoside (X-Gal)) in PBS. Ear clips that turned blue were identified as being *Hs6st1*$^{+/-}$ animals, while ear clips not turning blue were

identified as wild type. Wild type, *Hs6st1*$^{+/-}$ embryos and *Hs6st1*$^{-/-}$ embryos from *Hs6st1*$^{+/-}$ x *Hs6st1*$^{+/-}$ crosses were essentially genotyped as above using embryo paws, however LacZ staining was monitored at ~20 minute intervals to gauge β-galactosidase activity (development of blue colour intensity). At 40-60 minutes, β-galactosidase activity was moderate in *Hs6st1*$^{+/-}$ mutants (one copy of LacZ reporter), high in *Hs6st1*$^{-/-}$ mutants (two copies of LacZ reporter), and absent in wild type (no copies of LacZ reporter). PCR was later used to genotype *Hs6st1* mutants and was used to determine the genotype of *Hs2st* mutant animals and embryos (See section 2.2.3).

2.2.2 Mouse genomic DNA extraction

Mouse ear clips or embryo paws were digested in 0.25 ml tail tip lysis buffer (100 mM Tris-HCl, pH 8.5, 5 mM EDTA, 200 mM NaCl, 0.2% SDS) containing 50 μl/ml proteinase K at 55°C O/N. 150 μl of phenol:chloroform:isoamyl alcohol (25:24:1) (Sigma) was added to each tube and centrifuged at 13,000 rpm for 5 minutes. The top aqueous layer was transferred to fresh tubes containing 25 μl of 3M NaOAc and mixed with ~400 μl of 96% ethanol. Tubes were then centrifuged at 13,000 rpm for 5 minutes in a bench-top microfuge. The supernatant was decanted and the remaining pellet washed once in 70% EtOH, centrifuged at 13,000 rpm and the supernatant decanted. Remaining EtOH was evaporated using a thermo-cycler set at 55°C for 45 minutes. 200 μl of water was added to each pellet and re-suspended at 37°C overnight with shaking.

2.2.3 PCR genotyping

The PCR reaction used for *Hs2st* genotyping was 0.2 μl 10nM dNTPs, 2 μl 10X Perkin-Elmer buffer II, 2.2 μl 25 mM $MgCl_2$, 0.2 μl Perkin-Elmer amplitaq, 10.6 μl

sterile ddH_2O, and 1.2 μl primer mix (70 ng/μl each) (Table 1). The PCR reaction used for *Hs6st1* genotyping was 0.2 μl 10nM dNTPs, 2 μl 10X Perkin-Elmer buffer II, 1.6 μl 25 mM $MgCl_2$, 0.2 μl Perkin-Elmer amplitaq, 11.2 μl sterile ddH_2O, and 0.2 μl each primer (70 ng/μl each) (Table 1). PCR conditions for *Hs2st* genotyping were 30 cycles of 20 seconds at 94°C, 30 seconds at 60°C, 30 seconds at 72°C and 1 cycle of 5 minutes at 72°C. The PCR conditions for *Hs6st1* genotyping were 30 cycles of 30 seconds at 94°C, 30 seconds at 58°C, 30 seconds at 72°C and 1 cycle of 5 minutes at 72°C. The PCR products were visualized under ultraviolet light after 30 minute electrophoresis at 90V on a 2% agarose gel containing 1X TBE buffer + SYBR Safe (Invitrogen).

Table 1. **PCR Primers for *Hs2st* and *Hs6st1* Genotyping**

Allele	Forward 5' Primer	Reverse 3' Primer	Product Size (bp)
Hs2st$^+$	5'ATCAATGAATAATTGCCTAGGTC3'	5'GGGAAGAAATTCACCCCAACA3'	174
Hs2st$^-$	As Above	5'TACTCAGTGCAGTGCAGTCA3'	344
Hs6st1$^+$	5'ATGGTGACTGTGACCCACAA3'	5'GGGATATAGGGGACCTTGGA3'	179
Hs6st1$^-$	5'ACAGCTGCCAGGATCCTAAA3'	5'CCCACCTTGGCTGTAGTCAT3'	328

2.3 Reverse transcriptase (RT)-PCR

Approximately 5 mg of tissue was dissected from the optic chiasm or retina of E14.5 embryos and total RNA was extracted using an RNAeasy micro kit (Qiagen, Valencia, CA) according to the manufacturer's instructions. Using Sensiscript

Reverse Transcriptase kit (Qiagen), 1 μl of RNA was reverse transcribed to generate cDNA using oligo (dT)-15 primers (Promega, Madison, WI) according to the manufacturer's instructions.

To characterize the *Hs6st1*-gene trap allele, RT-PCR was performed on wild type cDNA, *Hs6st1*$^{+/-}$ mutant cDNA, and *Hs6st1*$^{-/-}$ mutant cDNA. Primer sequences were designed to target exon 1 to exon 2 of *HS6st1* gene (*Hs6st*$^{+}$) to identify the wild type transcript. Primer sequences were designed to target *HS6st1* exon 1 to CD4 of gene trap vector (*Hs6st*$^{-}$) to identify the mutant transcript. Primers were designed to target glyceraldehyde-3-phosphate dehydrogenase (*GAPDH*) which was used as an internal control (Table 2). RT-PCR was as follows; cDNA was denatured for 5 minutes at 95°C and cycled at 94°C denaturing for 30 seconds, 60°C annealing for 30 seconds, and 72°C extension for 40 seconds for a total of 35 cycles.

Table 2. **RT-PCR primers used to identify the *Hs6st1*-gene trap fusion transcript.**

Allele	Forward 5' Primer	Reverse 3' Primer	Product Size (bp)
Hs6st1^{+}	5'ACGACGTGATCGTCTTCCTG3'	5'TCACACATGTGCAAGGAGGT3'	379
Hs6st1^{-}	5'GACATGAAGGGCGACGAC3'	5'AGTAGACTTCTGCACAGACACC3'	500
GAPDH	5'GGGTGTGAACCACGAGAAAT3'	5'CCTTCCACAATGCCAAAGTT3'	121

2.3.1 Quantitative RT-PCR

To quantify the expression of *Hs2st*, *Hs6st1*, *Slit1*, *Slit2*, *Robo1*, and *Robo2*, we used Quantitative RT-PCR (Q-RTPCR) on optic chiasm cDNA and retinal cDNA extracted from wild type, *Hs2st*$^{-/-}$ mutants and *Hs6st1*$^{-/-}$ mutants (Table 3). Q-

RTPCR was done using Qiagen Quantitect SYBR Green PCR Kit as described by the manufacturer's instructions and a DNA Engine Opticon Continuous Fluorescence Detector (Genetic Research Instrumentation, Essex, UK). Target cDNA was normalized to the house keeping gene, *GAPDH* and quantification calculated from standard curves generated from the cDNA isolated from the optic chiasm and the retina. The PCR was as follows: hot start at 95°C for 15 minutes, followed by a 35 cycle reaction with 15 seconds denaturing at 94°C, 30 seconds annealing at 60°C, and 30 seconds extension at 72°C.

Table 3. **Q-RTPCR primers.**

Allele	Forward 5' Primer	Reverse 3' Primer	Product Size (bp)
Hs2st	5'GCTTCCTTCTGTCTTACCTTGCTG3'	5'AGCCCACCCTTTTCTTAGTCTCC3'	138
Hs6st1	5'ACGACGTGATCGTCTTCCTG3'	5'TGGAGAAGCGAGAGAAGAGC3'	159
Slit1	5'TCACTGACCTGCAGAACTGG3'	5'ACCATCTGGTCGAAGGTGAC3'	257
Slit2	5'CCTGCCAGATGATCAAGTGC3'	5'GCTGCTTCTGGTAATAGTCC3'	152
Robo1	5'GCCACTTCCATGCCTCTCAG3'	5'GTGCCTTGGACTGGACAGTG3'	187
Robo2	5'GCAGAAGTAAACCGGACGAA3'	5'CTCCAAGATTGCAGGCTCTC3'	164
GAPDH	5'GGGTGTGAACCACGAGAAAT3'	5'CCTTCCACAATGCCAAAGTT3'	121

2.4 Cloning

We used either pGEM-T Easy cloning systems (Promega) to create riboprobes for RNA *in situ* hybridization or TOPO-TA Cloning Systems (Invitrogen) to create DNA probes for Southern blot analysis. PCR amplified DNA fragments encoding the riboprobes and the DNA probes were ligated into the pGEM-T Easy vectors and the pCR 2.1-TOPO vectors, respectively following the manufacturer's instructions and these vectors were then transformed into TOP10 chemically competent *E. coli* cells (Invitrogen) following the manufacturer's instructions and incubated for 1 hour at 37°C. These cells were then plated onto pre-warmed LB agar (1% tryptone, 0.5% yeast extract, 1% NaCl, 1.5% agar, pH 7) + 50 µg/ml ampicillin plates and incubated O/N at 37°C. Positive white colonies were selected from blue colonies and LB medium was inoculated with single white colonies and incubated O/N at 37°C with shaking. Either minipreps (Qiagen) or midipreps (Qiagen) were used as described in the manufacturer's instructions to isolate and purify plasmid DNA carrying the probes.

2.5 Southern blot analysis

Wild type genomic DNA was extracted from the liver of E15.5 embryos as described in section 2.3, which yielded a high concentration of genomic DNA as determined by gel electrophoresis. 40 µl of mouse genomic DNA was digested with BamHI (>50U) and ClaI (>50U), 2 µl spermidine, and 10x buffer overnight at 37°C and loaded onto a 0.8% agarose gel and run for 16 hours at 40V in 1X TBE buffer without ethidium bromide. The next day, the gel was exposed to ethidium bromide for 20 minutes with shaking and briefly visualized under UV light. The gel was then transferred to 250 ml HCl mix (2.5% HCl) for 30 minutes with shaking. This was followed by 2x30 minutes Denaturation solution (0.4 M NaOH, 0.6 M NaCl) and 2x30 minutes in neutralization solution (1.5 M NaCl, 0.5 M Tris-HCl, pH 7.5). The gel was then

placed onto a blotting apparatus and the surface was dampened with 20x SSC. Hybond-N+ nylon membrane (Amersham Biosciences) was pre-soaked in 2x SSC and placed carefully onto the gel; this was followed by 2 pieces of pre-soaked Whatman 3MM paper. Any trapped bubbles were removed by rolling a pipette over the surface. One stack of paper towels was split into equal halves and placed on top of the Whatman 3MM paper and weighted down in a balanced fashion. After ~3 hours the Whatman 3MM paper and paper towels were replaced and left overnight to allow the DNA in the gel to transfer to the nylon membrane. The next day, the membrane was wrapped in saran wrap and placed into a UV incubator for 2 minutes. The membrane was then placed onto Whatman 3MM paper to remove excess moisture and placed into a 120°C oven for 15 minutes to ensure the DNA was fixed to the nylon membrane. The membrane was pre-hybridized using Church hybridization buffer (0.5 M $NaPO_4$, pH 7.2, 7% SDS, 1mM EDTA, 1% BSA) + 0.1 mg/ml denatured salmon sperm for 3 hours at 65°C in a rolling incubator. This was followed hybridization using Church hybridization buffer + radioactively-labelled DNA probes (See section 2.5.1) incubated overnight at 65°C in a rolling incubator. The next day, the membrane was washed several times in Church wash (1% SDS, 1mM EDTA, 40 mM $NaPO_4$, pH 7.2) and then exposed to MR X-ray film (Kodak) in an autoradiography cassette O/N at -70°C. The films were then developed (Hyper-processor, Amersham).

2.5.1 Southern blot DNA probe design

Intron 1 of the *Hs6st1* gene was predicted to have 3 BamHI cut sites and 1 ClaI cut site which would produce 5 segments within the *Hs6st1* intron1 according to MacVector Software. Using Primer3 software, we designed 5 sets of PCR primer pairs that were specific to each of the 5 segments of *Hs6st1* intron1 and would produce 5 different DNA probes (Table 4).

Table 4. **PCR primers used to generate Southern blot DNA probes.**

Probe	Forward 5' Primer	Reverse 3' Primer	Product Size (bp)
P1	5'CCTGTCATTTGCTG GCTGTTG3'	5'CTAAACGCTGGAAA GGGTTGC3'	394
P2	5'CCCCAGGCTCCATC TCTATGTTAG3'	5'CAAGTCCCCCATTTC CAGTAGTG3'	643
P3	5'TGGAGAAGACAGT GTTGTGGGC3'	5'CAGCAGAATGAGGC AGTCAAGC3'	575
P4	5'GAGCCTGAATGAA TGAACCCTCCTTC3'	5'CCTGTCCTGACTTCC TTTGGTG3'	467
P5	5'GGGGTGTCGTGGC TTTTTTC3'	5'TGCTTCCGTGTGAGT CAGGATG3'	642

PCR amplification of these probes was conducted using 0.2 µl 10nM dNTPs, 2 µl 10X Perkin-Elmer buffer II, 0.8 µl 25 mM $MgCl_2$, 0.2 µl Perkin-Elmer amplitaq, 10.6 µl sterile ddH_2O, and 0.2 µl primer each (70 ng/µl for each primer). PCR conditions were 30 cycles of 20 seconds at 94°C, 30 seconds at 60°C, 1 minute at 72°C and 1 cycle of 5 minutes at 72°C. The PCR products were visualized under ultraviolet light after 45 minute electrophoresis at 65V on a 1% agarose gel containing 1X TBE buffer + ethidium bromide. The PCR product bands were excised from the gel and the DNA extracted using a Qiagen Gel Extraction kit. This was followed by cloning (See section 2.4) and enzymatic excision of the DNA probe. 25 ng of the DNA probes were radioactively-labelled using Rediprime II Random Probe labelling system (Amersham) + 5µl of ^{32}P-dCTP in TE buffer and incubated at 37°C for 10 minutes. The reaction was stopped with 0.2M EDTA and the labelled DNA probe was isolated using Sephadex G50 columns (Amersham).

2.6 Histology

2.6.1 Fixation of brain tissue for vibratome sectioning

Following decapitation, embryonic heads were placed in 4% PFA/PBS overnight (O/N) at 4°C. For LacZ staining, 4% PFA/PBS was supplemented with 0.02% NP40, 0.01% sodium deoxycholate, 5 mM EGTA, and 2 mM $MgCl_2$. For *in situ* hybridization, 4% PFA/PBS was supplemented with 0.1% Tween-20 and the pH adjusted to 9.5. Heads were washed several times in PBS with shaking at room temp and then positioned in the coronal, horizontal, or sagittal plane in molten 4% low melting agarose/ddH_2O and allowed to set on ice. Either 100 µm or 200 µm thin sections were cut using a vibratome.

2.6.2 Fixation of brain tissue for microtome sectioning

Following decapitation, embryonic heads were placed in 4% PFA/PBS O/N at 4°C. The heads were washed several times in PBS at room temp with shaking and then placed in 70% ethanol for wax processing. Heads were positioned in the coronal, horizontal, or sagittal plane and embedded in paraffin wax using an automated tissue processor (Tissue-Tek, VIP, Sakura). Wax embedded heads were cut at 10 µm thin sections using a microtome (Reichert, Jung 2050) and floated onto poly-L-lysine (Sigma) coated glass slides or Superfrost Plus (VWR International) slides and the sections allowed to dry O/N at 37°C.

2.7 Expression

2.7.1 Expression of *Hs2st*$^{+/LacZ}$ and *Hs6st1*$^{+/LacZ\_IRES\_hPLAP}$ using LacZ staining

Heads were prepared as outlined in section 2.6.1. 200 µm sections were collected and rinsed several times with LacZ wash buffer (2mM $MgCl_2$, 0.02% NP40, 0.01% sodium deoxycholate in PBS) and transferred to LacZ staining solution (wash buffer supplemented with 5mM potassium ferricyanide, 5mM potassium ferrocyanide, and 1 mg/ml X-Gal), and stained at 37°C until LacZ expression was evident (as indicated by the development of a blue colour). Staining was stopped with 20 mM EDTA in PBS and post-fixed in 2% glyceraldehyde overnight at 4°C. Sections were transferred to glass slides, mounted in Aquatex (Merck, Germany) and allowed to set O/N at room temp in the dark. Images were generated using light microscopy with digital camera (Leica Microsystems, Germany).

2.7.2 *In situ* hybridization on thick 100 µm sections

Heads were prepared as outlined in section 2.6.1. 100 µm sections were floated onto Superfrost Plus (VWR International) glass slides and allowed to air dry overnight at room temperature. All steps were done at room temperature unless otherwise stated. Slides were placed in slide-mailers and washed in PBS + 0.1% Tween-20 (PBT) for 5 minutes. Sections were dehydrated in a 50%, 100% methanol/PBT series and then rehydrated in a75%, 50%, 25% methanol/PBT series each for 5 minutes. Slides were washed twice in PBT for 5 minutes and then placed in 6% H2O2/PBT for 1 hr. Slides were then washed 3xPBT for 5 minutes and placed in 5 µg/ml Proteinase K/PBT for 10 minutes. Slides were placed in 0.2% glycine/PBT for 10 minutes and washed for 5 minutes twice in PBT. Sections were post-fixed in 4% PFA/PBT pH 9.5 for 20 minutes and again washed for 5 minutes twice in PBT. Sections were

encircled with an Immedge lipid pen (Vector Laboratories, Burlingame, CA) and treated with prehybridization buffer (50% formamide/5x SSC, pH 4.5 supplemented with 1% SDS, 50 µg/ml tRNA, and 50 µg/ml heparin) for 1 hr at 65°C in a humidified chamber containing 50% formamide. RNA riboprobes were denatured for 5 minutes at 85°C and then placed on ice for 1 minute. Sections were then hybridized in the same humidified chamber O/N at 65°C with prehybridization buffer containing the denatured riboprobe (15 µl/ml). Post-hybridization washes consisted of 3x 20 minute washes in Solution 1 (50% formamide/5x SSC, pH 4.5 supplemented with 1% SDS) at 65°C; 3x 20 minute washes in Solution 3 (50% formamide/2x SSC, pH 4.5); and 3x 5 minute washes in 1X TBST (1.4M NaCl, 27mM KCl, 250 mM Tris-HCl, pH 7.5 + 1% Tween-20) at room temp. Sections were incubated for 1 hr in 10% sheep serum in 1X TBST at room temp and then incubated O/N in anti-digitoxinigen-Ab (1:2000) in 1% sheep serum in TBST at 4°C. The next day, unbound antibody was washed off using TBST at 90 minute intervals for the entire day at room temp and then stored at 4°C O/N. To produce the colour reaction, sections were washed 3x 10 minute in NTMT (100 mM NaCl, 100 mM Tris-HCl, pH 9.5, 50 mM $MgCl_2$, and 1% Tween-20) at room temp and then incubated in NTMT supplemented with NBT (4.5 µl/ml)/BCIP (3.5 µl/ml) stock solution until adequate colour development was observed. The colour reaction was stopped using several washes of PBS, post-fixed in 4% PFA/PBS, washed several more times in PBS and mounted in 90% glycerol/PBS before imaging.

2.7.2.1 Generation of DIG-labelled RNA riboprobes for *in situ* hybridization

Hs2st primers (Table 5) were designed to specifically target the 3'-UTR of the *Hs2st* transcript and PCR was used to amplify the target region using essentially the same conditions described for *Hs6st1* genotyping (1 minute elongation steps instead of 30 seconds). The PCR product was visualized using 2% gel electrophoresis + SYBR Safe (Invitrogen) under UV light and the PCR product band excised and purified using the Qiagen gel extraction kit as per supplier instructions.

Table 5. **Primers used for the generation of an Hs2st specific riboprobe.**

Allele	Forward 5' Primer	Reverse 3' Primer	Product Size (bp)
Hs2st RNA riboprobe	5'TGTGAACGGCTTAT GCACTC3'	5'CTGTGACAGCGACTT TCCAA3'	678

The purified PCR product was then ligated into the pGEM T-easy plasmid (Promega) as per supplier instructions and cloned (See Section 2.4), then sequenced (MWG sequencing) to confirm its identity and its orientation within the plasmid. *Hs6st1*, *Hs6st2*, and *Hs6st3* RNA riboprobe plasmids were kindly provided by K. Izvolsky (Sedita et al., 2004) and *Slit1*, *Slit2*, *Robo1*, and *Robo2* RNA riboprobe plasmids were kindly provided by L. Erskine (Erskine et al., 2000). The RNA riboprobe plasmids were linearized using restriction endonucleases at either the 5' end or the 3' end of the riboprobe insertion site to produce either sense-riboprobes (control) or anti-sense riboprobes (Table 6).

Table 6. **Description of the RNA antisense riboprobes used for *in situ* hybridization.**

RNA Riboprobe	Plasmid	Restriction enzyme	Polymerase	Product Size (bp)
Hs2st	pGEM-T Easy	EcoRI	T7	~700
Hs6st1	pPCR-Script AMP SK+	EcoRI	T3	~900
Hs6st2	pPCR-Script AMP SK+	EcoRI	T3	~900
Hs6st3	pPCR-Script AMP SK+	EcoRI	T3	~900
Slit1	pBluescript	BamHI	T7	~800
Slit2	pBluescript	XbaI	T7	~1,600
Robo1	pBluescript S/K+	EcoRI	T7	~1,000
Robo2	pBluescript S/K+	NotI	T7	~1,700

DIG-labelled antisense RNA riboprobes were generated as follows; 1 µl of 1 µg/µl of the linearized plasmid was mixed with 2 µl 10X buffer, 1 µl 10X DIG RNA nucleotide labelling mix (Roche, Germany), 0.5 µl RNAsin (40 U/ µl) (Promega) and 1 µl of either T3, T7, or Sp6 (20 U/ µl) polymerase (Roche) to a final volume of 20 µl. The reaction mix was incubated for 4 hours at 37°C. 2 µl of Rnase free, Dnase I (Qiagen) was added and incubated at 37°C for 10 minutes and the reaction then stopped by adding 2 µl 0.2 M EDTA, pH 8. The RNA riboprobes were precipitated O/N at -20°C using 2.5 µl 4M LiCl and 75 µl chilled 100% EtOH. The RNA riboprobes were centrifuged at 13,000 rpm for 5 minutes, the supernatant discarded and the riboprobes were again precipitated as described above for an additional 4 hours to remove any remaining unincorporated nucleotides. The RNA riboprobes were centrifuged at 13,000 rpm for 5 minutes and the supernatant discarded. The

RNA riboprobes were then washed in 70% EtOH and centrifuged at 13,000 rpm for 1 minute, the supernatant discarded, and the RNA riboprobes were re-suspended in 100 µl ddH_2O and stored at -20°C.

2.7.3 Immunohistochemistry

2.7.3.1 Neurofilament immunohistochemistry

Heads were prepared and processed as outlined in section 2.6.2 for neurofilament immunohistochemistry. Sections were de-waxed in xylene and rehydrated through an alcohol series, between which, endogenous peroxidase activity was blocked using 3% hydrogen peroxide in 90% methanol. Sections were microwaved in 10 mM sodium citrate buffer, pH 6, to unmask antigens, incubated in blocking buffer (20% goat serum/0.1% Tx/PBS) and then reacted with anti-neurofilament antibody (rabbit-anti-mouse pan-neurofilament NA1297, (BioMol, International)) at a 1:200 dilution and incubated at 4°C overnight. Sections were then incubated in secondary antibody (biotinylated, polyclonal goat-anti-rabbit, E0432 (DakoCytamation) at a 1:200 dilution for 1 hour, followed by Avidin and Biotinylated horseradish peroxidase macromolecular Complex (ABC) (Vector Laboratories) for 1 hour. Sections were then stained with 3, 3'-diaminobenzidine (DAB) (Vector Laboratories), dehydrated through an alcohol series and mounted in DPX.

2.7.3.2 Haematoxylin staining

Sections were processed as described in 2.7.3.2; however sections were not mounted in DPX. The sections were then placed into filtered 1% Harris Haematoxylin for 1 minute. Sections were washed by placing them into a running water bath until the

water was clear. Sections were then dehydrated through an alcohol series and finally cleared in xylene. The sections were then mounted in DPX.

2.7.3.3 L1 immunohistochemistry

Heads were prepared and processed as outlined in section 2.6.1. For L1 immunohistochemistry, 200 µm vibratome sections or flat mounted retinas were permeabilized for 15 minutes at room temp in permeabilization solution (PBS/1% Tx). Sections were then blocked using blocking solution (PBS/0.5% Tx + 10% goat serum) for 30 minutes at room temp. Rat anti L1 primary antibody (Chemicon, MAB5272) (1:50 dilution in blocking solution) was added to the sections and then stored O/N at 4°C. Sections were washed several times in PBS and then Alexa 568 goat anti rat secondary antibody (Invitrogen) (1:200 dilution in blocking solution) + 0.2 µM TOPRO3 was added and stored O/N at 4°C. The sections were washed several times in PBS and sections were mounted in Vectashield hard set on glass slides (Vector Laboratories).

2.8 Axon tract tracing with DiI and/or DiA

Heads were fixed as described in section 2.6.1. 1,1'-dioctadecyl-3,3,3',3'-tetramethyl-indocarbocyanine perchlorate (DiI) crystals and/or 4-(4-dihexadecylamino)styryl-N-methylpyridinium iodide (DiA) crystals were placed in locations that would contact and label axons. For RGC axons, crystals were packed or focally injected into the exposed retina of one eye and allowed to diffuse at room temp for 6 weeks in 4% PFA/PBS. For TCA/CTA axons, crystals were focally injected into the most caudal region (V1 of the visual cortex) of the cortex or the exposed dorsal thalamus after a portion of the cortex was removed and left to diffuse at room temp for 6 weeks in 4% PFA/PBS. For callosal axons, crystals were focally injected into the cingulate cortex of coronally sectioned brains and left to diffuse for

8 days at 37°C in 4% PFA/PBS. Heads were then placed in a 4% low melting agarose/ddH_2O and 200 μm sections were cut using a vibratome. Sections were cleared in 1:1 glycerol:PBS overnight at 4°C, and then further cleared in 9:1 glycerol:PBS containing the nuclear counter-stain TOPRO3 (1 μl/ml) overnight at 4°C. Sections were mounted in 100 μl Vectashield on glass slides (prevents TOPRO3 photo-bleaching) and sealed with nail polish. Stored at 4°C until dry. Images were generated using both an epifluorescense microscope (with TRITC filter) with digital camera (Leica Microsystems, Germany) and a TCS NT confocal microscope (Leica Microsystems, Germany). Quantification of DiI back-labelled RGCs was done on serial sections by counting RGCs observed at x20 objective.

2.9 Microscopy

2.9.1 Light microscopy

Slides were viewed using a Leica DMLB upright compound microscope (Leica, Nussloch, Germany). Images were taken using an attached Leica DSC480 digital camera and the images processed using Leica IM50 image management software.

2.9.2 Fluorescence microscopy

Fluorescent staining was observed using a Leica DMRE compound microscope associated with the Leica TCS NT Confocal system using Leica "Lite" software to take images. DiI=red, DiA=green, TOPRO3=blue. Alternatively, fluorescent staining was viewed using epifluorescence on a Leica DMLB upright compound microscope with a TRITC filter. Images were taken using an attached Leica DSC480

digital camera and the images processed using Leica IM50 image management software. DiI=orange, DiA=green, TOPRO3=red.

2.10 Statistical analysis

Sigmastat (Systat Software Inc.) and Excel (Microsoft) were used for data analysis. Parametric tests were performed where the data met the assumptions of being normally distributed (assessed by Kolmogorov-Smirnov Normality Test) and the sample populations had equal variance (assessed by Equal Variance Test). The parametric Student's t-test was used when two sample populations were directly compared (α=0.05). We used one-way ANOVA for multiple sample populations followed by the Holm-Sidak *post hoc* method for multiple comparisons versus a control group (α determined by *post hoc* test). In the case that the data did not meet the above assumptions, the non-parametric Mann-Whitney test was used when two sample populations were directly compared. We performed the non-parametric Kruskal-Wallis one-way ANOVA on ranks followed by the Dunn's *post hoc* method for multiple comparisons versus a control group (α determined by *post hoc* test). It is important to note that non-parametric tests were favoured when sample numbers were less than 4 regardless of whether they passed Normality tests and equal variance tests. Chi-Squared analysis was used to test the distribution of sample populations (α=0.05).

Chapter 3: Expression Patterns of *Hs2st* and *Hs6st1* in the Developing Mouse Central Nervous System.

3.1 Introduction

HSPGs are found in the ECM and on the surface of a wide range of animal cells. They have been shown to be involved in a number of developmental processes by interacting with growth factors, morphogens, axon guidance cues, and a myriad of other molecules. These interactions are made possible, at least in part, by the different modifying enzymes that act on the GAG chains of HSPGs (Bernfield et al., 1999; Esko and Lindahl, 2001). Hs2st and Hs6st1 are HSPG modifying enzymes responsible for adding sulphate groups to the 2-O position of hexuronic acids and the 6-O position of *N*-acetylglucosamines that make up the GAG chain, respectively. The expression of these HSPG modifying enzymes are under strict temporal and spatial regulation allowing for a high degree of control during development (Sedita et al., 2004; Yabe et al., 2005).

Expression patterns of both *Hs2st* and *Hs6st1* have previously been reported using *in situ* hybridization and Q-RTPCR, showing both distinct and overlapping expression in many regions of the developing prenatal and postnatal mouse CNS (Sedita et al., 2004; Yabe et al., 2005). We previously described the expression patterns of *Hs2st*$^{+/LacZ}$ and *Hs6st1*$^{+/LacZ\_IRES\_hPLAP}$ at the optic chiasm and the retina of the E15.5 mouse brain using a LacZ reporter that was integrated into the *Hs2st* gene and the *Hs6st1* gene via a gene trap vector. Expression of *Hs2st* and *Hs6st1* was analyzed at E15.5 as this is the peak phase of RGC genesis and retinal axon growth through the optic chiasm (Table 1, Chapter 1). Expression patterns using the LacZ reporter showed that both *Hs2st* and *Hs6st1* were well placed to influence RGC axon navigation at the retina and the optic chiasm of the developing mouse visual system (Pratt et al., 2006).

While using the gene trap vector's LacZ reporter was a quick and efficient way of determining expression patterns it had its disadvantages. In order for the trapped genes expression to be known, one of the alleles must carry the gene trap, which introduces a mutation in that allele. This heterozygous mutation may alter *Hs2st* or *Hs6st1* at the level of transcription, post-transcription, translation, and/or post translation. In addition, this method of determining expression of a gene is not ideal for quantitative measurements. Furthermore, it is not possible to identify the expression pattern of more than one gene carrying a LacZ reporter as the expression patterns of the genes would be indistinguishable. Using other methods in addition to the LacZ reporter, such as *in situ* hybridization and Q-RTPCR to identify cells that express *Hs2st* and *Hs6st1*, it is possible to accurately characterize the expression patterns of these two genes.

3.2 Aims

To identify cells that express *Hs2st* and *Hs6st1*, we utilized two different approaches. Using direct methods to detect gene expression, we performed RNA *in situ* hybridization using RNA riboprobes specific to either *Hs2st* or *Hs6st1* and Q-RTPCR. Using an indirect method to detect gene expression, we took advantage of the $Hs2st^{+/LacZ}$ and $Hs6st1^{+/LacZ\_IRES\_hPLAP}$ mouse lines that carried the LacZ reporter. We aimed to map the expression patterns of *Hs2st* and *Hs6st1* in an effort to determine regions where these HSPG modifying enzymes might be important in embryonic development. Particular interest was directed to regions where RGC axons of the visual system navigate, including the retina and the optic chiasm at E15.5 and the dLGN and the SC at E16.5. E15.5 is the peak phase of RGC genesis and retinal axon growth through the optic chiasm. During this period the permanent ipsilateral RGC axon projection develops and the adult pattern of decussation is established. E16.5 marks the time point at which RGC axons start arriving at the SC and collateral branches start projecting into the dLGN (Table 1, Chapter 1). We also investigated the expression patterns of *Hs2st* and *Hs6st1* in regions where the

TCA/CTA and the corpus callosum tracts navigate to determine a possible role for *Hs2st* and *Hs6st1* in mediating their axon guidance. We looked at the expression patterns of *Hs2st* and *Hs6st1* at E16.5, a stage where TCA/CTA and callosal axons are navigating through key decision points along their mutual paths (Table 2-3, Chapter 1). Furthermore, using RNA *in situ* hybridization, we aimed to determine whether the *LacZ* reporters accurately recapitulate the actual expression patterns of *Hs2st* and *Hs6st1* in the developing mouse CNS.

3.3 Results

3.3.1 *Hs2st* expression in the eye and the optic chiasm

To begin to examine the possible mechanisms by which Hs2st sulphation may regulate RGC axon guidance we looked at the expression of *Hs2st* in the retina and the optic chiasm of E15.5 embryos; the key time point of RGC genesis and optic chiasm formation. RNA *in situ* hybridization showed that *Hs2st* was uniformly expressed throughout the RGC layer of the mouse retina as observed in 100 µm horizontal sections (Figure 1B). Using both RNA *in situ* hybridization on 100 µm horizontal sections (Figure 1C) and LacZ staining ($Hs2st^{LacZ/+}$) on 200 µm horizontal sections (Figure1D-F, images provided by E. Martin) we showed that *Hs2st* was expressed within the cells surrounding the optic nerve. The comparable expression results observed in both the LacZ staining and *in situ* hybridization techniques provided evidence that the LacZ reporter faithfully recapitulated the normal expression of *Hs2st* in the retina and at the optic chiasm. Expression of $Hs2st^{LacZ/+}$ was shown to be highest at the ventral diencephalon where the optic nerve first makes contact; the future site of the optic chiasm (Figure 1C-F) as well as distributed along the caudal midline of the ventral diencephalon particularly in the region of the hypothalamic neuroepithelium (hTN) (Figure 1D-E, dotted line). Using neurofilament immunohistochemistry to label axons we were able to show the close

association between the regions of *Hs2st*$^{LacZ/+}$ expression at the optic chiasm and the navigating RGC axons as they enter the region of the optic chiasm as observed in 200µm horizontal sections (Figure 1F). We performed Q-RTPCR on wild type E14.5 optic chiasm tissue (n=3) and retinal tissue (n=3) to determine both the presence and amount of *Hs2st* transcript. Results showed the presence of *Hs2st* transcript in both the retina and the optic chiasm of E14.5 embryos. The expression levels of *Hs2st* were normalized to the ubiquitously expressed housekeeping gene *GAPDH*, with the expression of *Hs2st* being significantly higher at the optic chiasm than in the retina (mean ± SEM) (Mann-Whitney rank sum test, $P<0.05$) (Figure 1G).

Figure 1. **Expression of *Hs2st* in the retina of the eye and at the site of optic chiasm formation in E15.5 embryos**. (A) Diagram representing the horizontal plane of section used to describe the expression patterns of *Hs2st* in the E15.5 mouse eye and (B) at the ventral diencephalon where the optic chiasm forms (C-F). (B) RNA *in situ* hybridization on 100 µm horizontal sections showed *Hs2st* expression (violet stain) in the RGC layer of the retina. (C) *Hs2st* was also shown to be expressed in the cells surrounding the optic nerve (ON) and in a distinct pattern at the ventral diencephalon; the future site of the optic chiasm. The pattern of expression at the ventral diencephalon was consistent with the region first encountered by RGC axons as they arrive at the ventral diencephalon where they decide whether to cross the midline (dotted line running rostral to caudal) and enter the contralateral optic tract (OT) or be repelled from the midline and enter the ipsilateral OT. (D-E) LacZ staining (blue stain) of 200 µm horizontal sections of E15.5 embryos using the LacZ reporter of $Hs2st^{LacZ/+}$ corroborated the pattern of expression of *Hs2st* as reported using RNA *in situ* hybridization. Also, *Hs2st* expression was shown along the caudal midline of the ventral diencephalon as well as the region of the hypothalamic neuroepithilium (hTN) (dotted line in D-E). (F) Using neurofilament immunohistochemistry (brown stain) to label axons we showed the close association of *Hs2st* expression ($Hs2st^{LacZ/+}$, blue stain) at the ventral diencephalon with the RGC axons that form the characteristic "X" structure of the optic chiasm (boxed area) as observed in 200 µm horizontal sections of E15.5 embryos. (G) Q-RTPCR revealed expression of *Hs2st* in both the retina (n=3) and the optic chiasm (n=3) of E14.5 embryos, with the expression of *Hs2st* being significantly higher at the optic chiasm than in the retina (mean ± SEM) (Mann-Whitney rank sum test, $P<0.05$). The expression levels of *Hs2st* were normalized to the ubiquitously expressed housekeeping gene *GAPDH*. RPE, retinal pigmented epithelium; NE, nasal epithelium; TGG, trigeminal ganglion; VT, ventro-temporal; DN, dorso-nasal; VD, ventral diencephalon. Scale bars: 200 µm B; 400 µm C-F.

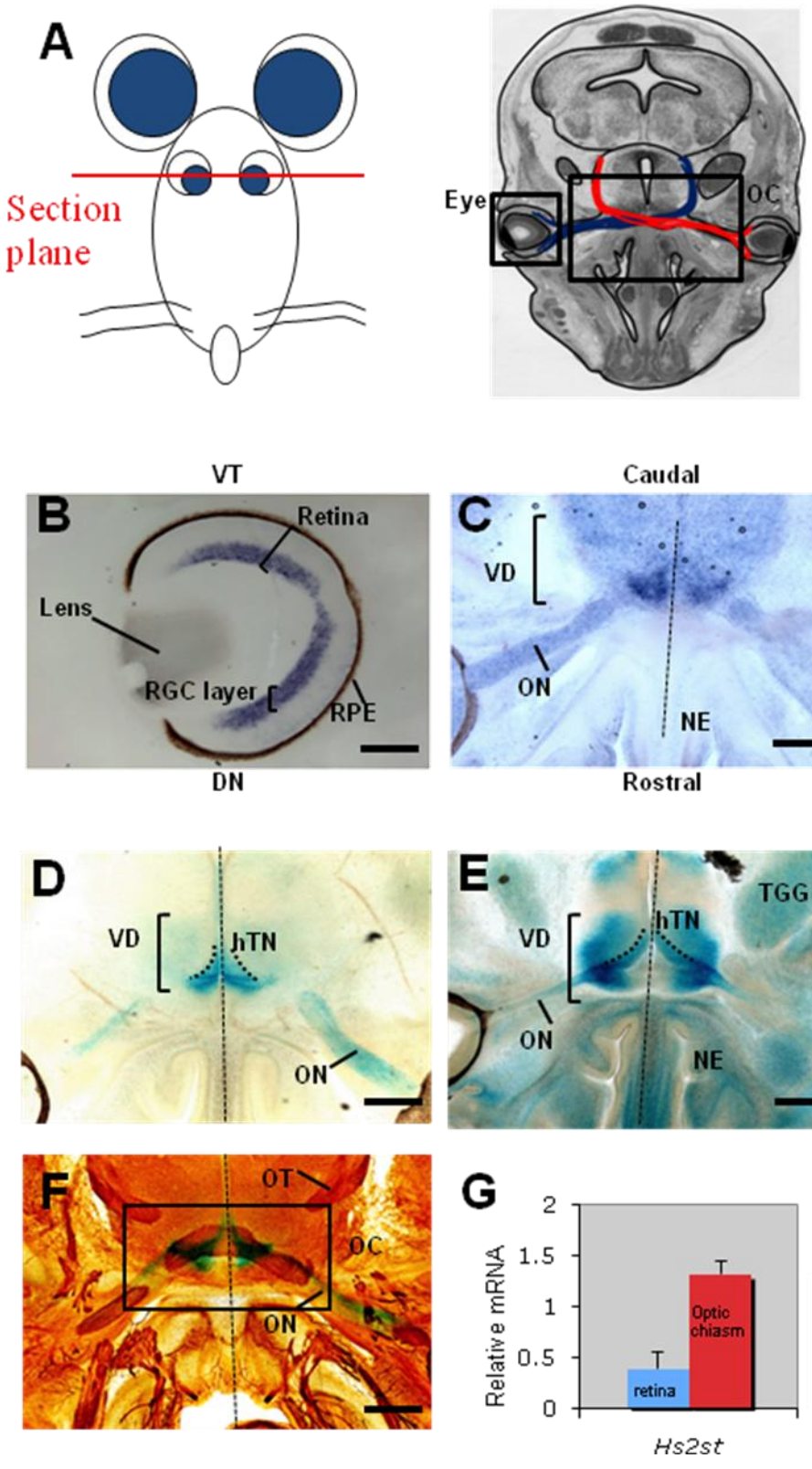
A
Section plane
Eye
OC
VT
Caudal
B
Retina
Lens
RGC layer
RPE
DN
C
VD
ON
NE
Rostral
D
VD
hTN
ON
E
TGG
VD
hTN
ON
NE
F
OT
OC
ON
G
Relative mRNA
2
1.5
1
0.5
0
retina
Optic chiasm
Hs2st

3.3.2 Expression of *Hs2st* in the thalamus and the SC as observed in sagittal sections.

We looked at *Hs2st* expression in other regions encountered by navigating RGC axons including both the dorsal thalamus and the superior colliculus, both major targets for RGC axon innervation. Using LacZ staining ($Hs2st^{LacZ/+}$) on 200 µm sagittal sections of E16.5 embryos we characterized the expression of *Hs2st* (Figure 2B-D). E16.5 is the time point at which RGC axons start projecting collaterals towards the dLGN. *Hs2st* expression was observed within the hypothalamus and ventral thalamus (Figure 2C), with particularly high expression around the fasciculated optic tract (Figure 2D). The relatively high expression in the ventral thalamus was in stark contrast to the low expression observed in the dorsal thalamus (Figure 2C-D). The dLGN of the dorsal thalamus, a major target for approximately 1/3 of all RGC axons in mice, showed little *Hs2st* expression. Observations of *Hs2st* expression in sagittal sections also revealed expression in the SC (major target for all navigating RGC axons) (Figure 2B). Expression of *Hs2st* was evident in the epithalamus; a site RGC axons are normally repelled from (Figure 2C). High *Hs2st* expression was observed in the developing cortex (Figure 2B) and has previously been described in detail (McLaughlin et al., 2003a).

Figure 2. **Expression of *Hs2st* in regions encountered by RGC axons as they navigate from the optic chiasm to the SC of E16.5 embryos**. (A) Diagram representing the sagittal plane of section used to describe the expression patterns of *Hs2st* in the E16.5 mouse brain. The optic tracts project dorsally from the optic chiasm over the surface of the hypothalamus and ventral thalamus in a tightly bundled organization before spreading out over the surface of the dorsal thalamus; the dLGN is located within the dorsal thalamus and is a major target for RGC axons that produce collaterals for innervation. RGC axons are re-organized into a tight bundle as they leave the region of the dLGN and are directed caudally avoiding the epithalamus and navigating towards the superior colliculus; a final target for all RGC axons. (B) LacZ staining (blue color) on 200 µm sagittal sections revealed highest $Hs2st^{+/LacZ}$ expression in the cortex and the superior colliculus (SC). (C) While *Hs2st* expression was observed in the ventral thalamus (VT) and epithalamus (epiT), virtually no *Hs2st* expression was observed in the dorsal thalamus (DT). (D) *Hs2st* was strongly expressed within the cells surrounding the optic tract (OT) as they navigate over the surface of the hypothalamus (HypoT). *Hs2st* was also expressed in the cortex and the SC (A). Scale bars: 1000 µm B; 400 µm C-D.

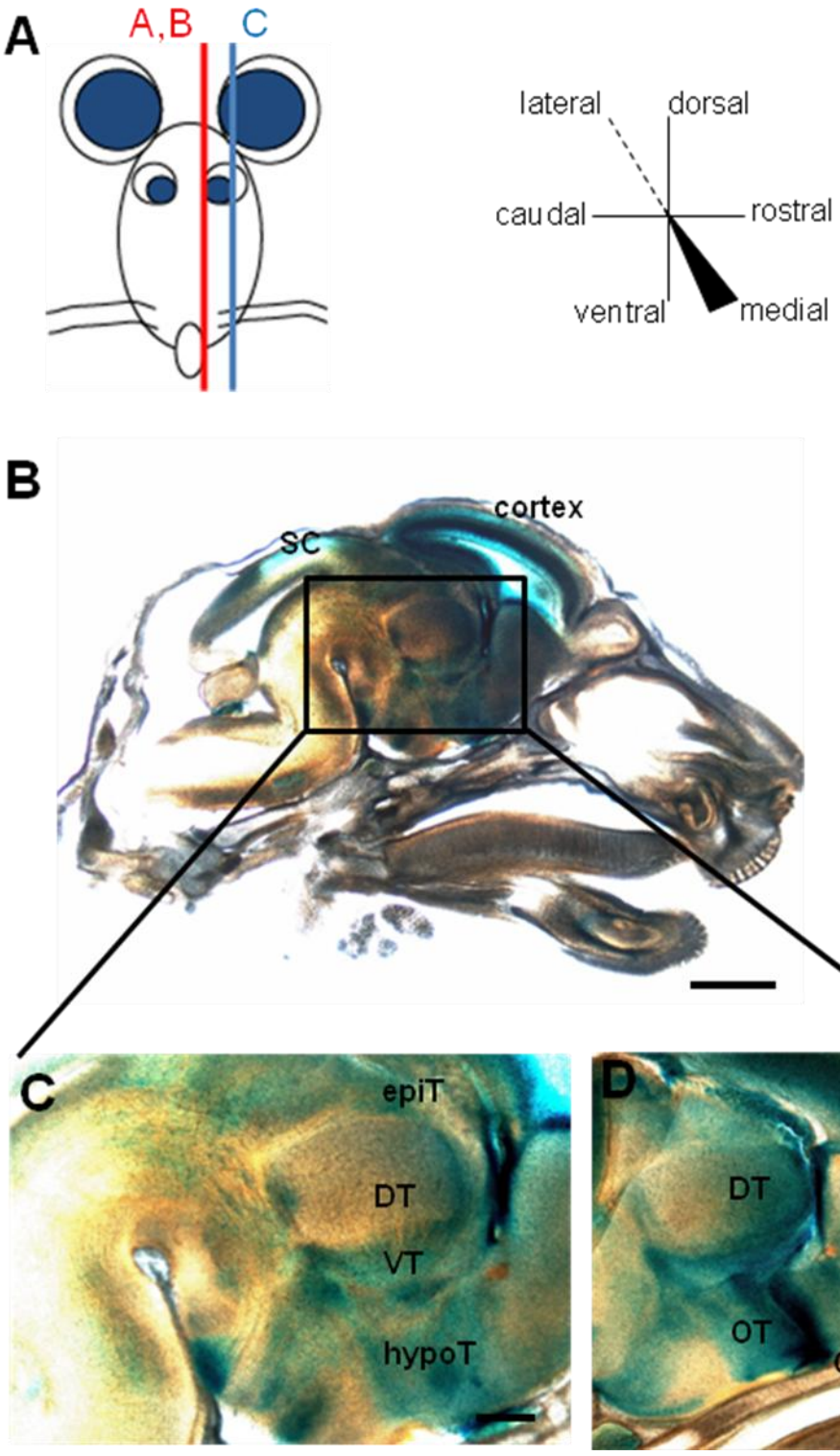
A
A,B
C
lateral
dorsal
caudal
rostral
ventral
medial
B
cortex
SC
C
epiT
DT
VT
hypoT
D
DT
OT
OC

3.3.3 Expression of *Hs2st* in the thalamus and cortex as observed in coronal sections.

The thalamus is a region of the diencephalon that can be anatomically and functionally regionalized into the ventral and dorsal thalamus (Rubenstein and Beachy, 1998). The ventral and dorsal thalamus can be further regionalized into histologically distinct nuclei at postnatal ages based primarily on gene expression and TCA:CTA targeting and/or origin (Nakagawa and O'Leary, 2001). This distinction becomes exceedingly difficult at earlier stages of development. However it is possible to broadly identify domains using anatomical structures such as the TCA tract as well as the medullary lamina which runs between the vLGN and the dLGN. Using LacZ staining (*Hs2st*$^{LacZ/+}$) we looked at regions of *Hs2st* expression in E16.5 mouse embryos in 200 µm coronal sections. E16.5 is a stage where TCA/CTA axons are navigating through key decision points along their mutual paths. Using neurofilament immunohistochemistry to label axons, we were able to observe the TCA/CTA tracts to determine whether these navigating axons encountered regions where *Hs2st* is expressed. *Hs2st* was shown to be expressed along the dorsal midline as well as in distinct regions of the hypothalamus, epithalamus and cortex (Figure 3B); reconfirming the *Hs2st* expression patterns observed in E16.5 sagittal sections (Figure 2). While *Hs2st* was shown to be expressed within the ventral thalamus, the dorsal thalamus had very little *Hs2st* expression with the exception of the vLGN (Figure 3B). Along the path of navigating TCA/CTA tracts, *Hs2st* expression overall was observed to be low. There was some *Hs2st* expression within the striatum, a site where the TCA/CTA tracts defasciculate, however the highest expression was observed in the cerebral cortex (Figure 3B). The *Hs2st* expression observed in the cerebral cortex was consistent with the patterns previously published (McLaughlin, et al., 2003).

Figure 3. **Expression of *Hs2st* in regions encountered by thalamocortical and corticothalamic axons as they navigate between the thalamus and the cortex of E16.5 embryos**. (A) Diagram representing the coronal plane of section used to describe the expression patterns of *Hs2st* in the E16.5 mouse brain. Thalamocortical axons (TCAs) originating in the dorsal thalamus (dT) and their reciprocal corticothalamic axons (CTAs) originating in the cortex project their axons through a number of emerging boundaries including the diencephalic/telencephalic boundary (DTB) and the pallial/sub-pallial boundary (PSPB) to reach their eventual targets in the cortex and dT, respectively. Using neurofilament immunohistochemistry to label axons (brown stain) we showed the association of regions expressing *Hs2st* with the route TCAs/CTAs take in the developing CNS at E16.5. (B) LacZ staining (blue stain) on 200 µm coronal sections showed $Hs2st^{+/LacZ}$ expression in both the hypothalamus (hypoT) and the epithalamus (epiT). Within the dorsal thalamus (dT), *Hs2st* expression was only observed in the presumptive vLGN, however this a region avoided by TCAs/CTAs. Expression of *Hs2st* was also observed dorso-medial to the PSPB within the striatum (stm). *Hs2st* was highly expressed within the ventricular zone of the cortex. CP, choroid plexus; VZ, ventricular zone. Scale bars: 400 µm B.

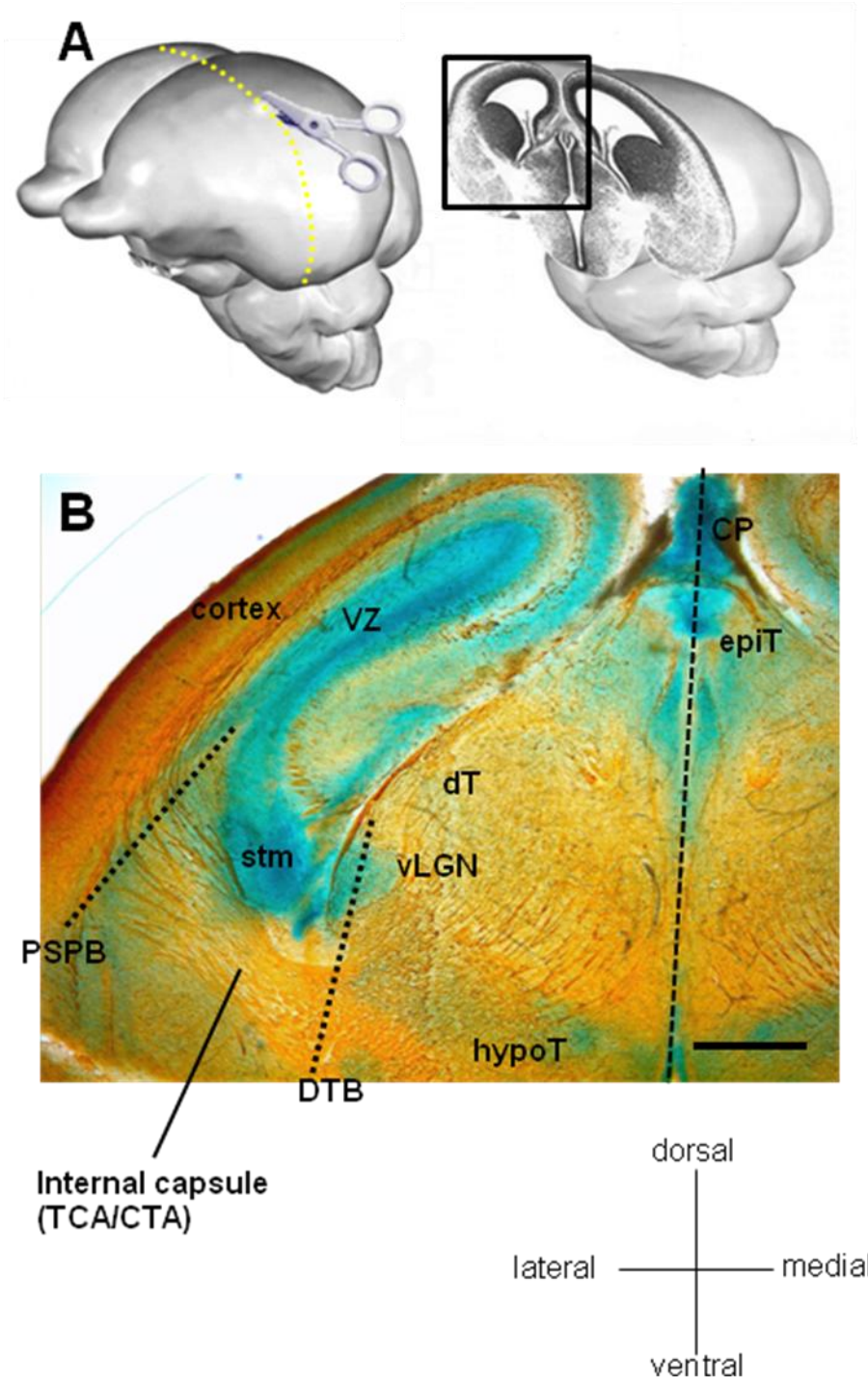
A
B
CP
cortex
VZ
epiT
dT
stm
vLGN
PSPB
hypoT
DTB
Internal capsule
(TCA/CTA)
dorsal
lateral
medial
ventral

3.3.4 Expression of *Hs6st1* in the eye and at the optic chiasm.

To determine the expression pattern of *Hs6st1* we used a combination of LacZ staining (*Hs6st1*$^{+/LacZ\_IRES\_hPLAP}$) and/or RNA *in situ* hybridization. *Hs6st1* expression was characterized in the eye and at the optic chiasm using horizontal sections of E15.5 embryos; the key time point of RGC genesis and optic chiasm formation. RNA *in situ* hybridization revealed expression of *Hs6st1* to be specifically and uniformly present in the RGC layer of the retina as observed in 100 µm sections (Figure 4B). There was *Hs6st1* expression around the optic nerve located at the region just after the optic nerve leaves the eye, but was not expressed along the full length of the optic nerve (Figure 4B-D). The optic chiasm showed a distinct pattern of *Hs6st1* expression as observed using both LacZ staining of 200 µm horizontal sections (Figure 4F-G, images provided by E. Martin) and RNA *in situ* hybridization of 100 µm horizontal sections (Figure 4C-E). These techniques produced the same results for *Hs6st1* expression confirming that the LacZ reporter faithfully recapitulated the normal expression of *Hs6st1* as determined using *in situ* hybridization. *Hs6st1* expression was particularly strong at the optic nerve-optic chiasm border where RGC axons are observed to defasciculate and enter the region of the optic chiasm (Figure 4C-D, F-G). The regions surrounding the optic chiasm including the caudal diencephalon lateral to the midline and the region rostral to the diencephalon at the midline of the pre-optic area showed high expression of *Hs6st1* (Figure 4C-G). Using neurofilament immunohistochemistry to label axons, we were able to show the close relationship between the navigating RGC axons and the distinct pattern of *Hs6st1* expression at the optic chiasm (Figure 4G). We performed Q-RTPCR on wild type E14.5 optic chiasm tissue (n=3) and retinal tissue (n=3) to determine both the presence and amount of *Hs6st1* transcript. Results showed the presence of *Hs6st1* transcript in both the retina and the optic chiasm of E14.5 embryos. The expression levels of *Hs6st1* were normalized to the ubiquitously expressed housekeeping gene *GAPDH*, with the expression of *Hs6st1* being significantly higher at the optic chiasm than in the retina (mean ± SEM) (Mann-Whitney rank sum test $P<0.05$) (Figure 4H).

Figure 4. **Expression of *Hs6st1* in the retina of the eye and at the site of optic chiasm formation in E15.5 embryos**. (A) Diagram representing the horizontal plane of section used to describe the expression patterns of *Hs6st1* in the E15.5 mouse eye and at the ventral diencephalon where the optic chiasm forms. (B) RNA *in situ* hybridization on 100 µm horizontal sections showed high *Hs6st1* expression (violet stain) in the RGC layer of the retina, the lens, and in a population of cells surrounding the most proximal region of the ON closest to the eye. (C-E) Using three adjacent 100 µm horizontal sections (ventral to dorsal: C to E) from the same embryo, *Hs6st1* was shown to be expressed in a distinct pattern within the ventral diencephalon with relatively high expression in the pre-optic area (POA), rostral to the 3rd ventricle (3V). The surface of the ventral diencephalon is the site where the optic chiasm (OC) forms. (F-G) LacZ staining (blue stain) of 200 µm horizontal sections of E15.5 embryos using the LacZ reporter of *Hs6st1*$^{+/LacZ\_IRES\_hPLAP}$ corroborated the expression of *Hs6st1* at the ventral diencephalon as observed by RNA *in situ* hybridization. *Hs6st1* expression was particularly strong at the region where the optic nerve first makes contact with the ventral diencephalon. Hs6st1 expression was also observed in the caudal diencephalon lateral to the midline and the region rostral to the diencephalon at the midline of the POA. (G) Using neurofilament immunohistochemistry to label axons (brown stain) we showed the close association of *Hs6st1* expression in *Hs6st1*$^{+/LacZ\_IRES\_hPLAP}$ in 200 µm horizontal sections at the ventral diencephalon with the RGC axons that form the characteristic "X" structure of the OC in E15.5 embryos. (H) Q-RTPCR revealed expression of *Hs6st1* in both the retina and the optic chiasm of E14.5 embryos, with the expression of *Hs6st1* being significantly higher at the optic chiasm (n=3) than in the retina (n=3) (mean ± SEM) (Mann-Whitney rank sum test $P<0.05$). The expression levels of *Hs6st1* were normalized to the ubiquitously expressed housekeeping gene *GAPDH*. RPE, retinal pigmented epithelium; TGG, trigeminal ganglion; NE, nasal epithelium; VT, ventro-temporal; DN, dorso-nasal. Scale bars: 200 µm B, G; 400 µm C-F.

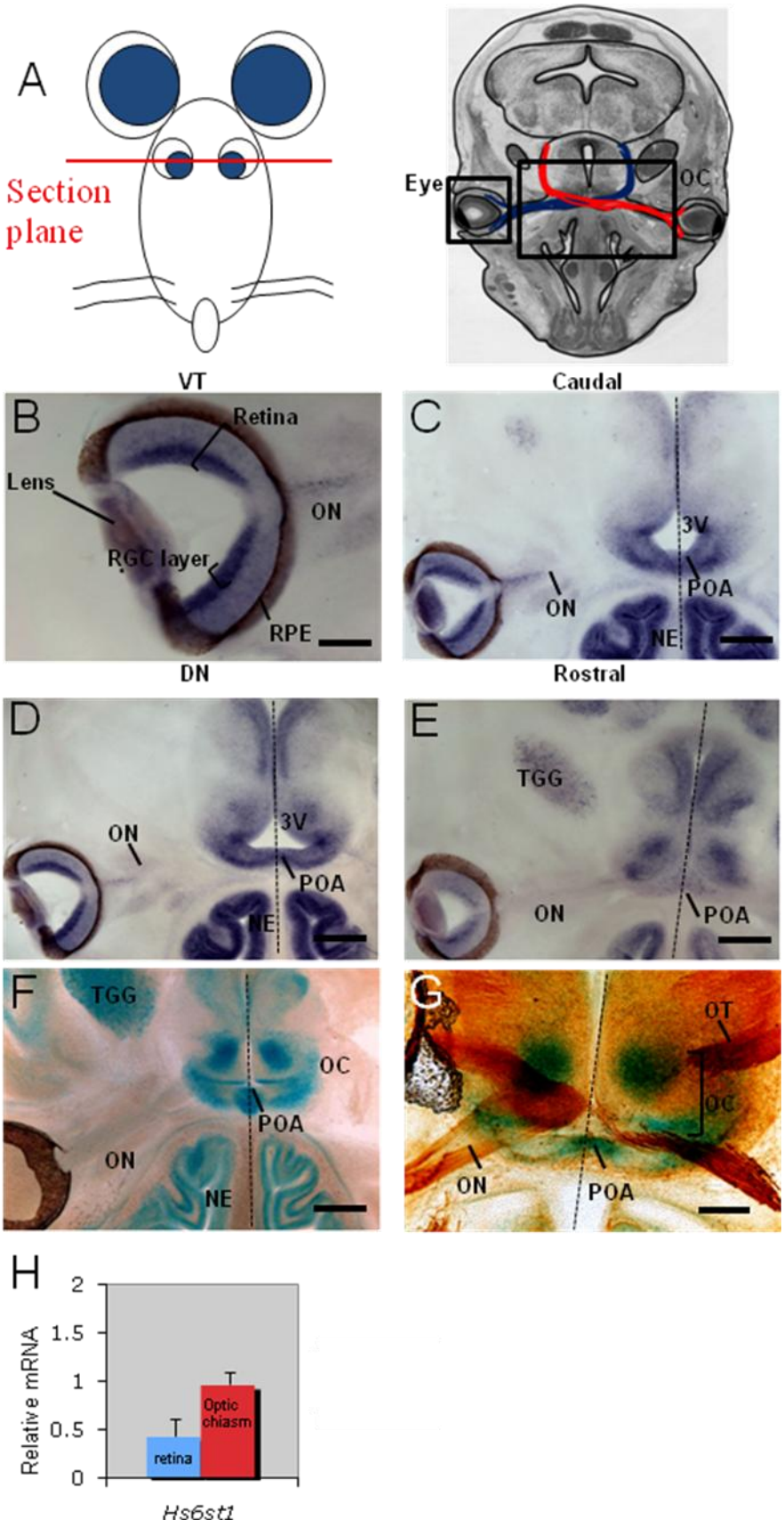
A
Section plane
VT
Eye
OC
Caudal
B
Retina
Lens
ON
RGC layer
RPE
DN
C
3V
POA
ON
NE
Rostral
D
ON
3V
POA
NE
E
TGG
ON
POA
F
TGG
OC
POA
ON
NE
G
OT
OC
ON
POA
H
Relative mRNA
2
1.5
1
0.5
0
retina
Optic chiasm
Hs6st1

3.3.5 Expression of *Hs6st1* in the thalamus and the SC as observed in sagittal sections.

Using LacZ staining (*Hs6st1*$^{+/LacZ\_IRES\_hPLAP}$) on 200 µm sagittal sections of E16.5 embryonic brains, we observed *Hs6st1* expression patterns at the hypothalamus, thalamus and superior colliculus; all key anatomical environments that RGC axons navigate through (Figure 5B-D). E16.5 is the time point at which RGC axons start projecting collaterals towards the dLGN. Examination of the *Hs6st1* expression patterns revealed high expression in the dorsal thalamus as well as the epithalamus (Figure 5D). The high expression of *Hs6st1* at the dorsal thalamus was coincident with the site of defasciculation and innervation of RGC axons into the dLGN. The pattern of *Hs6st1* expression was particularly interesting at the SC (Figure 5C). Strong *Hs6st1* expression was observed in both the superficial and deep layers of the SC. Within the differentiating fields of the SC, *Hs6st1* expression was less intense and absent in the superior tectal neuroepithilium. Collectively, *Hs6st1* expression was shown to have a high dorsal to low ventral gradient within the SC. *Hs6st1* expression was observed in more caudal regions of the midbrain as evidenced in the inferior tectal neuroepithilium of the inferior colliculus. There was a high rostral to low caudal gradient within the SC (Figure 5C). An *Hs6st1* expression gradient was also observed in the outer layer of the cortex with relatively high expression laterally and less expression medially (data not shown). These *Hs6st1* expression patterns may establish a link to retino-tectal mapping of RGC axons as they project towards their targets in the SC and/or TCA/CTA mapping.

Figure 5. **Expression of *Hs6st1* in regions encountered by RGC axons as they navigate from the optic chiasm to the SC of E16.5 embryos**. (A) Diagram representing the sagittal plane of section used to describe the expression patterns of *Hs6st1* in the E16.5 mouse brain. The optic chiasm forms on the ventral surface of the hypothalamus. The optic tracts project dorsally from the optic chiasm over the surface of the hypothalamus and ventral thalamus in a tightly bundled organization before spreading out over the surface of the dorsal thalamus; the dLGN is located within the dorsal thalamus and is a major target for RGC axons that produce collaterals for innervation into the dLGN. RGC axons are re-organized into a tight bundle and directed caudally avoiding the epithalamus and navigating towards the superior colliculus; a final target for all RGC axons. (B) LacZ staining (blue stain) on 200 µm sagittal sections showed high *Hs6st1*$^{+/LacZ\_IRES\_hPLAP}$ expression at the dorsal thalamus (DT), the epithalamus (EpiT), and in the superior colliculus. (C) Differential expression in the layers of the superior colliculus (SC) generated an expression gradient; high dorsal to low ventral and high rostral to low caudal. Some *Hs6st1* expression was also evident in the hypothalamus (HypoT) and the cortex (D). Scale bars: 1000 µm B; 100 µm C; 400 µm D.

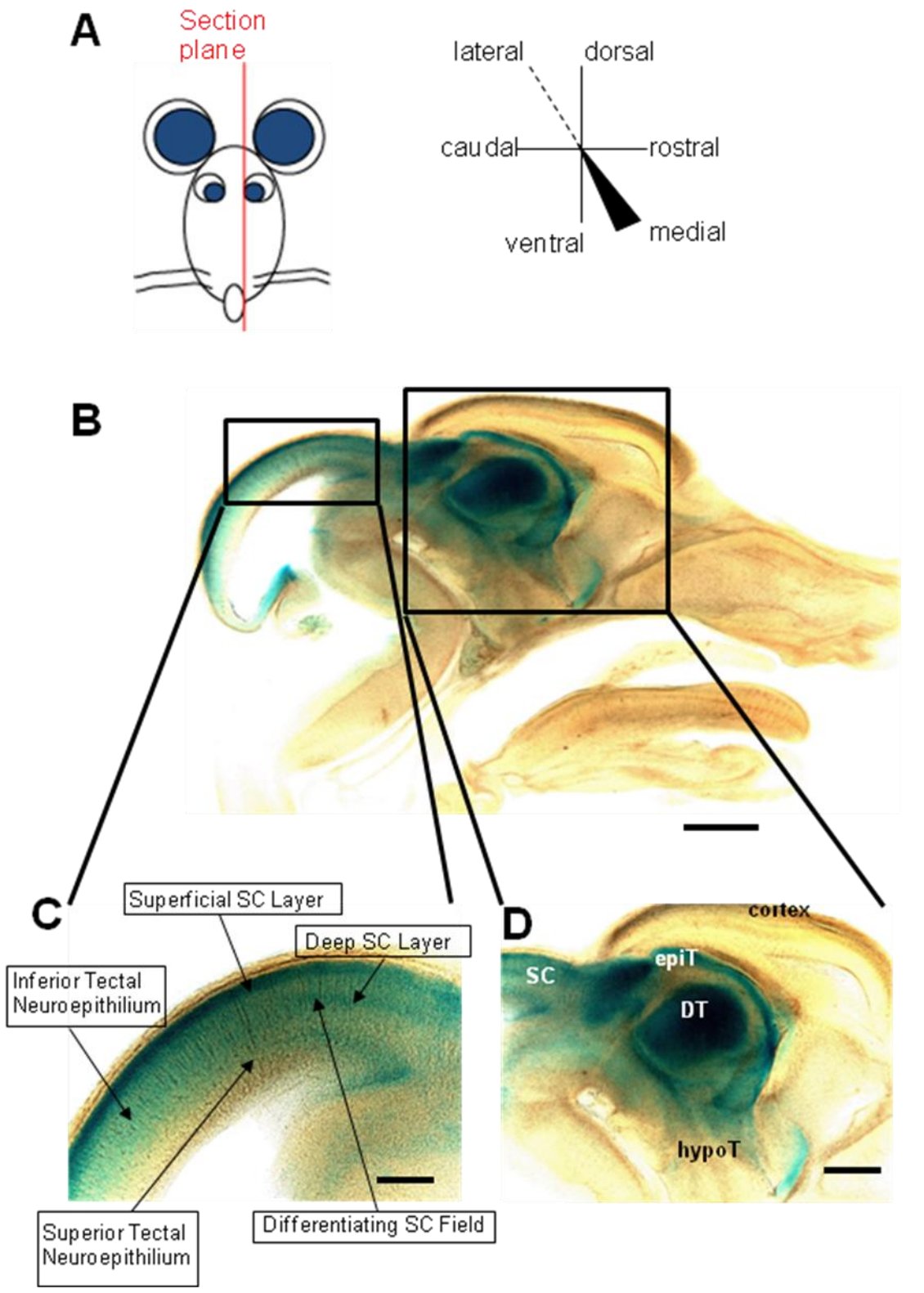
A
Section plane
lateral
dorsal
caudal
rostral
ventral
medial
B
C
Superficial SC Layer
Deep SC Layer
Inferior Tectal Neuroepithilium
Superior Tectal Neuroepithilium
Differentiating SC Field
D
cortex
epiT
SC
DT
hypoT

3.3.6 *Hs6st1* expression in the thalamus and cortex as observed in coronal sections.

RNA *in situ* hybridization on E16.5 mouse embryos revealed high *Hs6st1* expression in the dorsal thalamus, the epithalamus, along the midline of the brain, and in the cortex as observed in 100 µm coronal sections (Figure 6B-C). E16.5 is a stage where TCA/CTA axons are navigating through key decision points along their mutual paths. Observations of LacZ stained 200 µm coronal sections of E16.5 mouse embryos indicated relatively high *Hs6st1*$^{+/LacZ\_IRES\_hPLAP}$ expression within the developing mouse brain particularly in the region of the dorsal thalamus and the midline (Figure 6D). The expression of *Hs6st1* appeared to be highest at the dLGN. *Hs6st1* expression was also evident in the vLGN as well as other distinct regions of the dorsal thalamus (possibly corresponding to a number of presumptive thalamic nuclei) (Figure 6D-E). The path of the TCA/CTA tracts was identified using neurofilament immunohistochemistry (Figure 6D). The striatum showed *Hs6st1* expression consistent with the site TCA/CTA tracts defasciculate before entering/exiting the cortex, respectively (Figure 6C-D). While *Hs6st1* appeared to be expressed throughout the superficial layers of the cortex, the highest expression appeared to be in the cortical plate (CP) and the intermediate zone (IZ) (Figure 6D, arrows).

Figure 6. **Expression of *Hs6st1* in regions encountered by thalamocortical and corticothalamic axons as they navigate between the thalamus and the cortex of E16.5 embryos**. (A) Diagram representing the coronal plane of section used to describe the expression patterns of *Hs6st1* in the E16.5 mouse brain. RNA *In situ* hybridization (violet stain) on 100 µm coronal sections (B-C) and LacZ staining (blue stain) on 200 µm coronal sections (D-E) showed high *Hs6st1*$^{+/LacZ\_IRES\_hPLAP}$ expression in the dorsal thalamus (DT) and along the midline. Within the dorsal thalamus (dT), *Hs6st1* expression was observed in the vLGN and highly in the dLGN (E). Expression of *Hs6st1*was also observed in the striatum (stm), the epithalamus (epiT), as well as in the cortex. *Hs6st1* was specifically expressed in the intermediate zone (IZ) and the cortical plate (CP) of the cortex (C). Using neurofilament immunohistochemistry to label axons we showed the association of regions expressing *Hs6st1* with the TCA/CTA tract. EpiT, epithalamus. Scale bars: 400 µm B-D; 100 µm E.

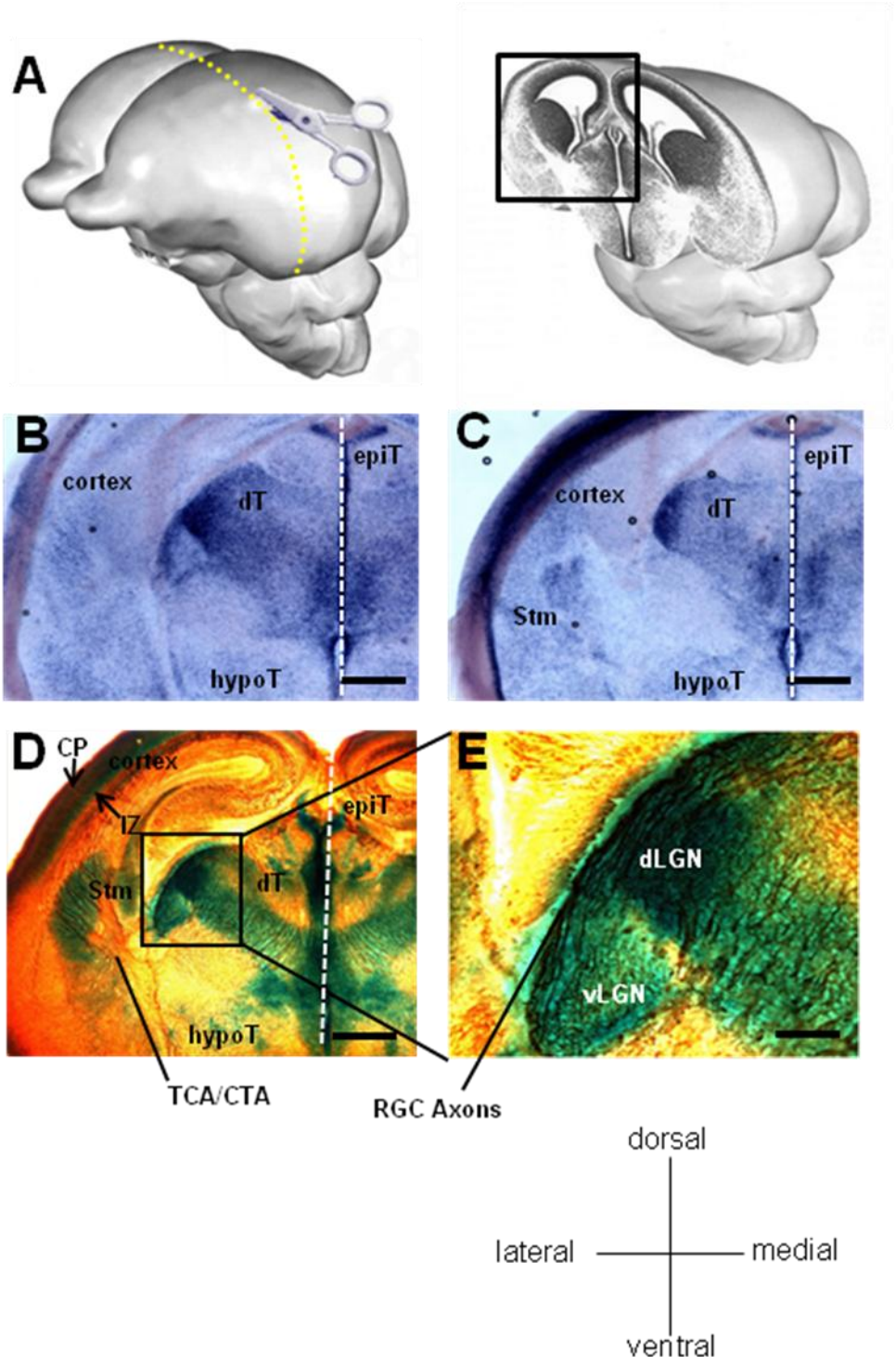
A
B
cortex
dT
epiT
hypoT
C
cortex
dT
epiT
Stm
hypoT
D
CP
cortex
IZ
epiT
Stm
dT
hypoT
TCA/CTA
E
dLGN
vLGN
RGC Axons
dorsal
lateral
medial
ventral

3.4 Discussion

HSPG sulphation has been shown to be critical to the normal development of many model organisms (Bulow and Hobert, 2006). In addition to mediating many critical developmental events through their interactions with morphogenic factors (Perrimon and Bernfield, 2000; Lin, 2004), HSPGs have been shown to be important in the development of axonal tracts in the developing mouse CNS (Lee and Chien, 2004; Hacker et al., 2005). We investigated the expression patterns of *Hs2st* and *Hs6st1* to determine regions where these genes may be important in development, particularly in regions where major axonal tracts must navigate through.

3.4.1 *Hs2st* is expressed at key choice points along the path of navigating RGC axons.

We previously showed the expression of *Hs2st* in the RGC layer and at the optic chiasm using a LacZ reporter (Pratt et al., 2006) and more recently, were able to re-confirm these expression patterns using RNA *in situ* hybridization in the embryonic mouse brain. Based on the identical expression patterns observed using these two different techniques, we were able to confirm the efficacy of the LacZ reporter as accurately reporting *Hs2st* expression in the developing mouse brain. The expression of *Hs2st* specifically in the RGC layer indicated a possible cell autonomous requirement for RGC axon navigation however, to complicate matters, *Hs2st* was also observed to be expressed in regions of the optic chiasm pointing to the possibility of a cell non-autonomous requirement for RGC axon navigation at this key choice point.

Interestingly, *Hs2st* expression was observed to be highest along the length of the optic nerve and along the length of the optic tract coincident with the tight bundling of RGC axons. The expression pattern of *Hs2st* suggests a possible role in RGC axon-axon interactions keeping them in close proximity to one another. This

hypothesis was consistent with the observation that RGC axons defasciculated at the dLGN, a region almost completely lacking *Hs2st* expression. The expression of *Hs2st* in the epithalamus may indicate a role in RGC axon guidance as this is a site where RGC axons are repelled from. Overall, the spatiotemporal distribution of *Hs2st* expression was shown to coincide with key choice points responsible for directing RGC axons from their site of origin in the retina to their targets in the dLGN and SC.

3.4.2 Expression of *Hs2st* indicates a possible role in directing TCA/CTA navigation in the developing mouse CNS

Our observations of the expression pattern of *Hs2st* along the path of the TCA/CTA tracts as well as previously published findings (McLaughlin et al., 2003a) revealed high expression in the ventricular zone and cortical plate of the cortex, a target and origin for TCA/CTA, respectively. This high *Hs2st* expression was in stark contrast to the low expression of *Hs2st* in the dorsal thalamus, an origin and target for TCA/CTA, respectively. It is possible that the requirement for Hs2st sulphation dictates axon guidance in this system as its spatiotemporal expression pattern is consistent with the time and place the TCA/CTA tracts develop in the mouse CNS.

3.4.3 Expression of *Hs6st1* indicates a possible role in RGC axon guidance at key choice points in the developing mouse CNS.

We previously showed the expression of *Hs6st1* in the RGC layer of the retina and at the optic chiasm using a LacZ reporter (Pratt et al., 2006) and more recently, were able to re-confirm these expression patterns using RNA *in situ* hybridization in the embryonic mouse brain. Based on the identical expression patterns observed using these two different techniques, we were able to confirm the efficacy of the LacZ

reporter as accurately reporting *Hs6st1* expression in the developing mouse brain. *Hs6st1* expression was observed at a place and a time when RGC axons navigate from the retina of the eye to the optic chiasm. Whether *Hs6st1* is required cell autonomously and/or cell non-autonomously in the guidance of RGC axons would be an interesting avenue of research. Observations of other regions where RGC axons navigate suggested an important role for Hs6st1 sulphation. The high expression of *Hs6st1* at the dLGN was consistent with this particular sulphation pattern being a possible factor in the defasciculation of the optic tract and/or the formation of collaterals for dLGN innervation by the RGC axons. In fact, the expression of *Hs6st1* within the dLGN appeared to be the highest region of expression in the developing mouse brain and may be an indication of its importance in this region; however Q-RTPCR must be performed before we can confirm this observation.

3.4.4 Expression of *Hs6st1* indicates a possible role in directing TCA/CTA navigation in the developing mouse CNS.

Our observations of the expression pattern of *Hs6st1* along the path of the TCA/CTA tracts revealed high expression in the cortical plate and the intermediate zone of the cortex as well as the striatum and regions of the dorsal thalamus. The expression patterns for *Hs6st1* in the cortex were inconsistent with previously published results where it was shown that *Hs6st1* was not expressed in the E16.5 cortex (Yabe et al., 2005). This may have been due to genetic background effects or the methods used to detect *Hs6st1* transcripts. The high *Hs6st1* expression in the dLGN indicates a possible role in the development of the visual system as this is the thalamic nucleus that integrates visual information with the visual cortex via the TCA/CTA tract. It is possible that the requirement for Hs6st1 sulphation dictates axon guidance in this system as its spatiotemporal expression pattern is consistent with the time and place the TCA/CTA tracts develop in the mouse CNS.

3.4.5 *Hs2st* and *Hs6st1* have both overlapping and non-overlapping patterns of expression in the developing mouse brain.

The *Hs2st* and *Hs6st1* expression patterns observed in the developing mouse CNS suggest that the patterns of HSPG sulphation are highly diverse. Within the developing mouse visual system we showed that both *Hs2st* and *Hs6st1* are co-expressed within the RGC layer of the retina. Expression of *Hs2st* and *Hs6st1* at the optic chiasm showed both regions of co-expression as well as regions of differential expression, suggesting the possibility that Hs2st sulphation and Hs6st1 sulphation have both unique functions as well as cooperative functions at the optic chiasm. While Hs2st sulphation appears to be important for RGC axon fasciculation along the optic nerves and optic tracts, Hs6st1 sulphation appears to be important for RGC axon defasciculation at the dLGN. Using mutant animals that lack Hs2st sulphation and/or Hs6st1 sulphation we plan to characterize the unique and/or redundant functions these sulphation patterns may have on axon guidance.

3.5 Summary

The dynamic expression patterns observed for *Hs2st* and *Hs6st1* indicate a possible role in the development of the mouse CNS and in particular the guidance of axons within the visual system and TCA/CTA tracts. The fact *Hs2st* and *Hs6st1* show both overlapping and non-overlapping expression patterns may suggest that the combination of these sulphation patterns dictate different aspects of axon guidance within these systems in agreement with a "heparan sulphate code". Observations of the axon guidance trajectories in the absence of *Hs2st* and/or *Hs6st1* will provide insight into their roles as possible factors in axon guidance in the developing mouse CNS.

Chapter 4: Characterization of the *Hs2st and Hs6st1*-Gene Trap Alleles.

4.1 Introduction

To define the roles both Hs2st and Hs6st1 have on axon guidance in the developing mouse CNS, we used knockouts that had been engineered using a gene trapping approach (Skarnes et al., 1995; Bullock et al., 1998; Leighton et al., 2001; Mitchell et al., 2001). Gene trapping of *Hs2st* and *Hs6st1* involved the non-targeted insertion of a gene trap vector into one of the introns of either *Hs2st* or *Hs6st1* gene creating a gene fusion. Gene trap insertions disrupt the function of the endogenous gene and place the gene trap under the control of either the *Hs2st* or *Hs6st1* promoter.

The random insertion of a gene trap vector was initially carried out in embryonic stem (ES) cells and subsequent screening using 5'-RACE identified two different lines carrying a gene trap in either the *Hs2st* gene (*Hs2st*$^{+/-}$) or *Hs6st1* gene (*Hs6st1*$^{+/-}$). These ES cells were then used to create chimeric embryos and germ-line mice. The gene trap vector used to disrupt *Hs2st* contained the bicistronic β-geo (β-galactosidase fused to neomycin phosphotransferase) reporter (*Hs2st*$^{+/LacZ}$) (Bullock et al., 1998) while the gene trap vector used to disrupt *Hs6st1* contained the bicistronic β-geo and the human placental alkaline phosphatase (hPLAP) reporter genes which was under the control of an internal ribosome entry site (IRES) (*Hs6st1*$^{+/LacZ\_IRES\_hPLAP}$) (Leighton et al., 2001; Mitchell et al., 2001).

Full characterization of the *Hs2st*$^{+/LacZ}$ allele had previously been described and showed gene trap integration into intron 4, which resulted in a truncated version of the *Hs2st* transcript (Bullock et al., 1998). *Hs2st* genotype was determined using PCR and involved a primer pair flanking the site of gene trap insertion as well as one reverse (3'-5') primer targeting the 5'region of the gene trap (Figure 1A). *Hs2st*$^{-/-}$

mutant animals died shortly after birth as a result of kidney agenesis (Bullock et al., 1998).

Previous work had described a mouse line that harboured an *Hs6st1*$^{+/LacZ\_IRES\_hPLAP}$ allele (Leighton et al., 2001; Mitchell et al., 2001), however full characterization of the gene trap insertion site into the *Hs6st1* gene was not reported so it was initially impossible to genotype embryos using the traditional PCR method used for *Hs2st* genotyping. Because of the random nature of gene trap insertion, genotyping can be difficult because the precise site of insertion is unknown. Instead, genotyping was performed by exploiting the *LacZ* reporter of the gene trap. Wild type tissue lacking the gene trap produced no colour when the tissue was treated with X-Gal. Tissue homozygous for the gene trap (2 copies of *LacZ*) produced a blue colour at a rate twice as fast as tissue heterozygous for the gene trap (1 copy of *LacZ*) when treated with X-Gal (Pratt et al., 2006).

LacZ staining was a fast, effective method of genotyping *Hs6st1*$^{-/-}$ embryos at earlier stages of development, but became less reliable at older ages due to X-Gal permeability issues. Because of this, there was no reliable method of genotyping postnatal animals, and thus, the status of older *Hs6st1*$^{-/-}$ animals could not be ascertained. Also, it was not possible to reliably identify mice carrying more than one gene trap allele. The proposed *Hs2st*$^{-/-}$*/Hs6st1*$^{-/-}$ double mutant embryos (See Chapter 6) are an example of a mutant line that could not be genotyped using LacZ staining. So, an alternative genotyping strategy had to be designed before attempting to make double mutants.

4.2 Aims

Here we aimed to determine whether insertion of the gene trap vector into the *Hs6st1* locus resulted in an *Hs6st1* null allele. In addition, we aimed to identify the location of gene trap insertion into the *Hs6st1* gene in an effort to design a PCR based method of genotyping *Hs6st1* animals. With this knowledge we hoped to determine the

postnatal survival of *Hs6st1*$^{-/-}$ mutant animals. Also, this method of genotyping was critical to creating the proposed *Hs2st*$^{-/-}$/*Hs6st1*$^{-/-}$ double mutant embryos to determine possible redundancy in their roles as modulators of axon guidance (See Chapter 6).

4.3 Results

4.3.1 Gene trap insertion into the *Hs2st* gene results in a null allele

The gene encoding the Hs2st enzyme used in this study was previously shown to be incapable of producing wild-type *Hs2st* mRNA due to the insertion of a gene trap vector (Bullock et al., 1998) and therefore, presumed unable to produce Hs2st protein (Figure 1A). Using RNA *in situ* hybridization we designed an antisense riboprobe to the 3'UTR of the *Hs2st* transcript and were able to corroborate the absence of a detectable *Hs2st* transcript in *Hs2st*$^{-/-}$ mutants (Figure 1). We were able to detect *Hs2st* mRNA in the retina of the eye, the optic nerve, and at the optic chiasm in 100 µm horizontal sections of E15.5 wild type embryos (Figure 1B). Using this same *Hs2st* specific antisense riboprobe, we were unable to detect the presence of *Hs2st* mRNA in *Hs2st*$^{-/-}$ mutant embryos (Figure 1C).

4.3.2 Gene trap insertion into the *Hs6st1* gene results in a null allele

Gene trap insertion into intron 1 of the gene encoding the Hs6st1 enzyme (Figure 2A) had previously been described (Leighton et al., 2001; Mitchell et al., 2001) however, disruption of the wild type *Hs6st1* transcript had not been ascertained. RT-PCR analysis of *Hs6st1* gene expression was performed on E14.5 wild type (n=3), *Hs6st1*$^{+/-}$ (n=3), and *Hs6st1*$^{-/-}$ mutant (n=3) retinal tissue and optic chiasm tissue

(Figure 2B). PCR primers designed to span exon1 to exon2 of *Hs6st1* mRNA revealed the presence of a 379 bp PCR product in wild type and *Hs6st1*$^{+/-}$ embryos, but no such PCR product was observed in the *Hs6st1*$^{-/-}$ mutant embryos (Figure 2B, i). PCR primers designed to span exon1 to the transmembrane domain (TM) of the gene trap (GT) revealed the presence of a 500 bp PCR product in the *Hs6st1*$^{+/-}$ and *Hs6st1*$^{-/-}$ mutant embryos, but no such PCR product was observed in the wild type embryos (Figure 2B, ii). Sequencing of the 500 bp PCR product confirmed a fusion transcript between *Hs6st1* exon1 and the TM domain of the gene trap vector (data not shown). GAPDH and a no reverse transcriptase (RT) reaction were used as positive and negative controls, respectively (Figure 2B, iii,iv). These results, taken together provide evidence of a disruption in wild type *Hs6st1* mRNA due to the insertion of a gene trap between exon1 and exon2 of the *Hs6st1* gene (Figure 2A-B). Using RNA *in situ* hybridization on 100 µm horizontal sections of E15.5 embryos we showed a distinct pattern of expression in the retina of the eye as well as the region surrounding the optic chiasm in wild type embryos using an *Hs6st1* antisense riboprobe specific to the 3'-UTR (Figure 2C). Using this same *Hs6st1* specific antisense riboprobe, we were unable to detect the presence of *Hs6st1* mRNA in *Hs6st1*$^{-/-}$ mutant embryos (Figure 2D).

Figure 1. **Description of the *Hs2st*-gene trap allele.** (A) Schematic representation of the *Hs2st*-gene trap allele. The *Hs2st* gene is found on chromosome 3 and is composed of 7 exons. The gene trap is composed of a splice acceptor (SA) and an open reading frame encoding a transmembrane domain from CD4 (TM) and a β-Geo cassette (LacZ and Neo) followed by a polyA site. The gene trap inserts into intron 4 of the *Hs2st* gene which has been shown to abolish wild type transcript. *Hs2st* genotype was determined using PCR. Primers (yellow arrow heads) flanking the gene trap insertion site identify the wild type allele while the 5' primer specific to intron 4 and a 3' primer specific to the 5' end of the gene trap (SA) identify the *Hs2st* mutant allele. (B) *In situ* hybridization using an *Hs2st* specific RNA antisense riboprobe directed to the 3'-UTR showed a distinct pattern of expression in 100 µm horizontal sections of wild type embryos including the cells surrounding the optic nerves and the ventral diencephalon where the optic chiasm forms (the pattern of *Hs2st* expression was described in detail in Chapter 3). (C) Observations of *Hs2st* expression in *Hs2st* mutant embryos revealed no detectable *Hs2st* expression within the cells surrounding the optic nerves nor in the ventral diencephalon where the optic chiasm forms. Scale bar: 400 µm B-C .

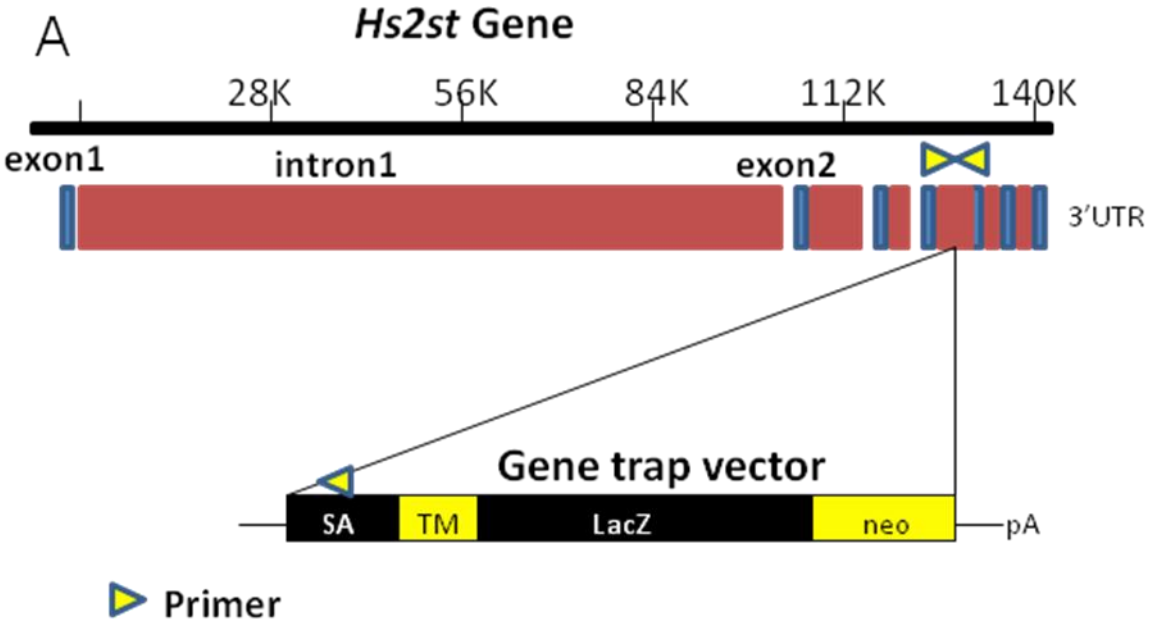
A
Hs2st Gene
28K
56K
84K
112K
140K
exon1
intron1
exon2
3'UTR
Gene trap vector
SA
TM
LacZ
neo
pA
Primer

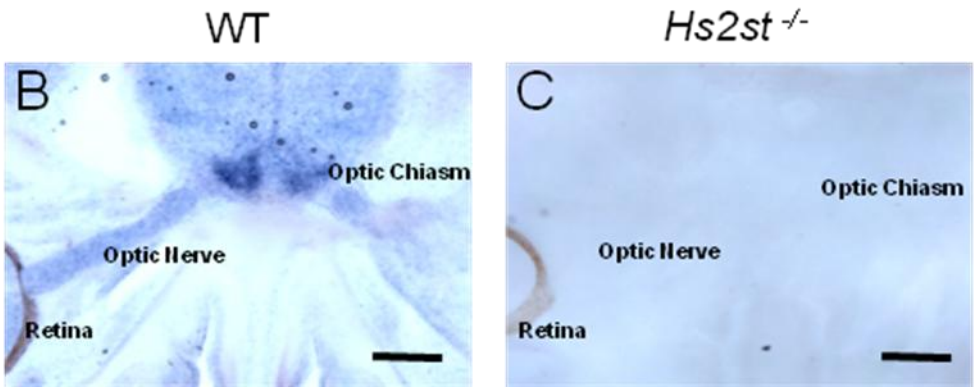
WT
Hs2st -/-
B
Optic Chiasm
Optic Nerve
Retina
C
Optic Chiasm
Optic Nerve
Retina

Figure 2. **Characterization of the *Hs6st1*-gene trap null allele.** (A) Schematic representation of the *Hs6st1*-gene trap allele. The *Hs6st1* gene is found on chromosome 1 and is composed of 2 exons separated by a ~35 kb intron. The gene trap vector is composed of a splice acceptor (SA) and an open reading frame encoding a transmembrane domain from CD4 (TM) and a β-Geo cassette (LacZ and Neo) as well as an internal ribosome entry site (IRES) and human placental alkaline phosphatase (hPLAP) coding region followed by a polyA site. The gene trap inserts into intron1 of the *HS6st1* gene which is predicted to abolish wild type transcript. (B) RT PCR on E14.5 *Hs6st1* wild type, heterozygous, and homozygous mutant embryos showing insertional mutagenesis of the gene trap into *Hs6st1*. (I) Primers (yellow arrow heads) designed to span exon1 to exon2 of *Hs6st1* show the presence of a PCR product in wild type and heterozygous embryos, but not in the homozygous mutant embryo. (II) Primers (yellow arrow heads) designed to target the gene trap (transmembrane domain, CD4) show its presence in the homozygous mutant and heterozygous embryo, but not in the wild type embryo. These results taken together provide evidence of an insertional mutation of the gene trap into the *Hs6st1* gene. (III) Glyceraldehyde-3-phosphate dehydrogenase (*GAPDH*) was used as an internal control for the presence of cDNA while (IV) RNA without reverse transcriptase was used as a negative control. (C) *In situ* hybridization using an *Hs6st1* specific RNA antisense riboprobe directed to the 3'-UTR showed a distinct pattern of expression in 100 µm horizontal sections of wild type embryos including the retina of the eye and the ventral diencephalon where the optic chiasm forms (the pattern of *Hs6st1* expression was described in detail in Chapter 3). (D) Observations of *Hs6st1* expression in *Hs6st1* mutant embryos revealed no detectable *Hs6st1* expression within the retina of the eye nor in the ventral diencephalon where the optic chiasm forms. Scale bar: 400 µm C-D.

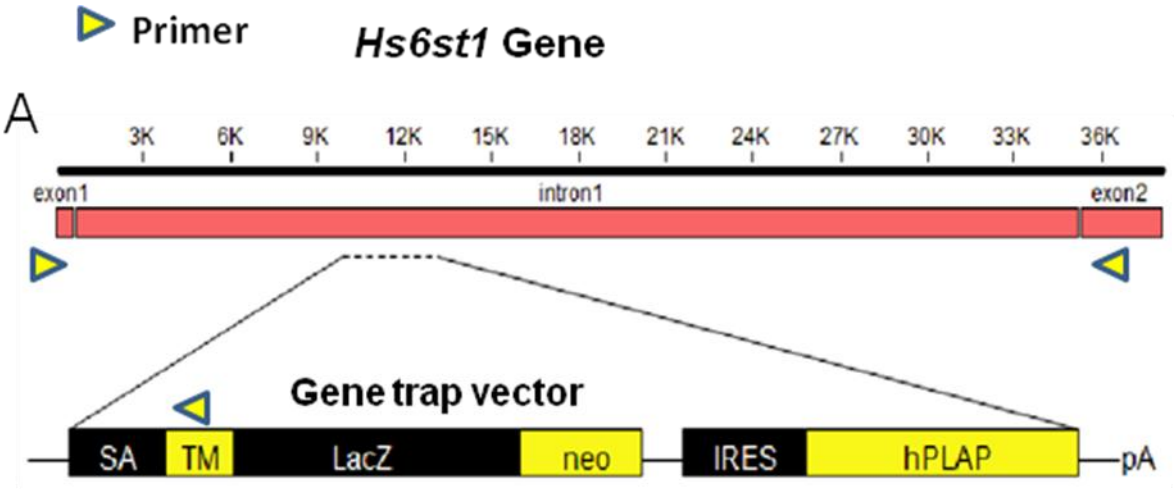
Primer
Hs6st1 Gene
A
3K
6K
9K
12K
15K
18K
21K
24K
27K
30K
33K
36K
exon1
intron1
exon2
Gene trap vector
SA
TM
LacZ
neo
IRES
hPLAP
pA

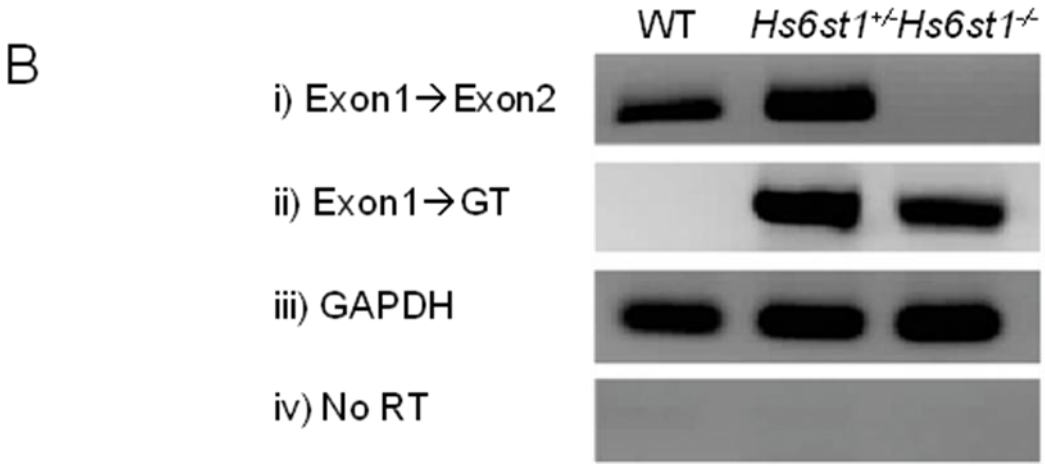
B
WT
Hs6st1+/-Hs6st1-/-
i) Exon1→Exon2
ii) Exon1→GT
iii) GAPDH
iv) No RT

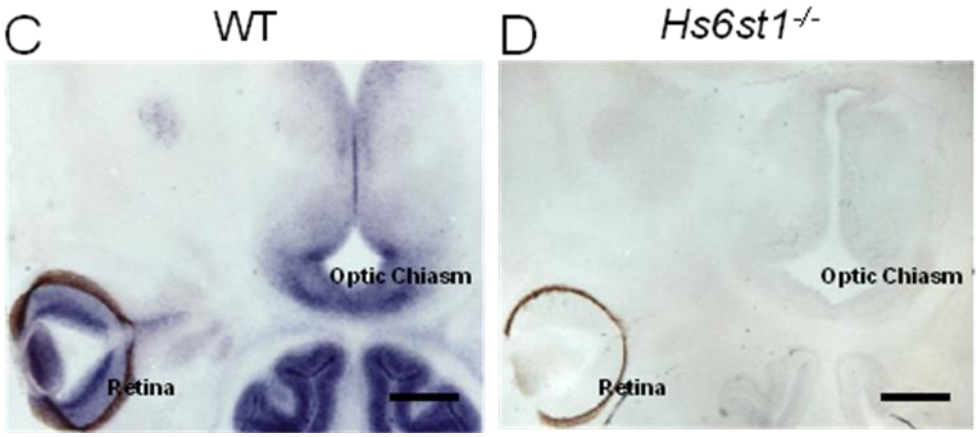
C
WT
D
Hs6st1-/-
Optic Chiasm
Retina
Optic Chiasm
Retina

4.3.3 Southern blot analysis identified the insertion site of the gene trap to a 1,100 bp region of intron1 within the *Hs6st1* gene

The insertion of the gene trap had previously been localized to the ~35 kb intron 1 of the *Hs6st1* gene through 5'RACE (Leighton et al., 2001; Mitchell et al., 2001) and we confirmed this by RT-PCR. In order to generate a PCR based approach to *Hs6st1* genotyping it was important to localize the gene trap insertion point to a smaller region of the large intron1. Briefly, the strategy used to further identify the insertion site of the *Hs6st1*-gene trap utilized Southern blot analysis. Enzymatically digested genomic DNA fragments were separated by gel electrophoresis and identified using radioactively-labelled DNA probes specific to regions of intron1. DNA fragments containing the gene trap insertion (*Hs6st1*$^{-}$) would be of a different size than the wild type (*Hs6st1*$^{+}$) fragments.

Genomic DNA from wild type, *Hs6st1*$^{+/-}$, and *Hs6st1*$^{-/-}$ mutant embryos was enzymatically digested using a combination of BamHI and ClaI restriction endonucleases and the fragments separated using gel electrophoresis. Through the creation of five (P1-P5) different radioactively labelled DNA probes generated by PCR and directed to different BamHI restriction fragments of wild type *Hs6st1* intron1, we were able to successively narrow the region of gene trap insertion to a ~7000 bp region of *Hs6st1* intron1 which was detected using the P3 probe (other probes gave no difference in size, data not shown) (Figure 3A-B). We were able to narrow down the site of gene trap insertion further, using a combination of BamHI and EcoRV digested genomic DNA and the P3 probe (Figure 3C-D). The final Southern blot analysis revealed a band size of ~3,900 bp in wild type tissue and a band size of 6,600 bp in *Hs6st1*$^{-/-}$ mutant tissue. Both bands were present in *Hs6st1*$^{+/-}$ tissue (Figure 3D). This digest pattern was consistent with an insertion of the gene trap to a ~1,100 bp region of *Hs6st1* intron1 (Figure 3C).

Figure 3. **Location of the gene trap vector into intron 1 of the *Hs6st1* locus.** (A) Southern blot analysis was performed on BamHI/ClaI digested genomic DNA from wild type, *Hs6st1*$^{+/-}$, and *Hs6st1*$^{-/-}$ tissue using radioactively labeled DNA probes (P1-P5). The *Hs6st1* gene trap was identified as inserting into a ~7,000 bp region of the 35 kb *Hs6st1* intron1 using the P3 probe. (B) The same P3 DNA probe was then used on BamHI/EcoRV digested genomic DNA from wild type, *Hs6st1*$^{+/-}$, and *Hs6st1*$^{-/-}$ tissue. The *Hs6st1* gene trap gene trap was identified as inserting into a ~1,100 bp region of the 35 kb *Hs6st1* intron1. (C) The Southern blot identified a ~6,600 bp DNA fragment which was consistent with an *Hs6st1*-gene trap fusion product and seen in Hs6st1$^{-/-}$ mutant and *Hs6st1*$^{+/-}$ tissue. The DNA probe identified a ~3,900 bp DNA fragment which was consistent with *Hs6st1* wild type product and seen in both wild type and *Hs6st1*$^{+/-}$ tissue.

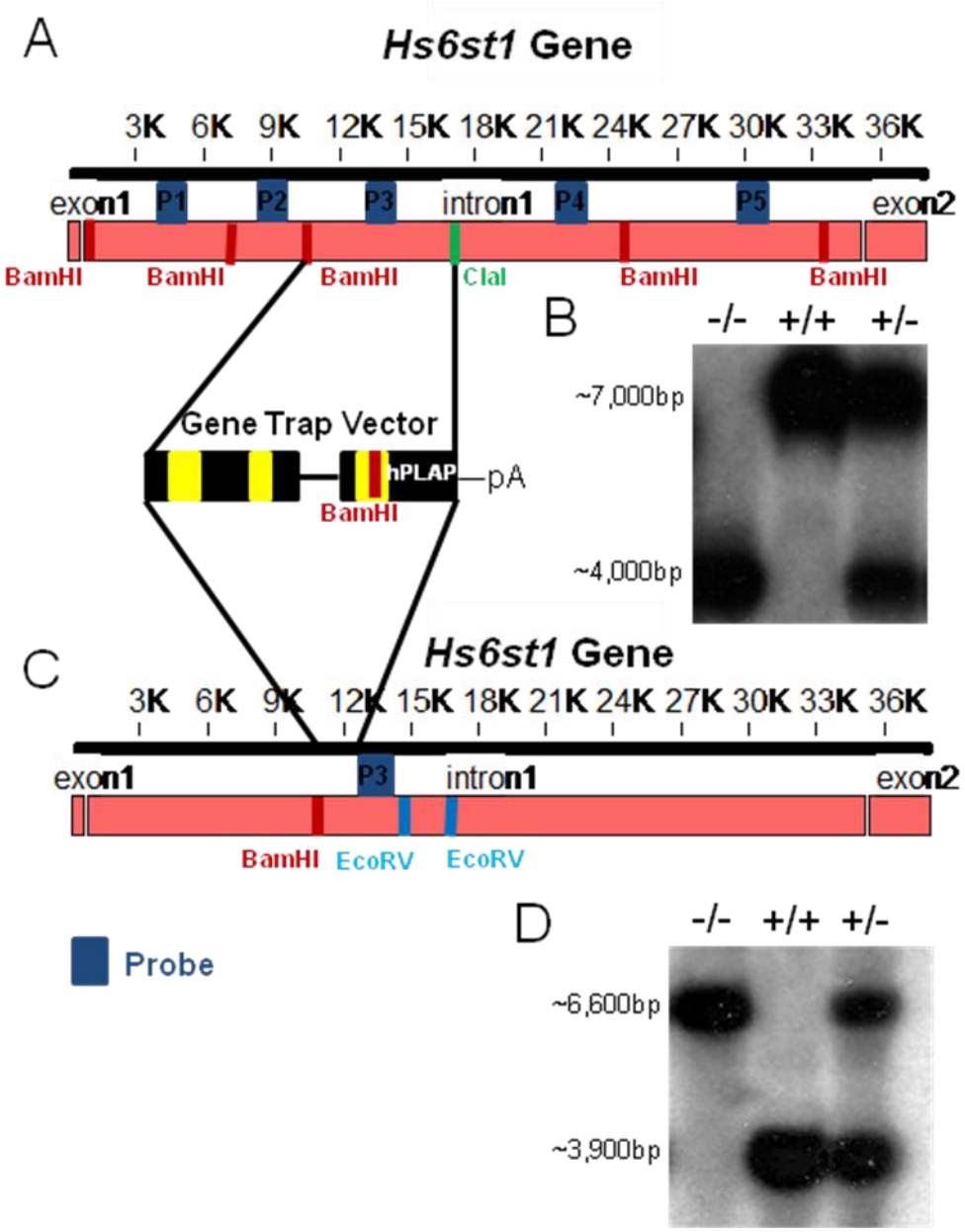
A
Hs6st1 Gene
3K 6K 9K 12K 15K 18K 21K 24K 27K 30K 33K 36K
exon1
P1
P2
P3
intron1
P4
P5
exon2
BamHI
BamHI
BamHI
ClaI
BamHI
BamHI
B
-/- +/+ +/-
~7,000bp
~4,000bp
Gene Trap Vector
hPLAP
pA
BamHI
C
Hs6st1 Gene
3K 6K 9K 12K 15K 18K 21K 24K 27K 30K 33K 36K
exon1
P3
intron1
exon2
BamHI
EcoRV
EcoRV
Probe
D
-/- +/+ +/-
~6,600bp
~3,900bp

4.3.4 PCR Genotyping of *Hs6st1*

Screening a series of primer pairs designed in and around the 1,100 bp region of *Hs6st1* intron1 eventually identified a PCR primer pair (PCR1) producing a 200 bp product in wild type and *Hs6st1*$^{+/-}$ embryos (Figure 4A-B). This 200 bp PCR product (PCR1) was absent in *Hs6st1*$^{-/-}$ mutant embryos and showed these primers flanked a region altered by the gene trap insertion (Figure 4B). However, despite numerous attempts it was not possible to identify a primer pair that bridged the gap between intron1 or intron2 and the gene trap (a fusion transcript). This was most likely due to rearrangements, deletions, and/or duplications resulting from the insertion of the gene trap which altered the wild type sequence of *Hs6st1* intron1. Instead, a primer pair (PCR2) designed to identify the gene trap specific hPLAP reporter was used which produced a 300 bp PCR product in *Hs6st1*$^{+/-}$ and *Hs6st1*$^{-/-}$ mutant embryos (Figure 4A-B). This 300 bp PCR product (PCR2) was absent in wild type animals (Figure 4A-B). This provides two separate PCRs that were used to identify the *Hs6st1* genotype; A 200 bp PCR product identifying the wild type allele (absent in *Hs6st1*$^{-/-}$ mutants) and a 300 bp PCR product to identify the *Hs6st1*-gene trap allele (absent in wild type). *Hs6st1*$^{+/-}$ embryos generated both PCR products (Figure 4A-B).

Figure 4. **PCR genotyping to identify the *Hs6st1*$^{-/-}$ mutant allele.** (A) Schematic representation of the primer sites (yellow arrow heads) used to identify the *Hs6st1* genotype. (B) PCR1 identified a ~200 bp region of *Hs6st1* intron1 where the gene trap inserted; this PCR product was absent in *Hs6st1*$^{-/-}$ mutant tissue, but present in wild type and *Hs6st1*$^{+/-}$ heterozygous tissue. PCR2 was designed to identify the hPLAP domain of the gene trap and produced a ~300 bp product; this PCR product was absent in wild type tissue, but present in *Hs6st1*$^{+/-}$ heterozygous and *Hs6st1*$^{-/-}$ mutant tissue.

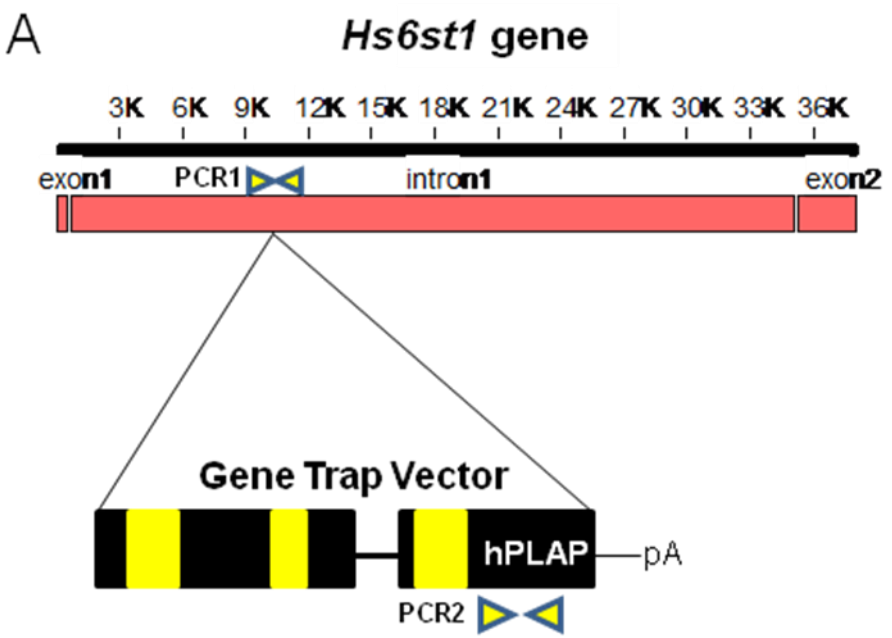
A
Hs6st1 gene
3K 6K 9K 12K 15K 18K 21K 24K 27K 30K 33K 36K
exon1
PCR1
intron1
exon2
Gene Trap Vector
hPLAP
pA
PCR2

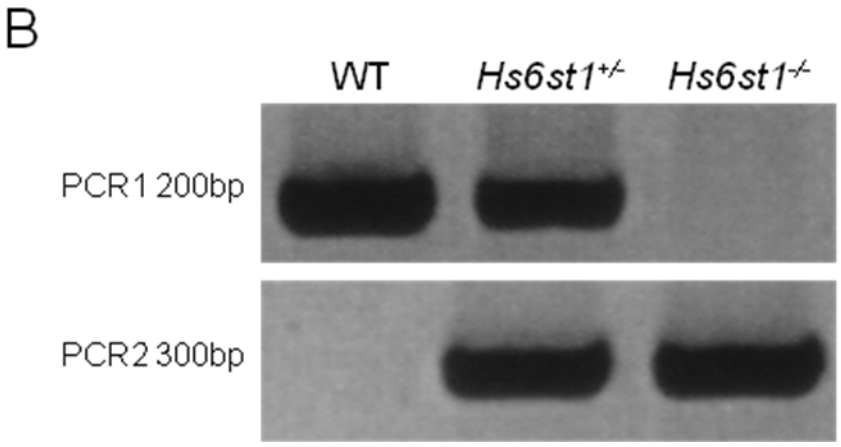
B
WT
Hs6st1+/-
Hs6st1-/-
PCR1 200bp
PCR2 300bp

4.3.5 *Hs6st1*$^{-/-}$ mice suffer postnatal lethality

Hs6st1$^{+/-}$ CBA mice were inter-crossed and their progeny were PCR genotyped at either E14.5 or at weaning. PCR genotyping results of E14.5 embryos did conform to Mendelian rules (Table 1). However, the genotyping results of weaned animals did not conform to Mendelian rules. Out of 100 animals genotyped at weaning, only 3 were observed to be *Hs6st1*$^{-/-}$ mutant. Chi-squared analysis showed the difference between the observed and expected values to be statistically significant with a P-value <0.0001 (Table 1). The accumulated data suggest that Hs6st1 sulphation is very important at later stages of development. We did not determine why *Hs6st1*$^{-/-}$ mutant animals had such a low postnatal survival rate, nor did we determine the health of the *Hs6st1*$^{-/-}$ mutant animals that did survive.

Table 1. **Viability of *Hs6st1*$^{-/-}$ mice produced by *Hs6st1*$^{+/-}$ / *Hs6st1*$^{+/-}$ inter-crosses and genotyped at E14.5 or at weaning.**

Age (%)	# of animals	Genotype	Observed (%)	Expected
E14.5	50	wild type	(13) 26%	25%
		Hs6st1$^{+/-}$	(24) 48%	50%
		Hs6st1$^{-/-}$	(13) 26%	25%
Weaning	100	wild type	(26) 26%	25%
		Hs6st1$^{+/-}$	(71) 71%	50%
		Hs6st1$^{-/-}$	(3) 3% **	25%

**Chi-squared analysis P<0.001

4.4 Discussion

To determine the physiological importance of Hs2st sulphation and Hs6st1 sulphation *in vivo* in mouse development we opted to characterize animals lacking these enzymes. Using the high throughput approach of gene trapping, mouse lines had been created that contained a gene trap within intron4 of the *Hs2st* gene locus and intron1 of the *Hs6st1* gene locus (Bullock et al., 1998; Leighton et al., 2001; Mitchell et al., 2001). While the *Hs2st*-gene trap allele had previously been characterized (Bullock et al., 1998), the precise nature of the disruption in *Hs6st1* gene expression had not been ascertained, and thus could not be confirmed as an *Hs6st1* null. Using RT-PCR, we were able to confirm the disruption of the *Hs6st1* gene transcript due to the insertion of a gene trap between exon1 and exon2 (Figure 2). The gene trap insertion introduced a premature poly-adenylation site which essentially removed exon2 from the transcript and created an *Hs6st1* exon1-gene trap fusion protein. Further corroboration of this result was shown using RNA *in situ* hybridization and showed no *Hs6st1* transcript in *Hs6st1*$^{-/-}$ mutant embryos when compared to wild type (Figure 2C-D). Using RNA *in situ* hybridization we also showed no *Hs2st* transcript in *Hs2st*$^{-/-}$ mutant embryos when compared to wild type (Figure 1B-C). Based on these findings, we concluded that no functional Hs6st1 protein could be produced. With no functional *Hs6st1*, we could now associate any developmental defects as being the likely result of HSPG 6-O-sulphation deficits.

Using a combination of Southern blotting and PCR we were able to identify (to within 200 bp) the location of gene trap insertion into the 35kb intron1 of the *Hs6st1* gene. One set of PCR primers was used to identify the *Hs6st1* wild type allele (200 bp PCR product), while a different set of PCR primers directed specifically to the hPLAP reporter of the gene trap (300 bp PCR product) was used to identify the *Hs6st1* mutant allele. Using this combination of PCRs, it was now possible to genotype *Hs6st1* animals accurately using PCR. This genotyping approach had the advantage (compared to the previously described LacZ staining method) of being able to accurately identify *Hs6st1* genotype at later stages of development. This approach also allowed us to proceed with attempts to generate *Hs2st*$^{-/-}$*/Hs6st1*$^{-/-}$

double mutants, as we could now confidently identify each genotype at each locus independently. The gene trap vector used to create *Hs2st* null animals did not carry the hPLAP reporter, and so, the primers we designed specifically identified the *Hs6st1* gene trap.

Using the PCR genotyping approach we were able to show normal *Hs6st1*$^{-/-}$ mutant survival prenatally (E14.5). However, only 3% of offspring genotyped at weaning were *Hs6st1*$^{-/-}$ mutant animals. We did not ascertain why there was such low survivability of postnatal *Hs6st1*$^{-/-}$ mutant animals, nor did we determine the health status of those *Hs6st1*$^{-/-}$ mutant animals that survived. Fortunately, an independent group had created a transgenic *Hs6st1*$^{-/-}$ mutant mouse line using conventional gene targeting in ES cells (Habuchi et al., 2007). They found normal Mendelian ratios at E14.5 however, the survivability of *Hs6st1*$^{-/-}$ mutant animals declined at later stages of development, with only 4% of the offspring being *Hs6st1*$^{-/-}$ mutant at postnatal day 1. The cause of this late embryonic lethality observed in *Hs6st1*$^{-/-}$ mutant animals was determined at least in part, to be a ~50% reduction in the number of foetal micro-vessels in the labyrinthine zone of the placenta. Gross observations of the placenta in our *Hs6st1*$^{-/-}$ mutant embryos did show a dark red discoloration that was not seen in the placentas of wild type embryos (data not shown). We presumed the high incidence of postnatal lethality in our *Hs6st1*$^{-/-}$ mutants is the result of placental defects as described in the *Hs6st1*$^{-/-}$ mutant animals described in Habuchi et. al., 2007. *Hs6st1*$^{-/-}$ mutant animals that did survive to adulthood (<4%) were shown to be smaller than their wild type littermates, but outwardly healthy, and fertile (Habuchi et al., 2007).

4.5 Summary

Using a combination of RT-PCR, Southern blotting, and PCR we were able to characterize the *Hs6st1*-gene trap allele. Using RT-PCR we showed that the insertion of the gene trap into the *Hs6st1* locus created a fusion transcript which resulted in a truncated version of the *Hs6st1* transcript. We presumed that the gene-

trapped-*Hs6st1* transcript was incapable of producing functional Hs6st1. Southern blotting and PCR were used to identify the site of gene trap insertion into the *Hs6st1* gene and a PCR genotyping strategy was developed. Using the *Hs6st1* genotyping strategy, we showed that *Hs6st1*$^{-/-}$ mutant animals had low postnatal survival with only 3% of offspring carrying the *Hs6st1*$^{-/-}$ null allele surviving to weaning. Using this PCR genotyping strategy, we were now able to accurately identify the proposed *Hs2st/Hs6st1* compound mutants (See Chapter 6).

Chapter 5: Loss of Hs2st Sulphation or Hs6st1 Sulphation Results in Distinct Axon Guidance Defects in the Developing Mouse CNS.

In this chapter I provide evidence supporting the "heparan sulphate code" hypothesis where 2-O-sulphation and 6-O-sulphation of HSPGs regulate distinct aspects of RGC axon navigation at the optic chiasm. Based on the available data, we hypothesize that Hs2st sulphation is specifically required for Slit1-Robo2 signaling and Hs6st1 sulphation is specifically required for Slit2-Robo2 signaling in guiding RGC axons at the optic chiasm. Observations of *Hs2st*$^{-/-}$ mutant and *Hs6st1*$^{-/-}$ mutant axon guidance in other regions of the visual system (retina and dLGN) as well as other axonal systems (TCA/CTA tract and corpus callosum) known to be regulated by Slit-Robo signaling show different phenotypes to those of *Slit/Robo* mutants. These observations indicate that the role Hs2st sulphation and Hs6st1 sulphation have on axon guidance is not absolute, but rather reflective of the context in which they are encountered and also on the type of axon that encounters them.

5.1 Introduction

Preliminary observations of RGC axon navigation in *Hs2st*$^{-/-}$ mutants and *Hs6st1*$^{-/-}$ mutants focused primarily on the regions of the retina and the optic chiasm (Pratt et al., 2006). RGC axons were observed to have abnormal trajectories at the optic chiasm, coincident with regions where *Hs2st* and/or *Hs6st1* were expressed. In addition, the RGCs themselves were shown to express both *Hs2st* and *Hs6st1*. Key molecular optic chiasm markers were shown to be unaltered in *Hs2st*$^{-/-}$ mutants and *Hs6st1*$^{-/-}$ mutants suggesting that changes in gross anatomical morphology was not causing the optic chiasm defects observed. Slit-Robo signalling was implicated as a

possible mechanism for the RGC axon guidance defects at the optic chiasm showing that *Hs6st1*$^{-/-}$ mutant RGC axons were less responsive to Slit2 repulsion *in vitro*.

In *Hs2st*$^{-/-}$ mutants, ectopic RGC axons were observed to navigate caudally from the optic chiasm along the midline of the ventral diencephalon. Also, the *Hs2st*$^{-/-}$ mutant optic chiasm was described as disorganized with RGC axons navigating erratically within the confines of the optic chiasm. Observations of *Hs6st1*$^{-/-}$ mutants showed an approximately four-fold increase in the number of RGC axons navigating to the contralateral eye. Conclusions based on these results showed that Hs6st1 sulphation is normally required to stop ectopic RGC axons entering the contralateral optic nerve. Hs2st sulphation was shown to be required to stop ectopic RGC axons growing caudally up the midline of the ventral diencephalon as well as being important in maintaining normal optic chiasm boundaries (Pratt et al., 2006). These observations indicated important and distinct roles for 2-O-sulphation and 6-O-sulphation of HSPGs in regulating RGC axon navigation at the developing optic chiasm.

Based on the *Hs2st*$^{-/-}$ mutant and *Hs6st1*$^{-/-}$ mutant phenotypes observed at the optic chiasm, we proposed the hypothesis that these specific sulphation modifications were critical to Slit1 and Slit2 signalling, respectively through the Robo2 receptor. This hypothesis was based on the RGC axon midline wandering phenotype observed in *Hs2st*$^{-/-}$ mutants phenocopying *Slit1*$^{-/-}$ mutants (Plump et al., 2002), and the ectopic retino-retinal projection observed in *Hs6st1*$^{-/-}$ mutants phenocopying *Slit2*$^{-/-}$ mutants (Tom Pratt, unpublished data) as well as the *Robo2*$^{-/-}$ mutants showing the additive phenotypes of both *Slit1*$^{-/-}$ mutants and *Slit2*$^{-/-}$ mutants (Plachez et al., 2008).

5.2 Aims

In this chapter we set out to extend our analysis of a “heparan sulphate code” for axon guidance by looking at the optic chiasm in more detail and examining other axonal tracts for defects in *Hs2st*$^{-/-}$ mutant and *Hs6st1*$^{-/-}$ mutant embryos and

associate these defects with Slit-Robo signaling. In *Hs2st*$^{-/-}$ mutants we aimed to quantify the defects occurring at the optic chiasm. In *Hs6st1*$^{-/-}$ mutants we attempted to identify whether a specific group of RGCs were responsible for the ectopic retino-retinal projection. In addition, we looked at the importance of differential HSPG sulphation patterns in other regions of the visual system where *Hs2st* and/or *Hs6st1* are expressed, including the retina, the optic tract, and one of the main targets for RGC axons, the dLGN; all regions shown to require Slit-Robo signaling for normal development. Furthermore, we aimed to describe the importance of Hs2st sulphation and Hs6st1 sulphation in contributing to axon guidance in other axonal systems including the thalamocortical tract and the corpus callosum; axonal systems known to require Slit-Robo signaling.

5.3 Results

5.3.1 Loss of Hs2st sulphation or Hs6st1 sulphation cause distinct RGC axon guidance defects resulting in increased optic chiasm width at the midline.

While strong qualitative evidence had been provided describing RGC axons escaping the normal boundary of the optic chiasm in *Hs2st*$^{-/-}$ mutant embryos (Pratt et al., 2006), quantification of this defect had never been performed. Using DiI tract tracing to label RGC axons, we were able to quantify the axon guidance defects previously described in the *Hs2st*$^{-/-}$ mutant optic chiasm (Pratt et al., 2006). Observations of the *Hs2st*$^{-/-}$ mutant optic chiasm at E15.5 showed a number of ectopic RGC axons navigating across the midline prior to arriving at the optic chiasm and forming an additional tract ventral and rostral to the normal optic chiasm (Figure 1B; white arrow). To quantitatively measure this defect at the optic chiasm we planned to measure the width of the optic chiasm at the midline. 200 µm serial stacked, horizontal sections were imaged and the images manually aligned using Photoshop software to view the entire optic chiasm. We defined the optic chiasm to

include any RGC axon that was DiI labeled and therefore, single RGC axons that were observed were included in the measurements. Rostro-caudal measurements of the optic chiasm were taken at the anatomical midline using Image J software. We found a significant increase in the rostro-caudal width of the *Hs2st*$^{-/-}$ mutant optic chiasm (n=7) when compared to the wild type (n=5) as observed in horizontal, stacked sections (One way ANOVA, multiple comparisons versus a control group (Holm-Sidak method), $P<0.05$) (Figure 1B-C,E).

We also carried out quantitative measurements of the *Hs6st1*$^{-/-}$ mutant optic chiasm to further establish differences in *Hs2st*$^{-/-}$ mutant and *Hs6st1*$^{-/-}$ mutant phenotypes at the optic chiasm. However, besides there being distinct differences in optic chiasm phenotypes in the *Hs2st*$^{-/-}$ mutant and *Hs6st1*$^{-/-}$ mutant, we did show that the *Hs6st1*$^{-/-}$ mutant optic chiasm was also wider at the midline when compared to the wild type optic chiasm. Unilateral DiI tract tracing of E15.5 *Hs6st1*$^{-/-}$ mutant RGC axons indicated axon guidance defects at the caudal midline of the optic chiasm. This defect appeared as a peak at the caudal midline of the *Hs6st1*$^{-/-}$ mutant optic chiasm that was unlike the midline wandering previously observed in the *Hs2st*$^{-/-}$ mutant optic chiasm (Figure 1D; white arrow) (Pratt et al., 2006). Rostro-caudal measurements of the *Hs6st1*$^{-/-}$ mutant optic chiasm were taken in the same manner as described for the *Hs2st*$^{-/-}$ mutant optic chiasm. The data indicated a significant increase in the rostro-caudal width of the *Hs6st1*$^{-/-}$ mutant optic chiasm (n=5) when compared to wild type (n=5) as observed in horizontal, stacked sections (One way ANOVA, multiple comparisons versus a control group (Holm-Sidak method), $P<0.05$) (Figure 1B,D-E).

To determine the trajectories RGC axons were taking within the optic chiasm, we used neurofilament immunohistochemistry on thin wax sections. This enabled us to identify individual trajectories of RGC axons within the optic chiasm. While the neurofilament antibody was not an RGC axon specific antibody, it was easy to distinguish the characteristic optic chiasm from other axonal tracts. 10 µm horizontal wax sections of the optic chiasm were photographed, which showed more detail of the RGC axons as they navigate within the optic chiasm. A complement of all 10 µm sections of the optic chiasm images were manually aligned using

Photoshop software which showed the entire optic chiasm with their characteristic phenotypes as described above for wild type, *Hs2st*$^{-/-}$ mutant and *Hs6st1*$^{-/-}$ mutant embryos (Figure 2B-D). Moving from dorsal to ventral within the optic chiasm we were able to view RGC axons navigating ectopically along the caudal midline of the diencephalon in both the *Hs2st*$^{-/-}$ mutant (Figure 2F,I) and *Hs6st1*$^{-/-}$ mutant embryos (Figure 2G,J). While RGC axons were restricted to the border of the hypothalamic neuroepithilium in *Hs6st1*$^{-/-}$ mutant embryos (Figure 2J, asterisk within the dotted lines), RGC axons were observed to navigate in and around the hypothalamic neuroepithilium and directly along the midline in *Hs2st*$^{-/-}$ mutant embryos (Figure 2I, asterisk within the dotted lines). Moving further from dorsal to ventral, we observed the optic nerves just prior to the point where they meet to form the optic chiasm (ventral region of the optic chiasm) and found an ectopic projection of RGC axons along the pre-optic area in the *Hs2st*$^{-/-}$ mutant (Figure 2L,O black arrow); this ectopic navigation was not observed in either the wild type or the *Hs6st1*$^{-/-}$ mutant (Figure 2K,M-N,P). These ectopic RGC axons were observed to leave the fasciculated optic nerve prior to the site of optic chiasm formation and penetrate the pre-optic area around the third (hypothalamic) ventricle of the ventral diencephalon to form an ectopic tract ventral and rostral to the normal optic chiasm in *Hs2st*$^{-/-}$ mutant embryos (Figure 2C,F,I,L,O).

Figure 1. **Optic chiasm width along the rostro-caudal midline is increased in the absence of either Hs2st sulphation or Hs6st1 sulphation in E15.5 embryos.** (A) Diagram representing the horizontal plane of section used to describe the trajectory of RGC axons as they travel from the retina of the eye to the ventral diencephalon where RGC axons from each eye meet to form the characteristic "X" structure of the optic chiasm. DiI tract tracing (white color represents the DiI labeled RGC axons) revealed the structure of the optic chiasm in (B) wild type, (C) *Hs2st*$^{-/-}$ mutant, and (D) *Hs6st1*$^{-/-}$ mutant as observed in 200 µm horizontal sections when DiI was unilaterally placed into one retina (red arrow in "A"). In *Hs2st*$^{-/-}$ mutants the optic chiasm appeared wider along the rostro-caudal midline due to the formation of an ectopic tract rostral to the optic chiasm (C, white arrow). In *Hs6st1*$^{-/-}$ mutants the optic chiasm appeared wider along the rostro-caudal midline due to ectopic axon navigation along the caudal midline of the ventral diencephalon (D, white arrow). Width measurements of the optic chiasm were taken along the midline where the optic chiasm was taken to consist of any DiI RGC axon that could be detected using confocal microscopy (red arrow). The average width of the wild type optic chiasm (n=5) was 345µm±51µm (mean ± SEM). The average width of the *Hs2st*$^{-/-}$ mutant optic chiasm (n=7) was 448µm±30µm and the average width of the *Hs6st1*$^{-/-}$ mutant optic chiasm (n=5) was 435µm±25µm. The width of the optic chiasm was significantly greater in both the *Hs6st1*$^{-/-}$ mutant and the *Hs2st*$^{-/-}$ mutant, when compared to the wild type (One way ANOVA, multiple comparisons versus a control group (Holm-Sidak method), $P<0.05$). Scale bar: 200 µm B-D.

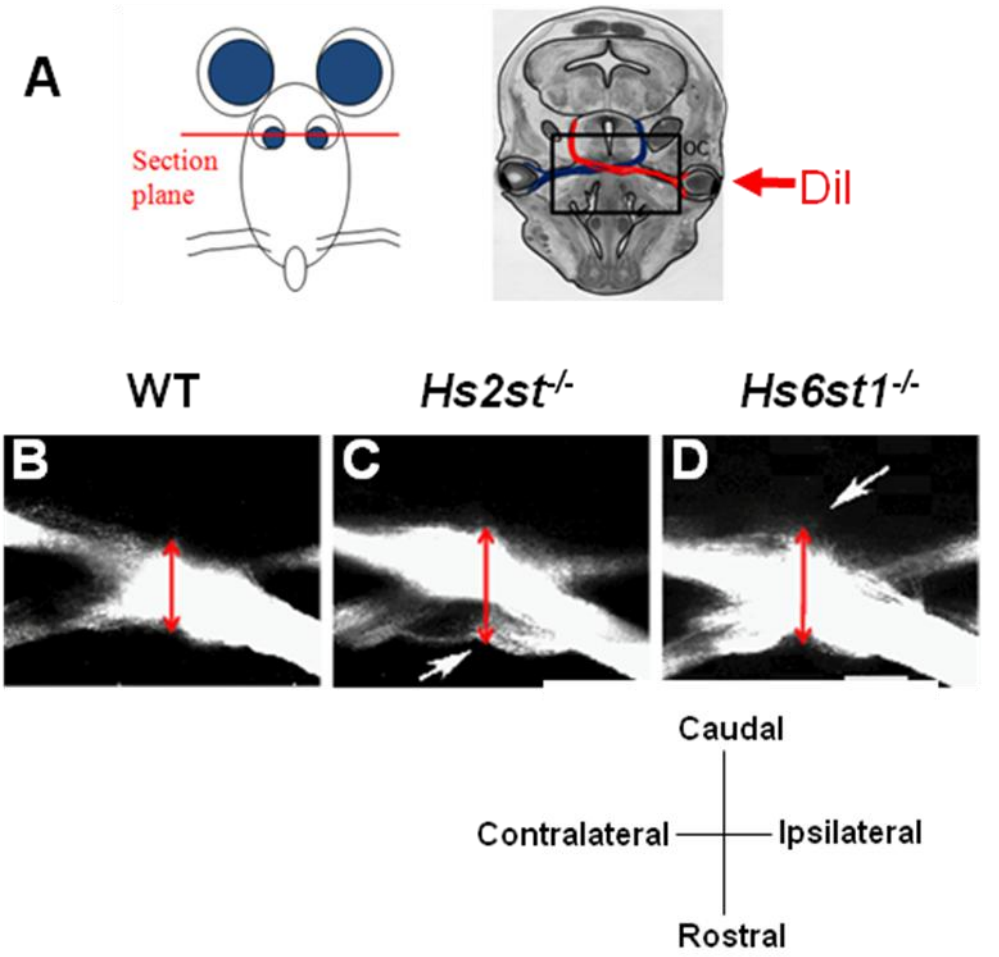
A
Section plane
OC
DiI
WT
Hs2st-/-
Hs6st1-/-
B
C
D
Caudal
Contralateral
Ipsilateral
Rostral

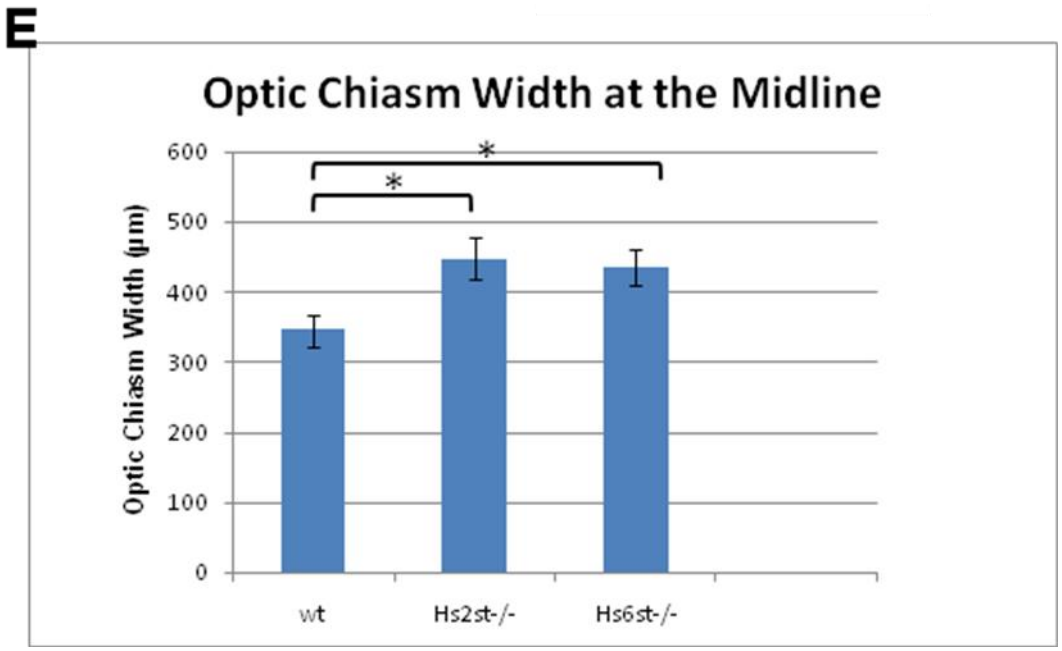
E
Optic Chiasm Width at the Midline
Optic Chiasm Width (µm)
600
500
400
300
200
100
0
*
*
wt
Hs2st-/-
Hs6st-/-

Figure 2. **Neurofilament immunohistochemistry revealed defects in optic chiasm development in both *Hs2st*$^{-/-}$ and *Hs6st1*$^{-/-}$ at E15.5 as observed in 10 µm horizontal sections.** (A) Diagram representing the horizontal plane of section used to describe the trajectory of RGC axons as they travel from the retina of the eye to the ventral diencephalon where RGC axons from each eye meet to form the characteristic "X" structure of the optic chiasm. Neurofilament immunohistochemistry (dark brown stain) was used to label axons and we were able to identify the RGC axons that constitute the optic chiasm because of the distinctive "X" structure formed at the ventral diencephalon. (B-D) stacked serial horizontal sections consisting of 30x 10 µm sections were manually aligned using Photoshop software and showed the characteristic phenotypes of the whole optic chiasm in (B) wild type (n=3), (C) *Hs2st*$^{-/-}$ mutants (n=3), and (D) *Hs6st1*$^{-/-}$ mutants (n=3). (E-J) stacked serial horizontal sections consisting of 15x 10 µm sections revealed the characteristics of the optic chiasm in more anterior regions of the optic chiasm and indicated the RGC axon navigation errors contributing to the midline wandering observed in *Hs2st*$^{-/-}$ mutants (F, I) and the caudal peak that formed in the *Hs6st1*$^{-/-}$ mutant optic chiasm (G, J); these phenotypes were not observed in wild type (E, H). While ectopic RGC axons were observed to penetrate the hypothalamic neuroepithilium (dotted line) in *Hs2st*$^{-/-}$ mutants (I, *), ectopic RGC axons were excluded from the hypothalamic neuroepithilium (dotted line) in *Hs6st1*$^{-/-}$ mutants (J, *). Moving from posterior to anterior, stacked serial horizontal sections consisting of 5x 10 µm sections indicated the RGC axon navigation errors contributing to the ectopic tract that forms rostral and anterior to the optic chiasm observed in *Hs2st*$^{-/-}$ mutants (L, O black arrow); this phenotype was not observed in either wild type (K, N) or *Hs6st1*$^{-/-}$ mutants (M, P). In *Hs2st*$^{-/-}$ mutant RGC axons were observed to penetrate the pre optic area (POA) rostral to the third ventricle (O). Black dotted line indicates the midline. Scale bars: 400 µm B-G, K-M; 200 µm H-J, N-P.

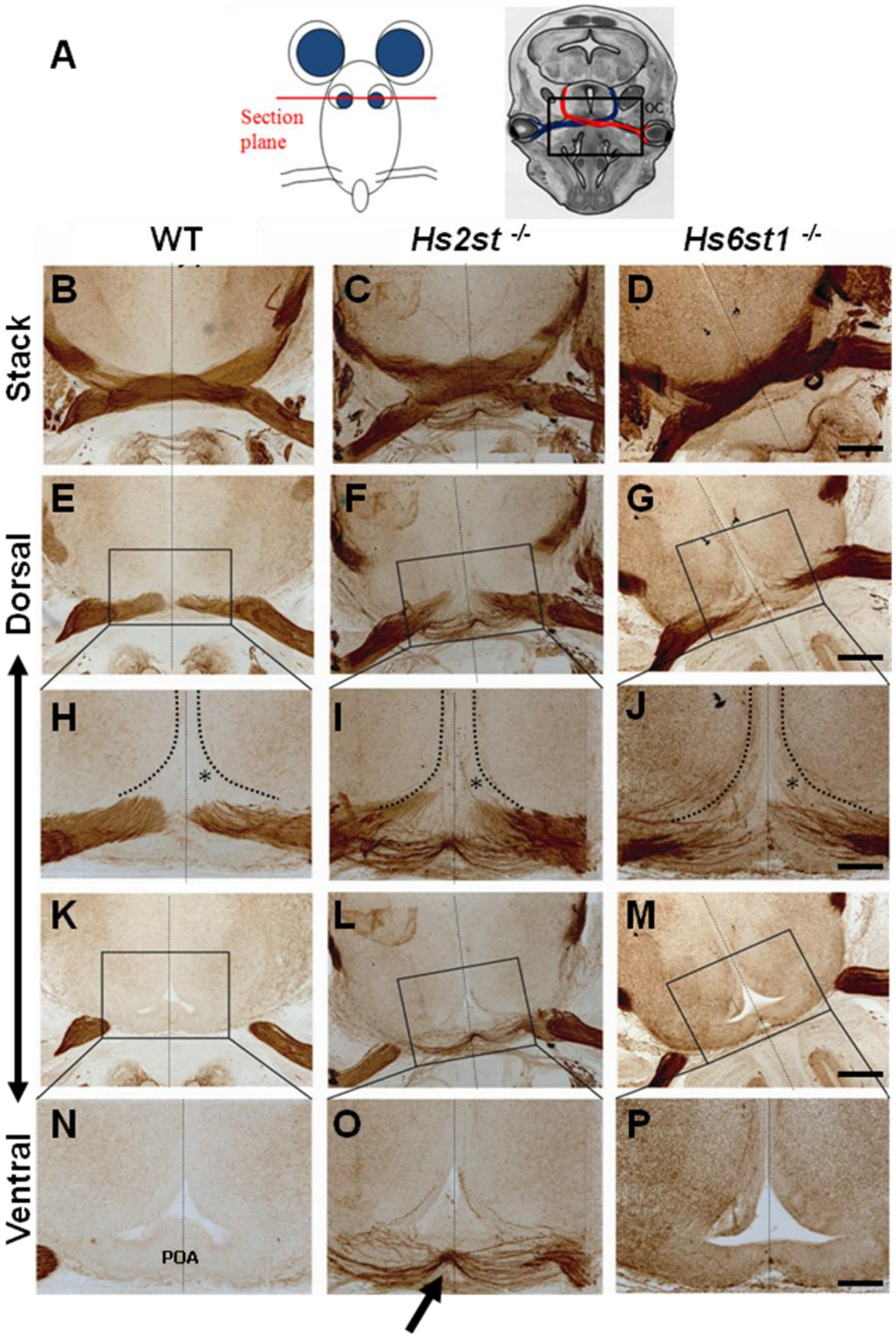
A
Section plane
oc
WT
Hs2st -/-
Hs6st1 -/-
Stack
Dorsal
Ventral
B
C
D
E
F
G
H
I
J
K
L
M
N
O
P
POA

5.3.2 *Hs6st1*$^{-/-}$ mutant RGC axons originating from both the DN and VT retina specifically target the VT region of the contralateral retina

Previous characterization of the *Hs6st1*$^{-/-}$ mutant revealed an increase in the number of RGC axons mis-projecting to the opposite eye (Pratt et al., 2006). We hypothesized that this ectopic projection was the result of a specific class of RGCs that were incapable of responding to specific guidance cues due to the loss of Hs6st1 sulphation. By regionalizing the retina into VT and DN domains, we aimed to test the possibility that the mis-guided RGC axons in our *Hs6st1*$^{-/-}$ mutants were either VT or DN in origin.

To determine whether a specific subpopulation of RGCs was contributing to the ectopic innervation of the contralateral *Hs6st1*$^{-/-}$ mutant retina, we divided the retina into VT and DN domains by using DiI/DiA tract tracing to see if RGCs from one region or the other was responsible for the ectopic innervations to the opposite eye (Figure 3A-C). Results of this labelling indicated that while *Hs6st1*$^{-/-}$ mutant RGCs from both VT and DN regions projected ectopic RGC axons to the opposite eye, all of these ectopic RGC axons specifically targeted the VT region of the opposite eye (n=6) (Figure 3A-C). While this experiment did not identify a specific population of RGCs that were responsible for the ectopic innervations to the opposite eye, we did show that RGCs that did mis-project to the opposite eye specifically targeted the VT region of the retina.

To quantify this result we focally labelled a proportion of the total RGCs by injecting DiI into either the DN (n=3) or VT (n=3) region of the retina of both wild type (n=3) and *Hs6st1*$^{-/-}$ mutant embryos (n=3) and counted the number of back-labelled RGC bodies in the opposite eye (mean ± SEM) (Figure 4B). Focal DiI injections into the DN region of the *Hs6st1*$^{-/-}$ mutant retina resulted in 14±4 RGC bodies being back-labelled in the contralateral retina while no RGC bodies were observed in the wild type (Figure 4C). Focal DiI injections into the VT region of the *Hs6st1*$^{-/-}$ mutant retina resulted in 82±6 RGC bodies being back-labelled in the contralateral retina while only 5±1 RGC bodies were observed in the wild type (Figure 4C). These results showed that the RGC axons projecting to the contralateral eye, while

originating in both the VT and DN regions of the retina, specifically innervated the VT region of the contralateral eye in wild type and in greater numbers in the contralateral eye of *Hs6st1*$^{-/-}$ mutants (Mann-Whitney rank sum test, P>0.05) (Figure 4). This result indicates that RGC axons are capable of responding to chemical guidance cues within the contralateral eye that direct them specifically to the VT region of the retina.

Figure 3. **RGCs originating in both the VT and DN retina mis-project to the VT region of the opposite eye in *Hs6st1*$^{-/-}$ mutants at E15.5.** DiI (red) and DiA (green) were both unilaterally injected into the retina of one eye (diagrammatically described in C) to separately label RGC axons in the VT and DN regions of the retina in *Hs6st1*$^{-/-}$ mutants, respectively (n=2) and observed in 200 µm horizontal sections that were counterstained with TOPRO3 (blue). DiI and DiA were also placed in the opposite regions of the retina to control for rate of diffusion of the two dyes (n=2) (data not shown). This was done in an effort to visualize the trajectories RGC axons take in the (A) *Hs6st1*$^{-/-}$ mutant optic chiasm and determine if either VT or DN RGC axons are responsible for the retino-retinal projection observed in *Hs6st1*$^{-/-}$ mutants. (B) In all cases, we showed that RGCs (colored red) originating in both the VT and DN regions of the wild type and *Hs6st1*$^{-/-}$ mutant retina projected their axons to the opposite eye and specifically targeted the VT retina (B-C). V, ventral; D, dorsal; N, nasal; T, temporal. Scale bars: 200 µm A; 100 µm B.

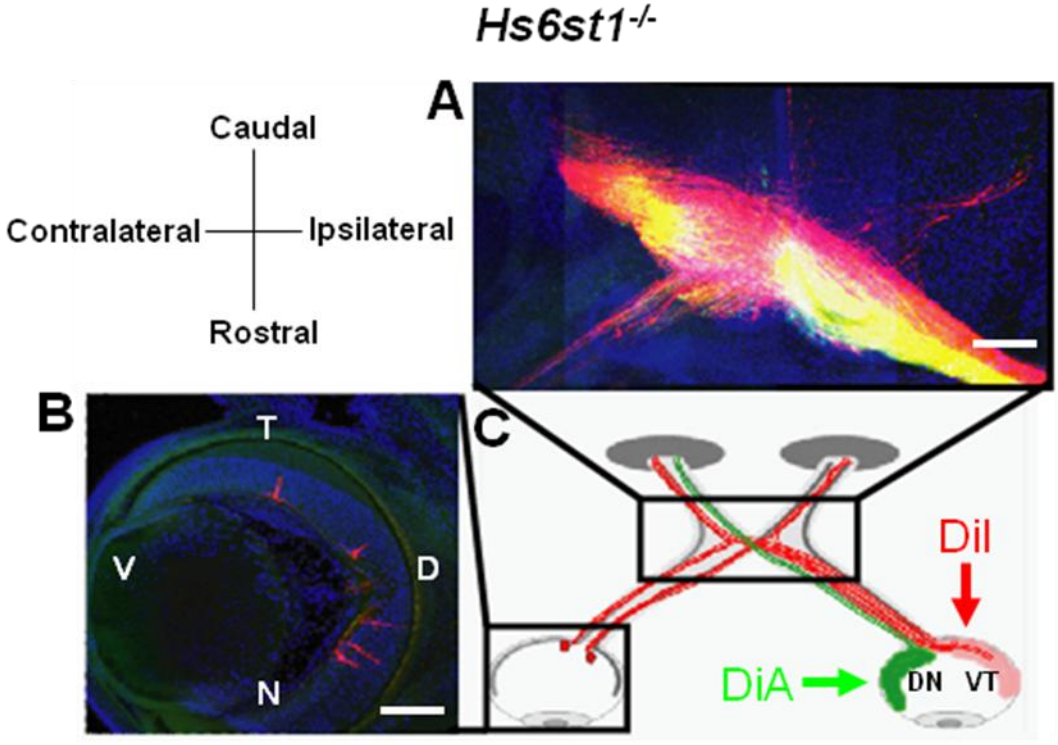
Hs6st1-/-
A
Caudal
Contralateral
Ipsilateral
Rostral
B
T
V
D
N
C
DiI
DiA
DN
VT

Figure 4. **Quantitative evidence showing *Hs6st1*$^{-/-}$ mutant RGC axons that mis-project to the opposite eye specifically target the VT region of the retina.** (A) Diagram representing the horizontal plane of section used to describe the trajectory of RGC axons and the placement of DiI (red arrow) allowing for retrograde labeling of RGC bodies in the opposite eye. (B) DiI (red) was placed unilaterally into either the DN region of the eye in wild type (n=3) and *Hs6st1*$^{-/-}$ mutants (n=3) or the VT region of one eye in wild type (n=3) and *Hs6st1*$^{-/-}$ mutants (n=3) and in some cases counterstained with TOPRO3 (blue). (C) The total number of back-labeled RGC bodies were counted in the opposite eye and revealed a large number of RGC bodies targeting the VT region of the *Hs6st1*$^{-/-}$ mutant retina when compared to the number of labeled RGC bodies targeting the DN region of the *Hs6st1*$^{-/-}$ mutant retina (Mann-Whitney rank sum test, $P<0.05$). While very few RGC axons navigated to the opposite eye in wild types, those that did were also shown to target the VT retina specifically suggesting that axons that ectopically enter the region of the opposite eye are still responding to axon guidance cues (Mann-Whitney rank sum test, $P>0.05$). Scale bars: large image 400 µm; small images 50 µm.

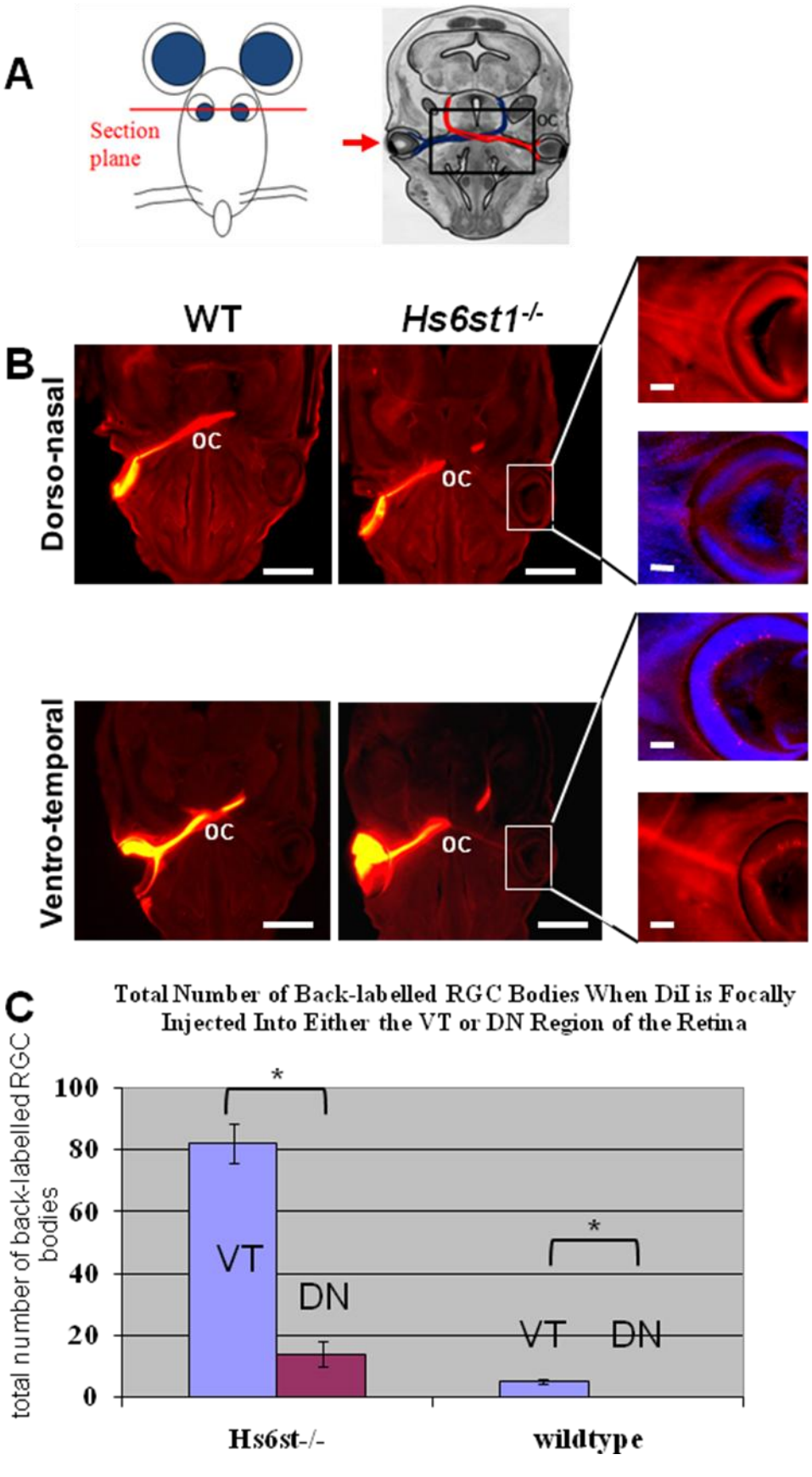
A
Section plane
OC
B
WT
Hs6st1-/-
Dorso-nasal
Ventro-temporal
OC
C
Total Number of Back-labelled RGC Bodies When DiI is Focally Injected Into Either the VT or DN Region of the Retina
total number of back-labelled RGC bodies
100
80
60
40
20
0
*
*
VT
DN
VT
DN
Hs6st-/-
wildtype

5.3.3 RGC axons navigating in the retina of the eye are restricted to the OFL in *Hs6st1*$^{-/-}$ mutants.

Previous findings had shown that in *Slit2*$^{-/-}$ mutants and more severely in *Slit1*$^{-/-}$/*Slit2*$^{-/-}$ double mutants, RGC axons ectopically exit the OFL of the retina (Thompson et al., 2006b). Based on our hypothesis that Hs6st1 sulphation is required for Slit2 signalling we predicted that we may see a similar defect in the retina of *Hs6st1*$^{-/-}$ mutants. L1 (axon specific marker) immunohistochemistry was used to identify RGC axons and show any RGC axons that might be ectopically navigating outside the OFL or erratically within the OFL. To observe the trajectories taken by *Hs6st1*$^{-/-}$ mutant RGC axons, we observed the RGC axons in both 200 µm coronal sections (Figure 5A-B) and as flattened whole-mounts (Figure 5C-F). We did not observe RGC axons ectopically exiting the OFL in *Hs6st1*$^{-/-}$ mutants (Figure 5B) nor did we observe any unusual RGC axon trajectories within the OFL (Figure 5D, F). This suggested that the *Hs6st1*$^{-/-}$ mutant RGC axons were behaving normally i.e. they were restricted to OFL and did not phenocopy *Slit2*$^{-/-}$ mutants. One possible explanation is that the loss of Hs6st1 sulphation in the retina is being compensated for by other enzymes capable of 6-O-sulphation and therefore Slit2 signaling is unaffected. This possibility is addressed further in Chapter 8.

Figure 5. **RGC axons do not exit the optic fiber layer aberrantly in the *Hs6st1*$^{-/-}$ mutant eye.** RGCs originating in the retina of the eye project their axons into the optic fiber layer (OFL) and their axons navigate towards the optic disc (OD) where they will exit the eye to form the optic nerves. Using the axonal marker L1, we performed L1 immunohistochemistry to observe RGC axon trajectories in the retinas of E15.5 wild type (n=6) (A, C, E) and *Hs6st1*$^{-/-}$ mutants (n=6) (B,D,F). Observations of RGC axons (red) in coronally sectioned eyes revealed no differences between (A) wild type (n=3) and (B) *Hs6st1*$^{-/-}$ mutants (n=3); sections were counterstained with TOPRO3 (blue). Observations of RGC axon trajectories in flat-mounted retinas revealed no differences between (C, E) wild type (n=3) and (D-F) *Hs6st1*$^{-/-}$ mutants (n=3). DN, dorso-nasal; VT, ventro-temporal. Scale bars: 200 µm A-D; 100 µm E-F.

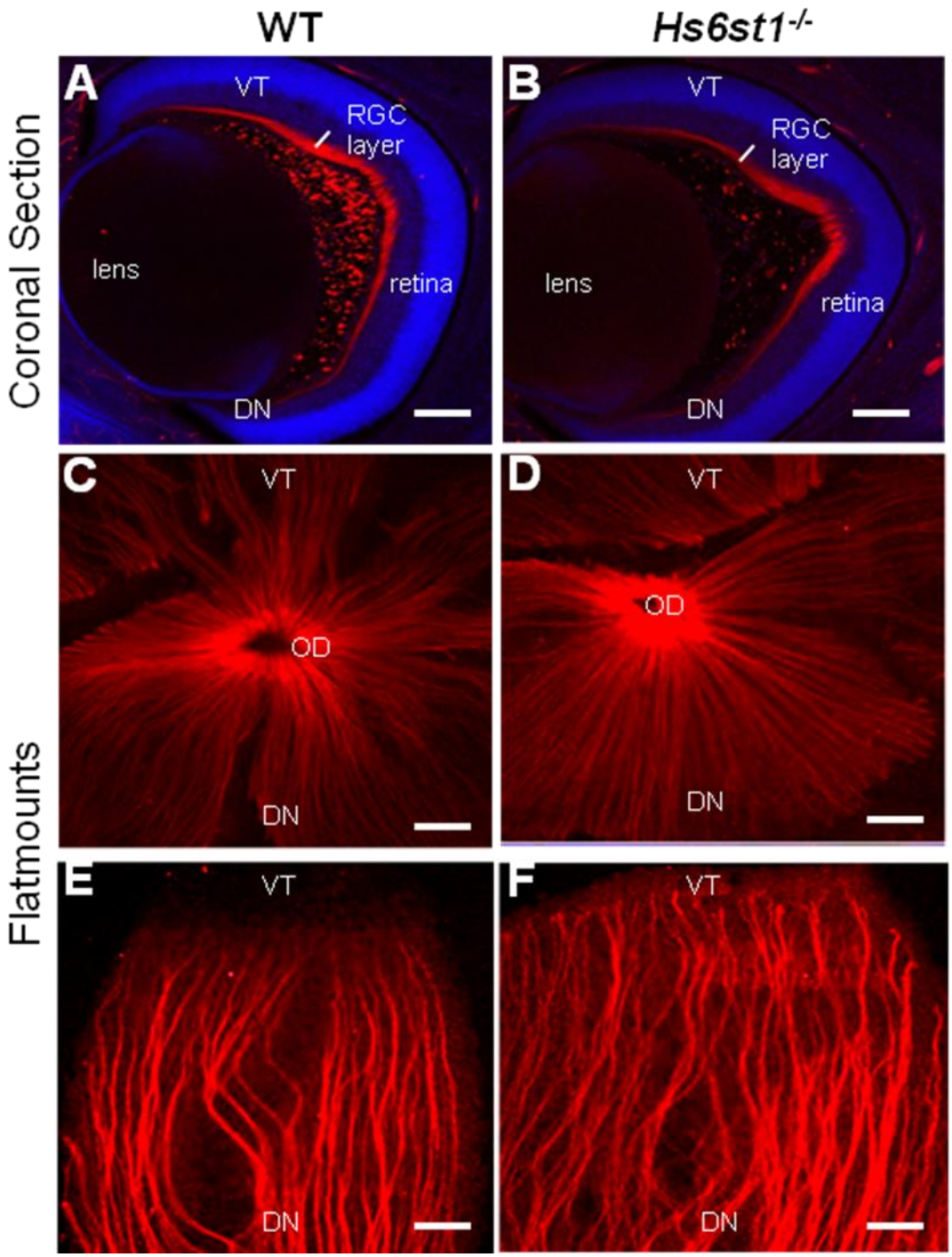
WT
Hs6st1-/-
Coronal Section
Flatmounts
A
B
C
D
E
F
VT
RGC
layer
lens
retina
DN
OD

5.3.4 RGC axons show increased defasciculation at the dLGN in *Hs6st1*$^{-/-}$ mutant mice

Because of the relatively high expression of *Hs6st1* at the dLGN in the embryonic mouse (Chapter 3), we decided to characterize the navigation of RGC axons in the *Hs6st1*$^{-/-}$ mutant at the dLGN; a major target for RGC axons. Using DiI tract tracing, we labelled the contralateral optic tract by placing DiI crystals into the retina of the contralateral eye allowing us to investigate the navigation of RGC axons as they travelled from the optic chiasm to the dLGN. The E17.5 optic tract was observed using stacked sagittal sections (3 x 200 µm serial sections constituted the entire optic tract) in wild type, *Hs2st*$^{-/-}$ mutant, and *Hs6st1*$^{-/-}$ mutant embryos (Figure 6B-D). The optic tract was observed to be tightly fasciculated as it travelled over the surface of the ventral thalamus with no evidence of navigation errors in *Hs2st*$^{-/-}$ mutants or *Hs6st1*$^{-/-}$ mutants (Figure 6B-D). Observations of the optic tract at the dLGN showed no difference in defasciculation in the *Hs2st*$^{-/-}$ mutant, but the *Hs6st1*$^{-/-}$ mutant optic tract did have increased defasciculation at the dLGN when compared to the wild type (Figure 6E). The degree of defasciculation at the dLGN was measured by drawing a rostral-to-caudal line (red dotted arrow) encompassing any RGC axon labelled with DiI along the width of the optic tract using Image J software. This line was positioned 2 µm away from and parallel to the striatum medullaris (red dotted line), an easily identifiable anatomical structure for reference. Width measurements (mean ± SEM) of the optic tract confirmed a significant increase in the defasciculation of RGC axons at the dLGN in *Hs6st1*$^{-/-}$ mutants (n=3) (Kruskal-Wallis One way ANOVA on ranks, $P>0.05$) when compared to wild type (n=3) (Figure 6E). There was no significant difference in the width of the optic tract in *Hs2st*$^{-/-}$ mutants (n=3) when compared to wild type embryos (n=3) (Figure 6E).

Figure 6. **A loss of Hs6st1 sulphation results in an increase in the defasciculation of the optic tract at the dLGN.** (A) Diagram representing the sagittal plane of section used to describe the trajectory of RGC axons within the optic tract as they navigate over the surface of the diencephalon (box shows the region observed in B-D). (B-D) DiI (grey color) was unilaterally injected into the retina of an E17.5 eye to label RGC axons and the contralateral optic tract was observed in serial stacked 200 µm sagittal sections. Comparing (B) wild type (n=3), (C) *Hs2st*$^{-/-}$ mutants (n=3), and (D) *Hs6st1*$^{-/-}$ mutants (n=3), revealed a wider, more defasciculated optic tract at the dLGN in *Hs6st1*$^{-/-}$ mutants (D). Using the striatum medullaris as a landmark (red dotted line), measurements were made 2 µm away and parallel to the striatum medullaris (red dotted arrow) using Image J software and included any axon that was DiI labeled (B-D). There appeared to be an increase in the width of the optic tract at the dLGN in *Hs6st1*$^{-/-}$ mutants when compared to either *Hs2st*$^{-/-}$ mutants or wild type (Kruskal-Wallis One way ANOVA on ranks, P>0.05) (E). Scale bars: 200 µm B-D.

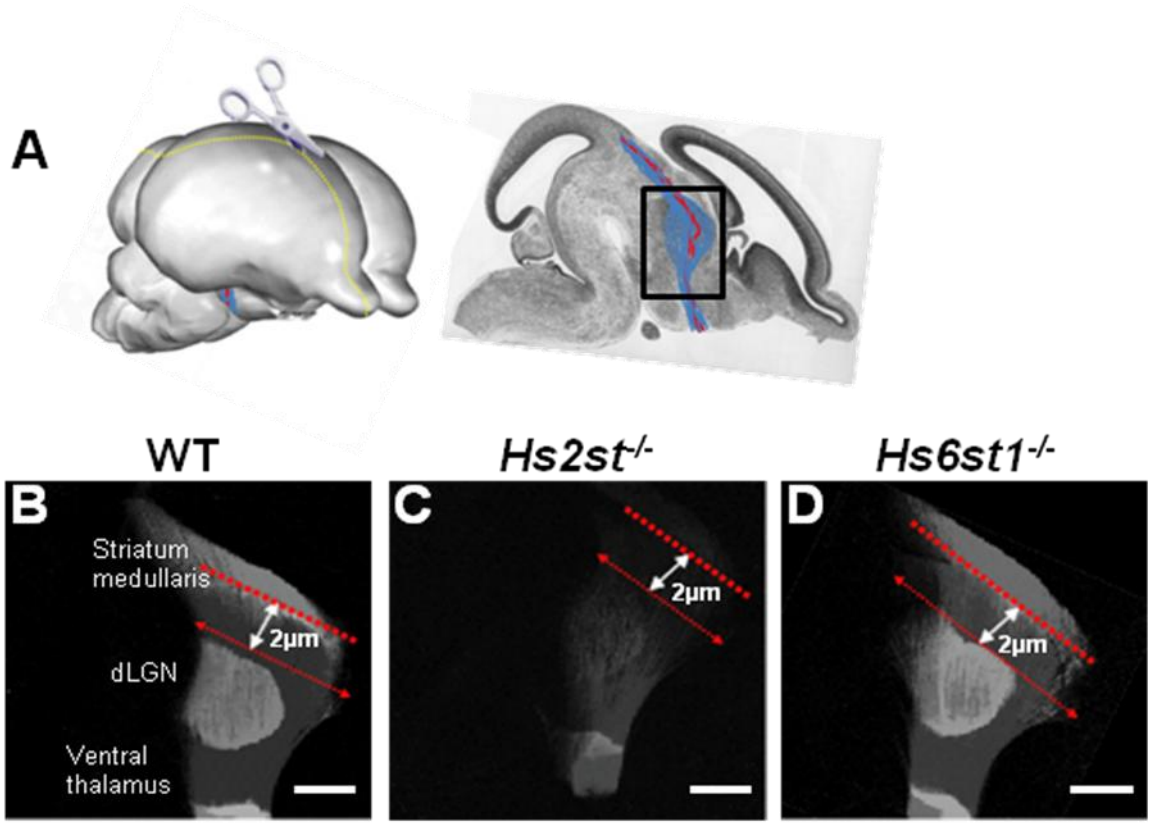
A
WT
Hs2st-/-
Hs6st1-/-
B
C
D
Striatum medullaris
dLGN
Ventral thalamus
2µm
2µm
2µm

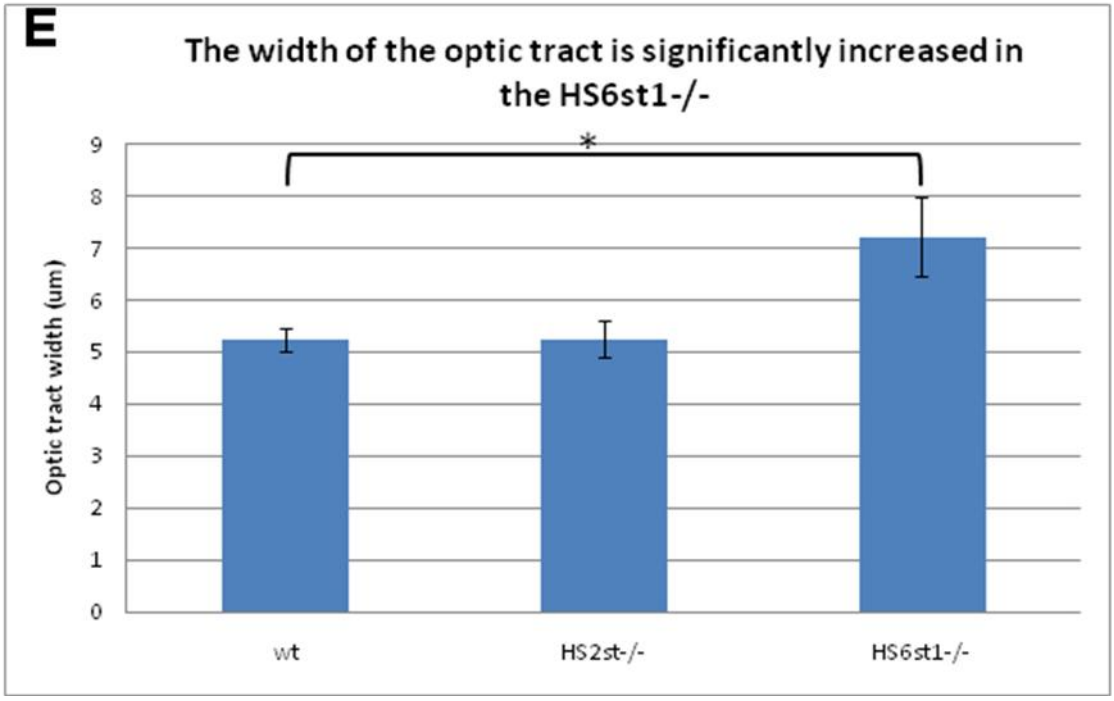
E
The width of the optic tract is significantly increased in the HS6st1-/-
Optic tract width (um)
0
1
2
3
4
5
6
7
8
9
*
wt
HS2st-/-
HS6st1-/-

5.3.5 Axon guidance defects were not observed in the TCA/CTA tracts of *Hs2st*$^{-/-}$ mutant or *Hs6st1*$^{-/-}$ mutant embryos.

The TCA tract and its reciprocal CTA tract collectively function to integrate sensory information arriving in the dorsal thalamus to higher order processing centers in the cerebral cortex. Previous work had established the importance of Slit-Robo signaling in TCA/CTA tract formation where they showed that in the absence of Slit2 or Robo2 and more severely in the absence of both Slit1/Slit2 or Robo1/Robo2 that these axons mis-navigate outside the normal boundaries of the TCA/CTA tract (Bagri et al., 2002; Lopez-Bendito et al., 2007). We therefore looked at the formation of these axonal tracts in *Hs2st*$^{-/-}$ mutants and *Hs6st1*$^{-/-}$ mutants. Based on our Hs2st/Slit1 : Hs6st1/Slit2 hypothesis, we predicted that there may be axon guidance defects in the *Hs2st*$^{-/-}$ mutants and/or *Hs6st1*$^{-/-}$ mutants similar to those previously described in *Slit* mutants and/or *Robo* mutants. Observations of the TCA and CTA tracts using a combination of DiI (Figure 7B, D, F) and DiI/DiA (Figure 7C, E, G) tract tracing indicated no significant differences when E17.5 *Hs2st*$^{-/-}$ mutants (Figure 7D-E) and *Hs6st1*$^{-/-}$ mutants (Figure 7F-G) were compared to the wild type (Figure 7B-C). DiI or DiI/DiA was placed into the most caudal region of the cortex where the V1 domain of the visual cortex was located to anterogradely label the CTA axons and retrogradely label the TCA axons (Figure 7A). There was no observable difference in tract formation when DiI and DiA were placed into the dorsal thalamus of E17.5 *Hs2st*$^{-/-}$ mutant or *Hs6st1*$^{-/-}$ mutant brains when compared to wild type (data not shown). Using 200 µm coronal sections we were able to confirm that the *Hs2st*$^{-/-}$ mutant (Figure 7D-E) and *Hs6st1*$^{-/-}$ mutant (Figure 7F-G) TCA/CTA tracts navigated their stereotyped path from cortex to dorsal thalamus in a manner consistent with wild type (Figure 7B-C). Using both DiI and DiA we showed that, not only did the tracts execute the expected trajectories from origin to target, but they also mapped to the correct region within the dLGN (Figure 7C,E,G). DiI placed into the most caudal position of V1 mapped to the most lateral position of the dLGN, while DiA placed into the rostral region of V1 mapped to the medial position of the dLGN. These results show that the TCA/CTA tracts develop normally in *Hs2st*$^{-/-}$ mutants and *Hs6st1*$^{-/-}$ mutants producing none of the defects

previously described in Slit/Robo mutants. One possibility to explain the lack of an *Hs6st1*$^{-/-}$ mutant phenotype in TCA/CTA tract development is that the loss of Hs6st1 sulphation in the dorsal thalamus and cortex is being compensated for by other enzymes capable of 6-O-sulphation and therefore Slit2 signaling is unaffected. This possibility is addressed further in Chapter 8.

Figure 7. **The TCA tract and its reciprocal CTA tract show no gross alterations in either tract morphology or patterning in the absence of either Hs2st sulphation or Hs6st1 sulphation.** E17.5 brains were either (B, D, F) DiI labeled (red) or (C, E, G) DiI/DiA labeled (red/green) into (A) the visual cortex and observed in 200 µm coronal sections. DiI tract tracing revealed normal TCA/CTA trajectories in (D) *Hs2st*$^{-/-}$ mutants (n=3) and (F) *Hs6st1*$^{-/-}$ mutants (n=3), when compared to (B) wild type (n=3). DiI/DiA revealed no differences in gross patterning of TCAs/CTAs when (C) wild type (n=3) was compared to (E) *Hs2st*$^{-/-}$ mutants (n=3) or (G) *Hs6st1*$^{-/-}$ mutants (n=3). DiI placed in the caudal region of the visual cortex labeled axons in the lateral region of the dLGN while DiA placed in the rostral region of the visual cortex labeled axons in the medial region of the dLGN (A, C, E, G). DTB; diencephalic/telencephalic boundary, PSPB; pallial/sub-pallial boundary. Scale bars: 400 µm B,D,F; 200 µm C,E,G.

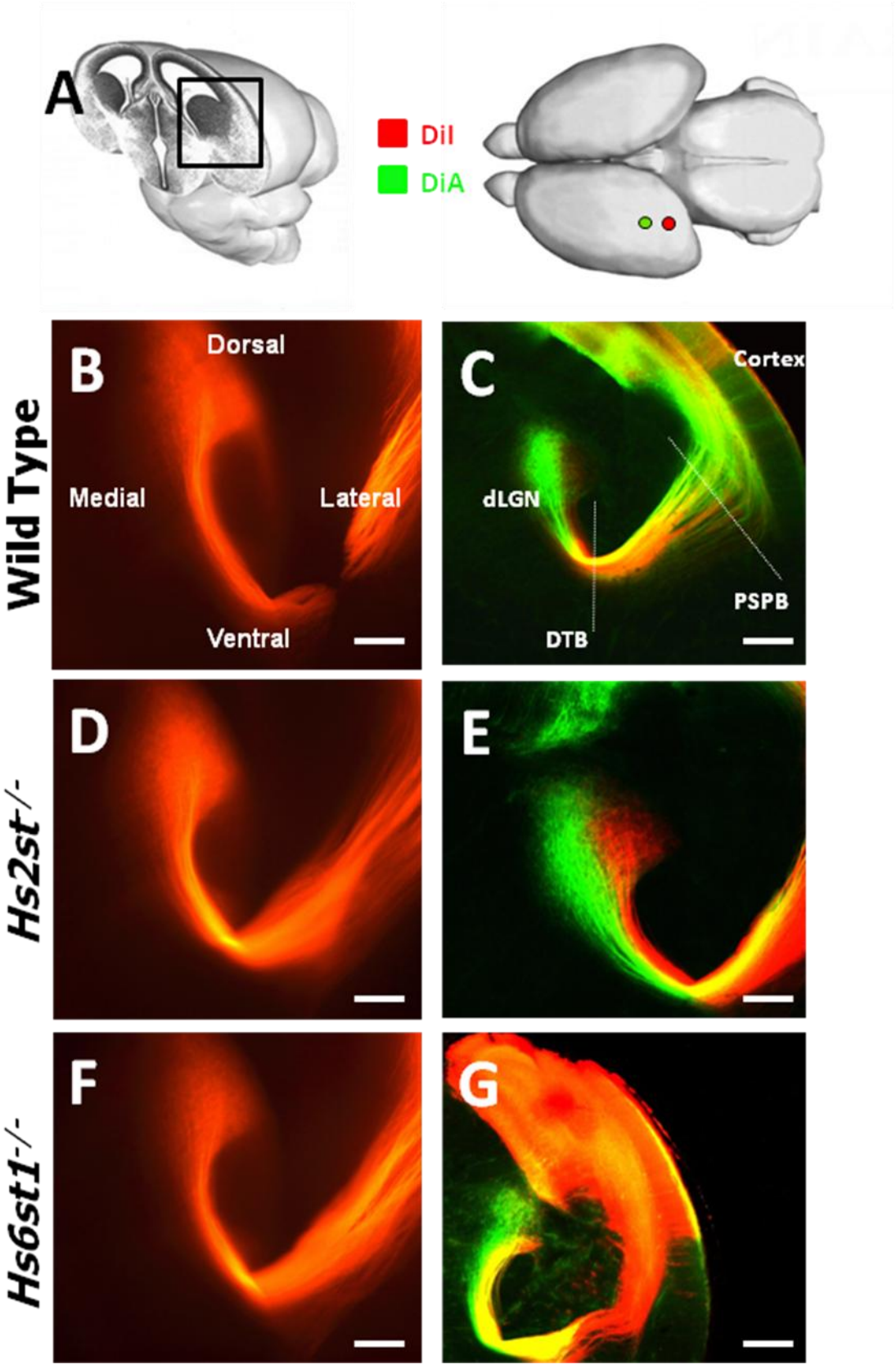
A
DiI
DiA
Wild Type
B
Dorsal
Medial
Lateral
Ventral
C
Cortex
dLGN
PSPB
DTB
Hs2st-/-
D
E
Hs6st1-/-
F
G

5.3.6 *Hs6st1*$^{-/-}$ mutants and *Hs2st*$^{-/-}$ mutants show defects in the development of the corpus callosum

The corpus callosum is a major commissural tract that links the two cortical hemispheres. The development of the corpus callosum has previously been shown to be defective in *Slit2*$^{-/-}$ mutants and *Robo1*$^{-/-}$ mutants and more severely in *Slit1*$^{-/-}$ */Slit2*$^{-/-}$ double mutants and *Robo1*$^{-/-}$*/Robo2*$^{-/-}$ double mutants where a number of callosal axons were described as forming Probst bundles after failure to cross the midline (Bagri et al., 2002; Andrews et al., 2006; Lopez-Bendito et al., 2007). We decided to look at the development of the corpus callosum in *Hs2st*$^{-/-}$ mutants and *Hs6st1*$^{-/-}$ mutants to see if they had similar defects observed in *Slit* mutants and/or *Robo* mutants and thus test our hypothesis that Slit-Robo signaling requires specific HSPG sulphation patterns to function. Characterization of the corpus callosum involved neurofilament immunohistochemistry and haematoxylin counterstaining of E17.5 wax embedded brains (Figure 8); a stage when callosal axons have normally started crossing the midline (Figure 8A). In both *Hs2st*$^{-/-}$ mutant (n=3) (Figure 8D-E) and *Hs6st1*$^{-/-}$ mutant (n=3) embryos (Figure 8F-G), there was an absence of callosal axons crossing the midline, when compared to their wild type littermates (Figure 8B-C) as observed in multiple sections of the mouse brain where the corpus callosum develops. However, this result did not rule out the possibility that what we were observing was a delay in the development of the corpus callosum. DiI and DiA were placed on opposite sides of the midline of E17.5 brains in a position that would label callosal axons (Figure 9A). Using this tract tracing technique we showed that the callosal axons in *Hs6st1*$^{-/-}$ mutants navigated correctly towards the midline, but were unable to cross the midline (Figure 9C,E) unlike wild type littermates (Figure 9B,D). Instead, these callosal axons were ectopically deflected ventrally without ever crossing the midline of the mouse brain. Further work is required to determine the mechanisms involved in the observed *Hs6st1*$^{-/-}$ mutant phenotype. While neurofilament staining suggested that axons were not able to cross the midline in *Hs2st*$^{-/-}$ mutants (Figure 8D-E), the fate of these axons has yet to be determined using DiI/DiA tract tracing.

Figure 8. **Loss of either Hs2st sulphation or Hs6st1 sulphation results in the absence of callosal axons crossing the midline.** (A) Diagram representing the coronal plane of section used to describe the trajectory of callosal axons as they navigate from one cortical hemisphere to the other (box shows the region observed in B-G). We used the neurofilament antibody to label axons and using immunohistochemistry (brown stain) we were able to characterize the route callosal axons make at the midline (dotted line) in E17.5 brains and observed in 10 µm coronal sections; haematoxylin (blue) was used to counter-stain cell bodies. While callosal axons were observed to cross the midline in E17.5 (B, arrow-C) wild type (n=3), no clear evidence was shown for callosal axon midline crossing in either (D, arrow-E) *Hs2st*$^{-/-}$ mutants (n=2) or (F, arrow-G) *Hs6st1*$^{-/-}$ mutants (n=3) as observed in multiple sections from rostral to caudal. Scale bars: 200 µm B-G.

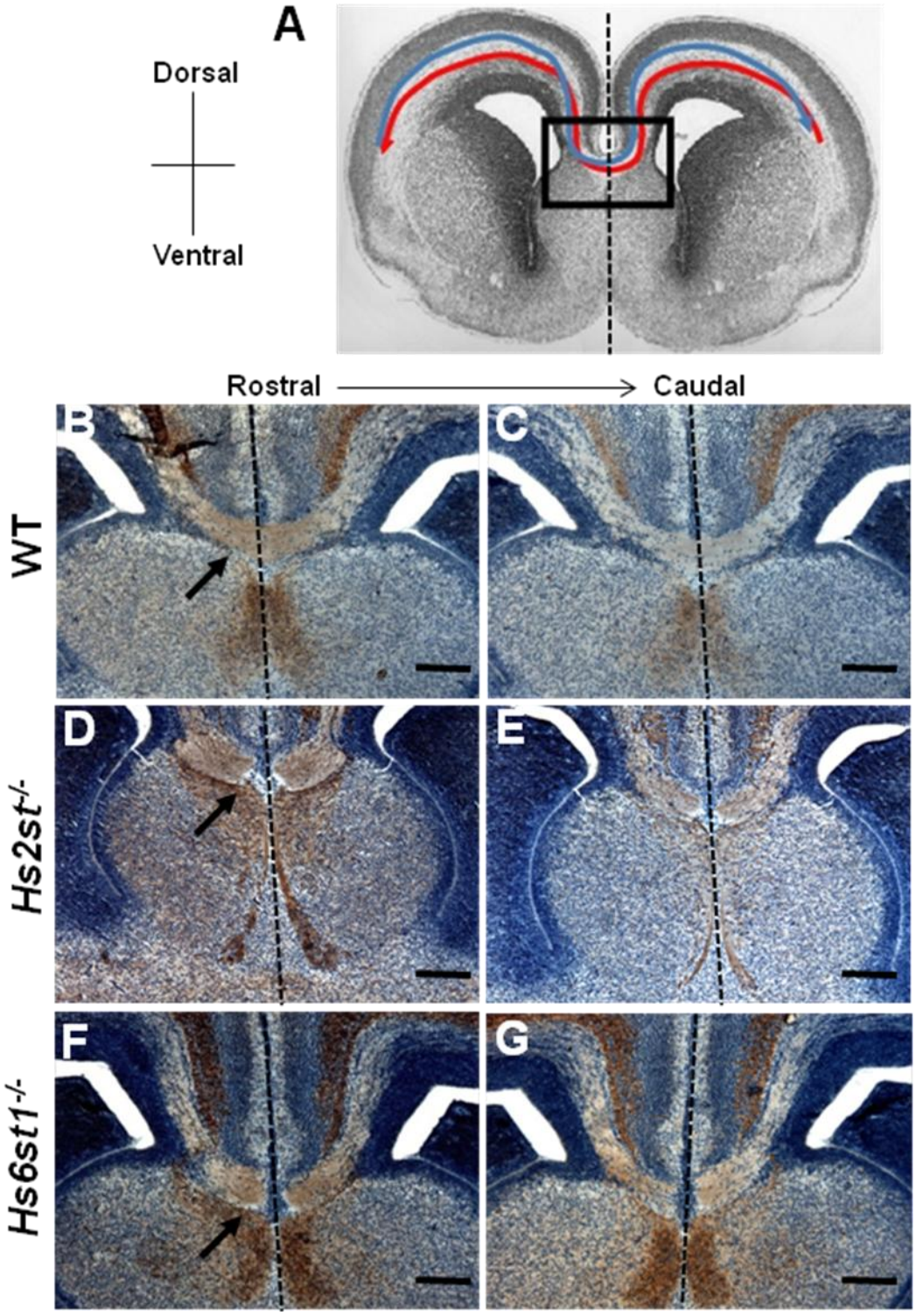
A
Dorsal
Ventral
Rostral
Caudal
B
C
WT
D
E
Hs2st-/-
F
G
Hs6st1-/-

Figure 9. **Loss of Hs6st1 sulphation results in ectopic navigation of callosal axons along the ventral midline.** (A) Diagram representing the coronal plane of section used to describe the trajectory of callosal axons as they navigate from one cortical hemisphere to the other and the placement of DiI (red) and DiA (green) (box shows the region observed in B-E). DiI was placed into the cingulate cortex on one side of the E17.5 brain, while DiA was placed into the cingulate cortex on the other side of the E17.5 brain to label callosal axons originating on either side of the developing brain and look at their trajectories in 200 µm coronal sections. Callosal axons were observed to cross the midline (observed using the nuclear stain TOPRO3, blue (B-C)) in wild type at E17.5 (n=3) (B-D) while no callosal axons were observed to cross the midline in the absence of Hs6st1 sulphation (n=3) (C-E). Instead, callosal axons were observed to deflect from the midline and navigate ectopically along the ventral midline (C-E). Scale bars: 200 µm B-E.

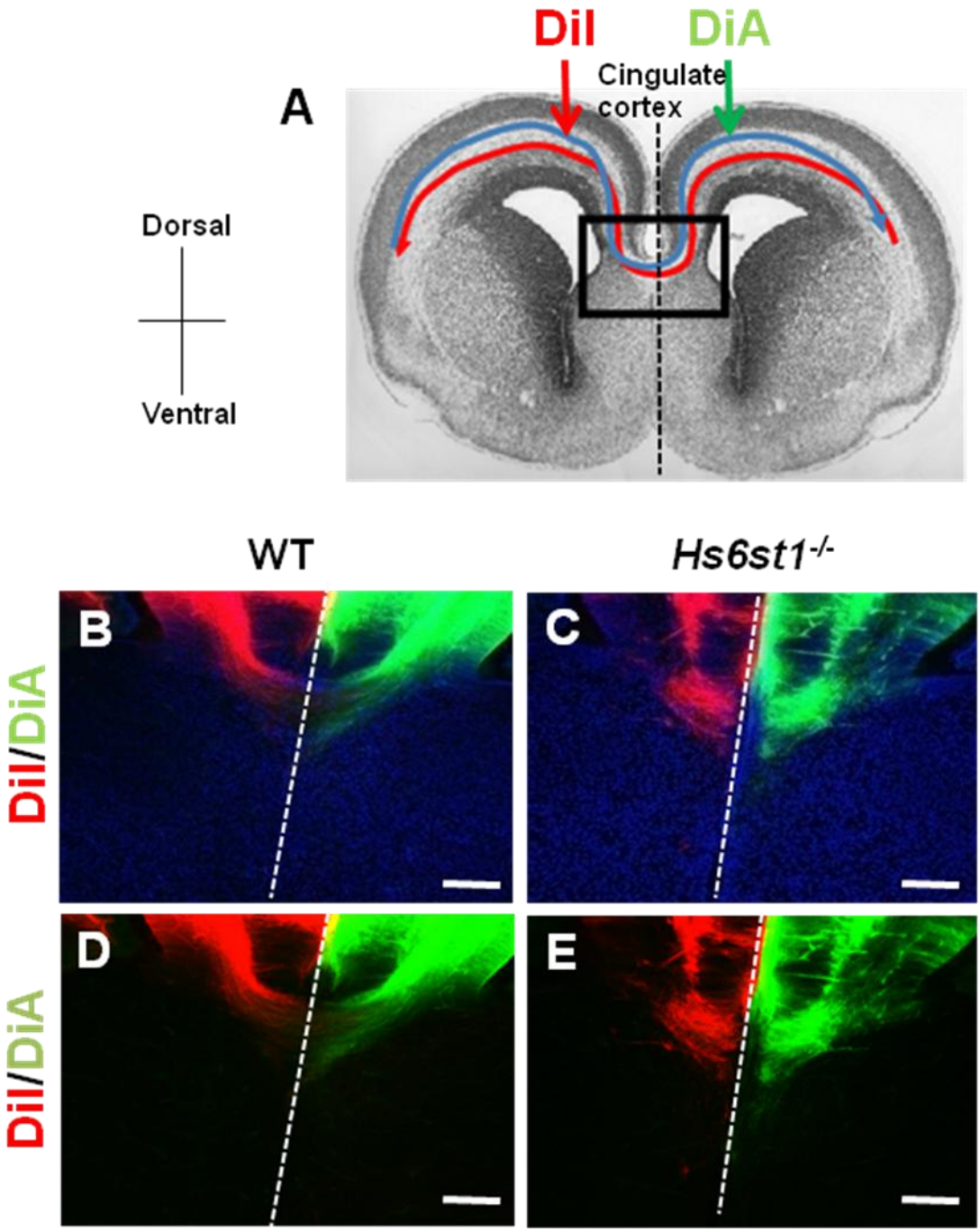
DiI
DiA
A
Cingulate cortex
Dorsal
Ventral
WT
Hs6st1-/-
B
C
D
E
DiI/DiA
DiI/DiA

5.4 Discussion

Path-finding of navigating axons relies on a number of complex regulatory mechanisms that collectively act to guide them from source to target (Dickson, 2002; Schnorrer and Dickson, 2004; Tanaka et al., 2008). Within the ECM, in which axons navigate, are differentially modified HSPGs. These differentially modified HSPGs have been shown to be crucial in mediating different aspects of neuronal development. Because of their structural diversity and their role in axon guidance, the "heparan sulphate code" hypothesis was postulated (Bulow and Hobert, 2004). This hypothesis postulated that different HSPG modifications confer different axon navigation responses as the growth cones traverse the local environment. The *Hs2st*$^{-/-}$ mutant and *Hs6st1*$^{-/-}$ mutant phenotypes reported here provide insight into the importance of HSPG sulphation patterns in regulating axon guidance in the developing mouse CNS.

5.4.1 Loss of either Hs2st sulphation or Hs6st1 sulphation results in distinct optic chiasm defects, both of which culminate in an increase in the width of the optic chiasm at the midline.

In support of the heparan sulphate code hypothesis (Bulow and Hobert, 2004), previous results established that a loss of either Hs2st sulphation or Hs6st1 sulphation resulted in distinct axon guidance defects at the E15.5 mouse optic chiasm (Pratt et al., 2006). The optic chiasm was characterized at E15.5 because this corresponded with the peak phase of RGC genesis and RGC axon guidance through the optic chiasm as well as the time when the permanent ipsilateral projection was forming. Loss of Hs2st sulphation was shown to result in RGC axons escaping the normal boundary of the optic chiasm. Loss of Hs6st1 sulphation resulted in RGC axons mis-navigating to the opposite eye. We carried out further characterization of the optic chiasm in *Hs2st*$^{-/-}$ mutants and *Hs6st1*$^{-/-}$ mutants to provide more evidence

to support the hypothesis that Hs2st sulphation and Hs6st1 sulphation differentially mediate the axon guidance molecules Slit1 and Slit2 at the optic chiasm, respectively and add further evidence for a "heparan sulphate code" in vertebrates.

5.4.2 Further characterization of the *Hs2st*$^{-/-}$ mutant phenotype at the optic chiasm

Utilizing DiI tract tracing to label RGC axons, we measured the width of the E15.5 optic chiasm at the midline in horizontal sections. Our results showed clear, statistically significant evidence that a loss of Hs2st sulphation resulted in an increase in the width of the optic chiasm when compared to wild type. Interestingly, the source of this increased optic chiasm width was observed to be the result of an ectopic tract anterior and rostral to the normal optic chiasm and not because of a general widening of the optic chiasm. The ectopic axonal tract observed in the *Hs2st*$^{-/-}$ mutant was reminiscent of the ectopic optic chiasm previously described in both *Slit1*$^{-/-}$*/Slit2*$^{-/-}$ double mutants and *Robo2*$^{-/-}$ mutants (Plump et al., 2002; Plachez et al., 2008). Using neurofilament immunohistochemistry on thin wax sections, we were able to identify the origin of the observed ectopic tract in *Hs2st*$^{-/-}$ mutants. RGC axons were observed to leave the fasciculated optic nerve before they reached the optic chiasm and navigate ectopically into the pre-optic area along the ventro-rostral surface of the third ventricle; a region usually repulsive to RGC axons.

The pre-optic area is a site of both *Slit1* and *Slit2* expression in wild type with *Slit1* expression flanking either side of the optic nerve as it enters the region of the optic chiasm and *Slit2* expressed at the midline of the pre-optic area (Figure 10D) (Erskine et al., 2000). The fact that RGC axons penetrated this usually non-permissive region suggested that *Hs2st*$^{-/-}$ mutant RGC axons were either incapable of responding to guidance cues (possibly Slit1) or the expression patterns of these guidance cues were altered in the *Hs2st*$^{-/-}$ mutant. Using Q-RTPCR and *in situ* hybridization, we looked at the expression of *Slit1, Slit2, and Robo1, Robo2* in *Hs2st*$^{-/-}$ mutants (See Chapter 7) and showed no significant alteration in expression patterns of these genes that

would explain the mutant phenotypes. We therefore concluded that the loss of Hs2st sulphation resulted in defects in Slit-Robo signaling at the pre-optic area. It is interesting to note that the ectopic tract observed in the pre-optic area of *Hs2st*$^{-/-}$ mutants was only observed in *Slit1*$^{-/-}$/*Slit2*$^{-/-}$ double mutants and not phenocopied in *Slit1*$^{-/-}$ mutants. One explanation is that in the absence of Slit1, Slit2 is capable of diffusing to the region normally occupied by Slit1 and compensating for the loss.

5.4.3 Further characterization of the *Hs6st1*$^{-/-}$ mutant phenotype at the optic chiasm

A loss of Hs6st1 sulphation was previously reported to result in an increase in the number of RGC axons mis-navigating to the opposite eye (Pratt et al., 2006). We concluded that the axon guidance defects were not the result of optic chiasm morphology defects, and implicated the repulsive guidance cue Slit2 as having a likely role in the *Hs6st1*$^{-/-}$ mutant phenotype. We showed that RGC axons from retinal explants lacking Hs6st1 sulphation had a significantly reduced chemo-repulsive response to cells expressing *Slit2 in vitro* (Pratt et al., 2006).

Further characterization of E15.5 *Hs6st1*$^{-/-}$ mutants involved optic chiasm width measurements using DiI tract tracing to label the RGC axons. Our data demonstrated a significant increase in the width of the optic chiasm in *Hs6st1*$^{-/-}$ mutants when compared to wild type embryos. However, the defects observed at the *Hs6st1*$^{-/-}$ mutant optic chiasm were different to those defects observed in *Hs2st*$^{-/-}$ mutants, i.e. there was no evidence of an ectopic tract within the pre-optic area. The observed increase in the width of the optic chiasm appeared to be the result of RGC axons mis-navigating along the caudal midline to form a peak. Neurofilament immunohistochemistry revealed that RGC axons within the optic chiasm appeared to deflect from the midline in *Hs6st1*$^{-/-}$ mutants and were propelled caudally along the midline.

While there are a number of chemical guidance cues that have been shown to dictate the navigation of RGC axons at the optic chiasm, Slits and their Robo receptors are the most likely guidance molecule candidates to explain the defects observed in both *Hs2st*$^{-/-}$ mutants and *Hs6st1*$^{-/-}$ mutants (Figure 10) (Erskine and Herrera, 2007). Slit1/Slit2 and their Robo receptors have been shown to be expressed at the optic chiasm and RGC layer of the retina, respectively (Erskine et al., 2000) (Figure 10D), Slit-Robo signalling has been shown to require HSPGs (Hu, 1999; Liang et al., 1999; Hussain et al., 2006) and Slit-Robo signalling is known to provide chemo-repulsive guidance cues to RGC axons (Plump et al., 2002). Furthermore, *Slit1*$^{-/-}$*/Slit2*$^{-/-}$ double mutants and *Robo2*$^{-/-}$ mutants have ectopic chiasms, ventral midline wandering of RGC axons and ectopic navigation of RGC axons to the contralateral eye (Plump et al., 2002; Plachez et al., 2008) (Figure 10G), all phenotypes observed in either *Hs2st*$^{-/-}$ mutants or *Hs6st1*$^{-/-}$ mutants. *Slit1*$^{-/-}$ mutants show ventral midline wandering (Plump et al., 2002) (Figure 10F) of RGC axons from the optic chiasm and unpublished data (Tom Pratt) has indicated that *Slit2*$^{-/-}$ mutants have an increased ectopic projection of RGC axons to the opposite eye (Figure 10E). All of these results considered, it is tempting to suggest that differential sulphation patterns on HSPGs differentially regulate different aspects of Slit-Robo signalling. Based on these results, we hypothesize that Hs2st sulphation is required to mediate Slit1-Robo2 signalling and Hs6st1 sulphation is required to mediate Slit2-Robo2 signalling. Future plans include both *in vitro* and *in vivo* techniques to determine whether this hypothesis is correct (See Chapter 9).

Figure 10. **Summary of RGC axon navigation at the E15.5 optic chiasm and the navigation errors that occur in *Hs2st*$^{-/-}$ mutants, *Hs6st1*$^{-/-}$ mutants and *Slit-Robo* mutants.** The phenotypes observed in (C) *Hs2st*$^{-/-}$ mutant and (B) *Hs6st1*$^{-/-}$ mutant optic chiasm closely resembles phenotypes observed in (F) *Slit1*$^{-/-}$ mutants and (E) *Slit2*$^{-/-}$ mutants, respectively. (G) *Slit1*$^{-/-}$*/Slit2*$^{-/-}$ double mutants and *Robo2*$^{-/-}$ mutants show the additive mutant phenotypes observed in the single (C) *Hs2st*$^{-/-}$ and (B) *Hs6st1*$^{-/-}$ knockouts. Based on the expression patterns of (A) *Hs2st* and *Hs6st1* and (D) *Slit1* and *Slit2* as well as their respective mutant phenotypes, it is possible that Hs2st sulphation and Hs6st1 sulphation are important in regulating Slit-Robo signaling.

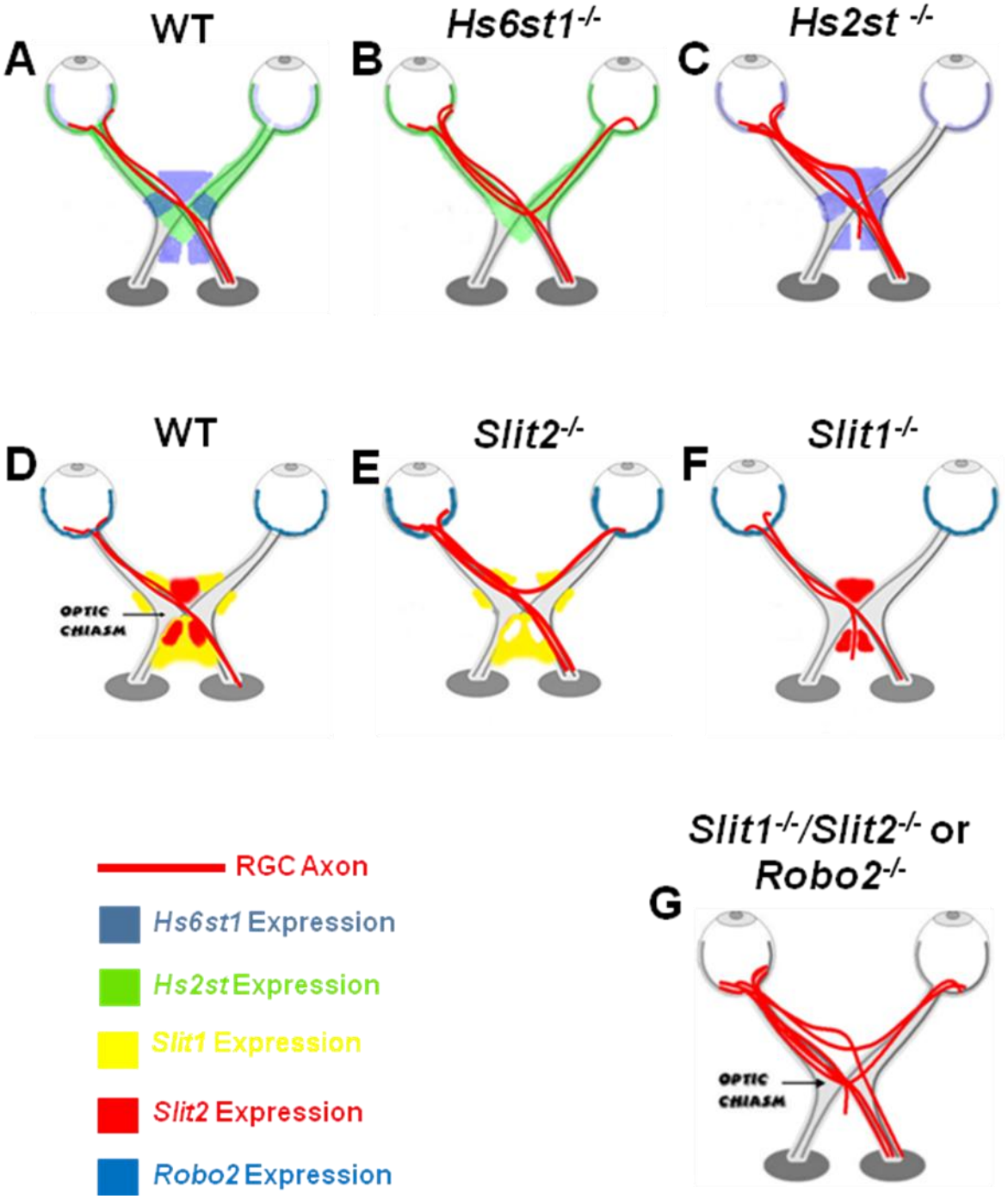
A
WT
B
Hs6st1-/-
C
Hs2st -/-
D
WT
OPTIC CHIASM
E
Slit2-/-
F
Slit1-/-
RGC Axon
Hs6st1 Expression
Hs2st Expression
Slit1 Expression
Slit2 Expression
Robo2 Expression
G
Slit1-/-/Slit2-/- or Robo2-/-
OPTIC CHIASM

5.4.4 *Hs6st1*$^{-/-}$ mutant RGC axons originating from both the DN and VT retina specifically target the VT region of the contralateral retina

In mice, all RGCs from the DN region of the retina project their axons towards contralateral targets of the visual system. Within the VT region of the retina, most RGCs are observed to project their axons to contralateral targets in the visual system, while a small percentage (3% of the total) of RGC axons are observed to project their axons to ipsilateral targets. The 3% of RGC axons that make up the ipsilateral portion of the mouse visual system gives rise to a small range of binocular vision in mice (Drager and Olsen, 1980). While this anatomical segregation of different RGCs within the retina is by far the best characterized, there are a number of different types of retinal ganglion cells that make up the RGC layer of the retina (Sun et al., 2002b).

In normal mouse embryonic development a number of RGC axons are observed to navigate towards the opposite eye, only to be pruned later in development. While the functions of these RGC axons are unknown, hypotheses have been suggested which claim they are just aberrant axons with no function, or that they play a role in axon path finding and/or patterned retinal activity (Torborg and Feller, 2005).

To determine if there was a specific population of RGCs that targeted the opposite eye we used focal injections of either DiI or DiA into either the DN or VT region of the wild type and *Hs6st1*$^{-/-}$ mutant mouse retina. However, results showed there was no bias towards RGCs from the VT retina or the DN retina sending their axons to the opposite eye. While this result does not rule out the possibility of a specific class of RGC being responsible for the retino-retinal projection it becomes exceedingly difficult to identify a specific class of RGC due to the heterogenous distribution within the retina. Another possibility for the retino-retinal projection may be explained by RGC axon positional effects within the optic chiasm. RGC axons navigating in more rostral regions of the optic chiasm may be mis-directed into the contralateral optic nerve due to a path of least resistance. More work is required

before we can determine the mechanism for the ectopic retino-retinal projection of RGC axons to the opposite eye.

It is interesting that while ectopic RGC axons could not be distinguished as being either VT or DN in origin, we did show that all ectopic RGC axons that did enter the contralateral eye specifically targeted the VT region of the retina. This suggested that wild type and *Hs6st1*$^{-/-}$ mutant RGC axons that mis-navigated to the contralateral eye were capable of responding to either chemo-attractive guidance cues within the VT retina or chemo-repulsive guidance cues within the DN retina. While we did not attempt to determine which guidance cues these ectopic RGC axons were responding to, we were interested to know whether these ectopic RGC axons were entering the OFL of the contralateral retina or if they were wandering outside of the OFL (Discussed below).

5.4.5 RGC axons are restricted to the OFL of the retina in *Hs6st1*$^{-/-}$ mutants

Previous work reported defects in RGC axon guidance specifically within the VT region of the retina in *Slit2*$^{-/-}$ and more severely *Slit1*$^{-/-}$*/Slit2*$^{-/-}$ mice (Thompson et al., 2006b). In these mutants, RGC axons were described as exiting the OFL aberrantly as they navigated towards the optic disc due to the absence of Slit1/Slit2 repulsion. Nevertheless, all RGC axons were shown to be capable of exiting the eye and navigating to the optic chiasm. Using DiI tract tracing and L1 immunohistochemistry, we looked at the trajectories of RGC axons in the retina of *Hs6st1*$^{-/-}$ mutants however; we did not observe any phenocopy of the defects described in *Slit2*$^{-/-}$ mutants showing that all RGC axons were restricted to the OFL of the retina. It is interesting to note that not only were the intra-retinal RGC axons restricted to the OFL in *Hs6st1*$^{-/-}$ mutants, but also the inter-retinal RGC axons that were specifically targeting the VT region of the contralateral retina. One possible explanation is that the loss of Hs6st1 sulphation in the retina is compensated for by other enzymes capable of 6-O-sulphation. Using *in situ* hybridization, we looked at

the expression of two genes capable of 6-O-sulphation (*Hs6st2* and *Hs6st3*) and found that *Hs6st3* is highly expressed in the retina (Chapter 8).

5.4.6 *Hs6st1*$^{-/-}$ mutant RGC axons showed increased defasciculation at the dLGN.

After making the decision at the mouse optic chiasm to either cross the midline and form the contralateral optic tract or be repelled from crossing the midline (Williams et al., 2003) and form part of the ipsilateral optic tract, RGC axons navigate over the surface of the diencephalon and terminate at the SC. While all RGC axons terminate at the SC in rodents, at the surface of the dorsal thalamus the optic tracts are observed to defasciculate and ~33% of these RGC axons send branches that innervate the dLGN (Martin, 1986). Our findings revealed an increase in the defasciculation of *Hs6st1*$^{-/-}$ mutant RGC axons as they traversed the dLGN without any other defects in the rest of the optic tract consistent with high *Hs6st1* expression at the dLGN (See Chapter 3). While there are few axon guidance molecules that have been implicated in directing RGC axons within the optic tract, Slit-Robo signalling has been shown to direct RGC axons within the optic tract. Previous work in *Slit1*$^{-/-}$*/Slit2*$^{-/-}$ double mutant animals showed RGC axons leaving the fasciculated optic tract and navigating over the pial surface within the telencephalon as well as ectopically entering the usually repulsive epithalamus (Thompson et al., 2006a). While we did not see either of these phenotypes in either the *Hs2st*$^{-/-}$ mutants or *Hs6st1*$^{-/-}$ mutants, it is possible that either there was a genetic background effect or there was a compensation event for the loss of Hs2st sulphation and/or Hs6st1 sulphation. Observations of the optic tract as it traversed the dLGN showed an increase in the defasciculation of RGC axons when *Hs6st1*$^{-/-}$ mutants were compared to wild type or *Hs2st*$^{-/-}$ mutants. This has recently been described in *Robo2*$^{-/-}$ mutants where they showed an increase in the defasciculation of RGC axons at the dLGN (Plachez et al., 2008). While it is yet to be determined whether the RGC axons have increased defasciculation or an increase in the number of collaterals at the dLGN, the

Hs6st1$^{-/-}$ mutant phenotype does phenocopy the previously described *Robo2*$^{-/-}$ mutant phenotype and adds support to the hypothesis that HSPG sulphation patterns differentially regulate Slit-Robo signalling.

5.4.7 TCA/CTA tract formation does not appear to depend on either Hs2st sulphation or Hs6st1 sulphation.

Observations of the mouse TCA tract at E17.5 did not reveal any major defects in development. While HSPGs have been shown to be important in the formation of this tract (Kinnunen et al., 1999), it appears that both Hs2st sulphation and Hs6st1 sulphation by themselves, are not critical. Slit-Robo signaling has been shown to be important in the formation of the mouse TCA/CTA tracts with mutants showing severe axon guidance defects (Bagri et al., 2002; Lopez-Bendito et al., 2007). While these results do not support the hypothesis that Hs2st sulphation and Hs6st1 sulphation critically regulate Slit-Robo signaling, there are a number of possible explanations. HSPGs have been shown to be capable of sulphation compensation in the absence of particular sulphation enzymes and may explain the absence of a phenotype in *Hs2st*$^{-/-}$ mutant and/or *Hs6st1*$^{-/-}$ mutant embryos (Merry et al., 2001; Habuchi et al., 2007; Sugaya et al., 2008). Not only is there the possibility of compensatory effects in sulphation deficits of HSPGs, but also compensatory effects by different types of HSPGs that may differentially interact with Slit-Robo signaling i.e. HSPGs that are capable of interacting with Slit-Robo in the absence of Hs2st sulphation and/or Hs6st1 sulphation. We have shown that *Hs6st2* is highly expressed at the dLGN and is known to sulphate the same region of HSPGs as Hs6st1 and may compensate for the loss of Hs6st1 sulphation in *Hs6st1*$^{-/-}$ mutants (See Chapter 7).

5.4.8 Loss of Hs6st1 sulphation or Hs2st sulphation results in the failure of callosal axons to cross the midline at E17.5

Observations of E17.5 mouse brains indicated the absence of midline crossing of callosal axons in the absence of either Hs2st sulphation or Hs6st1 sulphation. Axons appeared to correctly navigate their way from the cortex to the midline, however at the midline callosal axons were never observed to cross. While the absence of callosal axons to make it across the midline may have been due to developmental delay, we showed that at least in the *Hs6st1*$^{-/-}$ mutants, callosal axons ectopically navigated along the ventral midline to form Probst bundles. This acallosal phenotype has been observed in a number of mouse models including *Netrin1*$^{-/-}$ mutant animals (Serafini et al., 1996). While Robo1$^{-/-}$ mutants and *Slit2*$^{-/-}$ mutants and more severely *Robo1*$^{-/-}$*/Robo2*$^{-/-}$ double mutants and *Slit1*$^{-/-}$*/Slit2*$^{-/-}$ double mutants have been shown to have defects in midline crossing of callosal axons at E17.5, they do not exactly phenocopy the phenotype observed in *Hs6st1*$^{-/-}$ mutants. Both *Robo1*$^{-/-}$ mutants and *Slit2*$^{-/-}$ mutants as well as *Robo1*$^{-/-}$*/Robo2*$^{-/-}$ double mutants and *Slit1*$^{-/-}$*/Slit2*$^{-/-}$ double mutants show that while some callosal axons are able to cross the midline at E17.5, many of them are incapable, instead forming Probst bundles (Bagri et al., 2002; Andrews et al., 2006; Lopez-Bendito et al., 2007). There are a number of possible reasons why the loss of Hs6st1 sulphation results in the failure of callosal axons to navigate across the midline. Tissue morphology may be disrupted including the glial structures that have been implicated in corpus callosum formation (Lindwall et al., 2007). It is possible that a loss of Hs6st1 sulphation results in the failure of callosal axons to respond to one or more of the axon guidance cues known to regulate corpus callosum formation. Further work is required before conclusions can be made (See Chapter 8). While preliminary work has shown that *Hs2st*$^{-/-}$ mutant callosal axons fail to cross the midline, more work is required to determine the extent and reason for this phenotype.

5.5 Summary

Observations of axonal tracts within the mouse CNS indicate that their development while being dependent on HSPGs, are differentially dependent on the status of HSPG sulphation modifications as hypothesized by the "heparan sulphate code" (Bulow and Hobert, 2004). Here we show that Hs2st sulphation and Hs6st1 sulphation differentially regulate different aspects of axon guidance in different axonal systems. While mounting evidence suggests that Hs2st sulphation is absolutely required for Slit1-Robo2 signaling and Hs6st1 sulphation is absolutely required for Slit2-Robo2 signaling in optic chiasm development, this association is not so clear in other regions of CNS development. Taking into account the possibility of redundancy in CNS development and the fact that the function of many axon guidance molecules are reflective of the context in which they are encountered and also on the type of axon involved, it is not surprising that a simple set of rules not be sufficient to explain the complexity of axon guidance in the developing CNS.

Chapter 6: Characterization of RGC Axon Navigation at the Optic Chiasm of Compound *Hs2st/Hs6st1* Mutants.

6.1 Introduction

Disruption of either *Hs2st* or *Hs6st1* resulted in distinct axon guidance phenotypes at the optic chiasm. These distinct phenotypes were shown to phenocopy aspects of *Slit1*$^{-/-}$ mutants and *Slit2*$^{-/-}$ mutants and prompted us to propose the hypothesis that Hs2st was uniquely required for Slit1 signalling and Hs6st1 was uniquely required for Slit2 signalling (Pratt et al., 2006).

It is possible that Hs2st and Hs6st1 also have redundant functions in optic chiasm formation where the loss of one Hst is insufficient to cause a defect, but the loss of both Hs2st and Hs6st1 results in defects not observed in either of the single Hst mutants. In order to gain further insight into the phenotypes observed in *Hs2st*$^{-/-}$ mutant and *Hs6st1*$^{-/-}$ mutant mice embryos, we planned to create *Hs2st*$^{-/-}$/*Hs6st1*$^{-/-}$ double mutants. Generation of such mutants would answer whether these two enzymes have unique and/or redundant functions in optic chiasm development.

Unfortunately we were unable to simply inter-cross *Hs2st*$^{-/-}$ mutant mice with *Hs6st1*$^{-/-}$ mutant mice since *Hs2st*$^{-/-}$ mutant mice die perinatally due to renal agenesis (Bullock et al., 1998) and *Hs6st1*$^{-/-}$ mutant mice have low postnatal survival (See Chapter 4). Using the newly designed PCR genotyping strategy to identify *Hs6st1*$^{-/-}$ mutants (See Chapter 4) it was now possible to identify the genotypes of compound *Hs2st/Hs6st1* mutants.

6.2 Aims

We aimed to generate *Hs2st*$^{-/-}$/*Hs6st1*$^{-/-}$ double mutants as well as the intermediate compound *Hs2st/Hs6st1* mutant genotypes possible from inter-crossing *Hs2st*$^{+/-}$ /*Hs6st1*$^{+/-}$ animals. Using *Hs2st*$^{-/-}$/*Hs6st1*$^{-/-}$ double mutants we planned to determine whether *Hs2st* and *Hs6st1* have unique and/or redundant functions in optic chiasm formation in the developing mouse visual system.

In the event *Hs2st* and *Hs6st1* have unique functions in optic chiasm development, we predict *Hs2st*$^{-/-}$/*Hs6st1*$^{-/-}$double mutants to show an additive phenotype of the single *Hs2st*$^{-/-}$ mutant (midline wandering and ectopic RGC axon navigation into the pre-optic area) and *Hs6st1*$^{-/-}$ mutant (ectopic retino-retinal projection). If however, *Hs2st* and *Hs6st1* have redundant functions in optic chiasm development, we predict *Hs2st*$^{-/-}$/*Hs6st1*$^{-/-}$double mutants to have a more severe phenotype than the simple addition of the single *Hs2st*$^{-/-}$ mutant and *Hs6st1*$^{-/-}$ mutant phenotypes. We planned to quantify the compound *Hs2st/Hs6st1* mutant phenotypes observed at the optic chiasm by counting the number of retino-retinal projections and measuring the width of the optic chiasm at the midline using the same techniques used for *Hs2st* and *Hs6st1* single mutants described in Chapter 5.

6.3 Results

6.3.1 *Hs2st*$^{-/-}$*/Hs6st1*$^{-/-}$ double mutants suffer early embryonic death

Hs2st$^{+/-}$*/Hs6st1*$^{+/-}$ CBA mice were inter-crossed and their progeny were PCR genotyped at E15.5. PCR genotyping results of E15.5 embryos did not conform to Mendelian rules (Table 1). Chi-squared analysis showed the difference between the observed and expected numbers of *Hs2st*$^{-/-}$/*Hs6st1*$^{-/-}$ double mutant embryos to be statistically significant with a P-value <0.05 (Table 1). Based on Mendelian rules,

we expected 1/16 of genotyped embryos to be *Hs2st*$^{-/-}$/*Hs6st1*$^{-/-}$ double mutant; however no E15.5 embryos were observed to carry this genotype. Embryos lacking either *Hs2st*$^{-/-}$ or *Hs6st1*$^{-/-}$ combined with a heterozygous mutation in either *Hs6st1*$^{+/-}$ or *Hs2st*$^{+/-}$ respectively, were observed to survive to E15.5 in predicted numbers. This result showed that one copy of either *Hs2st* or *Hs6st1* was enough to prevent early embryonic death in *Hs6st1*$^{-/-}$ or *Hs2st*$^{-/-}$ embryos, respectively. The accumulated data suggests that Hs2st sulphation and Hs6st1 sulphation together, are critical to early embryonic development. Embryos lacking the two *Hs2st* alleles and the two *Hs6st1* alleles die before E15.5, while embryos lacking 3 out of the four Hst alleles are capable of surviving to E15.5.

Table 1. ***Hs2st*$^{-/-}$/*Hs6st1*$^{-/-}$ double mutants do not survive to E15.5.**

Age	# of animals	Genotype	Observed (%)	Expected (%)
E15.5	159	wild type	(10) 6.3%	6.3%
		Hs2st$^{+/+}$/*Hs6st1*$^{+/-}$	(19) 11.9%	12.6%
		Hs2st$^{+/+}$/*Hs6st1*$^{-/-}$	(12) 7.5%	6.3%
		Hs2st$^{+/-}$/*Hs6st1*$^{+/+}$	(17) 10.7%	12.6%
		Hs2st$^{+/-}$/*Hs6st1*$^{+/-}$	(41) 25.8%	24.5%
		Hs2st$^{+/-}$/*Hs6st1*$^{-/-}$	(20) 12.6%	12.6%
		Hs2st$^{-/-}$/*Hs6st1*$^{+/+}$	(10) 6.3%	6.3%
		Hs2st$^{-/-}$/*Hs6st1*$^{+/-}$	(30) 18.9%	12.6%
		Hs2st$^{-/-}$/*Hs6st1*$^{-/-}$	(0) 0%**	6.3%

**Chi-squared analysis $P<0.05$

6.3.2 No evidence for functional redundancy between Hs2st and Hs6st1 in the formation of the ectopic retino-retinal projection.

We previously showed that a loss of Hs6st1 sulphation resulted in an increase in the number of ectopic RGC axons mis-projecting from one eye to the other eye in the developing mouse visual system (Pratt et al., 2006). To test whether Hs2st sulphation and Hs6st1 sulphation were functionally redundant in optic chiasm development, we counted the number of RGC axons that mis-projected to the opposite eye in compound *Hs2st/Hs6st1* mutants. Using E15.5 embryos, we unilaterally injected DiI into the eye and counted the number of back-labelled RGC bodies in the opposite eye (mean ± SEM). DiI labelled RGC bodies were counted in serial 200 μm horizontal sections of the contralateral retina using epifluorescence microscopy to identify the morphologically distinct RGC cell bodies. RGC counts revealed no significant increase in the number of RGC axons mis-projecting to the opposite eye in *Hs2st*$^{-/-}$*/Hs6st1*$^{+/+}$ mutants (n=4), *Hs2st*$^{-/-}$*/Hs6st1*$^{+/-}$ double mutants (n=6), or *Hs2st*$^{+/-}$*/Hs6st1*$^{+/-}$ double mutants (n=7) when compared to wild type (n=5) (Figure 1A, C, E). RGC counts revealed a significant increase in the number of mis-projecting RGC axons to the opposite eye in *Hs2st*$^{+/+}$*/Hs6st1*$^{-/-}$ mutants (n=4) and *Hs2st*$^{+/-}$*/Hs6st1*$^{-/-}$ double mutants (n=4) when compared to wild type (n=5) (Student's t-test, $P<0.05$), however no significant difference was observed between *Hs2st*$^{+/+}$*/Hs6st1*$^{-/-}$ mutants and *Hs2st*$^{+/-}$*/Hs6st1*$^{-/-}$ double mutants (Figure 1B, D, E).

Figure 1. **Loss of Hs6st1 sulphation results in a significant increase in the retino-retinal projection irrespective of *Hs2st* genotype.** The trajectories of RGC axons were observed in 200 µm horizontal sections when DiI (red) was unilaterally placed into the retina of the eye (red arrow in B) of E15.5 embryos; sections were counterstained with the nuclear counterstain TOPRO3 (blue). In (A) wild type embryos capable of Hs6st1 sulphation, few RGC axons were observed to mis-navigate from one eye to the other as observed in (C) back-labeled RGC bodies in the opposite eye. In (B) *Hs6st1*$^{-/-}$ mutant embryos lacking Hs6st1 sulphation, a large number of RGC axons were observed to mis-navigate from one eye to the other as observed in (D) back-labeled RGC bodies in the opposite eye. (E) We counted the number of back-labeled RGC bodies in the contralateral eye (mean ± SEM) and showed there was no statistical evidence for an increase in the retino-retinal projection in *Hs2st*$^{-/-}$ mutants 65±17 (n=4), *Hs2st*$^{+/-}$*/Hs6st1*$^{+/-}$ double mutants 119 ±25 (n=7), or *Hs2st*$^{-/-}$*/Hs6st1*$^{+/-}$ double mutants 84±25 (n=6) when compared to wild type 59±18 (n=5). While there was a statistically significant increase in the number of back-labeled RGC bodies in *Hs6st1*$^{-/-}$ mutants 894±219 (n=4) and *Hs2st*$^{+/-}$*/Hs6st1*$^{-/-}$ double mutants 865±191 (n=4) when compared to the wild type, there was no significant difference when they were compared to each other ((Kruskal-Wallis one way ANOVA on ranks, pair wise multiple comparisons (Dunn's method), $P<0.05$). RGCs, retinal ganglion cells; L, lens. Scale bars: 400 µm A-B; 100 µm C-D.

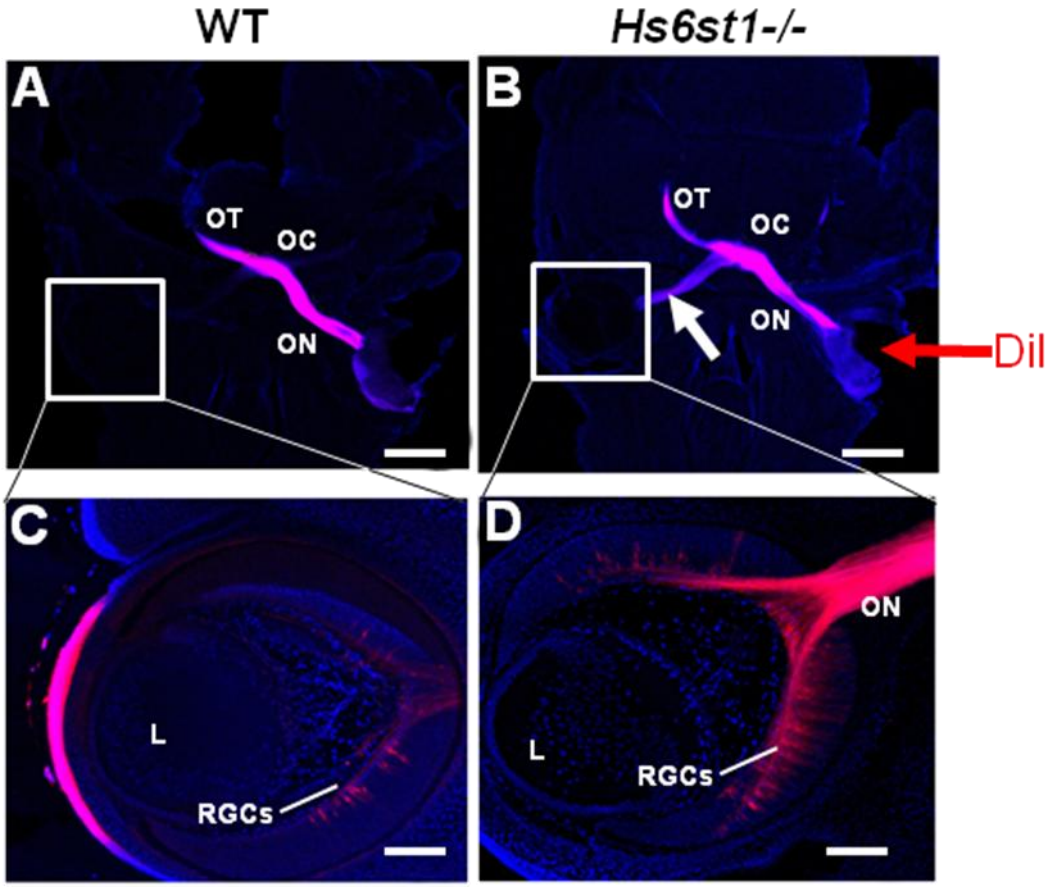
WT
Hs6st1-/-
A
B
OT
OC
ON
Dil
C
D
L
RGCs

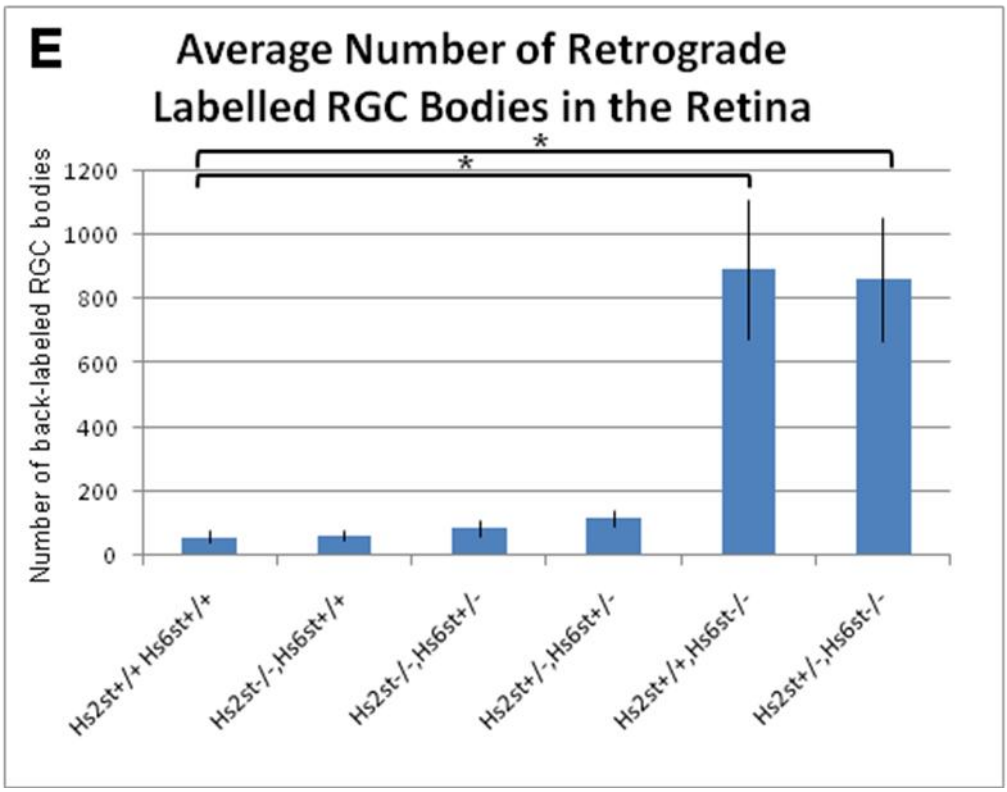
E
Average Number of Retrograde Labelled RGC Bodies in the Retina
Number of back-labeled RGC bodies
1200
1000
800
600
400
200
0
*
*
Hs2st+/+ Hs6st+/+
Hs2st-/-,Hs6st+/+
Hs2st-/-,Hs6st+/-
Hs2st+/-,Hs6st+/-
Hs2st+/+,Hs6st-/-
Hs2st+/-,Hs6st-/-

6.3.3 *Hs2st*$^{-/-}$*/Hs6st1*$^{+/-}$ and *Hs2st*$^{+/-}$*/Hs6st1*$^{-/-}$ double mutants do not provide any evidence for functional redundancy between Hs2st and Hs6st1 at the optic chiasm.

Observations of optic chiasm formation in *Hs2st*$^{-/-}$ mutants and *Hs6st1*$^{-/-}$ mutants revealed distinct defects at the optic chiasm resulting in a significant increase in the width of the optic chiasm at the midline when compared to wild type (see Chapter 5). To look for evidence of functional redundancy between Hs2st and Hs6st1, we measured the width of the optic chiasm in compound *Hs2st/Hs6st1* mutants. Using E15.5 embryos, we unilaterally injected DiI into the eye to label RGC axons. 200 µm serial stacked, horizontal sections of the DiI labeled brain were imaged and the images manually aligned using Photoshop software to view the entire optic chiasm. We defined the optic chiasm to include any RGC axon that was DiI labeled and therefore, single RGC axons that were observed were included in the measurements. Rostro-caudal measurements of the optic chiasm were taken at the anatomical midline using Image J software. We found a significant increase in the rostro-caudal width of the optic chiasm in *Hs2st*$^{-/-}$*/Hs6st1*$^{+/+}$ mutants (n=7) (Student's t-test, $P < 0.05$) and the *Hs2st*$^{-/-}$*/Hs6st1*$^{+/-}$ double mutants (n=4) were also shown to be wider when compared to the wild type (n=5). While both *Hs2st*$^{-/-}$*/Hs6st1*$^{+/+}$ mutants and *Hs2st*$^{-/-}$*/Hs6st1*$^{+/-}$ double mutants showed the characteristic ectopic projection into the pre-optic area (See Chapter 5), no morphological or quantitative differences at the optic chiasm were observed between *Hs2st*$^{-/-}$*/Hs6st1*$^{+/+}$ mutants and *Hs2st*$^{-/-}$*/Hs6st1*$^{+/-}$ double mutants (Figure 2A-B,D). The rostro-caudal width of the optic chiasm in *Hs2st*$^{+/+}$*/Hs6st1*$^{-/-}$ mutants (n=5) was shown to be significantly increased (Student's t-test, $P<0.05$) and the width of the *Hs2st*$^{+/-}$*/Hs6st1*$^{-/-}$ double mutants (n=3) was also shown to be increased (n=5). Both *Hs2st*$^{+/+}$*/Hs6st1*$^{-/-}$ mutants and *Hs2st*$^{+/-}$*/Hs6st1*$^{-/-}$ double mutants showed the characteristic ectopic caudal peak at the midline (See Chapter 5) however no morphological or quantitative differences were observed at the optic chiasm when *Hs2st*$^{+/+}$*/Hs6st1*$^{-/-}$ mutants and *Hs2st*$^{+/-}$*/Hs6st1*$^{-/-}$ double mutants were compared (Figure 2A-C,D).

Figure 2. ***Hs2st*$^{-/-}$*/Hs6st1*$^{+/-}$ and *Hs2st*$^{+/-}$*/Hs6st1*$^{-/-}$ double mutants do not result in a more severe optic chiasm phenotype.** DiI tract tracing (white color in grey scale) revealed the structure of the optic chiasm in (A) wild type, (B) *Hs2st*$^{-/-}$ mutants lacking Hs2st sulphation, and (C) *Hs6st1*$^{-/-}$ mutants lacking Hs6st1 sulphation as observed in 200 µm horizontal sections when DiI was placed into the retina of one eye (large red arrow in C) of E15.5 embryos. In mutants lacking Hs2st sulphation the optic chiasm appeared wider along the rostro-caudal midline due to the formation of an ectopic tract rostral to the optic chiasm (B, white arrow). In mutants lacking Hs6st1 sulphation the optic chiasm appeared wider along the rostro-caudal midline due to ectopic axon navigation along the caudal midline of the ventral diencephalon (C, white arrow). Width measurements of the optic chiasm were taken along the midline where the optic chiasm was taken to consist of any DiI RGC axon that could be detected using confocal microscopy (red arrow). The width (mean ± SEM) of the wild type optic chiasm (n=5) was 345µm±51µm. The width of the *Hs2st*$^{-/-}$ mutant optic chiasm (n=7) was 448µm±30µm and the width of the *Hs6st1*$^{-/-}$ mutant optic chiasm (n=5) was 435µm±25µm. The width of the optic chiasm was significantly greater in both the *Hs6st1*$^{-/-}$ mutant and the *Hs2st*$^{-/-}$ mutant, when compared to the wild type (one way ANOVA, multiple comparisons versus a control group (Holm-Sidak method), $P<0.05$). The width of the optic chiasm in *Hs2st*$^{-/-}$*/Hs6st1*$^{+/-}$ double mutants (n=4) was 438±45 µm while the width of the optic chiasm in *Hs2st*$^{+/-}$*/Hs6st1*$^{-/-}$ double mutants (n=3) was 447±44 µm which were comparable to results observed in *Hs2st*$^{-/-}$ mutants and *Hs6st1*$^{-/-}$ mutants, respectively. Scale bar: 200 µm A-E.

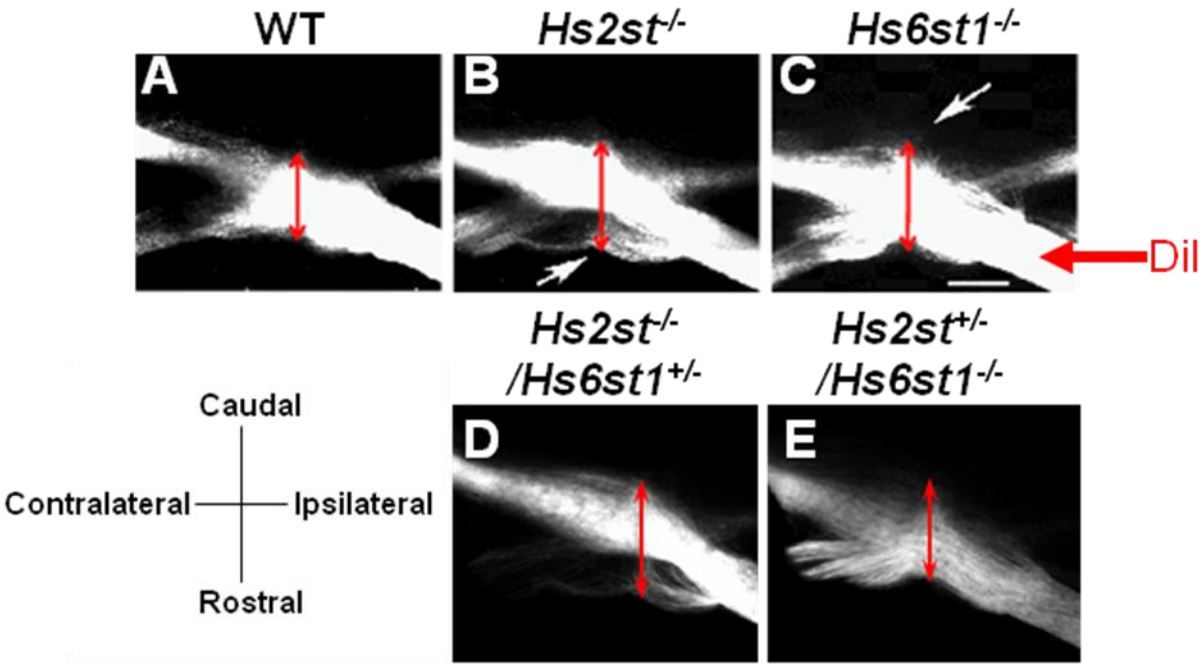
WT
Hs2st-/-
Hs6st1-/-
A
B
C
DiI
Caudal
Contralateral
Ipsilateral
Rostral
Hs2st-/-
/Hs6st1+/-
Hs2st+/-
/Hs6st1-/-
D
E

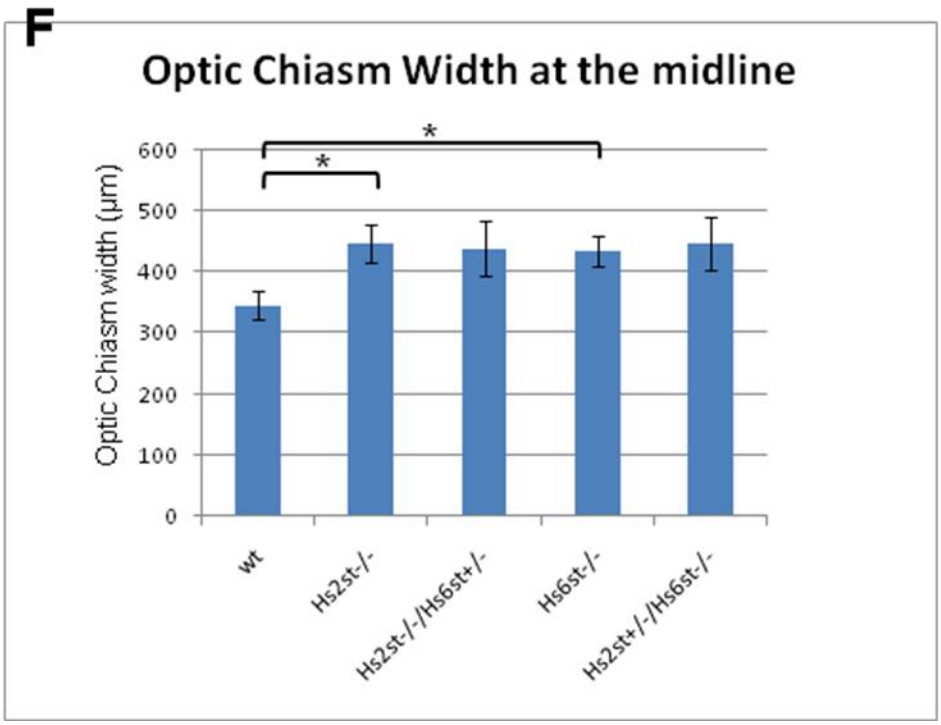
F
Optic Chiasm Width at the midline
Optic Chiasm width (µm)
600
500
400
300
200
100
0
*
*
wt
Hs2st-/-
Hs2st-/-/Hs6st+/-
Hs6st-/-
Hs2st+/-/Hs6st-/-

6.4 Discussion

Previous work on the role *Hs2st* and *Hs6st1* have on RGC axon guidance at the optic chiasm showed distinct phenotypes when either Hs2st sulphation or Hs6st1 sulphation was lost suggesting unique roles in optic chiasm formation (Pratt et al., 2006). These results provided evidence that differential sulphation patterns at the optic chiasm were individually important for different axon navigation cues. However, these results did not rule out the possibility that *Hs2st* and *Hs6st1* also have redundant functions in mediating axon guidance at the optic chiasm, possibly through interactions with other axon guidance cues.

6.4.1 Early embryonic death in *Hs2st*$^{-/-}$/*Hs6st1*$^{-/-}$ double mutants suggests the possibility for functional redundancy in early embryonic development.

In order to address the possibility that Hs2st and Hs6st1 have redundant functions in axon guidance, we attempted to generate *Hs2st*$^{-/-}$/*Hs6st1*$^{-/-}$ double mutants and characterize their RGC axon guidance at the optic chiasm. Unfortunately, we discovered that these mutants died early in embryonic development at a stage before RGC axons arrived at the optic chiasm. This early embryonic lethality is a common theme in animals carrying a mutation(s) in genes responsible for HSPG modifications indicating the importance of HSPG modifications in embryonic development (See Chapter 1, Table1). The fact *Hs2st*$^{-/-}$/*Hs6st1*$^{-/-}$ double mutants die early in development, while *Hs2st*$^{-/-}$ mutants and *Hs6st1*$^{-/-}$ mutants survive to birth suggested a possible redundancy in Hs2st and Hs6st1 function. Possible explanations for the early embryonic death observed in *Hs2st*$^{-/-}$/*Hs6st1*$^{-/-}$ double mutants are 1) Hs2st and Hs6st1 are required in the same critically important developmental pathway suggesting functional redundancy or 2) Hs2st function is required for one developmental pathway while Hs6st1 is required for another

developmental pathway; a loss of both pathways results in early embryonic death. It will be of interest to determine when and why *Hs2st*$^{-/-}$*/Hs6st1*$^{-/-}$ double mutants die.

6.4.2 *Hs2st*$^{-/-}$*/Hs6st1*$^{+/-}$ double mutants and *Hs2st*$^{+/-}$*/Hs6st1*$^{-/-}$ double mutants show no evidence for functional redundancy between Hs2st and Hs6st1 in optic chiasm development.

Characterization of the optic chiasm in compound *Hs2st/Hs6st* mutants showed no morphological or quantitative differences between *Hs2st*$^{-/-}$*/Hs6st1*$^{+/+}$ mutants and *Hs2st*$^{-/-}$*/Hs6st1*$^{+/-}$ double mutants or *Hs2st*$^{+/+}$*/Hs6st1*$^{-/-}$ mutants and *Hs2st*$^{+/-}$*/Hs6st1*$^{-/-}$ double mutants. The evidence to date, suggests that Hs2st and Hs6st1 have unique functions in optic chiasm formation. However, we cannot rule out the possibility that a single copy of either *Hs2st* or *Hs6st1* is sufficient to maintain a signalling pathway that shows a redundant requirement for Hs2st and Hs6st1 function without characterizing *Hs2st*$^{-/-}$*/Hs6st1*$^{-/-}$ double mutants. Consistent with this, we have yet to identify an *Hs2st*$^{+/-}$ or *Hs6st1*$^{+/-}$ phenotype.

While we have shown that it is not possible to generate *Hs2st*$^{-/-}$*/Hs6st1*$^{-/-}$ double mutants through inter-crossing mutant animals, future plans will involve an alternative approach using conditional mutants via the *Cre-loxP* system to generate *Hs2st*$^{-/-}$*/Hs6st1*$^{-/-}$ double mutants specifically targeted to the developing CNS. This approach is described in more detail in Chapter 9.

6.5 Summary

We have confirmed that *Hs2st*$^{-/-}$*/Hs6st1*$^{-/-}$ double mutants die at a stage before optic chiasm development can be characterized. Furthermore, we have confirmed that *Hs2st*$^{-/-}$*/Hs6st1*$^{+/-}$ double mutants and *Hs2st*$^{+/-}$*/Hs6st1*$^{-/-}$ double mutants show no increase in the severity of the optic chiasm phenotypes previously described for

Hs2st$^{-/-}$ mutants and *Hs6st1*$^{-/-}$ mutants, respectively. Based on the results to date, it is still unclear whether *Hs2st* and *Hs6st1* can act redundantly to mediate axon guidance at the optic chiasm without looking at *Hs2st*$^{-/-}$/*Hs6st1*$^{-/-}$ double mutants.

Chapter 7. Expression of *Slit1*/*Slit2* at the Optic Chiasm and *Robo1*/*Robo2* in the Retina of *Hs2st*$^{-/-}$ Mutants and *Hs6st1*$^{-/-}$ Mutants.

7.1 Introduction

Based on our observations of optic chiasm development in *Hs2st*$^{-/-}$ mutants and *Hs6st1*$^{-/-}$ mutants we developed the hypothesis that Hs2st sulphation was critical to Slit1-Robo2 signaling and Hs6st1 sulphation was critical to Slit2-Robo2 signaling at the optic chiasm. We hypothesized a mechanism whereby 2-O-sulphated and 6-O-sulphated modified HSPGs differentially modulated Slit-Robo signaling by stabilizing the interaction between the Slit ligand at the optic chiasm and the Robo receptor on the surface of the RGC growth cone. However, taking into account the incredible functional diversity of HSPGs it is possible that alterations in HSPG 2-O-sulphation and/or 6-O-sulphation may indirectly affect Slit-Robo signaling by altering their expression levels. In this scenario, *Hs2st*$^{-/-}$ mutants and/or *Hs6st1*$^{-/-}$ mutants would have defective Slit-Robo signaling because Slit ligands were not available at the optic chiasm and/or Robo receptors were not available on the surface of navigating growth cones. To test this hypothesis, we used *in situ* hybridization and Q-RTPCR to characterize the expression patterns of *Slits* at the optic chiasm and *Robos* in the retina of the eye in *Hs2st*$^{-/-}$ mutants and *Hs6st1*$^{-/-}$ mutants.

7.2 Results

7.2.1 Expression of *Slit1* at the optic chiasm is not altered in *Hs2st*$^{-/-}$ mutants, but significantly down-regulated in *Hs6st1*$^{-/-}$ mutants.

To determine whether *Slit1* expression was altered at the optic chiasm of *Hs2st*$^{-/-}$ mutants and/or *Hs6st1*$^{-/-}$ mutants we used RNA *in situ* hybridization and Q-RTPCR. Observations of *Slit1* expression using RNA *in situ* hybridization on 100 µm horizontal sections of E14.5 embryos revealed comparable patterns of expression when *Hs6st1*$^{-/-}$ mutants (Figure 1B) were compared to wild type (Figure 1A). Expression of *Slit 1* was comparable to previously published results (Erskine et al., 2000). We performed Q-RTPCR on optic chiasm tissue extracted from E14.5 wild type embryos (n=3), *Hs2st*$^{-/-}$ mutant embryos (n=4), and *Hs6st1*$^{-/-}$ mutant embryos (n=3). The expression levels of *Slit1* were normalized to the ubiquitously expressed housekeeping gene *GAPDH*. Results showed the levels of *Slit1* expression to be comparable in wild type and *Hs2st*$^{-/-}$ mutants, however *Slit1* expression was shown to be reduced in *Hs6st1*$^{-/-}$ mutants at half the amount observed in wild type (mean ± SEM) (Kruskal-Wallis one way ANOVA on ranks, multiple comparisons versus a control group (Dunn's method) , $P>0.05$) (Figure 1C).

Figure 1. **Expression of *Slit1* at the optic chiasm is normal in *Hs2st*$^{-/-}$ mutants, but significantly down-regulated in *Hs6st1*$^{-/-}$ mutants.** Using RNA *in situ* hybridization, we looked at the expression of *Slit1* in 100 µm horizontal sections of E14.5 wild type embryos (A) and *Hs6st1*$^{-/-}$ mutant embryos (B). Similar expression patterns were observed in wild type and *Hs6st1*$^{-/-}$ mutants showing expression in the RGC layer of the eye and in a distinct pattern at the ventral diencephalon; the future site of the optic chiasm. Q-RTPCR revealed normal expression of *Slit1* at the optic chiasm of *Hs2st*$^{-/-}$ mutants (n=4), when compared to wild type (n=3). *Slit1* expression was shown to be down-regulated in *Hs6st1*$^{-/-}$ mutants at the optic chiasm (mean ± SEM) (Kruskal-Wallis one way ANOVA on ranks, multiple comparisons versus a control group (Dunn's method), $P>0.05$) (C). The expression levels of *Slit1* were normalized to the ubiquitously expressed housekeeping gene *GAPDH*. Scale bars: 400 µm A-B.

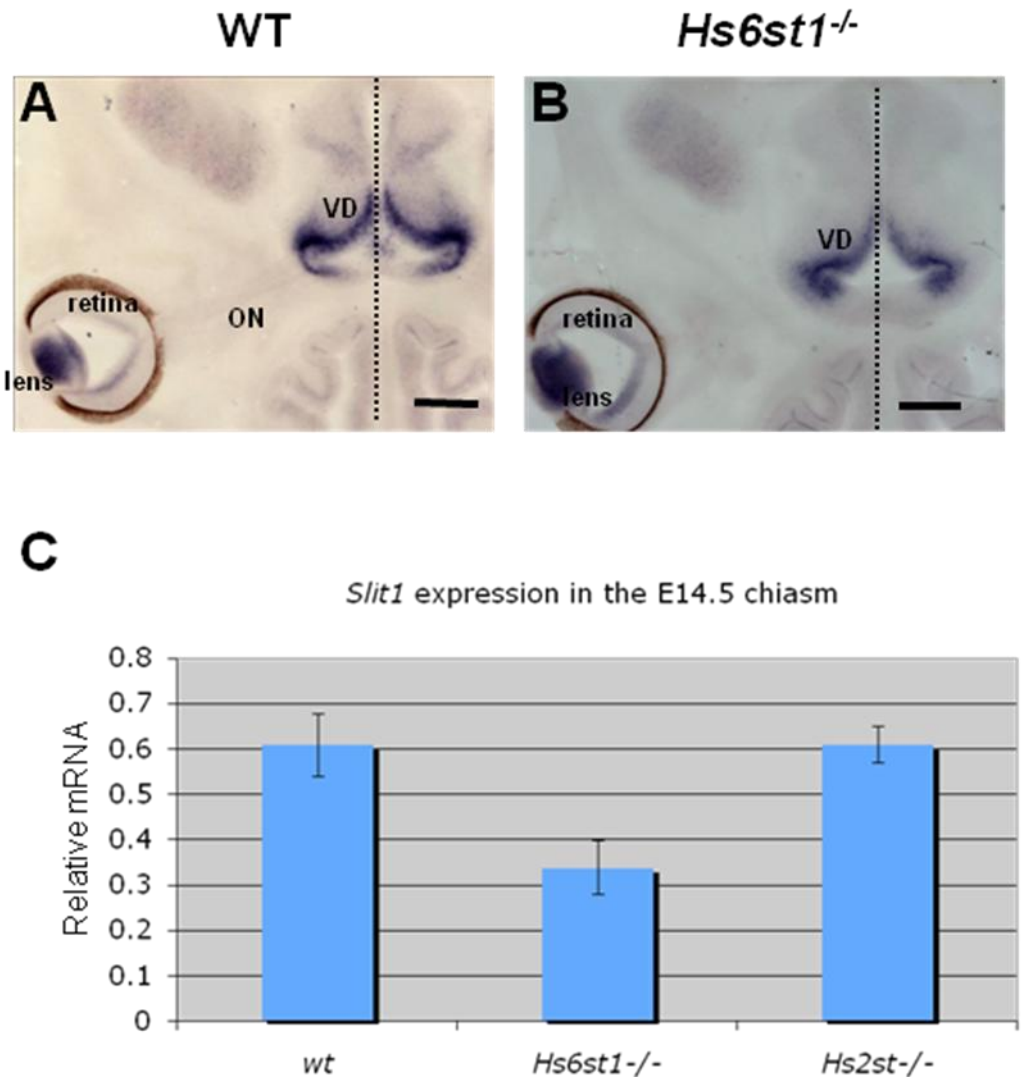
WT
Hs6st1-/-
A
B
VD
retina
ON
lens
VD
retina
lens
C
Slit1 expression in the E14.5 chiasm
Relative mRNA
0.8
0.7
0.6
0.5
0.4
0.3
0.2
0.1
0
wt
Hs6st1-/-
Hs2st-/-

7.2.2 Expression of *Slit2* at the optic chiasm is not altered in *Hs2st*$^{-/-}$ mutants or *Hs6st1*$^{-/-}$ mutants.

To determine whether *Slit2* expression was altered at the optic chiasm of *Hs2st*$^{-/-}$ mutants and/or *Hs6st1*$^{-/-}$ mutants we used RNA *in situ* hybridization and Q-RTPCR. Observations of *Slit2* expression using RNA *in situ* hybridization on 100 µm horizontal sections of E14.5 embryos revealed comparable patterns of expression when *Hs6st1*$^{-/-}$ mutants (Figure 2B) were compared to wild type (Figure 2A). Expression of *Slit2* was comparable to previously published results (Erskine et al., 2000) with the noticeable differences that *Slit2* was expressed along the length of the optic nerve with particularly high expression at the optic disc/optic nerve border. We performed Q-RTPCR on optic chiasm tissue extracted from E14.5 wild type embryos (n=3), *Hs2st*$^{-/-}$ mutant embryos (n=4), and *Hs6st1*$^{-/-}$ mutant embryos (n=3). The expression levels of *Slit2* were normalized to the ubiquitously expressed housekeeping gene *GAPDH*. Results showed the levels of *Slit2* expression to be comparable in wild type and *Hs2st*$^{-/-}$ mutants. While *Slit2* expression was shown to be reduced in *Hs6st1*$^{-/-}$ mutants when compared to wild type, *Slit2* was not significantly reduced (mean ± SEM) (Kruskal-Wallis one way ANOVA on ranks, multiple comparisons versus a control group (Dunn's method), $P>0.05$) (Figure 2C).

Figure 2. **Expression of *Slit2* at the optic chiasm is normal in *Hs2st*$^{-/-}$ mutants and *Hs6st1*$^{-/-}$ mutants.** Using RNA *in situ* hybridization, we looked at the expression of *Slit2* in 100 µm horizontal sections of E14.5 wild type embryos (A) and *Hs6st1*$^{-/-}$ mutant embryos (B). Similar expression was observed in wild type and *Hs6st1*$^{-/-}$ mutants showing expression in the RGC layer of the eye, within the cells surrounding the optic nerve and in a distinct pattern at the ventral diencephalon; the future site of the optic chiasm. Q-RTPCR revealed normal expression of *Slit2* at the optic chiasm of *Hs2st*$^{-/-}$ mutants (n=4) and *Hs6st1*$^{-/-}$ mutants (n=3) when compared to wild type (n=3) (mean ± SEM) (Kruskal-Wallis one way ANOVA on ranks, multiple comparisons versus a control group (Dunn's method) , $P>0.05$) (C). The expression levels of *Slit2* were normalized to the ubiquitously expressed housekeeping gene *GAPDH*. Scale bars: 400 µm A-B.

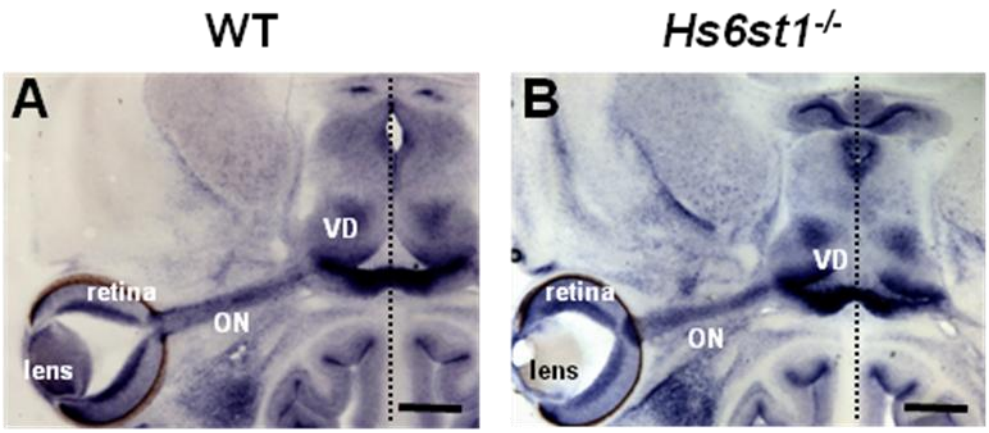
WT
Hs6st1-/-
A
B
VD
retina
ON
lens
VD
retina
ON
lens

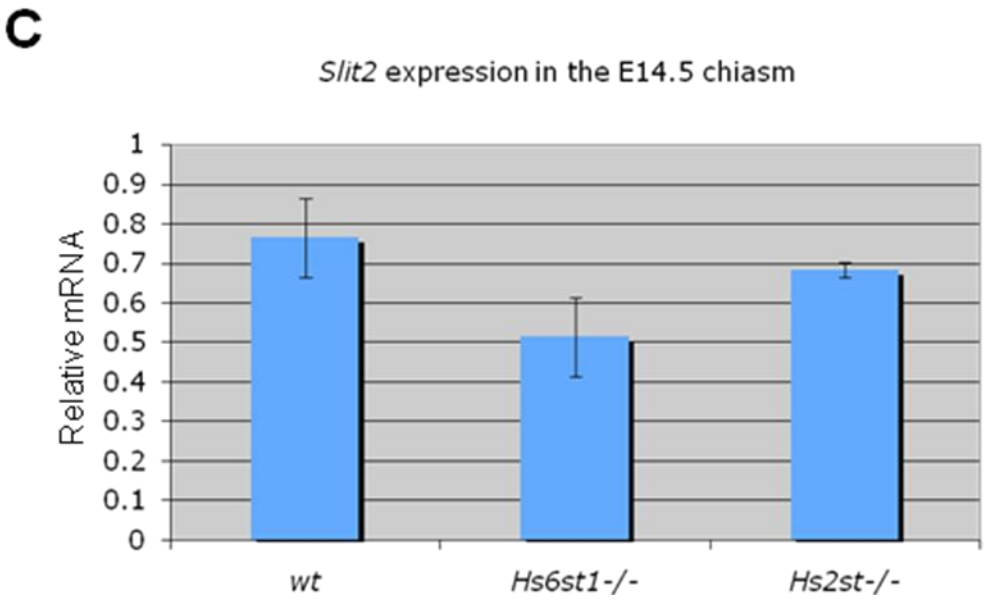
C
Slit2 expression in the E14.5 chiasm
Relative mRNA
1
0.9
0.8
0.7
0.6
0.5
0.4
0.3
0.2
0.1
0
wt
Hs6st1-/-
Hs2st-/-

7.2.3 Expression of *Robo1* and *Robo2* in the retina are not altered in *Hs2st*$^{-/-}$ mutants or *Hs6st1*$^{-/-}$ mutants.

To determine whether *Robo1* and/or *Robo2* expression were altered in the retina of *Hs2st*$^{-/-}$ mutants and/or *Hs6st1*$^{-/-}$ mutants we used RNA *in situ* hybridization and Q-RTPCR. Observations of *Robo1* expression using RNA *in situ* hybridization on 100 µm horizontal sections of E14.5 embryos revealed comparable patterns of expression when *Hs6st1*$^{-/-}$ mutants (Figure 3B) were compared to wild type (Figure 3A). There were also no observable differences in *Robo2* expression when *Hs6st1*$^{-/-}$ mutants (Figure 4B) were compared to wild type (Figure 4A). Expression of *Robo1* and *Robo2* were comparable to previously published results (Erskine et al., 2000). We performed Q-RTPCR on retinal tissue extracted from E14.5 wild type embryos (n=3), *Hs2st*$^{-/-}$ mutant embryos (n=4), and *Hs6st1*$^{-/-}$ mutant embryos (n=5). The expression levels of *Robo1* and *Robo2* were normalized to the ubiquitously expressed housekeeping gene *GAPDH*. Results showed the levels of *Robo1* (Figure 3C) and *Robo2* (Figure 4C) expression to be comparable in wild type, *Hs2st*$^{-/-}$ mutants, and *Hs6st1*$^{-/-}$ mutants (mean ± SEM) (Kruskal-Wallis one way ANOVA on ranks, multiple comparisons versus a control group (Dunn's method), $P>0.05$).

Figure 3. **Expression of *Robo1* in the eye is normal in *Hs2st*$^{-/-}$ mutants and *Hs6st1*$^{-/-}$ mutants.** Using RNA *in situ* hybridization, we looked at the expression of *Robo1* in 100 µm horizontal sections of E14.5 wild type embryos (A) and *Hs6st1*$^{-/-}$ mutant embryos (B). Similar expression was observed in wild type and *Hs6st1*$^{-/-}$ mutants showing expression in a punctuate manner around the RGC layer of the eye. Q-RTPCR revealed normal expression of *Robo1* in the retina of *Hs2st*$^{-/-}$ mutants (n=4) and *Hs6st1*$^{-/-}$ mutants (n=5) when compared to wild type (n=3) (mean ± SEM) (Kruskal-Wallis one way ANOVA on ranks, multiple comparisons versus a control group (Dunn's method), $P>0.05$) (C). The expression levels of *Robo1* were normalized to the ubiquitously expressed housekeeping gene *GAPDH*. Scale bars: 200 µm A-B.

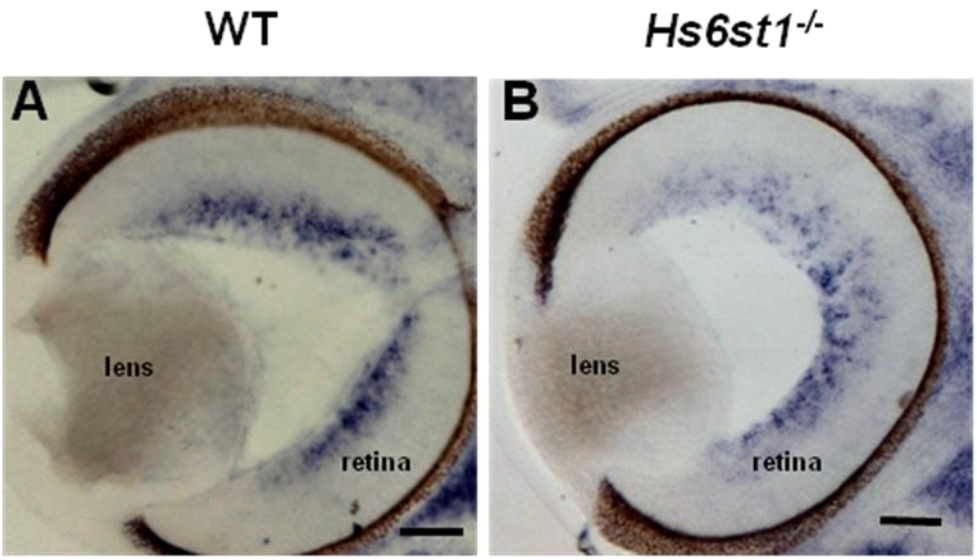
WT
Hs6st1-/-
A
B
lens
retina
lens
retina

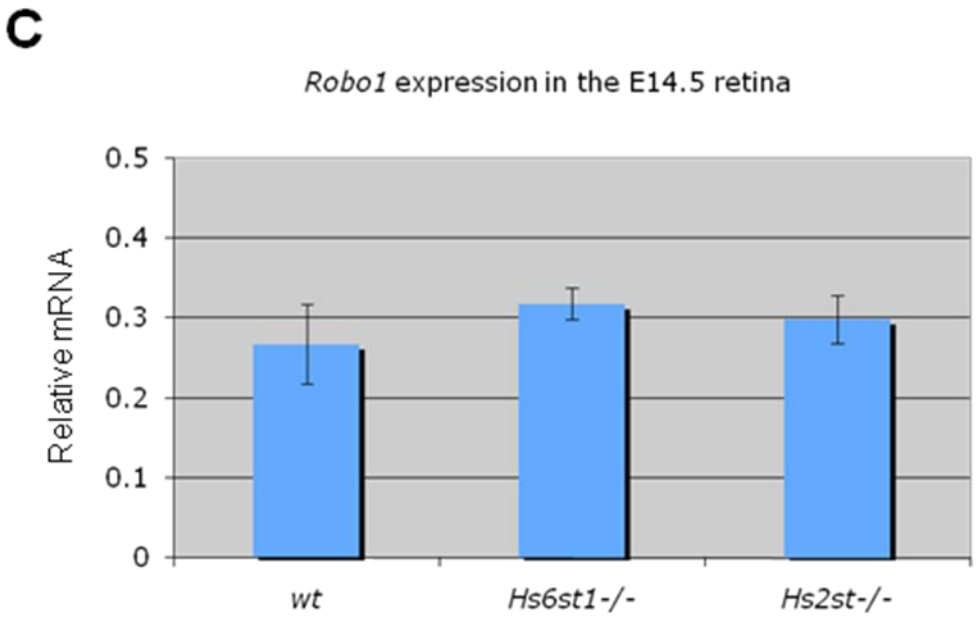
C
Robo1 expression in the E14.5 retina
Relative mRNA
0.5
0.4
0.3
0.2
0.1
0
wt
Hs6st1-/-
Hs2st-/-

Figure 4. **Expression of *Robo2* in the eye is normal in *Hs2st*$^{-/-}$ mutants and *Hs6st1*$^{-/-}$ mutants.** Using RNA *in situ* hybridization, we looked at the expression of *Robo2* in 100 µm horizontal sections of E14.5 wild type embryos (A) and *Hs6st1*$^{-/-}$ mutant embryos (B). Similar expression was observed in wild type and *Hs6st1*$^{-/-}$ mutants showing expression within the RGC layer of the eye. Q-RTPCR revealed normal expression of *Robo2* in the retina of *Hs2st*$^{-/-}$ mutants (n=4) and *Hs6st1*$^{-/-}$ mutants (n=5) when compared to wild type (n=3) (mean ± SEM) (Kruskal-Wallis one way ANOVA on ranks, multiple comparisons versus a control group (Dunn's method), P>0.05) (C). The expression levels of *Robo2* were normalized to the ubiquitously expressed housekeeping gene *GAPDH*. Scale bars: 200 µm A-B.

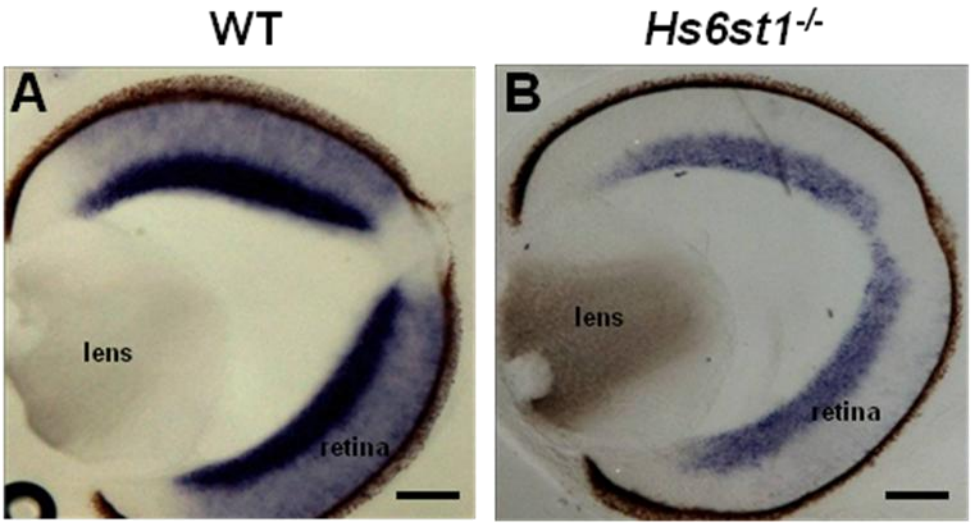
WT
Hs6st1-/-
A
B
lens
retina
lens
retina

C

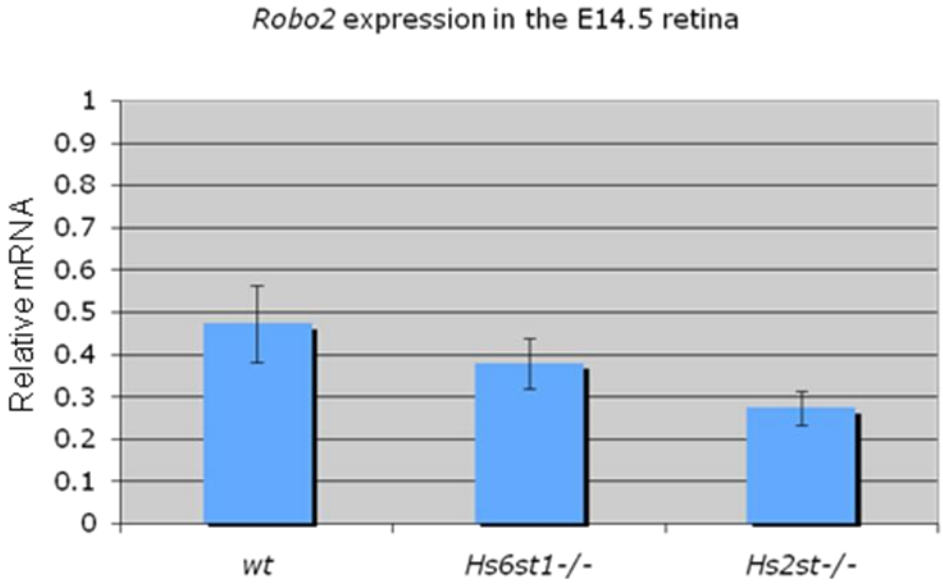
Robo2 expression in the E14.5 retina
Relative mRNA
1
0.9
0.8
0.7
0.6
0.5
0.4
0.3
0.2
0.1
0
wt
Hs6st1-/-
Hs2st-/-

7.3 Discussion

7.3.1 Hs2st sulphation and Hs6st1 sulphation are not likely important in regulating Slit-Robo expression at the optic chiasm or in the retina.

Previous work into the roles HSPG sulphation patterns have on RGC axon navigation at the optic chiasm led us to the Hs2st-Slit1-Robo2; Hs6st1-Slit2-Robo2 hypothesis where we suggested that these differentially sulphated HSPGs acted to mediate the interaction between the Slit ligands and their Robo receptor. However, it was conceivable that differentially sulphated HSPGs have distinct roles in regulating gene transcription through pathways that regulate *Slit* and/or *Robo* expression. To test this hypothesis, we looked at the expression patterns of *Slit1* and *Slit2* at the optic chiasm and *Robo1* and *Robo2* in the retina of the eye to determine whether their expression was affected by the loss of either Hs2st sulphation and/or Hs6st1 sulphation. The results showed that *Slit2*, *Robo1*, and *Robo2* expression were not significantly affected in *Hs2st*$^{-/-}$ mutants or *Hs6st1*$^{-/-}$ mutants. *Slit1* expression was observed to be significantly down-regulated at the optic chiasm of *Hs6st1*$^{-/-}$ mutants. However, the fact that *Slit1* expression was observed to be down-regulated in *Hs6st1*$^{-/-}$ mutants did not explain the characteristic retino-retinal projection observed in *Hs6st1*$^{-/-}$ mutants. Even if *Slit1* expression is down-regulated at the optic chiasm, neither *Slit1*$^{-/-}$ mutants nor *Slit1*$^{+/-}$ mutants result in the retino-retinal projection observed in *Hs6st1*$^{-/-}$mutants (Tom Pratt, unpublished data) (Plump et al., 2002). Based on our findings, we can now conclude that altered Slit-Robo expression in *Hs2st*$^{-/-}$ or *Hs6st1*$^{-/-}$ mutants does not explain their mutant phenotypes, leaving the remaining possibility that Hs2st sulphation and Hs6st1 sulphation regulate distinct aspects Slit-Robo signaling by mediating their interactions at the surface of the navigating RGC axon growth cone.

Chapter 8: Characterization of the *Hs6st* Isoforms *Hs6st1*, *Hs6st2*, and *Hs6st3* in the Developing Mouse CNS.

8.1 Introduction

Our work characterizing the role of Hs6st1 sulphation on optic chiasm development led us to the hypothesis that Hs6st1 sulphation was required for Slit2 signaling. However, we found several locations in the developing mouse CNS where Slit2 signaling was required for axon guidance, but where we did not find defects in *Hs6st1*$^{-/-}$ mutant axon guidance (See Chapter 5). A possible explanation for this discrepancy is that HSPG 6-O-sulphation is supplied by other enzymes capable of 6-O-sulphation. There are three *Hs6st* isoforms (*Hs6st1*, *Hs6st2*, and *Hs6st3*) known in mice, all of which are capable of HSPG 6-O-sulphation. These Hs6st isoforms have been shown to have similar substrate specificities, but differential expression patterns (Habuchi et al., 2000; Smeds et al., 2003; Sedita et al., 2004).

Slit2 signaling has previously been implicated in RGC axon navigation in the retina. Observations of *Slit2*$^{-/-}$ mutants and more severely in *Slit1*$^{-/-}$/*Slit2*$^{-/-}$ double mutants showed that RGC axons were capable of escaping the normal boundary of the OFL of the retina (Thompson et al., 2006b). Slit2 signaling has also been implicated in TCA/CTA tract formation in the developing mouse CNS. Observations of *Slit2*$^{-/-}$ mutants and *Slit1*$^{-/-}$/*Slit2*$^{-/-}$ double mutants showed TCA/CTA navigation errors where thalamic axons mis-navigated into the hypothalamic region and cortical axons ectopically mis-navigated across the ventral midline (Bagri et al., 2002; Andrews et al., 2006; Lopez-Bendito et al., 2007). We did not see any defects in *Hs6st1*$^{-/-}$ mutant axon guidance in the retina or in the TCA/CTA tracts (Chapter 5).

8.2 Aims

To test the hypothesis that the loss of Hs6st1 sulphation was being compensated for by the presence of Hs6s2 and/or Hs6st3, we aimed to characterize the expression of *Hs6st2* and *Hs6st3* in regions where RGC axons must navigate (eye and optic chiasm) and regions where TCA/CTA tracts navigate (dorsal thalamus and cortex).

8.3 Results

8.3.1 Expression of *Hs6st1*, *Hs6st2* and *Hs6st3* in the retina and optic chiasm

Previous work describing the expression patterns of these *Hs6st* isoforms showed that *Hs6st1* was predominantly expressed in epithelial and neural-derived tissues, whereas *Hs6st2* expression was more mesenchymal, and *Hs6st3* expression appeared in a more restricted manner (Sedita et al., 2004). While a detailed description of *Hs6st1* expression has previously been shown in the retina of the eye and at the optic chiasm (Pratt et al., 2006), no one has ever specifically looked at the expression of *Hs6st2* and *Hs6st3* in the retina of the eye and at the optic chiasm. We determined the expression patterns of *Hs6st1*, *Hs6st2* and *Hs6st3* in the retina and at the optic chiasm at E14.5 using *in situ* hybridization on 100 µm horizontal sections. *Hs6st1* expression was observed in the RGC layer, the region of the optic nerve closest to the eye, and in a distinct pattern at the optic chiasm as previously described in E15.5 embryos (See Chapter 3) (Figure 1A). *Hs6st2* expression was not observed in the RGC layer of the eye and very little *Hs6st2* expression was observed at the optic chiasm (Figure 1B). High *Hs6st3* expression was evident in the RGC layer and there was also low expression of *Hs6st3* around the optic chiasm (Figure 1C).

Figure 1. **Expression patterns of *Hs6st1*, *Hs6st2*, and *Hs6st3* in the retina and the optic chiasm.** Using RNA *in situ* hybridization, we looked at the expression of the three *Hs6st* isoforms in 100 µm horizontal sections of E14.5 wild type embryos. (A) *Hs6st1* expression was observed in the RGC layer as well as in a distinct pattern at the ventral diencephalon where the optic chiasm will form with particularly high expression where the optic nerve first encounters the ventral diencephalon. (B) *Hs6st2* expression was not present in the retina and little expression was observed at the ventral diencephalon. (C) *Hs6st3* expression was observed to be high in the RGC layer of the eye, but only low expression at the ventral diencephalon. Black dotted line represents the midline. VD, ventral diencephalon; NE, nasal epithelium. Scale bars: 400 µm A-C.

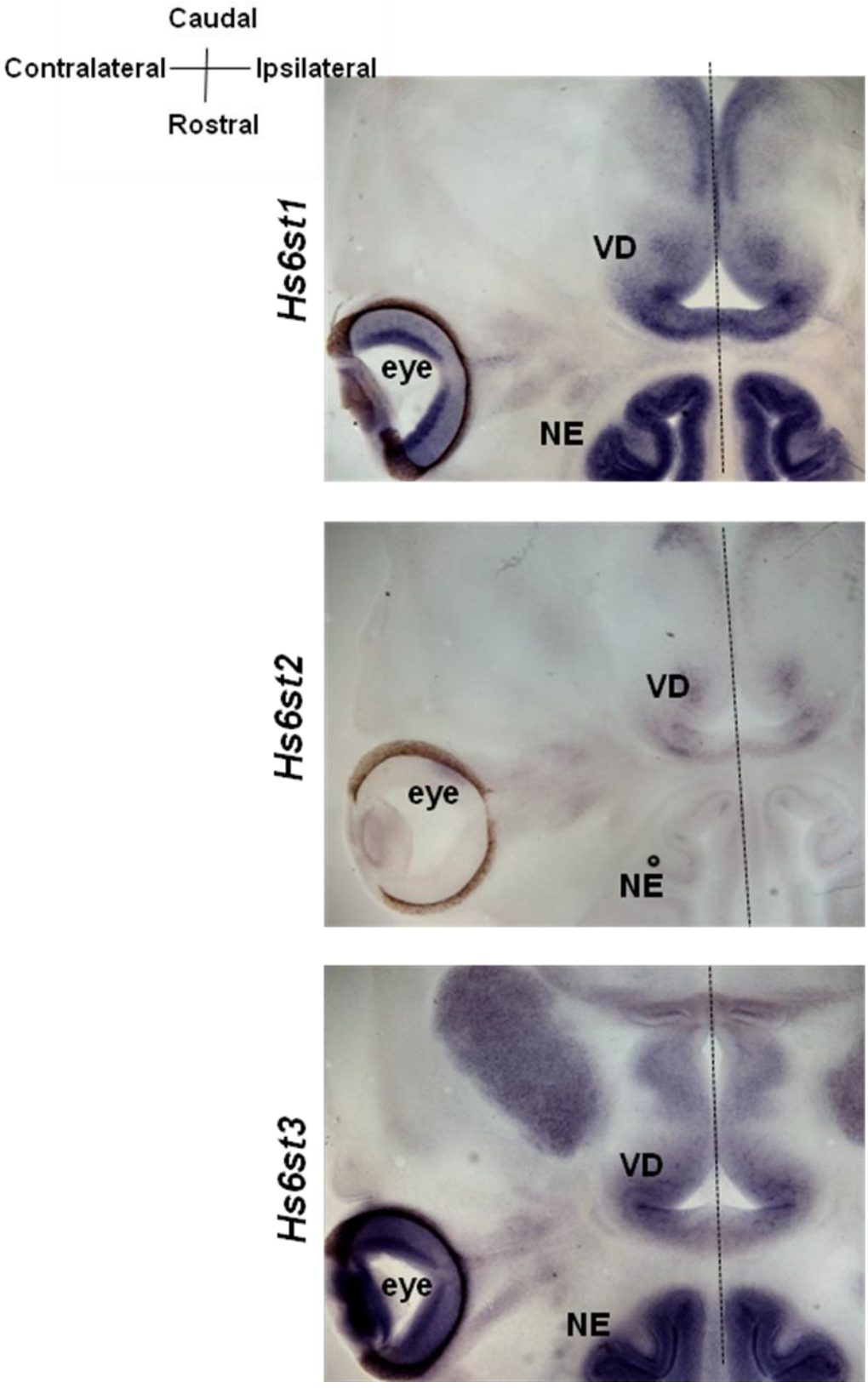
Caudal
Contralateral
Ipsilateral
Rostral
Hs6st1
VD
eye
NE
Hs6st2
VD
eye
NE
Hs6st3
VD
eye
NE

8.3.2 Expression of *Hs6st1*, *Hs6st2* and *Hs6st3* in the forebrain.

We next determined the expression patterns of *Hs6st1*, *Hs6st2* and *Hs6st3* in the thalamus and the cortex at E14.5 using *in situ* hybridization on 100 µm coronal sections of E14.5 embryos. There was low expression of *Hs6st1* throughout most regions of the forebrain (Figure 2A), while *Hs6st2* expression was more restricted (Figure 2B). High expression of *Hs6st1* was observed throughout most of the dorsal thalamus and along the length of the midline. *Hs6st1* expression was also observed in the epithalamus as well as the cortical plate of the cortex dorsal to ventral gradient (Figure 2A). High expression of *Hs6st2* was observed in a more lateral region of the dorsal thalamus when compared to the *Hs6st1* expression pattern. There was also *Hs6st2* expression in the striatum, the region of the internal capsule, and in a dorsal to ventral gradient within the cortical plate of the cortex (Figure 2B). Very little *Hs6st3* expression was observed in the thalamus and the cortex (Figure 2C).

Figure 2. **Expression patterns of *Hs6st1*, *Hs6st2*, and *Hs6st3* in the thalamus and the cortex.** Using RNA *in situ* hybridization, we looked at the expression of the three *Hs6st* isoforms in 100 µm coronal sections of E14.5 wild type embryos. (A) *Hs6st1* expression was observed to be high in the dorsal thalamus (DT) and the cortical plate of the cortex. Hs6st1 was also observed to be expressed in the ventricular surface of the ganglionic eminence (GE), the epithalamus (EpiT) and along the midline (black dotted line). (B) *Hs6st2* was also observed to be highly expressed in the DT, but restricted to a more lateral region of the DT. *Hs6st2* expression was also observed in the region of the internal capsule (IC), the striatum (Stm), the GE, and the cortical plate of the cortex. (C) *Hs6st3* was not highly expressed in either the thalamus or the cortex. Scale bars: 400 µm A-C.

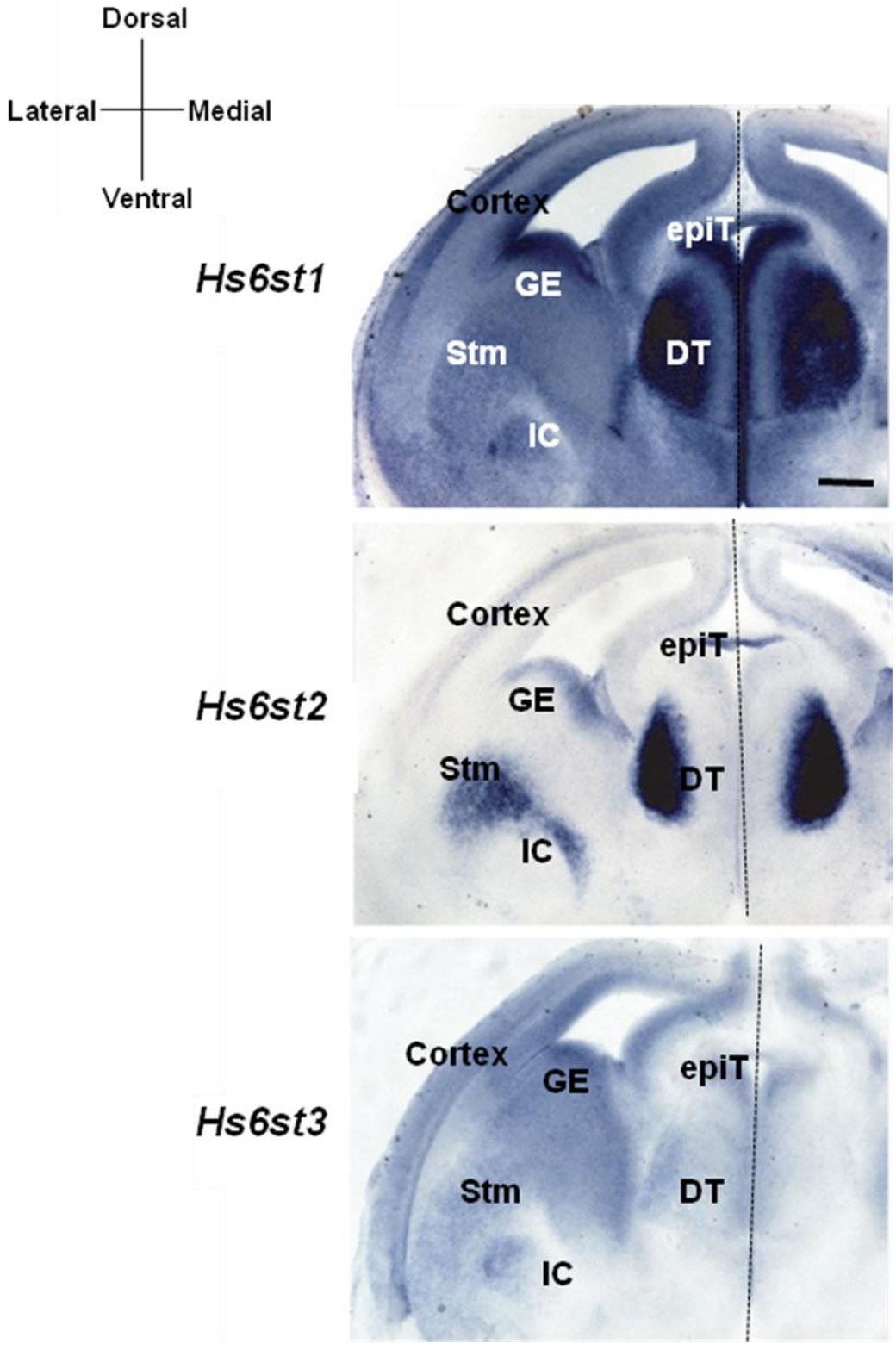
Dorsal
Lateral
Medial
Ventral
Hs6st1
Cortex
epiT
GE
Stm
DT
IC
Hs6st2
Cortex
epiT
GE
Stm
DT
IC
Hs6st3
Cortex
GE
epiT
Stm
DT
IC

8.4 Discussion

There are three isoforms of the *Hs6st* gene responsible for 6-O-sulphation (*Hs6st1*, *Hs6st2*, and *Hs6st3*) which show differential expression patterns, but similarities in substrate specificity (Habuchi et al., 2000; Smeds et al., 2003; Sedita et al., 2004). *Hs6st1* has previously been described as being predominantly expressed in neural derived tissue, whereas *Hs6st2* expression is more mesenchymal, and *Hs6st3*is expressed in a more restricted manner. While we had previously described the expression of *Hs6st1* in the developing CNS (See Chapter 3), we had not characterized the expression of *Hs6st2* and *Hs6st3* in the developing mouse CNS.

8.4.1 *Hs6st3* expression in the retina may compensate for the loss of Hs6st1 sulphation in *Hs6st1*$^{-/-}$ mutants.

Our hypothesis proposing that Hs6st1 sulphation was critical to Slit2-Robo2 signaling led us to the RGC layer of the eye where *Slit2*$^{-/-}$ mutants had previously been shown to result in RGC axon guidance defects (Thompson et al., 2006b). Because *Slit2*$^{-/-}$ mutants resulted in ectopic navigation of RGC axons outside the RGC layer we reasoned that this mutant phenotype would also be observed in our *Hs6st1*$^{-/-}$ mutants. However, observations in the retina of the eye of *Hs6st1*$^{-/-}$ mutants showed no RGC axon navigation defects (See Chapter 5). To explain this observation, we speculated that the loss of Hs6st1 sulphation was being compensated for by other Hs6st enzymes, which led us to look at the expression patterns of *Hs6st2* and *Hs6st3*. We showed that *Hs6st3* was highly expressed in the RGC layer, suggesting that Hs6st3 was capable of compensating for the loss of Hs6st1 sulphation in the RGC layer. It would be of interest to look at the affects *Hs6st1*$^{-/-}$ */Hs6st3*$^{-/-}$ double mutants would have in RGC axon guidance in the retina (See Chapter 9 for future plans).

8.4.2 *Hs6st2* expression in the dorsal thalamus and cortex may compensate for the loss of Hs6st1 sulphation in *Hs6st1*$^{-/-}$ mutants.

Previous work identified Slit2-Robo signaling as being critical to the development of the TCA/CTA tracts (Bagri et al., 2002), therefore we looked for evidence to support the hypothesis that Hs6st1 sulphation was critical to Slit2-Robo signaling by characterizing TCA/CTA tract development in *Hs6st1*$^{-/-}$ mutants. Despite there being very high expression of *Hs6st1* in the dorsal thalamus and expression in the cortex, we did not observe any major defects in TCA/CTA tract formation in *Hs6st1*$^{-/-}$ mutants. To explain this observation, we speculated that the loss of Hs6st1 sulphation was compensated for by other Hs6st enzymes, which led us to look at the expression patterns of *Hs6st2* and *Hs6st3* in the thalamus and the cortex. We observed *Hs6st2* to be highly expressed in the dorsal thalamus as well as in the cortical plate of the cortex consistent with regions where *Hs6st1* is expressed. In the absence of Hs6st1 sulphation, we propose an Hs6st2 sulphation dependant compensation in TCA/CTA tract development in *Hs6st1*$^{-/-}$ mutants. Future work will depend on the access *of Hs6st1*$^{-/-}$*/Hs6st2*$^{-/-}$ double mutant (See Chapter 9 for future plans).

8.5 Summary

We have shown that Hs6st1 sulphation is critical to axon guidance at key decision points likely through its actions in mediating Slit2 signaling. However, we have also identified key choice points that while requiring Slit2 signaling, do not appear to require Hs6st1 sulphation. Here we propose the possibility of compensatory effects in *Hs6st1*$^{-/-}$ mutant axon guidance when either *Hs6st2* and/or *Hs6st3* are co-expressed. We observed expression of *Hs6st2* to be highest in the dorsal thalamus, in a more laterally restricted pattern than *Hs6st1* which was also shown to be highly expressed in the dorsal thalamus. *Hs6st3* was observed to be highly expressed in the

RGC layer of the eye overlapping the high expression of *Hs6st1* in the RGC layer of the eye. The co-expression of *Hs6st1* and *Hs6st2* in the dorsal thalamus and cortex as well as co-expression of *Hs6st1* and *Hs6st3* in the RGC layer of the eye is particularly interesting as their expression patterns may explain why we did not see axon guidance defects in these regions in *Hs6st1*$^{-/-}$ mutants.

Chapter 9: Final Discussion

9.1 Summary of work to date

Hs2st and *Hs6st1* were shown to be expressed in both distinct and overlapping regions along the putative paths of many axonal tracts in the developing CNS (Chapter 3). While it had previously been shown that *Hs2st*$^{-/-}$ mutant animals die perinatally due to renal agenesis (Bullock et al., 1998), *Hs6st1*$^{-/-}$ mutant animals survival postnatally had not been ascertained. Using a PCR genotyping strategy to identify *Hs6st1* animals, we showed that *Hs6st1*$^{-/-}$ mutant animals have late embryonic lethality with only 3% of offspring carrying an *Hs6st1* null allele surviving to weaning (Chapter 4).

Observations of embryonic development in both *Hs2st*$^{-/-}$ mutant and *Hs6st1*$^{-/-}$ mutant embryos showed that a loss of either Hs2st sulphation or Hs6st1 sulphation resulted in distinct RGC axon guidance defects at the optic chiasm suggesting there was a "heparan sulphate code" in place for optic chiasm development (Pratt et al., 2006). Further observations of optic chiasm formation in the *Hs2st*$^{-/-}$ mutant and *Hs6st1*$^{-/-}$ mutant lead us to start formulating the hypothesis that Hs2st sulphation was required for Slit1-Robo2 signaling at the optic chiasm and Hs6st1 sulphation was required for Slit2-Robo2 signaling at the optic chiasm (Chapter 5). This hypothesis was based primarily on the fact that *Hs2st*$^{-/-}$ mutants phenocopied aspects of *Slit1*$^{-/-}$ mutants (RGC axons escaping the normal boundary of the optic chiasm) (Plump et al., 2002) and *Hs6st1*$^{-/-}$ mutants phenocopied aspects of *Slit2*$^{-/-}$ mutants (retino-retinal projection) (Tom Pratt, unpublished data), while *Robo2*$^{-/-}$ mutants showed all of the mutant phenotypes described in *Slit1*$^{-/-}$*/Slit2*$^{-/-}$ double mutants (Plump et al., 2002; Plachez et al., 2008).

To see if there was further evidence to support this hypothesis, we looked at other regions where axon guidance was known to be regulated by Slit-Robo signaling and showed defects in optic tract development in *Hs6st1*$^{-/-}$ mutants as well as defects in

corpus callosum development in both *Hs2st*$^{-/-}$ mutants and *Hs6st1*$^{-/-}$ mutants suggesting a possible link between specific HSPG sulphation patterns and Slit-Robo signaling (Chapter 5).

To determine whether Hs2st sulphation and Hs6st1 sulphation act redundantly in mediating axon guidance, we attempted to generate *Hs2st*$^{-/-}$/*Hs6st1*$^{-/-}$ double mutants, however they were shown to die very early in development. Compound mutants lacking three out of four alleles showed no differences in phenotype suggesting that one copy of either *Hs2st* or *Hs6st1* was sufficient to mediate HSPG sulphation dependant axon guidance at the optic chiasm. It was not possible to determine whether Hs2st and Hs6st1 were capable of acting redundantly without looking at *Hs2st*$^{-/-}$/*Hs6st1*$^{-/-}$ double mutants (Chapter 6).

Using a combination of *in situ* hybridization and Q-RTPCR, we were able to show that the loss of either Hs2st sulphation or Hs6st1 sulphation did not affect the expression of *Slit1* or *Slit2* at the optic chiasm, not did their loss affect *Robo1* or *Robo2* expression in the retina. Based on this, we hypothesized a mechanism whereby Hs2st sulphation and Hs6st1 sulphation differentially mediate Slit-Robo signaling at the surface of the navigating axon growth cone (Chapter 7).

Finally, we described a possible explanation for previous observations showing that the loss of Hs6st1 sulphation had no affect on RGC axon guidance in the retina or TCA/CTA tract formation even though Slit2 was previously shown to be critical to their axon guidance decisions in these regions. Hs6st1 is one of three isoforms capable of HSPG 6-O-sulphation and we hypothesized that the loss of Hs6st1 was being compensated for by the presence of Hs6st2 and/or Hs6st3 in the retina and the TCA/CTA tract. Using *in situ* hybridization we showed *Hs6st1* and *Hs6st2* were co-expressed in the dorsal thalamus and cortex suggesting possible redundant functions in TCA/CTA tract formation. *Hs6st1* and *Hs6st3* were shown to be co-expressed in the RGC layer of the retina suggesting possible redundant functions in RGC axon navigation in the retina of the eye (Chapter 8). In this Chapter, the focus will primarily address the questions that have yet to be answered and plans for future work that will aim to resolve these questions.

9.2 Future directions

9.2.1 Does Hs2st sulphation specifically regulate Slit1 signaling and Hs6st1 sulphation specifically regulate Slit2 signaling.

We have established that Hs2st sulphation and Hs6st1 sulphation have distinct roles in RGC axon guidance at the mouse optic chiasm. A loss of Hs2st sulphation resulted in the mis-navigation of RGC axons into the pre-optic area (Chapter 5) as well as along the ventral midline of the diencephalon, which was never seen in either the wild type or *Hs6st1*$^{-/-}$ mutant optic chiasm (Pratt et al., 2006). Interestingly, these mutant axon guidance phenotypes phenocopy mutant axon guidance phenotypes previously described in *Slit1*$^{-/-}$ mutants (midline wandering) and *Slit1*$^{-/-}$*/Slit2*$^{-/-}$ double mutant (mis-navigation into the pre-optic area) animals (Plump et al., 2002). A loss of Hs6st1 sulphation resulted in a significant increase in the number of RGC axons that navigated from one eye to the other which was not observed in either the wild type or *Hs2st*$^{-/-}$ mutant optic chiasm (Pratt et al., 2006). Interestingly, this mutant axon guidance phenotype phenocopies a recently observed phenotype in *Slit2*$^{-/-}$ mutants (Tom Pratt, unpublished data) and was previously observed in *Slit1*$^{-/-}$*/Slit2*$^{-/-}$ double mutant animals and *Robo2*$^{-/-}$ mutant animals (Plump et al., 2002; Plachez et al., 2008). Based on the mutant phenotypes observed, we have generated a hypothesis that Hs2st sulphation is essential to regulating Slit1-Robo2 signaling at the optic chiasm, while Hs6st1 sulphation is essential to regulating Slit2-Robo2 signaling at the optic chiasm. To address this hypothesis, we have planned both *in vitro* and *in vivo* techniques to establish the molecular mechanisms involved in HSPG sulphation mediated Slit-Robo signaling.

9.2.1.1 *In vitro* approach to determining whether Slit1 signaling specifically requires Hs2st sulphation and Slit2 signaling specifically requires Hs6st1 sulphation.

Previous *in vitro* work showed that the RGC axons from retinal explants lacking Hs6st1 sulphation lacked the chemo-repulsive response to Slit2 (Pratt et al., 2006). Using a similar approach described in Pratt et al. 2006, we plan to determine the response *Hs6st1*$^{-/-}$ mutant RGC axons exhibit when exposed to Slit1 conditioned medium. Based on our hypothesis, we would predict *Hs6st1*$^{-/-}$ mutant axons to be repelled in the presence of Slit1 as the full complement of Hs2st sulphation would remain intact in these *Hs6st1*$^{-/-}$ mutants. We also plan to determine the response *Hs2st*$^{-/-}$ mutant RGC axons exhibit when exposed to either Slit1 or Slit2. Based on our hypothesis, we would predict *Hs2st*$^{-/-}$ mutant RGC axons to be repelled normally from Slit2 as Hs6st1 sulphation is present, but lack a chemo-repulsive response to Slit1 conditioned medium due to the absence of Hs2st sulphation.

Previous *in vivo* work identified the importance of heparin 2-O-sulphation and 6-O-sulphation in *Xenopus* RGC navigation by using exogenously added chemically modified heparins. They showed that exogenously added heparan having a full complement of 2-O-sulphation and 6-O-sulphation resulted in RGC axon navigation errors, while a loss of either heparin 2-O-sulphation or 6-O-sulphation had no affect on RGC axon navigation (Irie et al., 2002). These results could be interpreted in two ways 1) the presence of exogenously added heparins disrupts axon guidance by chelating the axon guidance cues or 2) the presence of exogenously added heparins creates an alternative path for navigating RGC axons by allowing axon guidance cues to diffuse to other areas.

We plan to use exogenously added chemically modified heparins to determine their *in vitro* effects on wild type retinal explants exposed to Slits. If the presence of exogenously added heparins disrupts axon guidance by chelating Slit1 and/or Slit2, then we predict RGC axons to lack chemo-repulsion by Slit1 or Slit2 when 2-O and 6-O-sulphated heparan is added, respectively. When heparins lacking 2-O-sulphation

are added we predict RGC axons will be repelled from Slit1, but lack a chemo-repulsive response to Slit2, while adding heparins lacking 6-O-sulphation will result in RGC axon repulsion from Slit2, but lack a chemo-repulsive response to Slit1.

Another *in vitro* approach will involve the treatment of *Hs2st*$^{-/-}$ mutant and *Hs6st1*$^{-/-}$ mutant retinal cultures with chemically modified heparins. The aim will be to ascertain whether exogenously added heparins having a full complement of sulphation modifications will rescue RGC axon guidance responses to Slit1 and/or Slit2 in *Hs2st*$^{-/-}$ mutant and *Hs6st1*$^{-/-}$ mutant retinal cultures. If the presence of exogenously added heparins does not chelate Slit1 and/or Slit2 then we predict *Hs2st*$^{-/-}$ and *Hs6st1*$^{-/-}$ RGC axons to be repelled by Slit1 and Slit2, respectively because the fully sulphated heparins rescue the *Hs2st*$^{-/-}$ and *Hs6st1*$^{-/-}$ mutants.

9.2.1.2 Biochemical approach to determining whether Slit1 signaling specifically requires Hs2st sulphation and Slit2 signaling specifically requires Hs6st1 sulphation.

Previous work has shown that heparin is critical to Slit-Robo signaling showing that they form a ternary structure where heparin/HS is an integral component of the minimal Slit-Robo complex and functions to stabilize the relatively weak binding of Slit ligands to their Robo receptors (Hussain et al., 2006). To address whether Hs2st and/or Hs6st1 sulphation modifications are critical to heparan sulphate mediated Slit/Robo binding or regulating the availability of secreted Slit proteins we plan to utilize biochemical techniques. Using cell lysates from wild type, *Hs2st*$^{-/-}$ mutant, and *Hs6st1*$^{-/-}$ mutant embryos as a source of HSPGs we will test their abilities to bind to solid matrix immobilized Slit1 and Slit2 ligands. If our hypothesis is correct (Slit1 signaling requires Hs2st sulphation and Slit2 signaling requires Hs6st1 sulphation) we predict to see differences in wild type, *Hs2st*$^{-/-}$ mutant, and *Hs6st1*$^{-/-}$ mutant HSPGs ability to bind to Slit1 and/or Slit2. This biochemical method may also have the added benefit of revealing the type of HSPGs that are critical to Slit-Robo signaling.

Another question we plan to address involves the ability of differentially sulphated HSPGs to mediate the transduction of Slit-Robo signaling to the growth cone cytoskeleton. Previous work has shown that the transduction of Slit-Robo signaling involves the phosphorylation of β-catenin on a conserved tyrosine residue (Y459) resulting in the dissociation of β-catenin from N-cadherin which in turn, results in the loss of growth cone traction due to the uncoupling of the cell membrane from the actin cytoskeleton (Rhee et al., 2002; Rhee et al., 2007). This essentially results in the prevention of the growth cone from entering regions where Slits are present. Using wild type, *Hs2st*$^{-/-}$ mutant, and *Hs6st1*$^{-/-}$ mutant retinal explants exposed to either Slit1 or Slit2 we propose to test whether the phosphorylation status of β-catenin Y459 is altered in *Hs2st*$^{-/-}$mutants and/or *Hs6st1*$^{-/-}$ mutants when compared to wild type by utilizing quantitative immuno-fluorescence using a phosphorylated Y459 β-catenin specific antibody (Rhee et al., 2007). Based on our hypothesis, we would predict a decrease in the phosphorylation status of Y459 β-catenin in the absence of Hs2st sulphation in response to Slit1or Hs6st1 sulphation in response to Slit2 when compared to wild type indicating a possible defect in Slit-Robo signaling.

9.2.1.3 *In vivo* approach to determining whether Slit1 signaling specifically requires Hs2st sulphation and Slit2 signaling specifically requires Hs6st1 sulphation at the optic chiasm.

In vivo approaches to determine the molecular mechanisms involving HS sulphation patterns ability to differentially interact with Slit-Robo signaling will involve the use of two different mouse lines harboring a mutation in either Slit1 or Slit2. With the availability of *Slit1*$^{-/-}$ mutant animals and *Slit2*$^{-/-}$ mutant animals we plan to generate compound mutants in which Hst function and Slit function are simultaneously disrupted. If Slit1 signaling requires Hs2st sulphation, we predict that a loss of both *Slit1*$^{-/-}$ and *Hs2st*$^{-/-}$ will show defects similar to the defects observed in *Slit1*$^{-/-}$ mutants or *Hs2st*$^{-/-}$ mutants. We will test this by quantifying retino-retinal projections and optic chiasm width measurements. If Slit2 signaling requires Hs6st1 sulphation, we

predict that a loss of both Slit2 and Hs6st1 will show defects similar to the defects observed in *Slit2*$^{-/-}$ mutants or *Hs6st1*$^{-/-}$ mutants. Again, we will test this by quantifying retino-retinal projections and optic chiasm width measurements. We also plan to generate the compound *Slit1*$^{-/-}$*/Hs6st1*$^{-/-}$ double mutants and *Slit2*$^{-/-}$*/Hs2st*$^{-/-}$ double mutants. Based on our hypothesis, we would predict the phenotypes of these two compound mutants to show the same phenotype observed in *Slit1*$^{-/-}$*/Slit2*$^{-/-}$ double mutants suggesting that Slit1 and Hs2st as well as Slit2 and Hs6st1 act in series to control optic chiasm formation.

9.2.2 Do Hst enzymes have unique and/or redundant functions *in vivo*.

To determine whether *Hs2st* and *Hs6st1* have unique and/or redundant functions in axon guidance, we planned to generate the compound *Hs2st*$^{-/-}$*/Hs6st1*$^{-/-}$ double mutants. However, attempts to generate *Hs2st*$^{-/-}$*/Hs6st1*$^{-/-}$ double mutant embryos failed due to early embryonic death (Chapter 6). The fact *Hs2st*$^{-/-}$*/Hs6st1*$^{-/-}$ double mutant embryos died very early in development suggested that in the absence of both Hs2st sulphation and Hs6st1 sulphation, severe developmental processes controlling early embryonic development had been disrupted (possibly morphogen signaling). Embryos lacking either Hs2st sulphation or Hs6st1 sulphation alone were capable of surviving to birth suggesting that 1) Hs2st and Hs6st1 are required in the same critically important developmental pathway suggesting functional redundancy or 2) Hs2st function is required for one developmental pathway while Hs6st1 is required for another developmental pathway; a loss of both pathways results in early embryonic death. We plan to identify whether Hs2st sulphation and Hs6st1 sulphation have unique functions and/or redundant functions in embryonic mouse CNS development.

9.2.2.1 Generation of *Hs2st*$^{-/-}$/*Hs6st1*$^{-/-}$ double mutants to determine functional redundancy.

Previous work has indicated that Hs2st sulphation and Hs6st1 sulphation have unique functions at the optic chiasm, likely acting through Slit1 or Slit2, respectively (Chapter 5). However, it is possible that both Hs2st sulphation and Hs6st1 sulphation are simultaneously required in other processes of optic chiasm development and/or other processes involved in CNS development, where one sulphation pattern can compensate for the loss of the other sulphation pattern. To allow visual system development in the absence of Hs2st and Hs6st1 function we propose to use a conditional knockout strategy. We will use our *Hs2st*$^{+/-}$ mutant line and a previously characterized mouse line that contains a "floxed" *Hs6st1* allele (*Hs6st1*$^{flox/flox}$) (Izvolsky et al., 2008). Using this mutant mouse line it is possible to conditionally knockout the *Hs6st1 gene* in a spatially and temporally controlled manner. Using a *Nestin-Cre* mouse line it is possible to conditionally knockout *Hs6st1* specifically in the mouse brain (Dubois et al., 2006). Crossing these animals, it is possible to generate embryos that lack both *Hs2st* and *Hs6st1* (*Hs2st*$^{-/-}$ */Nestin*$^{Cre+}$/*Hs6st1* $^{flox/flox}$) specifically in the mouse CNS as outlined below:

1) *Hs2st*$^{+/-}$ x *Hs6st1*$^{+/floxed}$ = *Hs2st*$^{+/-}$/*Hs6st1*$^{+/floxed}$

Hs2st$^{+/-}$/*Hs6st1*$^{+/floxed}$ x *Nestin*$^{Cre+/Cre+}$ = ***Hs2st***$^{+/-}$***/Hs6st1***$^{+/floxed}$ ***/Nestin*** $^{Cre+/Cre+}$

2) *Hs2st*$^{+/-}$ x *Hs6st1*$^{floxed/floxed}$ = ***Hs2st***$^{+/-}$***/Hs6st1***$^{floxed/floxed}$

Hs2st$^{+/-}$***/Hs6st1***$^{floxed/floxed}$ x ***Hs2st***$^{+/-}$***/Hs6st1***$^{+/floxed}$ ***/Nestin*** $^{Cre+/Cre+}$

Embryos = ***Hs2st***$^{-/-}$***/Hs6st1*** $^{floxed/floxed}$ ***/Nestin***$^{Cre/+}$

This approach would allow us to determine the effect a loss of both Hs2st sulphation and Hs6st1 sulphation have on CNS development and determine whether they have unique and/or redundant functions in CNS development.

9.2.2.2 Generation of *Hs6st1*$^{-/-}$/*Hs6st2*$^{-/-}$ double mutants to determine functional redundancy in TCA/CTA tract formation.

Observations of TCA/CTA tract formation in the developing mouse CNS did not show any gross defects in *Hs2st*$^{-/-}$ mutant embryos or *Hs6st1*$^{-/-}$ mutant embryos (Chapter 5). While *Hs2st* was shown to be expressed in the cortex, *Hs6st1* was shown to be expressed in the cortex, striatum, and highly expressed in the dorsal thalamus; all important regions in TCA/CTA tract development (Chapter 3). The lack of a mutant phenotype particularly in the *Hs6st1*$^{-/-}$ mutant was not consistent with our hypothesis that *Hs6st1*$^{-/-}$ mutants phenocopy *Slit2*$^{-/-}$ mutants. In *Slit2*$^{-/-}$ mutant embryos, the TCA/CTA tract was shown to be defective, resulting in a more ventro-caudally extended tract and ectopic navigation into the hypothalamus (Bagri et al., 2002). One possible explanation for the normal formation of the TCA/CTA tract in *Hs6st1*$^{-/-}$ mutant embryos is that the loss of Hs6st1 sulphation is being compensated for. In addition to *Hs6st1*, there are two other isoforms, namely *Hs6st2* and *Hs6st3*. Observations of their expression patterns revealed high expression of *Hs6st2* at the dorsal thalamus as well as in the cortex, but low *Hs6st3* expression (Chapter 7). We therefore proposed that a loss of Hs6st1 sulphation is compensated for by the presence of Hs6st2 sulphation.

Previous work using *in vitro* experiments showed that in the absence of Hs6st1 sulphation, HSPG 6-O-sulphation was reduced, but not absent, however in the absence of both Hs6st1 and Hs6st2, almost no HSPG 6-O-sulphation was present (Sugaya et al., 2008). Using compound *Hs6st1*$^{-/-}$/*Hs6st2*$^{-/-}$ double mutants previously characterized in Sugaya et al. 2008, we plan to test whether the loss of *Hs6st1* can be compensated for by *Hs6st2* in TCA/CTA tract formation.

9.2.2.3 Generation of *Hs6st1*$^{-/-}$/*Hs6st3*$^{-/-}$ double mutants to determine functional redundancy in RGC axon navigation in the retina.

Observations of RGC axon navigation in the retina of the eye did not show any gross defects in *Hs6st1*$^{-/-}$ mutant embryos (Chapter 5). *Hs6st1* was shown to be highly expressed in the RGC layer of the retina (Chapter 3). The lack of a mutant phenotype in the *Hs6st1*$^{-/-}$ mutant was not consistent with our hypothesis that *Hs6st1*$^{-/-}$ mutants phenocopy *Slit2*$^{-/-}$ mutants. In *Slit2*$^{-/-}$ mutant embryos, the RGC axon navigation in the retina was shown to be defective, resulting in RGC axons ectopically navigating outside the normal boundary of the OFL (Thompson et al., 2006b). One possible explanation for the normal navigation of RGC axon in the retina of *Hs6st1*$^{-/-}$ mutant embryos is that the loss of Hs6st1 sulphation is being compensated for. Observations of other enzymes capable of HSPG 6-O-sulphation showed high expression of *Hs6st3* in the RGC layer of the eye (Chapter 7). We proposed that a loss of Hs6st1 sulphation is compensated for by the presence of Hs6st3 sulphation. To test this hypothesis we propose to generate *Hs6st1*$^{-/-}$/*Hs6st3*$^{-/-}$ double mutants to determine whether there is functional redundancy in RGC axon navigation in the retina. Sadly, as *Hs6st3*$^{-/-}$ mutant mice have not yet been generated, this will be a very time intensive experiment and therefore will not be an experiment carried out in the immediate future.

9.2.3 What are the mechanisms involved in Hs2st dependent and Hs6st1 dependent axon navigation in the corpus callosum

At E17.5 callosal axons are normally observed to have started crossing the midline, navigating towards their eventual targets in the contralateral cortex. Observations of E17.5 *Hs2st*$^{-/-}$ mutant and *Hs6st1*$^{-/-}$ mutant embryos showed that callosal axons had not yet crossed the midline. Further observations of the *Hs6st1*$^{-/-}$ mutant embryos at this age revealed that callosal axons ectopically navigated along the ventral midline

forming Probst bundles. Previous work on E17.5 *Slit2*$^{-/-}$ mutants and *Robo1*$^{-/-}$ mutants (Andrews et al., 2006), and more prominently in *Slit1*$^{-/-}$/*Slit2*$^{-/-}$ double mutant and *Robo1*$^{-/-}$/*Robo2*$^{-/-}$ double mutants, showed a hypocallosal phenotype where a proportion of callosal axons failed to cross the midline, forming Probst bundles (Bagri et al., 2002; Lopez-Bendito et al., 2007). The fact, the acallosal phenotype observed in *Hs6st1*$^{-/-}$ mutants did not phenocopy all aspects of the *Slit-Robo* mutant phenotypes does rule out the possibility that Slit-Robo signaling specifically requires specific Hs6st1 sulphation, but does suggest that other processes important to corpus callosum development are affected by the absence of Hs2st sulphation or Hs6st1 sulphation. This may include defects in other axon guidance molecules important in callosal axon navigation at the midline that are known to interact with HSPGs such as netrin1, ephrinB3, and semaphorin3b or Sema3f (Lindwall et al., 2007). Alternatively, the loss of Hs2st and/or Hs6st1 may affect midline glial development. Further characterization of both, *Hs2st*$^{-/-}$ mutant and *Hs6st1*$^{-/-}$ mutant corpus callosum development will involve DiI/DiA tract tracing at later embryonic ages to observe callosal axon behavior. Furthermore, a characterization of the glial structures known to be critical in the formation of the corpus callosum will be examined using GFAP immunohistochemistry. Finally, determining the molecular mechanisms affected in corpus callosum development in *Hs2st*$^{-/-}$ mutant and *Hs6st1*$^{-/-}$ mutant embryos using *in vitro* and *in vivo* techniques will show the similarities and/or differences in the way Hst enzymes regulate axon guidance in the major forebrain commissures, the optic chiasm and the corpus callosum.

9.3 Concluding Statement

My observations of axonal tracts within the mouse CNS indicate that their development while being dependant on HSPGs, are differentially dependant on the status of HSPG sulphation modifications as hypothesized by the "heparan sulphate code" (Bulow and Hobert, 2004). Here we show that Hs2st sulphation and Hs6st1

sulphation differentially regulate different aspects of axon guidance in different axonal systems. While mounting evidence suggests that Hs2st sulphation is absolutely required for Slit1-Robo2 signaling and Hs6st1 sulphation is absolutely required for Slit2-Robo2 signaling in optic chiasm development, this association is not so clear in other regions of CNS development. Taking into account the possibility of redundancy in CNS development and the fact that the function of many axon guidance molecules are not absolute, but rather, reflective of the context in which they are encountered and also on the type of axon they encounter, it is not surprising that a simple set of rules not be sufficient to explain the complexity of axon guidance in the developing CNS.

Happily there is a lot more to do and I look forward to doing it!

References

Aikawa J, Grobe K, Tsujimoto M, Esko JD (2001) Multiple isozymes of heparan sulfate/heparin GlcNAc N-deacetylase/GlcN N-sulfotransferase. Structure and activity of the fourth member, NDST4. J Biol Chem 276:5876-5882.

Andrews W, Liapi A, Plachez C, Camurri L, Zhang J, Mori S, Murakami F, Parnavelas JG, Sundaresan V, Richards LJ (2006) Robo1 regulates the development of major axon tracts and interneuron migration in the forebrain. Development 133:2243-2252.

Artigiani S, Comoglio PM, Tamagnone L (1999) Plexins, semaphorins, and scatter factor receptors: a common root for cell guidance signals? IUBMB Life 48:477-482.

Augsburger A, Schuchardt A, Hoskins S, Dodd J, Butler S (1999) BMPs as mediators of roof plate repulsion of commissural neurons. Neuron 24:127-141.

Bagnard D, Lohrum M, Uziel D, Puschel AW, Bolz J (1998) Semaphorins act as attractive and repulsive guidance signals during the development of cortical projections. Development 125:5043-5053.

Bagri A, Marin O, Plump AS, Mak J, Pleasure SJ, Rubenstein JL, Tessier-Lavigne M (2002) Slit proteins prevent midline crossing and determine the dorsoventral position of major axonal pathways in the mammalian forebrain. Neuron 33:233-248.

Barallobre MJ, Pascual M, Del Rio JA, Soriano E (2005) The Netrin family of guidance factors: emphasis on Netrin-1 signalling. Brain Res Brain Res Rev 49:22-47.

Bernfield M, Gotte M, Park PW, Reizes O, Fitzgerald ML, Lincecum J, Zako M (1999) Functions of cell surface heparan sulfate proteoglycans. Annu Rev Biochem 68:729-777.

Bhide PG, Frost DO (1991) Stages of growth of hamster retinofugal axons: implications for developing axonal pathways with multiple targets. J Neurosci 11:485-504.

Birgbauer E, Cowan CA, Sretavan DW, Henkemeyer M (2000) Kinase independent function of EphB receptors in retinal axon pathfinding to the optic disc from dorsal but not ventral retina. Development 127:1231-1241.

Black DL, Zipursky SL (2008) To cross or not to cross: alternatively spliced forms of the Robo3 receptor regulate discrete steps in axonal midline crossing. Neuron 58:297-298.

Bolz J, Uziel D, Muhlfriedel S, Gullmar A, Peuckert C, Zarbalis K, Wurst W, Torii M, Levitt P (2004) Multiple roles of ephrins during the formation of thalamocortical projections: maps and more. J Neurobiol 59:82-94.

Bourikas D, Pekarik V, Baeriswyl T, Grunditz A, Sadhu R, Nardo M, Stoeckli ET (2005) Sonic hedgehog guides commissural axons along the longitudinal axis of the spinal cord. Nat Neurosci 8:297-304.

Bradford D, Cole SJ, Cooper HM (2008) Netrin-1: Diversity in development. Int J Biochem Cell Biol.

Braisted JE, Tuttle R, O'Leary D D (1999) Thalamocortical axons are influenced by chemorepellent and chemoattractant activities localized to decision points along their path. Dev Biol 208:430-440.

Braisted JE, Catalano SM, Stimac R, Kennedy TE, Tessier-Lavigne M, Shatz CJ, O'Leary DD (2000) Netrin-1 promotes thalamic axon growth and is required for proper development of the thalamocortical projection. J Neurosci 20:5792-5801.

Brose K, Tessier-Lavigne M (2000) Slit proteins: key regulators of axon guidance, axonal branching, and cell migration. Curr Opin Neurobiol 10:95-102.

Brose K, Bland KS, Wang KH, Arnott D, Henzel W, Goodman CS, Tessier-Lavigne M, Kidd T (1999) Slit proteins bind Robo receptors and have an evolutionarily conserved role in repulsive axon guidance. Cell 96:795-806.

Brown A, Yates PA, Burrola P, Ortuno D, Vaidya A, Jessell TM, Pfaff SL, O'Leary DD, Lemke G (2000) Topographic mapping from the retina to the midbrain is controlled by relative but not absolute levels of EphA receptor signaling. Cell 102:77-88.

Brunet I, Weinl C, Piper M, Trembleau A, Volovitch M, Harris W, Prochiantz A, Holt C (2005) The transcription factor Engrailed-2 guides retinal axons. Nature 438:94-98.

Bullock SL, Fletcher JM, Beddington RS, Wilson VA (1998) Renal agenesis in mice homozygous for a gene trap mutation in the gene encoding heparan sulfate 2-sulfotransferase. Genes Dev 12:1894-1906.

Bulow HE, Hobert O (2004) Differential sulfations and epimerization define heparan sulfate specificity in nervous system development. Neuron 41:723-736.

Bulow HE, Hobert O (2006) The molecular diversity of glycosaminoglycans shapes animal development. Annu Rev Cell Dev Biol 22:375-407.

Butler SJ, Tear G (2007) Getting axons onto the right path: the role of transcription factors in axon guidance. Development 134:439-448.

Cang J, Kaneko M, Yamada J, Woods G, Stryker MP, Feldheim DA (2005) Ephrin-as guide the formation of functional maps in the visual cortex. Neuron 48:577-589.

Chan SO, Cheung WS, Lin L (2002) Differential responses of temporal and nasal retinal neurites to regional-specific cues in the mouse retinofugal pathway. Cell Tissue Res 309:201-208.

Charron F, Stein E, Jeong J, McMahon AP, Tessier-Lavigne M (2003) The morphogen sonic hedgehog is an axonal chemoattractant that collaborates with netrin-1 in midline axon guidance. Cell 113:11-23.

Chen Z, Gore BB, Long H, Ma L, Tessier-Lavigne M (2008) Alternative splicing of the Robo3 axon guidance receptor governs the midline switch from attraction to repulsion. Neuron 58:325-332.

Chilton JK (2006) Molecular mechanisms of axon guidance. Dev Biol 292:13-24.

Chisholm AD, Jin Y (2005) Neuronal differentiation in C. elegans. Curr Opin Cell Biol 17:682-689.

Chung KY, Shum DK, Chan SO (2000a) Expression of chondroitin sulfate proteoglycans in the chiasm of mouse embryos. J Comp Neurol 417:153-163.

Chung KY, Taylor JS, Shum DK, Chan SO (2000b) Axon routing at the optic chiasm after enzymatic removal of chondroitin sulfate in mouse embryos. Development 127:2673-2683.

Clark RA, Lin F, Greiling D, An J, Couchman JR (2004) Fibroblast invasive migration into fibronectin/fibrin gels requires a previously uncharacterized dermatan sulfate-CD44 proteoglycan. J Invest Dermatol 122:266-277.

Colamarino SA, Tessier-Lavigne M (1995) The axonal chemoattractant netrin-1 is also a chemorepellent for trochlear motor axons. Cell 81:621-629.

Colello RJ, Guillery RW (1990) The early development of retinal ganglion cells with uncrossed axons in the mouse: retinal position and axonal course. Development 108:515-523.

Coumoul X, Deng CX (2003) Roles of FGF receptors in mammalian development and congenital diseases. Birth Defects Res C Embryo Today 69:286-304.

Davy A, Soriano P (2005) Ephrin signaling in vivo: look both ways. Dev Dyn 232:1-10.

Deiner MS, Kennedy TE, Fazeli A, Serafini T, Tessier-Lavigne M, Sretavan DW (1997) Netrin-1 and DCC mediate axon guidance locally at the optic disc: loss of function leads to optic nerve hypoplasia. Neuron 19:575-589.

Dickson BJ (2002) Molecular mechanisms of axon guidance. Science 298:1959-1964.

Dickson BJ (2005) Wnts send axons up and down the spinal cord. Nat Neurosci 8:1130-1132.

Doi M, Uji Y, Yamamura H (1995) Morphological classification of retinal ganglion cells in mice. J Comp Neurol 356:368-386.

Drager UC (1985) Birth dates of retinal ganglion cells giving rise to the crossed and uncrossed optic projections in the mouse. Proc R Soc Lond B Biol Sci 224:57-77.

Drager UC, Hubel DH (1975) Physiology of visual cells in mouse superior colliculus and correlation with somatosensory and auditory input. Nature 253:203-204.

Drager UC, Olsen JF (1980) Origins of crossed and uncrossed retinal projections in pigmented and albino mice. J Comp Neurol 191:383-412.

Drager UC, Olsen JF (1981) Ganglion cell distribution in the retina of the mouse. Invest Ophthalmol Vis Sci 20:285-293.

Dubois NC, Hofmann D, Kaloulis K, Bishop JM, Trumpp A (2006) Nestin-Cre transgenic mouse line Nes-Cre1 mediates highly efficient Cre/loxP mediated recombination in the nervous system, kidney, and somite-derived tissues. Genesis 44:355-360.

Egea J, Klein R (2007) Bidirectional Eph-ephrin signaling during axon guidance. Trends Cell Biol 17:230-238.

Erskine L, Herrera E (2007) The retinal ganglion cell axon's journey: insights into molecular mechanisms of axon guidance. Dev Biol 308:1-14.

Erskine L, Williams SE, Brose K, Kidd T, Rachel RA, Goodman CS, Tessier-Lavigne M, Mason CA (2000) Retinal ganglion cell axon guidance in the mouse optic chiasm: expression and function of robos and slits. J Neurosci 20:4975-4982.

Esko JD, Lindahl U (2001) Molecular diversity of heparan sulfate. J Clin Invest 108:169-173.

Esko JD, Selleck SB (2002) Order out of chaos: assembly of ligand binding sites in heparan sulfate. Annu Rev Biochem 71:435-471.

Farrar NR, Spencer GE (2008) Pursuing a 'turning point' in growth cone research. Dev Biol 318:102-111.

Feldheim DA, Kim YI, Bergemann AD, Frisen J, Barbacid M, Flanagan JG (2000) Genetic analysis of ephrin-A2 and ephrin-A5 shows their requirement in multiple aspects of retinocollicular mapping. Neuron 25:563-574.

Feldheim DA, Nakamoto M, Osterfield M, Gale NW, DeChiara TM, Rohatgi R, Yancopoulos GD, Flanagan JG (2004) Loss-of-function analysis of EphA receptors in retinotectal mapping. J Neurosci 24:2542-2550.

Flanagan JG (2006) Neural map specification by gradients. Curr Opin Neurobiol 16:59-66.

Fransson LA, Belting M, Jonsson M, Mani K, Moses J, Oldberg A (2000) Biosynthesis of decorin and glypican. Matrix Biol 19:367-376.

Frisen J, Yates PA, McLaughlin T, Friedman GC, O'Leary DD, Barbacid M (1998) Ephrin-A5 (AL-1/RAGS) is essential for proper retinal axon guidance and topographic mapping in the mammalian visual system. Neuron 20:235-243.

Fujisawa H (2004) Discovery of semaphorin receptors, neuropilin and plexin, and their functions in neural development. J Neurobiol 59:24-33.

Garbe DS, Bashaw GJ (2004) Axon guidance at the midline: from mutants to mechanisms. Crit Rev Biochem Mol Biol 39:319-341.

Godement P, Salaun J, Imbert M (1984) Prenatal and postnatal development of retinogeniculate and retinocollicular projections in the mouse. J Comp Neurol 230:552-575.

Goodman CS (1996) Mechanisms and molecules that control growth cone guidance. Annu Rev Neurosci 19:341-377.

Goodman CS, Shatz CJ (1993) Developmental mechanisms that generate precise patterns of neuronal connectivity. Cell 72 Suppl:77-98.

Gorsi B, Stringer SE (2007) Tinkering with heparan sulfate sulfation to steer development. Trends Cell Biol 17:173-177.

Grobe K, Inatani M, Pallerla SR, Castagnola J, Yamaguchi Y, Esko JD (2005) Cerebral hypoplasia and craniofacial defects in mice lacking heparan sulfate Ndst1 gene function. Development 132:3777-3786.

Grobe K, Ledin J, Ringvall M, Holmborn K, Forsberg E, Esko JD, Kjellen L (2002) Heparan sulfate and development: differential roles of the N-acetylglucosamine N-deacetylase/N-sulfotransferase isozymes. Biochim Biophys Acta 1573:209-215.

Guimond S, Turner K, Kita M, Ford-Perriss M, Turnbull J (2001) Dynamic biosynthesis of heparan sulphate sequences in developing mouse brain: a potential regulatory mechanism during development. Biochem Soc Trans 29:177-181.

Habuchi H, Kobayashi M, Kimata K (1998) Molecular characterization and expression of heparan-sulfate 6-sulfotransferase. Complete cDNA cloning in

human and partial cloning in Chinese hamster ovary cells. J Biol Chem 273:9208-9213.

Habuchi H, Nagai N, Sugaya N, Atsumi F, Stevens RL, Kimata K (2007) Mice deficient in heparan sulfate 6-O-sulfotransferase-1 exhibit defective heparan sulfate biosynthesis, abnormal placentation, and late embryonic lethality. J Biol Chem 282:15578-15588.

Habuchi H, Tanaka M, Habuchi O, Yoshida K, Suzuki H, Ban K, Kimata K (2000) The occurrence of three isoforms of heparan sulfate 6-O-sulfotransferase having different specificities for hexuronic acid adjacent to the targeted N-sulfoglucosamine. J Biol Chem 275:2859-2868.

Habuchi H, Miyake G, Nogami K, Kuroiwa A, Matsuda Y, Kusche-Gullberg M, Habuchi O, Tanaka M, Kimata K (2003) Biosynthesis of heparan sulphate with diverse structures and functions: two alternatively spliced forms of human heparan sulphate 6-O-sulphotransferase-2 having different expression patterns and properties. Biochem J 371:131-142.

Hacker U, Nybakken K, Perrimon N (2005) Heparan sulphate proteoglycans: the sweet side of development. Nat Rev Mol Cell Biol 6:530-541.

Hansen MJ, Dallal GE, Flanagan JG (2004) Retinal axon response to ephrin-as shows a graded, concentration-dependent transition from growth promotion to inhibition. Neuron 42:717-730.

Hattar S, Kumar M, Park A, Tong P, Tung J, Yau KW, Berson DM (2006) Central projections of melanopsin-expressing retinal ganglion cells in the mouse. J Comp Neurol 497:326-349.

Haupt C, Huber AB (2008) How axons see their way--axonal guidance in the visual system. Front Biosci 13:3136-3149.

Herrera E, Marcus R, Li S, Williams SE, Erskine L, Lai E, Mason C (2004) Foxd1 is required for proper formation of the optic chiasm. Development 131:5727-5739.

Herrera E, Brown L, Aruga J, Rachel RA, Dolen G, Mikoshiba K, Brown S, Mason CA (2003) Zic2 patterns binocular vision by specifying the uncrossed retinal projection. Cell 114:545-557.

Hindges R, McLaughlin T, Genoud N, Henkemeyer M, O'Leary DD (2002) EphB forward signaling controls directional branch extension and arborization required for dorsal-ventral retinotopic mapping. Neuron 35:475-487.

Hinds JW, Hinds PL (1974) Early ganglion cell differentiation in the mouse retina: an electron microscopic analysis utilizing serial sections. Dev Biol 37:381-416.

Hopker VH, Shewan D, Tessier-Lavigne M, Poo M, Holt C (1999) Growth-cone attraction to netrin-1 is converted to repulsion by laminin-1. Nature 401:69-73.

Hu H (1999) Chemorepulsion of neuronal migration by Slit2 in the developing mammalian forebrain. Neuron 23:703-711.

Huberman AD, Murray KD, Warland DK, Feldheim DA, Chapman B (2005) Ephrin-As mediate targeting of eye-specific projections to the lateral geniculate nucleus. Nat Neurosci 8:1013-1021.

Hussain SA, Piper M, Fukuhara N, Strochlic L, Cho G, Howitt JA, Ahmed Y, Powell AK, Turnbull JE, Holt CE, Hohenester E (2006) A molecular mechanism for the heparan sulfate dependence of slit-robo signaling. J Biol Chem 281:39693-39698.

Huxlin KR, Goodchild AK (1997) Retinal ganglion cells in the albino rat: revised morphological classification. J Comp Neurol 385:309-323.

Illing RB, Wassle H (1981) The retinal projection to the thalamus in the cat: a quantitative investigation and a comparison with the retinotectal pathway. J Comp Neurol 202:265-285.

Inatani M (2005) Molecular mechanisms of optic axon guidance. Naturwissenschaften 92:549-561.

Inatani M, Yamaguchi Y (2003) Gene expression of EXT1 and EXT2 during mouse brain development. Brain Res Dev Brain Res 141:129-136.

Inatani M, Irie F, Plump AS, Tessier-Lavigne M, Yamaguchi Y (2003) Mammalian brain morphogenesis and midline axon guidance require heparan sulfate. Science 302:1044-1046.

Irie A, Yates EA, Turnbull JE, Holt CE (2002) Specific heparan sulfate structures involved in retinal axon targeting. Development 129:61-70.

Irie F, Okuno M, Matsumoto K, Pasquale EB, Yamaguchi Y (2008) Heparan sulfate regulates ephrin-A3/EphA receptor signaling. Proc Natl Acad Sci U S A 105:12307-12312.

Itoh K, Cheng L, Kamei Y, Fushiki S, Kamiguchi H, Gutwein P, Stoeck A, Arnold B, Altevogt P, Lemmon V (2004) Brain development in mice lacking L1-L1 homophilic adhesion. J Cell Biol 165:145-154.

Izvolsky KI, Lu J, Martin G, Albrecht KH, Cardoso WV (2008) Systemic inactivation of Hs6st1 in mice is associated with late postnatal mortality without major defects in organogenesis. Genesis 46:8-18.

Jeffery G (2001) Architecture of the optic chiasm and the mechanisms that sculpt its development. Physiol Rev 81:1393-1414.

Johnson KG, Ghose A, Epstein E, Lincecum J, O'Connor MB, Van Vactor D (2004) Axonal heparan sulfate proteoglycans regulate the distribution and efficiency of the repellent slit during midline axon guidance. Curr Biol 14:499-504.

Kantor DB, Chivatakarn O, Peer KL, Oster SF, Inatani M, Hansen MJ, Flanagan JG, Yamaguchi Y, Sretavan DW, Giger RJ, Kolodkin AL (2004) Semaphorin 5A is a bifunctional axon guidance cue regulated by heparan and chondroitin sulfate proteoglycans. Neuron 44:961-975.

Kaprielian Z, Imondi R, Runko E (2000) Axon guidance at the midline of the developing CNS. Anat Rec 261:176-197.

Kaprielian Z, Runko E, Imondi R (2001) Axon guidance at the midline choice point. Dev Dyn 221:154-181.

Keino-Masu K, Masu M, Hinck L, Leonardo ED, Chan SS, Culotti JG, Tessier-Lavigne M (1996) Deleted in Colorectal Cancer (DCC) encodes a netrin receptor. Cell 87:175-185.

Kennedy TE, Serafini T, de la Torre JR, Tessier-Lavigne M (1994) Netrins are diffusible chemotropic factors for commissural axons in the embryonic spinal cord. Cell 78:425-435.

Kidd T, Bland KS, Goodman CS (1999) Slit is the midline repellent for the robo receptor in Drosophila. Cell 96:785-794.

Kinnunen A, Niemi M, Kinnunen T, Kaksonen M, Nolo R, Rauvala H (1999) Heparan sulphate and HB-GAM (heparin-binding growth-associated molecule) in the development of the thalamocortical pathway of rat brain. Eur J Neurosci 11:491-502.

Klein R (2004) Eph/ephrin signaling in morphogenesis, neural development and plasticity. Curr Opin Cell Biol 16:580-589.

Kobayashi M, Habuchi H, Yoneda M, Habuchi O, Kimata K (1997) Molecular cloning and expression of Chinese hamster ovary cell heparan-sulfate 2-sulfotransferase. J Biol Chem 272:13980-13985.

Kruger RP, Aurandt J, Guan KL (2005) Semaphorins command cells to move. Nat Rev Mol Cell Biol 6:789-800.

Law CO, Kirby RJ, Aghamohammadzadeh S, Furley AJ (2008) The neural adhesion molecule TAG-1 modulates responses of sensory axons to diffusible guidance signals. Development 135:2361-2371.

Lee JS, Chien CB (2004) When sugars guide axons: insights from heparan sulphate proteoglycan mutants. Nat Rev Genet 5:923-935.

Lee JS, von der Hardt S, Rusch MA, Stringer SE, Stickney HL, Talbot WS, Geisler R, Nusslein-Volhard C, Selleck SB, Chien CB, Roehl H (2004) Axon sorting in the optic tract requires HSPG synthesis by ext2 (dackel) and extl3 (boxer). Neuron 44:947-960.

Leighton PA, Mitchell KJ, Goodrich LV, Lu X, Pinson K, Scherz P, Skarnes WC, Tessier-Lavigne M (2001) Defining brain wiring patterns and mechanisms through gene trapping in mice. Nature 410:174-179.

Lemke G, Reber M (2005) Retinotectal mapping: new insights from molecular genetics. Annu Rev Cell Dev Biol 21:551-580.

Li JP, Gong F, Hagner-McWhirter A, Forsberg E, Abrink M, Kisilevsky R, Zhang X, Lindahl U (2003) Targeted disruption of a murine glucuronyl C5-epimerase gene results in heparan sulfate lacking L-iduronic acid and in neonatal lethality. J Biol Chem 278:28363-28366.

Liang Y, Annan RS, Carr SA, Popp S, Mevissen M, Margolis RK, Margolis RU (1999) Mammalian homologues of the Drosophila slit protein are ligands of the heparan sulfate proteoglycan glypican-1 in brain. J Biol Chem 274:17885-17892.

Lin X (2004) Functions of heparan sulfate proteoglycans in cell signaling during development. Development 131:6009-6021.

Lin X, Perrimon N (2002) Developmental roles of heparan sulfate proteoglycans in Drosophila. Glycoconj J 19:363-368.

Lin X, Wei G, Shi Z, Dryer L, Esko JD, Wells DE, Matzuk MM (2000) Disruption of gastrulation and heparan sulfate biosynthesis in EXT1-deficient mice. Dev Biol 224:299-311.

Linden R, Perry VH (1983) Massive retinotectal projection in rats. Brain Res 272:145-149.

Lindwall C, Fothergill T, Richards LJ (2007) Commissure formation in the mammalian forebrain. Curr Opin Neurobiol 17:3-14.

Long H, Sabatier C, Ma L, Plump A, Yuan W, Ornitz DM, Tamada A, Murakami F, Goodman CS, Tessier-Lavigne M (2004) Conserved roles for Slit and Robo proteins in midline commissural axon guidance. Neuron 42:213-223.

Lopez-Bendito G, Molnar Z (2003) Thalamocortical development: how are we going to get there? Nat Rev Neurosci 4:276-289.

Lopez-Bendito G, Flames N, Ma L, Fouquet C, Di Meglio T, Chedotal A, Tessier-Lavigne M, Marin O (2007) Robo1 and Robo2 cooperate to control the guidance of major axonal tracts in the mammalian forebrain. J Neurosci 27:3395-3407.

Lund RD, Lund JS, Wise RP (1974) The organization of the retinal projection to the dorsal lateral geniculate nucleus in pigmented and albino rats. J Comp Neurol 158:383-403.

Ma L, Tessier-Lavigne M (2007) Dual branch-promoting and branch-repelling actions of Slit/Robo signaling on peripheral and central branches of developing sensory axons. J Neurosci 27:6843-6851.

Mann F, Harris WA, Holt CE (2004) New views on retinal axon development: a navigation guide. Int J Dev Biol 48:957-964.

Mann F, Ray S, Harris W, Holt C (2002) Topographic mapping in dorsoventral axis of the Xenopus retinotectal system depends on signaling through ephrin-B ligands. Neuron 35:461-473.

Manuel M, Pratt T, Liu M, Jeffery G, Price DJ (2008) Overexpression of Pax6 results in microphthalmia, retinal dysplasia and defective retinal ganglion cell axon guidance. BMC Dev Biol 8:59.

Marcus RC, Mason CA (1995) The first retinal axon growth in the mouse optic chiasm: axon patterning and the cellular environment. J Neurosci 15:6389-6402.

Marcus RC, Blazeski R, Godement P, Mason CA (1995) Retinal axon divergence in the optic chiasm: uncrossed axons diverge from crossed axons within a midline glial specialization. J Neurosci 15:3716-3729.

Martin PR (1986) The projection of different retinal ganglion cell classes to the dorsal lateral geniculate nucleus in the hooded rat. Exp Brain Res 62:77-88.

Matsumoto Y, Irie F, Inatani M, Tessier-Lavigne M, Yamaguchi Y (2007) Netrin-1/DCC signaling in commissural axon guidance requires cell-autonomous expression of heparan sulfate. J Neurosci 27:4342-4350.

McFarlane S, McNeill L, Holt CE (1995) FGF signaling and target recognition in the developing Xenopus visual system. Neuron 15:1017-1028.

McLaughlin D, Karlsson F, Tian N, Pratt T, Bullock SL, Wilson VA, Price DJ, Mason JO (2003a) Specific modification of heparan sulphate is required for normal cerebral cortical development. Mech Dev 120:1481-1488.

McLaughlin T, O'Leary DD (2005) Molecular gradients and development of retinotopic maps. Annu Rev Neurosci 28:327-355.

McLaughlin T, Hindges R, O'Leary DD (2003b) Regulation of axial patterning of the retina and its topographic mapping in the brain. Curr Opin Neurobiol 13:57-69.

McLaughlin T, Hindges R, Yates PA, O'Leary DD (2003c) Bifunctional action of ephrin-B1 as a repellent and attractant to control bidirectional branch extension in dorsal-ventral retinotopic mapping. Development 130:2407-2418.

Medeiros GF, Mendes A, Castro RA, Bau EC, Nader HB, Dietrich CP (2000) Distribution of sulfated glycosaminoglycans in the animal kingdom: widespread occurrence of heparin-like compounds in invertebrates. Biochim Biophys Acta 1475:287-294.

Mendes SW, Henkemeyer M, Liebl DJ (2006) Multiple Eph receptors and B-class ephrins regulate midline crossing of corpus callosum fibers in the developing mouse forebrain. J Neurosci 26:882-892.

Merry CL, Wilson VA (2002) Role of heparan sulfate-2-O-sulfotransferase in the mouse. Biochim Biophys Acta 1573:319-327.

Merry CL, Bullock SL, Swan DC, Backen AC, Lyon M, Beddington RS, Wilson VA, Gallagher JT (2001) The molecular phenotype of heparan sulfate in the Hs2st-/- mutant mouse. J Biol Chem 276:35429-35434.

Mitchell KJ, Pinson KI, Kelly OG, Brennan J, Zupicich J, Scherz P, Leighton PA, Goodrich LV, Lu X, Avery BJ, Tate P, Dill K, Pangilinan E, Wakenight P, Tessier-Lavigne M, Skarnes WC (2001) Functional analysis of secreted and

transmembrane proteins critical to mouse development. Nat Genet 28:241-249.

Moore SW, Tessier-Lavigne M, Kennedy TE (2007) Netrins and their receptors. Adv Exp Med Biol 621:17-31.

Morimoto-Tomita M, Uchimura K, Werb Z, Hemmerich S, Rosen SD (2002) Cloning and characterization of two extracellular heparin-degrading endosulfatases in mice and humans. J Biol Chem 277:49175-49185.

Nakagawa S, Brennan C, Johnson KG, Shewan D, Harris WA, Holt CE (2000) Ephrin-B regulates the Ipsilateral routing of retinal axons at the optic chiasm. Neuron 25:599-610.

Nakagawa Y, O'Leary DD (2001) Combinatorial expression patterns of LIM-homeodomain and other regulatory genes parcellate developing thalamus. J Neurosci 21:2711-2725.

Nakato H, Kimata K (2002) Heparan sulfate fine structure and specificity of proteoglycan functions. Biochim Biophys Acta 1573:312-318.

Negishi M, Oinuma I, Katoh H (2005) Plexins: axon guidance and signal transduction. Cell Mol Life Sci 62:1363-1371.

Nguyen-Ba-Charvet KT, Chedotal A (2002) Role of Slit proteins in the vertebrate brain. J Physiol Paris 96:91-98.

Nguyen Ba-Charvet KT, Brose K, Marillat V, Kidd T, Goodman CS, Tessier-Lavigne M, Sotelo C, Chedotal A (1999) Slit2-Mediated chemorepulsion and collapse of developing forebrain axons. Neuron 22:463-473.

Nguyen Ba-Charvet KT, Brose K, Ma L, Wang KH, Marillat V, Sotelo C, Tessier-Lavigne M, Chedotal A (2001) Diversity and specificity of actions of Slit2 proteolytic fragments in axon guidance. J Neurosci 21:4281-4289.

Niclou SP, Jia L, Raper JA (2000) Slit2 is a repellent for retinal ganglion cell axons. J Neurosci 20:4962-4974.

Nybakken K, Perrimon N (2002) Heparan sulfate proteoglycan modulation of developmental signaling in Drosophila. Biochim Biophys Acta 1573:280-291.

O'Leary DD (1992) Development of connectional diversity and specificity in the mammalian brain by the pruning of collateral projections. Curr Opin Neurobiol 2:70-77.

Ornitz DM (2000) FGFs, heparan sulfate and FGFRs: complex interactions essential for development. Bioessays 22:108-112.

Oster SF, Bodeker MO, He F, Sretavan DW (2003) Invariant Sema5A inhibition serves an ensheathing function during optic nerve development. Development 130:775-784.

Oster SF, Deiner M, Birgbauer E, Sretavan DW (2004) Ganglion cell axon pathfinding in the retina and optic nerve. Semin Cell Dev Biol 15:125-136.

Ozdinler PH, Erzurumlu RS (2002) Slit2, a branching-arborization factor for sensory axons in the Mammalian CNS. J Neurosci 22:4540-4549.

Pak W, Hindges R, Lim YS, Pfaff SL, O'Leary DD (2004) Magnitude of binocular vision controlled by islet-2 repression of a genetic program that specifies laterality of retinal axon pathfinding. Cell 119:567-578.

Pellegrini L (2001) Role of heparan sulfate in fibroblast growth factor signalling: a structural view. Curr Opin Struct Biol 11:629-634.

Perrimon N, Bernfield M (2000) Specificities of heparan sulphate proteoglycans in developmental processes. Nature 404:725-728.

Perry VH (1979) The ganglion cell layer of the retina of the rat: a Golgi study. Proc R Soc Lond B Biol Sci 204:363-375.

Perry VH, Oehler R, Cowey A (1984) Retinal ganglion cells that project to the dorsal lateral geniculate nucleus in the macaque monkey. Neuroscience 12:1101-1123.

Petros TJ, Rebsam A, Mason CA (2008) Retinal axon growth at the optic chiasm: to cross or not to cross. Annu Rev Neurosci 31:295-315.

Pfeiffenberger C, Cutforth T, Woods G, Yamada J, Renteria RC, Copenhagen DR, Flanagan JG, Feldheim DA (2005) Ephrin-As and neural activity are required for eye-specific patterning during retinogeniculate mapping. Nat Neurosci 8:1022-1027.

Pittman AJ, Law MY, Chien CB (2008) Pathfinding in a large vertebrate axon tract: isotypic interactions guide retinotectal axons at multiple choice points. Development.

Plachez C, Andrews W, Liapi A, Knoell B, Drescher U, Mankoo B, Zhe L, Mambetisaeva E, Annan A, Bannister L, Parnavelas JG, Richards LJ, Sundaresan V (2008) Robos are required for the correct targeting of retinal

ganglion cell axons in the visual pathway of the brain. Mol Cell Neurosci 37:719-730.

Plump AS, Erskine L, Sabatier C, Brose K, Epstein CJ, Goodman CS, Mason CA, Tessier-Lavigne M (2002) Slit1 and Slit2 cooperate to prevent premature midline crossing of retinal axons in the mouse visual system. Neuron 33:219-232.

Polleux F, Giger RJ, Ginty DD, Kolodkin AL, Ghosh A (1998) Patterning of cortical efferent projections by semaphorin-neuropilin interactions. Science 282:1904-1906.

Powell AW, Sassa T, Wu Y, Tessier-Lavigne M, Polleux F (2008) Topography of thalamic projections requires attractive and repulsive functions of Netrin-1 in the ventral telencephalon. PLoS Biol 6:e116.

Pratt T, Tian NM, Simpson TI, Mason JO, Price DJ (2004) The winged helix transcription factor Foxg1 facilitates retinal ganglion cell axon crossing of the ventral midline in the mouse. Development 131:3773-3784.

Pratt T, Conway CD, Tian NM, Price DJ, Mason JO (2006) Heparan sulphation patterns generated by specific heparan sulfotransferase enzymes direct distinct aspects of retinal axon guidance at the optic chiasm. J Neurosci 26:6911-6923.

Price DJ, Kennedy H, Dehay C, Zhou L, Mercier M, Jossin Y, Goffinet AM, Tissir F, Blakey D, Molnar Z (2006) The development of cortical connections. Eur J Neurosci 23:910-920.

Raper JA (2000) Semaphorins and their receptors in vertebrates and invertebrates. Curr Opin Neurobiol 10:88-94.

Rhee J, Buchan T, Zukerberg L, Lilien J, Balsamo J (2007) Cables links Robo-bound Abl kinase to N-cadherin-bound beta-catenin to mediate Slit-induced modulation of adhesion and transcription. Nat Cell Biol 9:883-892.

Rhee J, Mahfooz NS, Arregui C, Lilien J, Balsamo J, VanBerkum MF (2002) Activation of the repulsive receptor Roundabout inhibits N-cadherin-mediated cell adhesion. Nat Cell Biol 4:798-805.

Richards LJ, Plachez C, Ren T (2004) Mechanisms regulating the development of the corpus callosum and its agenesis in mouse and human. Clin Genet 66:276-289.

Ringstedt T, Braisted JE, Brose K, Kidd T, Goodman C, Tessier-Lavigne M, O'Leary DD (2000) Slit inhibition of retinal axon growth and its role in retinal axon pathfinding and innervation patterns in the diencephalon. J Neurosci 20:4983-4991.

Round J, Stein E (2007) Netrin signaling leading to directed growth cone steering. Curr Opin Neurobiol 17:15-21.

Rubenstein JL, Beachy PA (1998) Patterning of the embryonic forebrain. Curr Opin Neurobiol 8:18-26.

Sakai JA, Halloran MC (2006) Semaphorin 3d guides laterality of retinal ganglion cell projections in zebrafish. Development 133:1035-1044.

Schlessinger J, Plotnikov AN, Ibrahimi OA, Eliseenkova AV, Yeh BK, Yayon A, Linhardt RJ, Mohammadi M (2000) Crystal structure of a ternary FGF-FGFR-heparin complex reveals a dual role for heparin in FGFR binding and dimerization. Mol Cell 6:743-750.

Schnorrer F, Dickson BJ (2004) Axon guidance: morphogens show the way. Curr Biol 14:R19-21.

Sedita J, Izvolsky K, Cardoso WV (2004) Differential expression of heparan sulfate 6-O-sulfotransferase isoforms in the mouse embryo suggests distinctive roles during organogenesis. Dev Dyn 231:782-794.

Seeger M, Tear G, Ferres-Marco D, Goodman CS (1993) Mutations affecting growth cone guidance in Drosophila: genes necessary for guidance toward or away from the midline. Neuron 10:409-426.

Sefton AJ, Swinburn M (1964) Electrical activity of lateral geniculate nucleus and optic tract of the rat. Vision Res 4:315-328.

Serafini T, Colamarino SA, Leonardo ED, Wang H, Beddington R, Skarnes WC, Tessier-Lavigne M (1996) Netrin-1 is required for commissural axon guidance in the developing vertebrate nervous system. Cell 87:1001-1014.

Shu T, Richards LJ (2001) Cortical axon guidance by the glial wedge during the development of the corpus callosum. J Neurosci 21:2749-2758.

Shworak NW, HajMohammadi S, de Agostini AI, Rosenberg RD (2002) Mice deficient in heparan sulfate 3-O-sulfotransferase-1: normal hemostasis with unexpected perinatal phenotypes. Glycoconj J 19:355-361.

Silver J, Sidman RL (1980) A mechanism for the guidance and topographic patterning of retinal ganglion cell axons. J Comp Neurol 189:101-111.

Silver J, Lorenz SE, Wahlsten D, Coughlin J (1982) Axonal guidance during development of the great cerebral commissures: descriptive and experimental studies, in vivo, on the role of preformed glial pathways. J Comp Neurol 210:10-29.

Skarnes WC, Moss JE, Hurtley SM, Beddington RS (1995) Capturing genes encoding membrane and secreted proteins important for mouse development. Proc Natl Acad Sci U S A 92:6592-6596.

Smeds E, Habuchi H, Do AT, Hjertson E, Grundberg H, Kimata K, Lindahl U, Kusche-Gullberg M (2003) Substrate specificities of mouse heparan sulphate glucosaminyl 6-O-sulphotransferases. Biochem J 372:371-380.

Song HJ, Poo MM (1999) Signal transduction underlying growth cone guidance by diffusible factors. Curr Opin Neurobiol 9:355-363.

Sperry RW (1963) Chemoaffinity In The Orderly Growth Of Nerve Fiber Patterns And Connections. Proc Natl Acad Sci U S A 50:703-710.

Sretavan DW (1990) Specific routing of retinal ganglion cell axons at the mammalian optic chiasm during embryonic development. J Neurosci 10:1995-2007.

Sretavan DW, Feng L, Pure E, Reichardt LF (1994) Embryonic neurons of the developing optic chiasm express L1 and CD44, cell surface molecules with opposing effects on retinal axon growth. Neuron 12:957-975.

Sretavan DW, Pure E, Siegel MW, Reichardt LF (1995) Disruption of retinal axon ingrowth by ablation of embryonic mouse optic chiasm neurons. Science 269:98-101.

Steigemann P, Molitor A, Fellert S, Jackle H, Vorbruggen G (2004) Heparan sulfate proteoglycan syndecan promotes axonal and myotube guidance by slit/robo signaling. Curr Biol 14:225-230.

Stein E, Tessier-Lavigne M (2001) Hierarchical organization of guidance receptors: silencing of netrin attraction by slit through a Robo/DCC receptor complex. Science 291:1928-1938.

Stickens D, Zak BM, Rougier N, Esko JD, Werb Z (2005) Mice deficient in Ext2 lack heparan sulfate and develop exostoses. Development 132:5055-5068.

Stier H, Schlosshauer B (1995) Axonal guidance in the chicken retina. Development 121:1443-1454.

Stoykova A, Chowdhury K, Bonaldo P, Torres M, Gruss P (1998) Gene trap expression and mutational analysis for genes involved in the development of the mammalian nervous system. Dev Dyn 212:198-213.

Strigini M (2005) Mechanisms of morphogen movement. J Neurobiol 64:324-333.

Sugaya N, Habuchi H, Nagai N, Ashikari-Hada S, Kimata K (2008) 6-O-sulfation of heparan sulfate differentially regulates various fibroblast growth factor-dependent signalings in culture. J Biol Chem 283:10366-10376.

Sun W, Li N, He S (2002a) Large-scale morophological survey of rat retinal ganglion cells. Vis Neurosci 19:483-493.

Sun W, Li N, He S (2002b) Large-scale morphological survey of mouse retinal ganglion cells. J Comp Neurol 451:115-126.

Suter DM, Forscher P (1998) An emerging link between cytoskeletal dynamics and cell adhesion molecules in growth cone guidance. Curr Opin Neurobiol 8:106-116.

Tanaka DH, Yamauchi K, Murakami F (2008) [Guidance mechanisms in neuronal and axonal migration]. Brain Nerve 60:405-413.

Tear G, Seeger M, Goodman CS (1993) To cross or not to cross: a genetic analysis of guidance at the midline. Perspect Dev Neurobiol 1:183-194.

Tessier-Lavigne M, Goodman CS (1996) The molecular biology of axon guidance. Science 274:1123-1133.

Thompson H, Barker D, Camand O, Erskine L (2006a) Slits contribute to the guidance of retinal ganglion cell axons in the mammalian optic tract. Dev Biol 296:476-484.

Thompson H, Camand O, Barker D, Erskine L (2006b) Slit proteins regulate distinct aspects of retinal ganglion cell axon guidance within dorsal and ventral retina. J Neurosci 26:8082-8091.

Torborg CL, Feller MB (2005) Spontaneous patterned retinal activity and the refinement of retinal projections. Prog Neurobiol 76:213-235.

Torii M, Levitt P (2005) Dissociation of corticothalamic and thalamocortical axon targeting by an EphA7-mediated mechanism. Neuron 48:563-575.

Torres M, Gomez-Pardo E, Gruss P (1996) Pax2 contributes to inner ear patterning and optic nerve trajectory. Development 122:3381-3391.

Turnbull J, Drummond K, Huang Z, Kinnunen T, Ford-Perriss M, Murphy M, Guimond S (2003) Heparan sulphate sulphotransferase expression in mice and Caenorhabditis elegans. Biochem Soc Trans 31:343-348.

Tuttle R, Braisted JE, Richards LJ, O'Leary DD (1998) Retinal axon guidance by region-specific cues in diencephalon. Development 125:791-801.

Uziel D, Garcez P, Lent R, Peuckert C, Niehage R, Weth F, Bolz J (2006) Connecting thalamus and cortex: the role of ephrins. Anat Rec A Discov Mol Cell Evol Biol 288:135-142.

Van Vactor D, Flanagan JG (1999) The middle and the end: slit brings guidance and branching together in axon pathway selection. Neuron 22:649-652.

Van Vactor D, Wall DP, Johnson KG (2006) Heparan sulfate proteoglycans and the emergence of neuronal connectivity. Curr Opin Neurobiol 16:40-51.

Walsh FS, Doherty P (1997) Neural cell adhesion molecules of the immunoglobulin superfamily: role in axon growth and guidance. Annu Rev Cell Dev Biol 13:425-456.

Walz A, McFarlane S, Brickman YG, Nurcombe V, Bartlett PF, Holt CE (1997) Essential role of heparan sulfates in axon navigation and targeting in the developing visual system. Development 124:2421-2430.

Wang KH, Brose K, Arnott D, Kidd T, Goodman CS, Henzel W, Tessier-Lavigne M (1999) Biochemical purification of a mammalian slit protein as a positive regulator of sensory axon elongation and branching. Cell 96:771-784.

Wei G, Bai X, Gabb MM, Bame KJ, Koshy TI, Spear PG, Esko JD (2000) Location of the glucuronosyltransferase domain in the heparan sulfate copolymerase EXT1 by analysis of Chinese hamster ovary cell mutants. J Biol Chem 275:27733-27740.

Williams SE, Grumet M, Colman DR, Henkemeyer M, Mason CA, Sakurai T (2006) A role for Nr-CAM in the patterning of binocular visual pathways. Neuron 50:535-547.

Williams SE, Mann F, Erskine L, Sakurai T, Wei S, Rossi DJ, Gale NW, Holt CE, Mason CA, Henkemeyer M (2003) Ephrin-B2 and EphB1 mediate retinal axon divergence at the optic chiasm. Neuron 39:919-935.

Wilson VA, Gallagher JT, Merry CL (2002) Heparan sulfate 2-O-sulfotransferase (Hs2st) and mouse development. Glycoconj J 19:347-354.

Winberg ML, Noordermeer JN, Tamagnone L, Comoglio PM, Spriggs MK, Tessier-Lavigne M, Goodman CS (1998) Plexin A is a neuronal semaphorin receptor that controls axon guidance. Cell 95:903-916.

Yabe T, Hata T, He J, Maeda N (2005) Developmental and regional expression of heparan sulfate sulfotransferase genes in the mouse brain. Glycobiology 15:982-993.

Yamauchi K, Phan KD, Butler SJ (2008) BMP type I receptor complexes have distinct activities mediating cell fate and axon guidance decisions. Development 135:1119-1128.

Yoshikawa S, McKinnon RD, Kokel M, Thomas JB (2003) Wnt-mediated axon guidance via the Drosophila Derailed receptor. Nature 422:583-588.

Zhang F, Lu C, Severin C, Sretavan DW (2000) GAP-43 mediates retinal axon interaction with lateral diencephalon cells during optic tract formation. Development 127:969-980.

Zou Y, Lyuksyutova AI (2007) Morphogens as conserved axon guidance cues. Curr Opin Neurobiol 17:22-28.